UNIVERSITY OF MILAN

DEPARTMENT OF VETERINARY MEDICINE AND ANIMAL SCIENCES

PhD course in Veterinary and Animal Sciences

Cycle XXXVI

CHARACTERIZATION OF IMMUNE RESPONSE IN EXPERIMENTAL MOUSE MODELS

PhD Candidate

Dr. Luca Bertola

Supervisor: Dr. Camilla Recordati

Co-supervisor: Prof. Cristina Lecchi

PhD Course Coordinator: Prof. Fabrizio Ceciliani

Academic year 2022-2023.

1. TABLE OF CONTENTS

PREFACE

Immunology, the branch of medicine dedicated to the study of the Immune System, explores the complex defense mechanisms employed by living organisms to protect themselves against pathogens, foreign substances, and tumors. Immune system cellular and molecular components exert complex responses aimed at maintaining immune tolerance to self-proteins and cells and at defending the body against viruses, bacteria, fungi, protozoa, metazoan parasites, and cancer.

Advancements in immunology have deepened our knowledge of several basic biological processes and led to outstanding therapeutical improvements against both infectious agents and neoplastic conditions, among which vaccines and immunotherapy probably represent the most important discoveries.

The use of laboratory animals is of pivotal importance to investigate the complexities of the immune system. Among laboratory animals, rodents, particularly mice and rats, have emerged as indispensable tools for immunology investigations, since they share significant genetic, anatomic, and immunologic similarities with humans.

This thesis was aimed at characterizing immune system cells in both physiological and pathological conditions of laboratory mice through the application of histology, immunohistochemistry, and, when suitable, digital image analysis. After a general introduction to the immune system, four studies investigating immune cells in murine models, each introduced by a dedicated introduction, are presented, starting with steady state organs, and followed by inflammatory conditions and neoplastic disease.

1. INTRODUCTION TO THE IMMUNE SYSTEM

The immune system is a complex network of organs, cells and molecules aimed at protection against noxious stimuli and cancer development and at maintenance of self-tolerance (Kumar et al. 2018 b). The immune system is, in fact, able to detect components of pathogens, toxins or neoplastic cells, generally termed antigens, eliminating them, with minimal damage to the host tissues (Chaplin et al. 2010).

The immune response is broadly divided into 2 main categories: the quicker and less specific innate immunity and the secondary, specific, and more efficient adaptive immunity. Although didactically described as 2 distinct entities, innate and adaptive immune responses are deeply interconnected and represent a continuum of the same bodily response (Kumar et al. 2018 b).

1.1. Innate Immunity

Innate immunity relies on a combination of anatomical structures such as epithelial barriers of cutaneous or mucosal linings and on a set of cellular elements which share a limited number of antigen-recognizing molecules. Because these recognition molecules are expressed broadly on numerous cells in the body, and because these cells are strategically located in tissues with the highest chance of meeting a pathogen, innate immunity can act rapidly, within few hours, against target threats representing the first line of defense of the organism against pathogens and their toxins (Chaplin et al. 2010). Innate immunity deploys a stereotypical response against all pathogens and foreign substances and is, therefore, defined as non-specific (Kumar et al. 2018 b).

1.1.1. Epithelial Barriers

The epithelial covering of skin and of reproductive, respiratory, and gastro-intestinal mucosae functions as a mechanical barrier against pathogen penetration from the environment thanks to the presence of adherent cell junctions strongly interconnecting epithelial cells one to each other (Moens et al. 2012). However, these epithelia are not just inert barriers: intra-epithelial lymphocytes and the production and secretion of a plethora of antimicrobial peptides such as defensins and secretory immunoglobulins of the A class (IgAs) capable of eliminating pathogens or limiting their adhesion to mucosal surfaces, assist and boost epithelial protective activity (Kumar et al. 2018 b; Chaplin et al. 2010). Furthermore, mucus production and cilia movement aid in the elimination of exogenous particles, particularly in the respiratory tract. Even further than that, epithelial cells sense luminal and external microorganisms, selecting a commensal population of bacteria, fungi,

and protozoa of pivotal importance for organism homeostasis maintenance and for pathogens proliferation prevention (Moens and Veldhoen 2012, Constant 2021).

1.1.2. Cellular Elements

The innate immune response is carried out by numerous effector cells including polymorphonucleated granulocytes (neutrophils, eosinophils and basophils), monocytes, macrophages involved in both phagocytosis and cytokines production, innate lymphoid cells, natural killer cells and dendritic cells, the latter acting as antigen presenting cells (APCs) triggering the adaptive immune response (Kumar et al. 2018 b). All these cells exert their function along with epithelial cells, mast cells and endothelial cells.

1.1.2.1. Polymorphonucleated Granulocytes

Neutrophils are the first immune cells recruited to a site of inflammation by chemotactic molecules including C5a complement factor, IL-8 and leukotriene B4 (Nagy et al. 1984). These cells are specialized in bacterial and fungal phagocytosis, killing through both oxygen dependent and independent mechanism and can undergo NETosis, a particular form of cell death in which neutrophils extrude their DNA mixed to bactericidal molecules creating net-like structures entrapping pathogens and limiting extracellular infections (Nauseef 2007; Mesa 2013). Neutrophils can express MHC-II functioning as non-professional APCs stimulating T lymphocytes and activating the adaptive immune response and can modulate B and T cell maturations in lymph nodes through interaction with macrophages and dendritic cells, with still not-fully elucidated mechanisms (Yang et al. 2010; Li et al. 2019).

Similarly to neutrophils, albeit less effectively, eosinophils can phagocytose pathogens and kill them in phagosomes through the activity of lytic proteins such as major basic protein (MBP) and eosinophil cationic protein (ECP)(Lehrer et al.1989; Ramirez et al. 2018). Through degranulation, they release cytotoxic compounds active against helminths and other metazoan parasites (Ramirez et al. 2018). Eosinophils also carry out important immunomodulatory functions: they act as non-professional APCs presenting antigens on MHC-II molecules and stimulate T helper cells and B lymphocytes to produce IL-4 and IL-5 or parasite specific immunoglobulins respectively (Long et al. 2016; Mawhorter et al. 1994).

Basophils are the least common polymorphonucleated granulocytes found in peripheral blood. These cells release histamine, a vasoactive mediator, prostaglandins and leukotrienes, IL-4 and IL-5 and express high affinity receptors for the constant region of immunoglobulins E (FcεRI) (Chirumbolo et al. 2018). Although traditionally associated to allergic reactions

together with mast cells, basophils also participate to the anti-helminthic response releasing IL-4 and IL-13 and trigger adaptive immune response by secreting IL-6 stimulating T helper cells activation and proliferation (Wakahara et al. 2012; Webb et al. 2017).

1.1.2.2. Mononuclear Phagocytes

The mononuclear phagocyte system (MPS) comprises an heterogenous population of embryo and bone-marrow derived monocytes, macrophages (MΦs), and dendritic cells (DCs) found in all body systems and involved in a vast array of physiological and pathological functions comprising pathogen detection and destruction, stimulation of the adaptive response, tissue repair, and homeostasis maintenance (Figure 1) (Van furth 1972; Guilliams et al 2015).

Embryonal precursors originating from the yolk sack of the developing fetus (Yolk sack MΦs) or from the fetal liver (fetal liver monocytes) seed various tissues establishing a population of tissue-resident cells capable of constant self-renewal, independent from circulating monocytes (Yona and Gordon 2015). Examples of these cells are Kupffer cells in the liver, Langerhans cells in the skin or microglial cells in the central nervous system (Samokhvalov et al. 2007; Hoeffl et al. 2012; Ginhoux et al. 2010). Exceptions, however, exist with cardiac, intestinal, and dermal tissue resident mononuclear phagocytes requiring a constant renewal by circulatory, bone-marrow derived monocytes (Tamoutounour et al. 2013; Molawi et al. 2014). These tissue based MPS cells act against invading pathogens and necrotic cells and are fundamental in tissue development, remodeling, and homeostasis (McGrath et al. 2015; Wu et al. 2021).

Hematopoietic stem cells (HSCs) in the bone marrow give rise to common monocyte progenitors from which two subsets of monocytes develop: classical $Ly6C^{high}$ monocytes and non-classical $Ly6C^{low}$ monocytes (Zhao et al. 2018; Hettinger et al. 2013). While classical monocytes represent a circulatory reservoir of tissue resident cardiac, intestinal, and dermal MΦs and migrate into tissues, under physiologic or inflammatory conditions, differentiating into monocyte-derived MΦs or monocyte-derived DCs, non-classical monocytes remain in circulation, patrolling blood vessels, eliminating circulating debris and damaged endothelium (Guilliams et al 2014; Wynn et al. 2013).

From another maturation line of bone marrow HSCs, common dendritic cell precursors give rise to conventional and plasmacytoid DCs (cDCs and pDCs) through a series of intermediate maturation stages (Hettinger et al. 2013; Onai et al. 2007). Both cDCs and pDCs are tissue-based cells specialized in antigen phagocytosis and processing,

subsequently migrating to lymph nodes presenting antigens to T and B cells, thus representing the bridge between the innate and adaptive immune response (Kumar et al. 2018 b). cDCs are found in all tissues of the body, particularly at sites with greatest chance of meeting antigens such as skin or mucosae and are divided into cDCs type 1 and 2 based on transcriptional profiles, phenotype, and function (Guilliams et al. 2014; Guilliams and Van der 2015). While type 1 cDCs present antigens on MHC-I molecules triggering a T helper 1 mediated cytotoxic response, type 2 cDCs present antigens on MHC-II molecules, stimulating T helper 17 cells (Balan et al. 2019). Plasmacytoid DCs are found in lymphoid organs and morphologically resemble plasma cells. Upon activation they behave as DCs, developing dendritic processes and producing a high amount of type 1 INFs (Guilliams et al. 2014; Guilliams and Van der 2015).

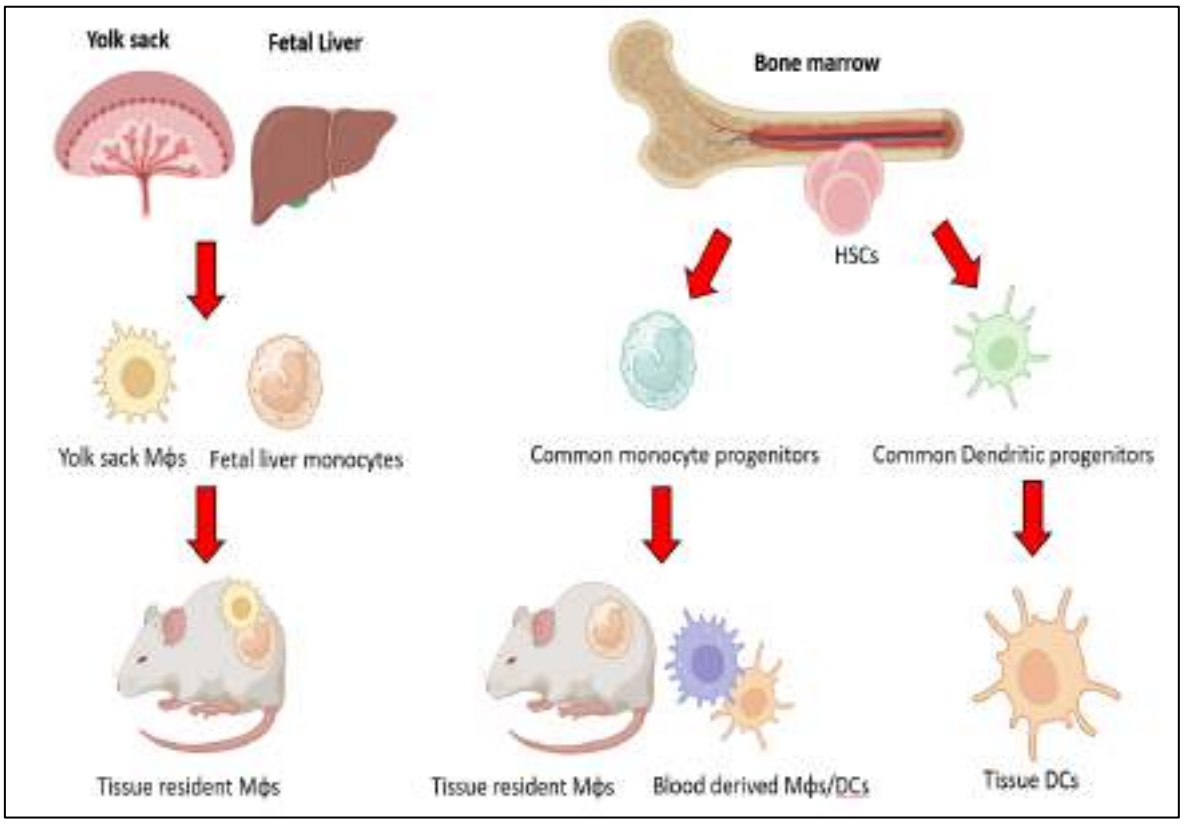

Figure 1. **MPS cells ontogenesis**. Yolk sack MΦs and Fetal liver monocytes give rise to most tissue resident macrophages. Hematopoietic stem cells (HSCs) in the bone marrow give rise to either classical and non-classical monocytes or to conventional and plasmacytoid DCs.

1.1.2.3. Innate Lymphoid Cells and Natural Killer Cells

Innate Lymphoid Cells (ILCs) are lymphoid progenitor-derived, tissue resident lymphocytes that lack T cell receptors and regulate the immune response through cytokines production (Kumar et al. 2018 b et al.2018; Eberl et al 2015). Currently, based on secreted cytokines, 3 subtypes of ILCs are recognized: type 1 ILCs activated by IL-12, IL-15 and IL-18 and producing TNF-α and INF-γ, Type 2 ILCs activated by IL-25 and IL-33 and producing IL-4, IL-5 and IL-13 and type 3 ILCs activated by IL-1β and IL-23 producing IL-17, IL-22 and granulocyte-macrophage colony stimulating factor (GM-CSF). These cells functionally mirror CD4+ T-helper 1, 2 and 17 cells, respectively (Eberl et al. 2015). A particular subset of ILCs are natural killer cells (NK cells), which can eliminate IgGs coated cells by means of CD16 receptor, in a process known as antibody-dependent cellular toxicity or kill infected or neoplastic cells characterized by decrease expression or loss of MHC-I molecules (Kumar et al. 2018 b; Liu et al. 2021).

1.1.2.4. Endothelial Cells and Mast cells

Beyond their functions in vascular hemodynamics and permeability regulation, endothelial cells carry out important immune functions such as pathogen and damage associated molecules recognition, cytokines secretion and antigens presentation through class I Major histocompatibility complex (Shao et al. 2020). Endothelial cells also express adhesion molecules such as P and E-selectins and vascular cell adhesion molecule (VCAM) which interact with leukocytes sialylated oligosaccharides and integrins respectively, favoring leukocytes rolling and subsequent endothelial firm adhesion, essential passages for diapedesis of inflammatory cells (Kumar et al. 2018 a; Filippi 2016).

Mast cells are found in close association to blood vessels, in the interstitial connective tissue of all organs and regulate vascular caliber and permeability through the release of vasoactive mediators such as histamine, thus playing a pivotal role in initiation of inflammation (Dimitriou et al. 2020). Activated mast cells also release cytokines, mainly IL-10 and TGF-β and chemokines recruiting and activating polymorphonucleated granulocytes (Menzies-Gow et al. 2004; Doener et al. 2013).

1.1.3. Plasma Proteins

Fundamental innate functions are played by soluble proteins circulating in blood such as mannose-binding lectin, C-reactive protein and the complement system. Mannose-binding lectin binds to a range of sugars found on viruses, bacteria, fungi, and protozoa allowing

complement fixation with an antibody and C1-indipendent manner, also known as the lectin pathway of activation (Turner 2003).

C-reactive protein is an acute inflammatory protein mainly synthesized by hepatocytes under the influence of IL-6, which binds to pathogen surface molecules favoring complement fixation or macrophages phagocytosis in a process knowns as opsonization (Sproston et al. 2018).

The complement system is composed of several blood circulating proteins produced by the liver. When activated, these proteins act in a cascade of bindings and cleavages, culminating with pathogen opsonization and elimination (Merle et al. 2015). The complement system can be activated, depending on the context, in three different manners: the classical (antibody-dependent), the alternative (antibody-independent) and the lectin pathways, all resulting in the cleavage of the inactive fragment C3 in the C3a and C3b fragments and in the production of the C5 fragment which subsequently allow the formation of the membrane attack complex (MAC) and the osmotic lysis of the target. (Dunkelberger et al.2010; Merle et al. 2015)

1.1.4. Pattern Recognition Receptors

The innate immune system can recognize a plethora of either pathogen associated molecules defined pathogen-associated molecular patterns (PAMPs) or released by damaged and necrotic cells, defined as damage-associated molecular patterns (DAMPs) through a set of receptors specific for different ligands, known as Pattern recognition receptors (PRRs) (Li and Wu 2021). Five different classes of PRRs have been described:

- Toll-like receptors (**TLRs**). Ten TLRs in humans and thirteen TLRs in mice, each recognizing different ligands have been identified both on the cellular surface and on the endosome membranes of a plethora of cells including MΦs, DCs, neutrophils, eosinophils, basophils, and epithelial cells (Li and Wu 2021; Kawai et al. 2010). Even though the majority of human and murine TLRs recognize bacterial molecules such as LPS, peptidoglycan or membrane-associated lipoproteins, some can recognize viral dsDNA or ssRNA (TLR7, TLR8, TLR9) or even protozoal components (murine TLR11 and TLR12) (Li and Wu, 2021, Kawai et al. 2010) triggering a signal transduction cascade leading to transcription factors activation and inflammatory cytokines production (O'neil 2007; Li and wu 2021).
- Nucleotide oligomerization domain (NOD)-like receptors (**NLRs**). More than 20 NLRs are found in epithelial cells and MΦs' cytoplasms. These receptors recognize

intra-cellular components of gram-positive and gram-negative bacteria such as muramyl dipeptide as well as viral ssRNA or "danger signals" of damaged cells (Li and Wu, 2021; Girardin et al. 2003; Geddes et al 2009). Upon activation NLRs initiate an intracellular signal cascade leading to cytokines production, NF-kB and interferon regulatory factors stimulation or even to caspase-1 activation with subsequent pyroptosis (Correa et al. 2012; Martinon 2007).

- C-type lectin receptors (**CLRs**). Several CLRs, mainly found on MΦs and DCs cells, can recognize pathogen sugar moieties (α-mannose, fucose) and glycoproteins. (Hoving et al. 2013). Although mainly involved in fungi-related molecules recognition (Nikolakopoulo et al. 2020) some CLRs recognize bacteria such as *Mycobacteria spp*. or *Yersinia pestis* or even viruses, though mostly with detrimental, immune-suppressive effects as observed with the human HIV (Chen et al. 2013) or Measles viruses (Miyake et al. 2013; Zhang et al. 2008; Harman et al. 2013; Avota et al. 2013).
- Retinoic acid-inducible gene-I (RIG-I)-like receptors (**RLRs**) can recognize intracytoplasmic viral RNA or short chains of viral dsDNA, prompting the production of different classes of interferons (INFs) (Rehwinkel et al. 2020; Li and Wu 2021). INFs act in an autocrine and paracrine manner activating the JAK-STAT pathway and promoting a virus-resistant state (Majoros et al. 2017).
- Absent in melanoma-2 (AIM2)-like receptors (**ALRs**) are cytosolic receptors that recognize intracytoplasmic bacterial or viral dsDNA triggering INFs class I secretion (Hansen 2011; Munoz-Wolf et al 2016; Wu et Li 2021).

The activation of one of these PRRs, generally leads to an intracellular signal cascade culminating in the activation of transcription factors and in the consequent production and secretion of molecules, mainly represented by adhesion molecules favoring inflammatory cells diapedesis or of pro and anti-inflammatory cytokines (Franchi et al. 2009; Lowrence 2009; Kawai et al. 2006).

1.1.5. Cytokines and Interferons

Cytokines are small, secreted proteins acting as mediators of inflammation, triggering, modulating, and eventually resolving inflammation (Liu et al. 2021; Kany et al. 2019). Although representing a complex set of molecules belonging to different families such as Tumor necrosis factors (TNFs), Interleukins (ILs), Lymphokines, Monokines, Interferons

(INFs), Colony stimulating factors (CSFs) and Transforming growth factors (TGFs), all cytokines share some common properties (Liu et al. 2021). They, in fact, act in an autocrine, paracrine or, in some instances, endocrine manner and often trigger cascades of production, as one cytokine often stimulates a target cell to produce more cytokines (Zhang et al. 2009). Different cytokines can exert the same biological function, a property known as redundancy, and, on the contrary, the same cytokine can exert different biological functions, a property known as pleiotropy. Cytokines redundancy and pleiotropy, together with their synergistic or antagonistic action, allow a subtle regulation of the immune response (Zhang et al. 2021).

Cytokines can be broadly divided into either pro-inflammatory cytokines such as IL-1, IL-6 and TNF-α or anti-inflammatory, immune-suppressive cytokines such as IL-4, IL-10 or TGF-β. Nevertheless, it has been recognized that the very same cytokine can play a pro or anti-inflammatory role depending on the inflammatory context (Zhang, Liu et al. 2021; Boshtam et al. 2017).

Among cytokines, interferons (INFs), so called because able to interfere with viral replication, play a notable role in viral infections, favoring an anti-viral state (Negishi et al. 2018). Based on the cellular receptor through which they signal, INFs are classified into three different types (Negishi et al. 2018):

- **Type I INFs** are generally produced by fibroblasts and innate immune cells after viral PAMPs recognition. Type I INFs bind to a membrane receptor known as IFN α/β receptor. Examples of type I INFs are INF-α, INF-β, INF-τ and INF-ω (Negishi et al. 2018).
- **Type II INF (INF- γ)** is produced by a plethora of cells comprising type 1 T helper cells and cytotoxic T cells, under the stimulation of IL-12 and bind to IFNGR receptor. INF-γ is the only member of type II INFs and is also involved in MΦs stimulation in the context of T helper 1 response.
- **Type III INFs (INF-λ1, INF-λ2, INF-λ3)** are the least characterized INFs. They are not highly expressed on hematopoietic cells and act mainly on epithelial surfaces, binding to a heterodimeric cytokine receptor composed of IL10R2 and IL28R subunits (Uzè et al. 2007).

As a result of INFs-receptor interaction several molecules are produced by target cells among which are P53 protein favoring apoptosis of virus-infected cells and protein kinase R (PKR) and RNAse L, which reduce both host and viral protein synthesis (Takaoka et al. 2003; Jha et al. 2011)

Table 1. Anatomical, cellular, and molecular components of the innate immune system. (Adapted from Aristizabal et al. 2013).

MECHANICAL BARRIERES		
Skin	Pathogen entrance prevention	
Mucosa	Pathogen entrance prevention, soluble antimicrobial peptide secretion	
CELLULAR COMPONENTS		
CELL TYPE	**FUNCTIONS**	**LOCATION**
Neutrophils	Microbial killing, NET formation	Blood. Tissues
Basophils	Histamine release. Active against parasites	Blood. Tissues
Eosinophils	Active against parasites and fungi	Blood. Tissues
Mast Cells	Vasodilation (heparin and histamine release). ECM remodeling and wound healing	Tissues
Monocytes	MΦs and DCs precursors. Endothelial debris phagocytosis	Blood
Macrophages	Phagocytosis. Stimulation of other immune cells	Tissues
Dendritic Cells	Antigen presentation to T cells	Tissues. Lymph nodes
Innate Lymphoid Cells	Immune response regulation	Tissues
Natural Killer cells	TCR-independent killing of neoplastic and viral-infected cells	Blood. Tissues
CELLULAR RECEPTORS		
TLRs	Recognition of extra and intra-cytoplasmic PAMPs and DAMPs	
NLRs	Recognition of intra-cytoplasmic PAMPs and DAMPs	
CLRs	Recognition of sugar moieties on Fungi, Bacteria and Viruses	
RLRs	Recognition of viral dsDNA and viral RNA	
ALRs	Recognition of viral and bacterial dsDNA	
CYTOKINES		
IL-1, IL-6	Pro-inflammatory effects	
TNF-α	Pro-inflammatory effects, Cell death promotion	
Type I, II and III INFs	Resistance to viral infections	
INF-γ	Macrophage activation. Resistance to intracellular pathogens	
IL-10	Suppression of cellular immunity; decreased cytokines production	
IL-12	INF- γ production by NK cells and T lymphocytes	
IL-15	NK cells proliferation	
TGF-β	Immune cells proliferation inhibition	
Chemokines	Immune cells chemotaxis	
…	….	
PLASMA PROTEINS		
Complement System	Opsonization and Pathogen lysis	
C Reactive Protein	Opsonization and Complement activation	
Mannose-binding lectin	Opsonization and Complement activation	

1.2. Adaptive Immunity

The adaptive immune system takes over the innate immune system when a noxious stimulus persists, acting days to weeks after the first exposure. Differently from the innate system, which recognizes a limited set of molecules shared among pathogens, the adaptive response targets specific components of a pathogen or its products, carrying out an extremely effective response and allowing the formation of memory cells, immediately reacting at the second exposure of the organism to the same antigen (Kumar et al. 2018 b; Molnar and Gair 2021).

1.2.1. Cellular Components of the Adaptive Immune System

Key effectors of innate immunity are T lymphocytes, exerting the so-called cellular immunity, active against neoplastic cells and intra cellular microbes and B lymphocytes, exerting the humoral immunity by transforming into antibodies-producing plasma cells, protective against extracellular microbes and their toxins and involved in the antibody-mediated killing (Kumar et al. 2018 b; Snyder, Cano and Lopera 2013). These cells are activated by professional (MΦs, DCs and B cells themselves) and less frequently non-professional (endothelial and epithelial cells) APCs, which phagocytose and process antigens in their cytoplasms, subsequently presenting them on MHC class I and II molecules (Sprent 1995).

1.2.1.1. T Lymphocytes

T lymphocytes origin from hematopoietic stem cells in the bone marrow and mature in the thymus (Cano and Lopera 2013). During their maturation, T cells acquire a multiproteic receptor called T cell receptor (TCR) composed of two variable antigen-binding chains (either αβ or γδ) and by an invariable domain (CD3/ CD247) (Wucherpfenning et al. 2010). TCRs recognize antigens presented on MHC-II molecules by APCs or on MHC-I of other cell types (Kapsemberg 2003; Eiz-Vesper et al. 2020).

After maturation, naïve, not activated, T cells migrate to secondary lymphoid organs (lymph nodes, spleen, tonsils, and mucosa-associated lymphoid tissues) where they can recognize antigens presented on MHC molecules (Cano and Lopera 2013). The binding of an antigen presented on MHC-I or MHC-II with the TCR, associated with the signal of a co-stimulatory molecule initiates an intracellular signal cascade, culminating with IL-2 production. IL-2 prompts T cells clonal expansion, generating large number of identical T lymphocytes all recognizing the antigen that initiated the proliferation process. After the clonal expansion, approximately 90% of these clones undergo apoptosis, which limits

excessive lymphocytes proliferation and contributes to high-affinity-clones selection (Malek et al. 2004).

T lymphocytes are divided, based on the expression of surface molecules, into CD4+ T helper (Th) cells and CD8+ T cytotoxic cells (Cano and Lopera 2013). T helper cells stimulate B cells to transform into plasma cell and produce different sets of cytokines, depending on their subtype:

- **Th1** are induced by INF-γ, and IL-12 secreted by DCs and MΦs and produce mainly INF-γ stimulating MΦs and triggering an immune response particularly active against intracellular pathogens and neoplastic cells. This subset is also involved in autoimmune diseases pathogenesis and delayed hyper-sensitivity. (Kumar et al. 2018 b; Cano and Lopera 2013)
- **Th2** are mainly induced by IL-4 and produce IL-4, IL-5 and IL-13 stimulating IgE production and eosinophils and mast cells activation. Th2 are therefore involved in allergic reactions and immune response against helminthic and metazoan parasites.
- **Th17** are induced by several molecules among which IL-1, IL-6 and TGF-β and produce IL-17 and IL-22, actively involved in monocytes and neutrophils recruitment active against extracellular bacteria and fungi.
- **T regulatory cells (Tregs)** are T cells expressing the forkhead box 3 transcription factor FoxP3. Endowed with immune-suppressive properties they are fundamental to prevent autoimmune diseases and to limit inflammatory-related tissue damage (Cano and Lopera 2013). They are also present in neoplastic tissues, usually favoring an immunosuppressive, tumor-permissive microenvironment (Li et al. 2020).
- **Th9 Th22 and Follicular helpers** are other, somewhat recently described T helper subtypes. While Th9 release IL-9 promoting mast cells activation and are mainly involved in anti-helminthic response, Th22 are induced by IL-6 and TNFs and mainly release IL-22 favoring the production of anti-microbial peptides and promoting neo-angiogenesis and fibrosis. (Eyerich et al. 2009; Ma et al. 2010). Follicular helpers are, instead, found in lymphoid germinal centers and stimulate B cells differentiation into plasma cells together with the production of antibodies of different isotypes and memory B cells formation (King 2009).

CD8+ Cytotoxic cells are instead capable of destroying neoplastic or infected cells inducing their apoptosis both through the release of cytolytic proteins such as perforin or granzyme or through the expression of surface proteins such as Fas ligand, triggering the extrinsic apoptosis pathway (Cox 2013; Lieberman 2003).

1.2.1.2. B Lymphocytes

B cells arise from bone-marrow derived hematopoietic stem cell precursors (Cano and Lopera 2013). During their maturation in the bone marrow, a process of gene recombination, initiated by the complex of proteins RAG1 and RAG2, allows the formation of a wide repertoire of membrane IgMs and IgDs, known as B cell receptors (BCRs) capable of recognizing 5 x 10^{13} antigens (Pieper et al.2013; Herzog et al. 2009; Kumar et al. 2018 b). B cells then migrate to secondary lymphoid organs organizing in follicles and receiving antigens through lymphatic circulation (Cano and Lopera 2013).

B lymphocytes are activated by two categories of antigens:

- **T cell dependent antigens**. These antigens are recognized by APCs and endocytosed, degraded and displayed on MHC-II complexes for recognition by T helper cells. T helper cells are, then, activated and express CD40 ligand and cytokines which stimulate B cells proliferation and differentiation into plasma cells
- **T cell independent antigens**. These antigens, mainly constituted by lipids and polysaccharides cannot bind to MHC molecules but are still recognized by BCRs, directly stimulating B cells proliferation and differentiation.

Whereas T cell independent antigens trigger a quite simple response, stimulating plasma cells producing IgMs, T cell dependent antigens stimulate a more complex response. T helpers can, in fact, stimulate the production of immunoglobulins of other classes than IgMs, in a process known as isotype switching and favor the production of antigens with high affinity for the target antigen, a quality known as affinity maturation (Kumar et al. 2018 b, Cano and Lopera 2013).

Different B cells subsets based on location, cell surface molecules and activation routes have been described:

- **B1 cells** express CD9 and CD45RA and populate the peritoneal and pleural cavities, recognizing self-components and bacterial antigens and subsequently transforming into plasma cells. They are the main source of circulating IgMs (Cano and Lopera 2013; Inoue and Kurosaki 2023).
- **Follicular B cells** also known as **B2 cells** are mainly located in follicles of the secondary lymphoid organs. They are activated by both T dependent and T independent antigens. Because they are located adjacent to the T cell zone of

lymphoid organs, they can easily interact with T helper cells, responding to lymph-borne antigen presented by APCs. However, follicular B cells can recirculate through the bone marrow where they are usually located around sinusoids, responding in a T-cell independent manner to circulating antigens (Cariappa et al. 2007; Pillai et al. 2009)

- **Marginal zone B cells** are mainly located in the splenic marginal zone, at the interface between the blood in the marginal sisus and the lymphoid tissue of the white pulp, but they can also be found in lymph node subcapsular sinus, in the tonsillar crypts' epithelium and in the sub-epithelial dome of intestinal Peyer's patches. These cells are activated both through T cell dependent and independent mechanisms but, interestingly, express high levels of TLRs, allowing them to participate in the innate immune response (Cerutti et al. 2013; Cano and Lopera 2013)
- **Memory B cells** originate in germinal centers of spleen, lymph nodes and mucosa associated lymphoid tissue and circulate in the bloodstream for decades in a quiescent state (Crotty et al. 2003). They share the same BCR of the original stimulated B cell and activate a quick and strong immune response when exposed to the original antigen (Weisel et al. 2017)
- **Regulatory B cells** contribute to maintain self-tolerance against self-antigens and to modulate and limit an excessive inflammatory response mainly through IL-10 production, inhibiting pro-inflammatory cytokines, reducing MHC-II molecule expression, and favoring Tregs differentiation (Cano and Lopera 2013; Mauri 2012). These cells also play a role in tumor development, mainly favoring a tumor-permissive microenvironment through cytotoxic response suppression (Michaud et al. 2021).

As already mentioned, B cells differentiate into plasma cells producing antibodies. Antibodies bind to microbes preventing them from infecting host cells or from adhering to mucosal surfaces, opsonizing them favoring their phagocytosis by macrophages and neutrophils which express receptor for the immunoglobulins Fcs tails or fixing the complement by the classical pathway (Kumar et al. 2018 b).

1.2.2. Lymphocytes Activation

Lymphocytes activation generally requires the recognition of antigens displayed on MHC molecules by means of TCR/BCRs and an additional signal given by costimulatory

molecules such as CD80 for T cells and CD40 for B cells (Kumar et al. 2018 b; Frauwirth et al. 2002; Kotsias et al. 2019). Professional and non-professional APCs in epithelia and tissues phagocytose and metabolize antigens and migrate to draining lymph nodes through lymphatic circulation (Kumar et al. 2018 b). Then, APCs display antigens on class I or II MHC molecules: class I MHC molecules display intracellular proteins, either normal cytoplasmic components or tumor or viral related proteins, while class II MHC molecules display extracellular antigens (Kumar et al. 2018 b; Kotsias et al. 2019).

CD8+ T cytotoxic cells recognize antigens displayed on class I MHC molecules, while CD4+ T helper cells recognize antigens displayed on class II MHC molecules, apart for some polysaccharides and lipids that cannot be exposed on MHC (Vos et al. 2000; Allman et al. 2019). The antigen recognition, together with the binding between CD80 and CD86 (B7 proteins) on APCs and CD28 on naïve T cells or between the complement c3b component and the protein complex formed by CD21, CD19 or CD81 (B cell coreceptor molecules) on B cells, activate an intracellular cascade (Kumar et al. 2018 b; Dempsey et al. 1996; Esensten et al. 2016). Activated lymphocytes proliferate and enter the bloodstream to reach the primary site of antigenic stimulation or remain in blood and blood-marrow sinusoids as memory cells (Kumar et al. 2018 b).

While activated CD8+ cytotoxic T lymphocytes destroy target infected or neoplastic cells, activated CD4+ T helper lymphocytes produce different classes of cytokines, differentiating into Th1, Th2, Th17 or other subtypes. T helper cells also produce CD40 ligand, which binds to the CD40 molecule on B cells surface, stimulating B cells proliferation and differentiation into plasma cells (Frauwirth et al. 2002; Kumar et al. 2018 b).

1.3. Immune System in Steady State Conditions

Apart from the constant protection against noxious stimuli, immune system cells and molecules have been associated with several physiological processes:

- **Embryogenesis.** Both innate and adaptive immune systems play a crucial role in regulating organogenesis of the developing fetus. It has been demonstrated, for example, that innate myeloid cells and MΦs are involved in ovary and testes morphogenesis and guide gonads vascular development, and that numerous tissue resident MΦs regulate target organs maturation (Gu et al. 2022; Feyaerts et al. 2022). Langerhans cells, in fact, support angiogenesis and regulate chemotaxis in the developing skin, while Kupffer cells have been associated with iron regulation and

erythropoiesis in the liver as red pulp MΦs in the developing spleen (Reynolds et al. 2021; Li et al. 2019; Kurotaki et al.2015). Although embryogenesis seems mostly regulated by cells of macrophagic origin, other immune cells are involved as well: in the central nervous system, CD4+ and CD8+ T cells have been associated to neurogenesis rate and in the early phases of pregnancy, maternal neutrophils have been shown to interact with T cells, inducing the differentiation of a pro-angiogenic population of regulatory T cells in fetal tissues. (Prinz et al. 2011; Nadkarni et al. 2016)

- **Tissue homeostasis.** After birth and after reaching maturity, the immune system contributes to tissue homeostasis maintenance, removing apoptotic debris and guaranteeing the proper function of several cellular elements in all systems (Antonangeli et al. 2021; Rankin et al. 2018). In the central nervous system, tissue-resident microglial cells support neuronal function and neuropile integrity while meningeal, choroid plexus and perivascular MΦs regulate cerebrospinal fluid composition and immune cells entry in the neuroparenchyma (Prinz et al- 2017). MΦs, eosinophils and innate lymphoid cells support white adipose tissue metabolic functions and stimulate, under the proper stimuli, the transition from white adipose tissue to brown adipose tissue, in a process known as "beiging", limiting obesity (Brestoff et al. 2014). Intracardiac MΦs can regulate electric conduction in cardiomyocites, particularly in the atrioventricular node (Hunselman et al. 2017).
- **Tissue repair.** Beyond killing pathogens the immune system promotes inflammation resolution and damage tissue repair. M2 MΦs play a pivotal role in tissue repair, by removing pathogens and necrotic debris and by producing mediators that stimulate fibroblasts proliferation and tissue cells replication such as IL-6, VEGF, and PDGF. (Kumar et al. 2018 a). The repair process is carried out by a complex interaction among immune cells, fibroblasts, mesenchymal stem cells and cells of the damaged tissue and has variable outcomes depending on damage severity as well as tissue-specific regenerative properties (Godwin et al. 2017). When a complete regeneration of the tissue cannot be achieved, there is deposition of scar tissue, mainly guided by TGF-β and IL-10.
- **Physiological functions**. Immune dysfunctions have been associated with neurological impairment and change in behavior. Disturbance of the delicate interactions between glial cells and neurons has been associated with autism, dementia and schizophrenia, highlighting the importance of immune system activity for neurologic functions (Rankin et al. 2018). Other than cellular elements, serum

and cerebrospinal fluid levels of numerous cytokines, particularly of IL-1 and TNFs have been associated with sleep propensity while others such as IL-4 and 10 with sleep inhibition (Majde et al. 2005). Increased or decreased levels of interleukins have also been shown to regulate other physiologic functions such as appetite or thermoregulation (Majde et al. 2005; Li et al 2021). If it is true that the immune system influences numerous physiologic functions, it is also true that immune system cells and mediators are, in their turn, influenced by processes such as aging, nutrients intake and sexual activity. It has, in fact, been demonstrated that advanced age is associated with a decreased response to self and foreign antigens and to a chronic low-grade inflammatory state and that a regular sexual activity increases secretory IgA in humans (Castelo-Blanco et al. 2013; Charnetski et al. 2004).

- **Microbiome selection.** In the last decades, the interaction between the immune system and the mucosal microbiome, especially of the gut, has been extensively studied unravelling a complex interplay (Thaiss et al. 2016). The immune system selects non-pathogenic viruses, bacteria, fungi and protozoa that, in turn, shape immune system functions, providing beneficial nutrients such as vitamins and short-chains fatty acids and promoting immune functions maturation (Shi et al. 2017). Dysbiosis of the gut microbiome has been associated with numerous disorders such as rheumatoid arthritis, asthma, and inflammatory bowel disease (Sartor 2008; Chen et al. 2016; Huang et al. 2015).

1.4. Immune System in Tumors

The immune system protects the organism from cancer development, constantly patrolling the body, detecting, and eliminating neoplastic clones. In the last decades the interaction between tumor and immune system has been extensively studied, giving rise to the so-called *immunoediting* concept in which three different phases known as elimination, equilibrium, and escape have been described (Gubin et al. 2022). A schematic representation of cancer immunoediting process can be seen in Figure 2.

Elimination. The elimination phase, also known as immunosurveillance, involves both adaptive and innate immune responses aimed at recognition and killing of neoplastic cells (Ponomarev et al. 2019). The most effective anti-tumoral response is carried out by CD8+ cytotoxic T lymphocytes which recognize tumor antigens presented on MHC-I and by NK cells, able to detect cells with low or no expression of MHC-I molecules (Mittal et al. 2014).

If the immune response successfully eliminates all cells undergone malignant transformation, neoplastic growth is prevented.

Equilibrium. The immune system exerts a Darwinian selection on neoplastic clones through the constant action of cytotoxic cells stimulated by INF-γ and IL-12 production (Walsh et al. 2023). As a result, the most immunogenic cells are eliminated while the less immunogenic cells survive, even for long periods of time, in a quiescent state. With time, neoplastic cells accumulate new mutations, increasing tumoral heterogeneity and giving rise to new, highly immune-resistant clones (Kim et al. 2013).

Escape. Neoplastic cells survived during the equilibrium phase progress to an overt neoplastic disease evading immune response either by "hiding" from the immune system or by activating mechanisms that suppress cytotoxic response (Kumar et al. 2018 b). Several neoplastic mechanisms of immune evasion have been recognized:

- **Antigen negative variants selection**. Neoplastic cells express a plethora of antigens, either in the form of abnormal proteins produced from mutated genes (neoantigens) or in the form of excessive expression of normal cellular proteins. These proteins are recognized by innate and adaptive immune cells, particularly cytotoxic T cells and destroyed (Kumar et al. 2018 b). The immune system thus eliminates the most immunogenic clones, selecting the less immunogenic ones which can survive and, ultimately, progress the disease.
- **MHC-I loss or reduced expression**. Neoplastic cells can reduce or lose the expression of MHC-I molecules, thus avoiding aberrant antigen exposure and the consequent immune response. NK cells are, however, able to recognize and kill cells with loss of MHC-I expression (Kumar et al. 2018 b; Dhatchinamoorthy et al. 2021).
- **Immune checkpoints molecules**. Neoplastic cells can promote the expression of molecules and receptors, with immune-modulatory effects. The most known are the Programmed death-1 (PD1) protein and its ligands PDL1 and PDL2 and the cytotoxic T lymphocyte antigen 4 receptor (CTLA4) and its ligands CD80 and CD86, also known as B7 molecules (Han et al. 2020; Van Coillie et al.2020). Neoplastic cells can overexpress PDL1 and PDL2 molecules, which prevent T cells activation by binding to their PD1 surface molecules. Tumor cells can also stimulate CTLA4 expression on T cells: the binding between CTL4 and the B7 molecules prevents the binding between the CTLA4 and the costimulatory molecule CD28, impeding T cell activation (Han et al. 2020; Van Coillie et al. 2020). In the last decades, monoclonal antibodies active against CTLA4 or PD1, and capable of blocking the immune-

suppressive pathways, have been produced with outstanding results in oncologic patients (Kumar et al. 2018 b; Liu et al. 2022).

- **Secretion of immune-suppressive factors**. Neoplastic cells produce several molecules able to suppress the immune response (Kumar et al. 2018 b). Among these mediators, IL-10 and TGF-B are widely recognized as the main immune suppressive intratumoral molecules (Mirlekar 2022).
- **T regulatory cells recruitment**. As already seen, tumor infiltrating T regulatory cells exert an immune suppressive immune response, with various mechanism including CTL4 induction on cytotoxic T cells, production of IL-10 and TGF-β and granzyme-mediated apoptosis induction of cytotoxic and NK cells (Gondek et al. 2005; Walker et al. 2011).
- **Macrophagic infiltration**. MΦs are an extremely plastic and heterogeneous population exerting multiple even contrasting functions (Kumar et al. 2018 b). In an oversimplified way, they can be classified as pro-inflammatory, anti-tumoral M1 macrophages and anti-inflammatory, pro-tumoral M2 macrophages, the latter involved in inflammatory response modulation, angiogenesis, and tissue repair promotion (Yunna et al. 2020). M2 tumor-infiltrating MΦs possess tumor-promoting properties, stimulating angiogenesis, producing immune-suppressive cytokines, and stimulating neoplastic cells proliferation (Allavena et al. 2007).

The study of these mechanisms and the deep understanding of the molecular pathways involved in cancer-related immune suppression has been the key to develop new drugs, mainly in the form of monoclonal antibodies, with outstanding improvements in the oncologic field (Kim and Cho 2021).

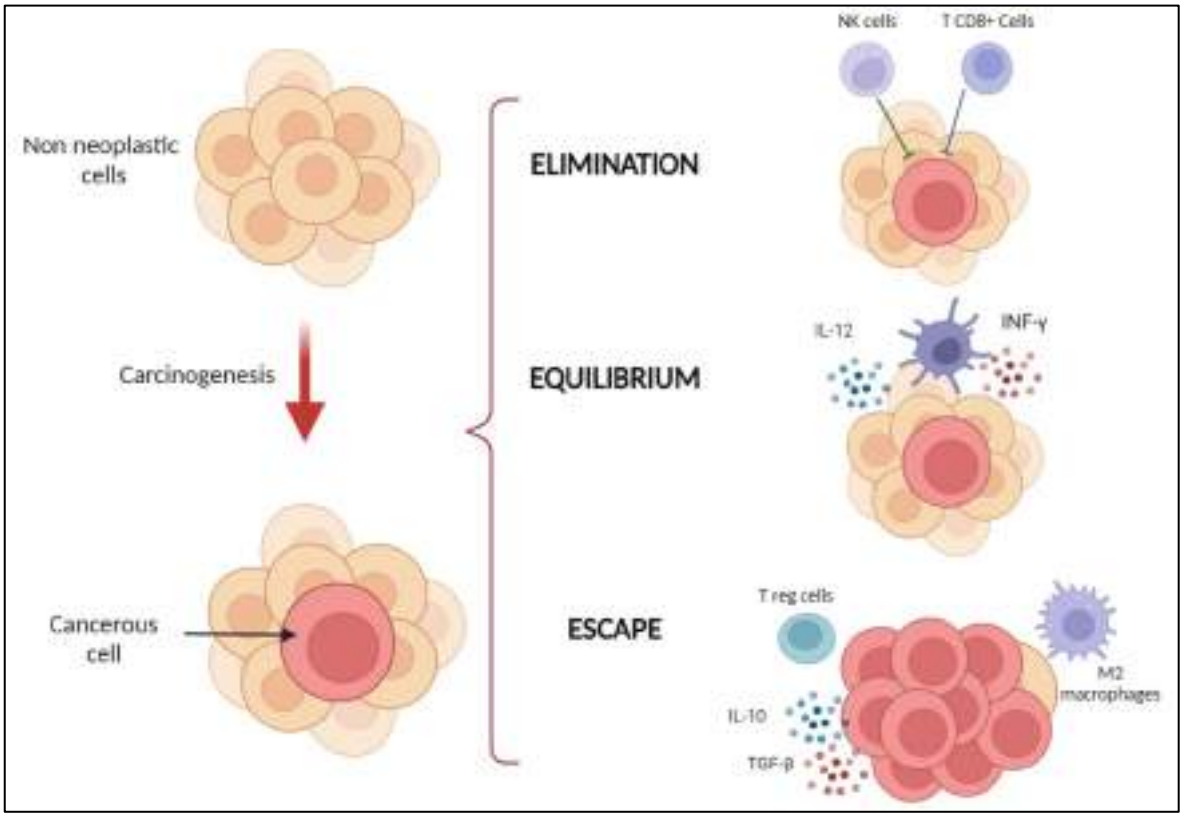

Figure 2. **Cancer immunoediting**. During the elimination phase, immune system cells, mainly CD8+ cytotoxic cells and NK cells remove neoplastic cells, preventing tumor development. Under the selective pressure of immune cells supported by IL-12 and IFN-γ secretion, resistant neoplastic clones can arise. These clones can activate several immune suppressive mechanisms comprising IL-10 and TGF-β secretion or Tregs and M2 oriented macrophages recruitment, supporting their growth and resulting in overt neoplastic disease.

1.5. Of Mice and Men: Immune System Similarities and Discrepancies.

Laboratory animals are widely used in biomedical research with up to 8,624,692 animals and 3,879,691 mice used every year in the European Union (Eu statistics). Among laboratory animals, mice are the most used and the most studied species: they are, in fact, easy to keep in animal enclosures, bred easily guaranteeing many animals in a low amount of time and, since their lifespan is of approximately 3 years, their entire life cycle can be investigated in a relatively short amount of time (Masopust et al. 2017).

Mice share more than 90% of the genome with human beings and it has been demonstrated that the general architecture and functioning of the immune system is preserved in the two species (Waterston et al. 2002; Haley 2003). Mice have been used to successfully investigate the immunopathogenesis of several human infectious diseases and to gain insights on numerous auto-immune and immunologic conditions (Bosma et al. 1983; Morel et al. 2004; Gomes-Solecki et al. 2017; Clever et al. 2023).

Nevertheless, some immune species-specific features have been recognized and must be bear in mind when translating data from the mouse model to humans. As a starting point, neutrophils, and lymphocytes ratio in the two species is different: even if a functional impact of this difference has still to be determined, neutrophils are the predominant population of circulating immune cells in humans, representing up to 70% of blood leukocytes while, in mice, lymphocytes are the predominant cell population, being up to 90% of circulating cells (Doeing et al. 2003). Concerning innate immunity, defensins are present in both species as important antimicrobial peptides, but, while, in humans, neutrophils are a major source of defensins, in mice, defensins are mainly produced by epithelial cells (Risso et al. 2000). Murine classical monocytes lack TLR4, TLR7, TLR8 and TLR10 response (Bjotrnson-Hooper ZB et al. 2022) and IL-15, a trophic cytokine for NK cells and memory T cells is expressed by human granulocytes and monocytes but only by some murine myeloid cells (Sellers et al. 2017). Differences in Arginase and iNOS expression by murine and human macrophages have, also, been demonstrated: even though both enzymes have been detected in human and murine MΦs, it seems that iNOS is less expressed by human MΦs and that, arginase, a murine marker of M2 MΦs, is preferentially expressed in azurophilic granules of human neutrophils (Zschaler et al. 2014; Munder et al 2005).

Differences in macrophage subsets ratio have also been recognized. Gata6+ peritoneal macrophages have been described in both species but while, in mice, they represent the most abundant population of cells, in humans they represent less than 10% of

the macrophages in the peritoneum with the predominant population being of CD206+, Lyve1+ cells (Han et al. 2024). In addition to that, type 2 DCs, present in both species, were more numerous in humans (Han et al 2024). Human and murine macrophages also display metabolic differences upon stimulation: LPS-activated, monocyte-derived macrophages fail, in fact, to undergo metabolic reprogramming towards glycolysis, relying on oxidative phosphorylation for ATP generation while, in murine LPS-activated bone marrow-derived macrophages, there is an increase of glycolysis with decreased oxygen consumption rate (Visajan et al. 2019).

Concerning adaptive immune system, while approximately 100% of murine T cells use CD28 as a costimulatory molecule only 80% of human CD4+ T helper cells and only 50% of human CD8+ cytotoxic cells express CD28. This highlights differences in T lymphocytes activation and potentially explains differences of treatment efficacy when using CD-28 blocking drugs (Lenschow et al. 1996; Mestas et al. 2004). Activated human CD4+ T cells trigger a more rapid and robust TH17 response than mice and highly express TNIP3, a NF-kB pathway inhibitor, which, on the contrary, appears to be non-functional in mice (Sellers et al. 2017). On the other hand, LAG3, an immune checkpoint molecule with inhibitory properties, is upregulated in activated murine T cells but not in human cells (Sellers et al. 2017). Furthermore, once activated, human T cells express MHC-II molecules while activated murine T cells do not. (Barnaba et al. 1994). As an additional difference, mice tend to have a higher percentage of γδ T cells in the intestinal mucosa compared to humans, and, while in both species they produce a notable amount of INF-γ, murine cells produce more IL-17 compared to the human counterpart (Sellers 2017).

Humans and mice also differ in immunoglobulins isotype production. Murine plasma cells produce IgA, IgD, IgE, IgM and 4 subtypes of IgGs (IgG1, IgG2a, IgG2b and IgG3) while human plasma cells express 2 classes of IgAs (IgA1 and IgA2), IgD, IgE, IgM and 4 subtypes of IgG (IgG1, IgG2, IgG3 and IgG4) (Mestas et al. 2004; Snapper 1999). Even though the different subtypes differ in the ability to bind FcRs or to fix the complement system, functional differences between the two species are, generally, considered irrelevant (Mestas et al. 2004).

Immune differences of mice and men are reviewed in detail in Mestas et al. 2004; Bailey et al. 2013; Zschaler et al. 2014; Sellers et al. 2017; Evren et al. 2020). Despite all the aforementioned differences that must be kept in mind, mice remain the most used animal model in biomedical research and provide invaluable data in several medical fields, comprising immunology (Mestas et al. 2004; Masopust et al. 2017).

1.6. Immunohistochemical Markers for Murine Immune Cells Characterization

Immunohistochemical phenotyping of immune system cells serves as a fundamental approach in the field of immunology, enabling the precise identification and characterization of immune cell populations within tissue specimens, preserving both cellular morphology and tissue architecture. Unlike other methods, immunohistochemistry enables the localization of immune cells within examined organs and provides information on cells morphology as well as on their interactions with other cell types, both in physiological conditions and in pathological contexts. To achieve a complete characterization, different antibodies must be applied to identify the vast array of cell types making up the immune system.

Provided below is a brief overview of the antibodies applied in this thesis. Technical details on stain protocols can be found in supplemental Table 1 and in the material and methods sections of each work.

Iba1. The Ionized calcium binding adaptor molecule 1 (Iba1) is a 17-kDa calcium-binding protein with an actin-bundling activity involved in membrane ruffling and phagocytosis in macrophages and microglial cells as well as in calcium and RHO proteins pathway signaling (Oshawa et al. 2004). Although initially described as a microglia specific marker, Iba1 is now considered a pan-macrophagic marker and its expression has been reported in numerous macrophage populations and, more recently, also in cDCs and MoDCs (Kohler et al. 2007; Elizondo et al. 2017; Elizondo et al. 2019).

F4/80. F4/80 is a murine-specific, cell-surface 160-kDa glycoprotein with an epithelial growth factor-like extracellular domain and a seven-transmembrane motif like those observed in G protein-coupled receptors with still not well determined function (Cassado 2017). F4/80 has been found to be expressed in mature macrophages as well as some tissue-resident macrophages such as Langerhans cells and Kupffer cells and is used as a macrophagic marker in murine tissues (Vermaelen et al. 2004).

MARCO. MARCO (Macrophage Receptor with Collagenous structure) is a 210-kDa scavenger class A receptor expressed by some subsets of macrophages and involved in binding and internalization of bacterial components such as LPS as well as in inflammatory response modulation (Kraal et al. 2010). This marker is particularly expressed by splenic marginal zone macrophages, and lymph node macrophages highlighting their specialization in lymph-borne antigens capture (Kraal et al. 2010).

CD206. CD206, also known as macrophage mannose receptor, is a 175-kDa transmembrane glycoprotein that belongs to the C-type lectin family, expressed predominantly by subsets of tissue macrophages, but also by selected lymphatic or liver endothelial cells and mesangial cells (Azad et al. 2014). CD206 binds to a wide range of ligands such as peptide hormones, lysosome enzymes, mannose and fucose glycoproteins, collagen as well as microbial DNA and is involved in endogenous molecule clearance and antigen processing and presentation triggering an anti-inflammatory response (Nielsen et al. 2020). CD206 is, therefore, used as a M2 macrophages marker in murine tissues (Kaku et al. 2014).

Arginase 1. Arginase 1 is a key enzyme of the urea cycle responsible for the hydrolysis of L-arginine to L-ornithine and urea, highly expressed in liver and moderately to minimally expressed in other tissues such as pancreas, stomach, brain and cells of myeloid lineage, including neutrophils and myeloid-derived suppressor cells (MDSCs) (Yang and Ming 2014; Barron et al. 2017; Rodriguez et al 2013). In macrophages, Arginase 1 expression decreases the intra-cytoplasmic L-arginine which, in inflammatory context, serves as substrate for NO production, hence decreasing the pro-inflammatory capacity of these cells, directing their phenotype towards an alternative activation (Yang et al. 2014). As CD206, Arginase 1 is a marker of alternatively activated M2 macrophages.

Ym1 (Chil3). Ym1, also known as chitinase-like protein 3 (Chil3), is a rodent-specific member of the chitinase-like proteins, a class of chitin degrading enzymes with roles in innate immunity against chitin-containing pathogens (Raes et al. 2002). Ym1 is produced by neutrophils and macrophages and is considered a marker of alternatively activated M2 macrophages in murine tissues (Kang et al. 2022). Ym1 is constitutively expressed by some tissue-resident macrophages such as alveolar or splenic macrophages, although its specific functions remain poorly understood (Kang et al. 2022).

iNOS. Three forms of nitric oxide synthase (NOS) exist in tissues: the endothelial (eNOS) the neuronal (nNOS) and the inducible (iNOS) isoforms. While eNOS and nNOS are constitutively expressed by tissues, where they are involved in vessel caliber regulation and neurotransmission, iNOS is not normally present in physiological conditions and is induced by pro-inflammatory cytokines and or bacterial components (Sharma et al. 2007; Cinelli et al. 2019). iNOS converts L-arginine to L-citrulline with concomitant production of nitric oxide, essential for pathogen clearance and is, therefore, considered a marker of classically activated M1 macrophages (Xue et al. 2018).

HO-1. Heme oxygenase-1 is a 32-kDa inducible enzyme, part of the heat shock protein family, that converts heme groups into biliverdin, carbon monoxide and iron (Vijayan et al. 2018). This enzyme is induced in several conditions such as hypoxia and oxidative stress and has antioxidant and anti-inflammatory properties. It has been demonstrated that macrophage exposure to heme can lead to an anti-inflammatory M2 phenotype and HO-1 is, therefore, considered a marker of alternatively activated macrophages in murine tissues (Vijayan et al. 2018).

MHC-II. MHC-II molecules are heterodimers composed of an α and β chain, normally expressed by professional antigen presenting cells such as dendritic cells and macrophages where it is involved in the activation of the innate immune response (Duffy et al. 2017). After phagocytosis and processing of extracellular proteins, cells expose target peptides onto MHC-II molecules for T helper cells recognition (Duffy et al. 2017). It has been demonstrated that M1 macrophages are characterized by high levels of MHC-II while low levels of MHC-II favor a M2 response (Baumgart et al. 1998). MHC-II expression has also been recognized in a plethora of cells comprising thymic, intestinal, biliary, and bronchial epithelial cells and even tumoral cells (Schrumpf et al. 2015; Wosen et al. 2018; Axelrod et al. 2019).

CD3ε. The CD3ε peptide, together with the CD3γ, δ, and ζ subunits and with the α/β or γ/δ heterodimers, form the T cell receptor complex, involved in the recognition of antigens bound to MHC molecules (Mariuzza et al. 2019). Since the TCR is expressed on T cells membranes, this marker is used for the detection of these cells in murine tissues.

B220. B220, also known as CD45, is a 220-kDa transmembrane protein expressed on the surface of B cells and involved in B cells maturation as well as in signal transduction initiation upon B cell receptor engagement by antigens. In murine tissues B220/CD45 is a pan B cells marker (Bleesing et al. 2003).

CD4 and CD8. CD4 is a 55-kDa co-receptor molecule expressed on the surface of T helper lymphocytes, composed of 4 immunoglobulins-like domains. CD4 stabilizes the binding between TCR and the peptide-MHC-II complex and activates T helper cells, inducing various cytokines sets secretion (Miceli et al. 1991). CD8 is a co-receptor molecule expressed predominantly on cytotoxic T lymphocytes, composed of an α and β chains linked by a disulfide bond. By interacting with antigens bound to MHC-I, CD8 stabilizes the binding between TCR and the peptide-MHC I complex, prompting T cell activation and

target cell lysis (Miceli et al. 1991). CD4 and CD8 are, therefore, utilized as markers for T helper cells and T cytotoxic cells detection respectively.

FoxP3. FoxP3, is a transcription factor composed of a forkhead domain, responsible for DNA binding, a leucine zipper like domain and a zinc finger motif with unknown function that plays a key role in the development and maturation of Tregs (Mercer et al. 2009). The nuclear expression of Foxp3 is a marker of T regulatory cells in murine specimens.

Ly6G. LY6G, also known as lymphocyte antigen 6 complex, locus G, is a protein that is primarily expressed on the surface of mature neutrophils. This marker is particularly useful in distinguishing neutrophils form other leukocytes in murine tissues.

2. AIM OF THE THESIS

This PhD research project aimed to investigate immune system functions in healthy and pathologic experimental murine models, through immunohistochemical characterization of immune cell populations in healthy steady state, inflammatory and neoplastic settings.

The following fields were investigated:

Study I – Mononuclear phagocyte system cells in murine healthy organs and selected pathological conditions.

Study II – Sex-dependent modulation of inflammation in a murine caerulein-induced acute pancreatitis model.

Study III – Comparison between two methods of digital image analysis (hot-spot fields vs whole-slide) for the assessment of immune cell infiltrations in a murine caerulein-induced acute pancreatitis model.

Study IV – Tumor immune system interaction in a murine model of orthotopic pleural mesothelioma.

3. STUDY I. IMMUNOHISTOCHEMICAL CHARACTERIZATION OF CELLS OF THE MONONUCLEAR PHAGOCYTE SYSTEM IN THE MOUSE

3.1. Introduction

An introduction to murine MPS cells origin, function and classification can be found in the thesis introduction, chapter 1.1.2.2.

MPS cells identification and characterization represent a significant challenge in the biomedical research due to the significant phenotypic and functional overlapping among cells (Guilliams et van de Laar, 2015). This is further complicated by cellular plasticity, since MPS cells can often rapidly transform into one another, but is of critical importance to shed light on physiological functions and diseases' pathogenesis (Guilliams et van de Laar, 2015). Among the plethora of available useful techniques, including next generation sequencing, transcriptomics, proteomics and flow cytometry, valuable data can be obtained through immunohistochemistry which allows identification of MPS cells in the morphological and spatial context of the tissue, providing information not only on cells themselves but also on interactions with other cells, hence on their functions (Hume et al. 1983; Chow et al. 2011; Nakagawa et al. 2017; Nordlohne et al. 2021).

Although numerous studies investigated MPS cells through immunohistochemistry in the mouse, reports are often limited in organs evaluated and antibodies used and often investigate only pathological conditions or mice with specific mutations or under specific experimental conditions (Hume et al. 1983; Hume et al. 1984; Perry et al 1985; Zhu et al. 2017; Le et al. 2021). The aim of this study was, therefore, to phenotypically characterize MPS cells in healthy murine tissues through the application of a wide panel of macrophagic immunohistochemical markers. Furthermore, the panel of antibodies was applied to a subset of representative pathological conditions, to assess its effectiveness in detecting variations of MPS cells between healthy and pathological conditions and to investigate its applicability to pathological samples. By doing so, we sought to provide thorough information on MPS cells distribution in tissues.

3.2. Materials and Methods

For the investigation, formalin-fixed paraffin embedded (FFPE) samples were retrieved from the archives of the Mouse &Animal Pathology Laboratory (MAPLab).

Healthy tissues

For healthy tissues, FFPE samples from 9 C57BL/6N male mice and 7 C57BL/6N female mice ranging from 4.5 to 12 months and from 2 C57BL/6J male mice and 3 C57BL6/J female mice of 4 months were selected. Only control, not manipulated animals without spontaneous background lesions were included in the study. Sections from liver, gallbladder, spleen, kidney, adrenal glands, lymph nodes, pancreas, testes, lungs, heart, and thymus were evaluated as reported in Table 1.

Selected pathological conditions

For pathological conditions, FFPE samples from a total of 4 mice were selected, including the liver of a 9-month-old, female Crl:CD1-*Foxn1*^{nu} *nude* mouse with a spontaneous necro-suppurative hepatitis, the lungs of a CD40L$^{-/-}$ C57BL/6 mouse experimentally infected with *Pneumocystis murina*, a SCID mouse with human synovial sarcoma xenograft transplant and a tdTomato$^{+/+}$ C57BL/6 mouse with murine fibrosarcoma syngeneic transplant. Organs and tissues evaluated are listed in Table 2.

Serial sections for each healthy or pathological case were cut at 4 µm and processed for immunohistochemistry directed towards Iba1, F4/80, MARCO, CD206, Arginase 1, Ym1, iNOS, HO1 and MHC-II. For all markers adequate positive controls (murine lymphoid organs) and negative controls (omission of primary antibody) were included. Immunohistochemical protocols and a list of the positive controls implemented in the study are summarized in supplemental Table 1.

Table 1. List of organs of healthy C57BL/6 mice examined per sex and age.

	Total Number	4 mo		4.5 mo		6 mo		9 mo		12 mo	
		M (2)	F (3)	M (2)	F (0)	M (3)	F (3)	M (1)	F (1)	M (3)	F (3)
LIVER	16	\	\	2	\	3	3	1	1	3	3
GALLBLADDER	13	\	\	2	\	\	3	1	1	3	3
SPLEEN	16	\	\	2	\	3	3	1	1	3	3
KIDNEY	16	\	\	2	\	3	3	1	1	3	3
PANCREAS	8	2	3	\	\	1	1	\	\	1	\
TESTIS	3	\	n/a	\	\	3	n/a	\	n/a	\	n/a
ADRENAL	5	\	\	\	\	\	\	\	\	2	3
LYMPH NODES	3	3	\	\	\	\	\	\	\	1	2
LUNG	7	2	3	2	\	\	\	\	\	\	\
HEART	5	2	3	\	\	\	\	\	\	\	\
THYMUS	5	2	3	\	\	\	\	\	\	\	\

Table 2. List of pathologic samples included in the study

Strain	**Age**	**Sex**	**Pathological condition**	**Organ/Tissue evaluated**
Crl:CD1-*Foxn1nu*	9 mo	F	Necrosuppurative Hepatitis of undetermined etiology	Liver
CD40L$^{-/-}$ C57BL/6	9-12 mo	F	Experimental *Pneumocystis murina* infection	Lung
SCID	\	\	Human Synovial Sarcoma (Xenograft Transplant)	Skeletal muscle (quadriceps)
TdTomato$^{+/+}$ C57BL/6	\	\	Murine Fibrosarcoma (Syngeneic Transplant)	Skeletal muscle (quadriceps)

For all markers, except for F4/80, 4 μm sections underwent deparaffinization and heat induced epitope retrieval (HIER) in a water bath for 40 min at 100°C (Dewax and HIER Buffer H, Thermo Scientific Lab Vision, cat. No. TA-999-DHBH). For F4/80 staining, slides were deparaffinized and hydrated through serial passages in alcohol, rinsed in PBS and unmasked with 1% trypsin for 30 minutes at 37°. All slides were then rinsed in PBS and placed in an autostainer (Lab Vision® Autostainer 480S-2D Thermo Fischer scientific) after application of PAP pen (Liquid Daido Sangyo Co. Ltd.). In the autostainer, endogenous peroxidase activity was blocked by incubating sections with 3% H_2O_2 for 10 minutes. Slides were rinsed, incubated with PBS containing 10% normal goat serum (IBA1, MARCO, CD206, Ym1, iNOS, HO-1) or 10% normal rabbit serum (F4/80, Arginase 1, MHC-II) for 30 min at room temperature to prevent nonspecific background staining and subsequently incubated for 1 hour at room temperature with primary antibodies (Table 3). Sections were rinsed in PBS and incubated with a biotinylated secondary antibody (goat anti-rabbit, Vector Laboratories, USA, cat. No. BA-1000 for IBA1, MARCO, CD206, Ym1, iNOS, HO1; rabbit anti-rat Vector Laboratories, USA, cat. No. BA-4001 for F4/80 and MHC-II; rabbit anti-goat Vector Laboratories, USA, cat. No. BA-5000 for Arginase 1) and labelled through avidin-biotin-peroxidase procedure (VECTASTAIN® Elite ABC-Peroxidase Kit Standard, Vector Laboratories, USA, cat. No.PK-6100). The immunoreaction was visualized with 3,3'-diaminobenzidine substrate (DAB, Peroxidase DAB Substrate Kit, Vector Laboratories, USA, cat. No. SK-4105). Sections were counterstained with Mayer's hematoxylin, dehydrated in a graded alcohol series and coverslipped with resinous mounting medium.

All slides were digitalized at 40x high resolution (0.23 μm x pixel) through the NanoZoomer-XR Digital slide scanner (Hamamatsu, C12000) at the Unitech Nolimits facility (UNIMI, Milan). Digital slides were visualized using the NDP.view2 Viewing software (Hamamatsu, U12388-01).

3.3. Evaluation of markers expression in normal and pathological mouse tissues

For each tissue, the number and shape of IHC-positive cells to each marker were evaluated under a light microscope. The number of positive cells was semi-quantitatively scored according to the following criteria: \ (absence of positive cells), + (rare positive cells), ++ (moderate number of positive cells), +++ (numerous positive cells), ++++ (myriads of positive cells). According to their shape, cells were classified as round (no dendritic processes), spindle (narrow, elongated cells), stellate (cells with two or more dendritic

processes) or polymorphic (round, spindle, and stellate without a predominant cellular morphology).

For each cell population, two parameters were additionally evaluated: staining intensity and staining pattern. Staining intensity was evaluated through a semi-quantitative scoring system as + (weak staining intensity), ++ (moderate staining intensity), and +++ (strong staining intensity). The staining pattern was described as either nuclear, cytoplasmic and/or membranous.

When cells with different shapes were present in the same anatomical location or when cells with the same shape but different staining intensity with the same antibody were present in the same location, they were considered as distinct populations. In the former case, the amount of cells of a particular subpopulation was expressed in percentage, i.e. % of positive cells to a specific marker with that particular shape on the total positive cells to that marker in the tissue.

3.4. Results and Discussion

Raw data of the semiquantitative evaluation are reported in supplemental Tables 2 to 19.

3.4.1. Healthy organs

Liver. Four main mononuclear phagocyte populations are described in the liver, namely capsular macrophages (CMφs) in the hepatic capsule, resident Kupffer cells in sinusoids, a minor subset of pDCs in the hepatic parenchyma and monocyte-derived macrophages (MoMφs), monocyte-derived DCs (MoDCs) and conventional dendritic cells (cDCs) mainly populating portal spaces (Kulle et al. 2022; Lau et al. 2003; Rahman et al. 2013; Bleriot et al. 2019). A few Iba1+ and F4/80+ spindle cells were detected within the capsule and identified as CMφs. Although MHC-II expression has been reported in CMφs, we did not observe any MHC-II positive signal in our samples (Bleriot et al 2019). We identified numerous intra-sinusoidal stellate Iba1+, F4/80+, MARCO+, rarely HO-1+ and MHC-II+ cells consistent with Kupffer cells (Figure 1, A-D). MARCO+ Kupffer cells were present in periportal and midzonal and only rarely in centrilobular areas and have in fact been correlated to host defense against bacterial infections and to tolerogenic and anti-inflammatory functions, particularly in periportal regions (Devey et al 2009, Björkström NK 2022 Paris and Henderson 2022). Rare round Iba1+, F4/80+, MARCO+, Ym1+ and HO-1+ macrophages were found within portal and centrilobular vessels lumen and classified as circulatory monocytes (Figure 1, D-E). In portal spaces, moderate numbers of Iba1+,

F4/80+, MHC-II+, rarely MARCO+ stellate cells were classified as either MoMφs, MoDCs or cDCs (English et al. 2022).

Gallbladder. Limited data regarding MPS cell populations of the gallbladder are available, with most reports focusing on inflammatory, degenerative, or neoplastic conditions and no classification of MPS cells in the normal organ has been proposed so far (Hadson and Hopwood, 1986; Guarino et al. 2008; Li et al. 2023). A moderate number of predominantly stellate Iba1+, F4/80+ cells in the lamina propria and rare to moderate Iba1+, F4/80+ and CD206+ spindle cells in the muscular layer were identified (Figure 2, A-C). Rare stellate MHC-II+ cells in the lamina propria were also present. These cells could either be a population of resident macrophages or represent MoMΦs or MoDCs/cDCs recapitulating the subsets observed in the intra-hepatic biliary tree. While CD206 is considered a marker of alternatively activated M2 macrophages, possibly involved in gallbladder homeostasis, it can also be expressed by DCs, thus complicating classification attempts (Taylor et al. 2005; Mondanelli et al. 2017). Occasionally, Iba1+, F4/80+, MHC-II- cells exhibited intra-epithelial cytoplasmic processes. F4/80+ cells with intra-epithelial processes have been previously described in the gallbladder but, although morphologically reminiscent of DCs, it was not possible to unequivocally define their origin (Hume et al. 1984).

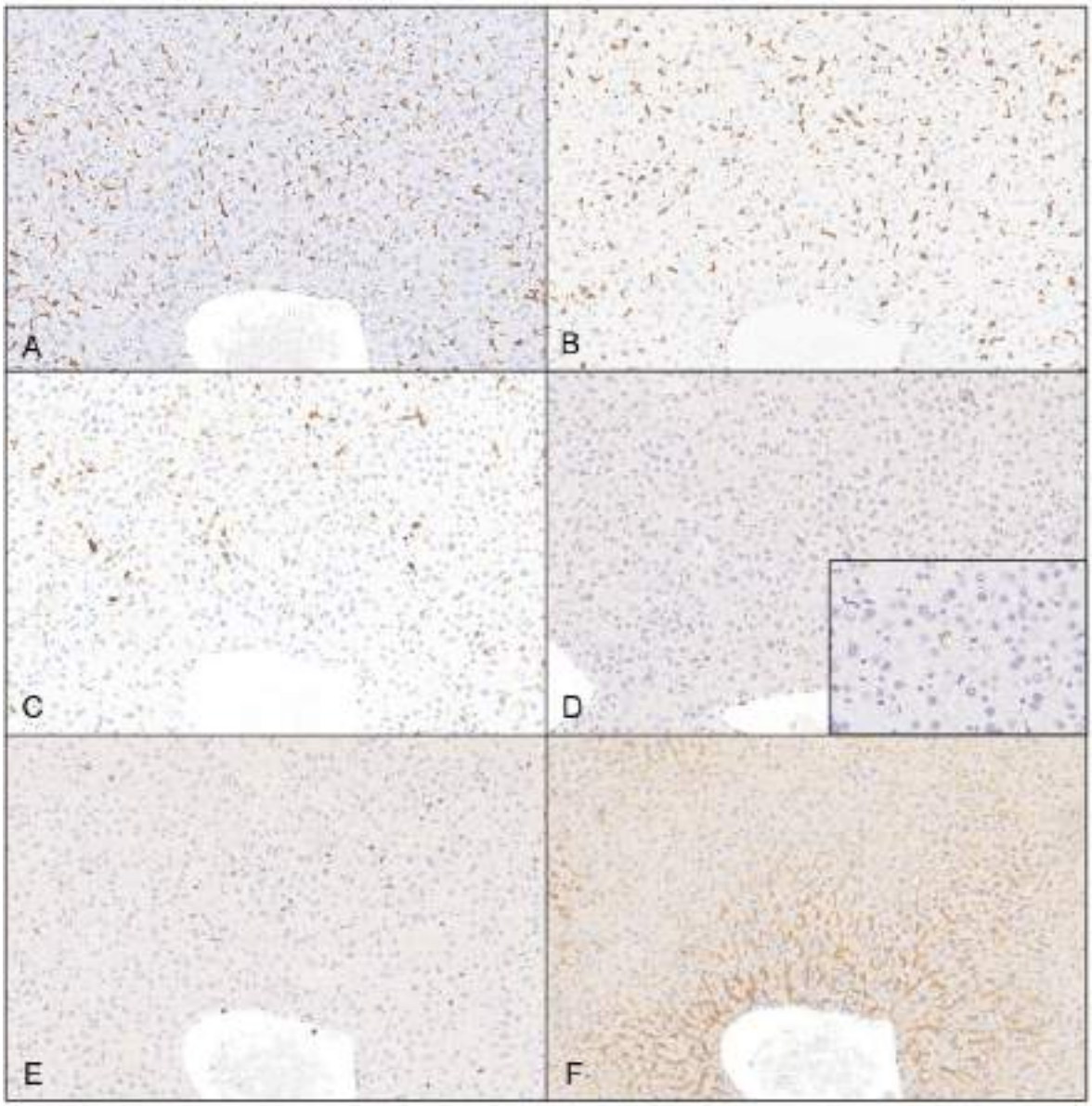

Figure 1. **Liver A**. Immunohistochemistry for F4/80, 20x **B**. Immunohistochemistry for Iba1, 20x. Numerous stellate Iba1+, F4/80+ Kupffer cells were identified along sinusoids of all regions of the hepatic lobule. **C**. Immunohistochemistry for MARCO, 20x. A moderate number of stellate MARCO+ Kupffer cells were stained with rare to absent positivity in the centrilobular region. **D.** Immunohistochemistry for HO-1, 20x. Rare stellate HO-1+ Kupffer cells are found in the sinusoids. Note the round positive monocyte on the endothelium of the centrilobular vein. **Inset,** 80x: A stellate HO1+ Kupffer cell is visible in a sinusoid. **E.** Immunohistochemistry for Ym1, 20x. Round Ym1+ cells interpreted as circulatory monocytes/ myeloid cells were observed in sinusoids. **F**. Immunohistochemistry for CD206, 20x. No positive cells were identified in sinusoids and centrilobular veins. Note the CD206+ endothelial cells of sinusoids surrounding centrilobular vein.

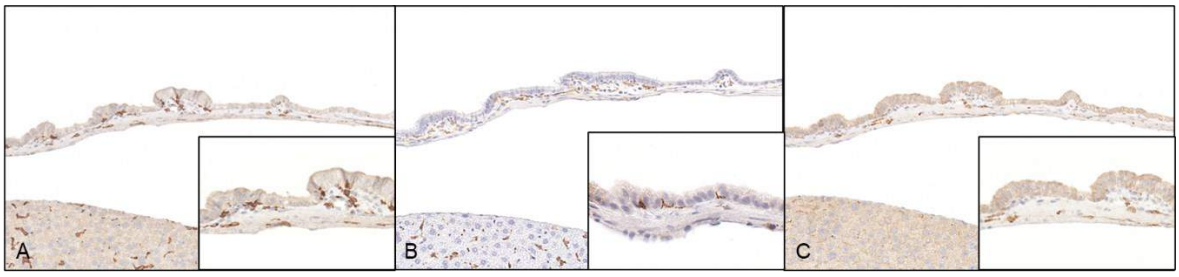

Figure 2. **Gallbladder**. **A**. Immunohistochemistry for Iba1, 20x. **Inset:** 80x **B**. Immunohistochemistry for F480, 20x. **Inset:** 80x **C**. Immunohistochemistry for CD206, 20x. **Inset:** 80x A moderate number of stellate to spindle and occasional round Iba1+, F4/80+ and CD206+ cells were identified in the gallbladder lamina propria and muscular layer. Note the presence of cytoplasmic F4/80+ processes, extending in the gallbladder epithelium in the B inset.

Spleen. The splenic parenchyma, composed of red and white pulp separated by a marginal sinus, hosts different subsets of mononuclear phagocytes namely red pulp macrophages (RPMφs) in the red pulp and white pulp macrophages (WPMφs) in the white pulp comprising marginal metallophilic macrophages (MMMφs) and marginal zone macrophages (MZMφs) located in the inner and outer regions of the marginal zones respectively, tingible body macrophages (TBMφs) and follicular dendritic cells (FDCs) in lymphoid germinal centers, as well as a plethora of MoDCs/ cDCs/ pDCs, particularly located in the T zone and marginal sinus areas (Hey et al. 2012; Fujiyama et al. 2019; McIlroy 2001; Cesta et al. 2006; Sathe et al. 2008). Numerous Iba1+, F4/80+ and HO-1+, moderate numbers of MHC-II+ and rare MARCO+, CD206+, Ym1+ polymorphic cells and Arginase 1+ round cells, were identified in the red pulp (Figure 3, A-D). Although MHC-II and HO-1 could also be expressed by DCs in the red pulp, most of these cells most-likely represent RPMφs involved in hemocatheresis (Fukaya et al.2012; Kurotaki et al. 2015). Apart from rare Ym1+ polymorphic cells consistent with tissue resident Mφs, Ym1 staining detected numerous small round cells interpreted as immature myeloid cells in the context of physiological extramedullary myelopoiesis (Nio et al. 2004; Kang et al. 2022). Concerning the white pulp, 4 main MPS cell subsets were identified. In the germinal centers of lymphoid follicles, stellate Iba1+, MHC-II+, HO1+ cells were classified as FDCs, while round Iba1+, MHC-II+, occasionally HO1+ cells with intra-cytoplasmic apoptotic bodies as TBMΦs (Figure 3,

E-F). Notably, TBMΦs were marked only with Iba1 and MHC-II and occasionally by HO1. It has been in fact recognized that TBMφs are devoid of most MPS surface markers including F4/80 (Leluoard et al 2010, Bonnardel et al. 2015). In the marginal zone (MZ), Iba1+, MARCO- cells in the inner MZ and Iba1+, MARCO+ in the peripheral MZ were identified as MMMΦs and MZMΦs, respectively. Since there is not a clear demarcation between the outer and inner regions of the marginal zone in murine spleens, MARCO positivity allowed for the definitive identification of MZMΦs, as this scavenger receptor is specifically expressed by this macrophagic subset specialized in blood-borne particles capture (Figure 3, C)(Cesta 2006; Borges da Silva 2015). A moderate number of MHC-II+ cells was additionally detected in the marginal zone. Since MZMΦs and MMMΦs are reportedly MHC-II-, these cells most likely represent either MoDCs or cDCs (McGaha et al. 2011; Eloranta et al. 2019). Interestingly, although F4/80 is considered a pan macrophagic marker and low F4/80 expression in MMMΦs and MZMΦs by flow cytometry has been reported in literature, no to rare F4/80+ cells were identified in splenic marginal zones in our samples (Figure 3, B) (Fujiyama et al 2019; Borges da Silva 2015). Lastly, numerous Iba1+, HO-1+ and rare F4/80+ round to stellate cells were identified in PALS and follicular mantle zone and classified as either WPMΦs/ MoMΦs, while Iba1+ and MHC-II+ cells as MoDCs /cDCs or pDCs (Cesta, 2006; Hey et al. 2012).

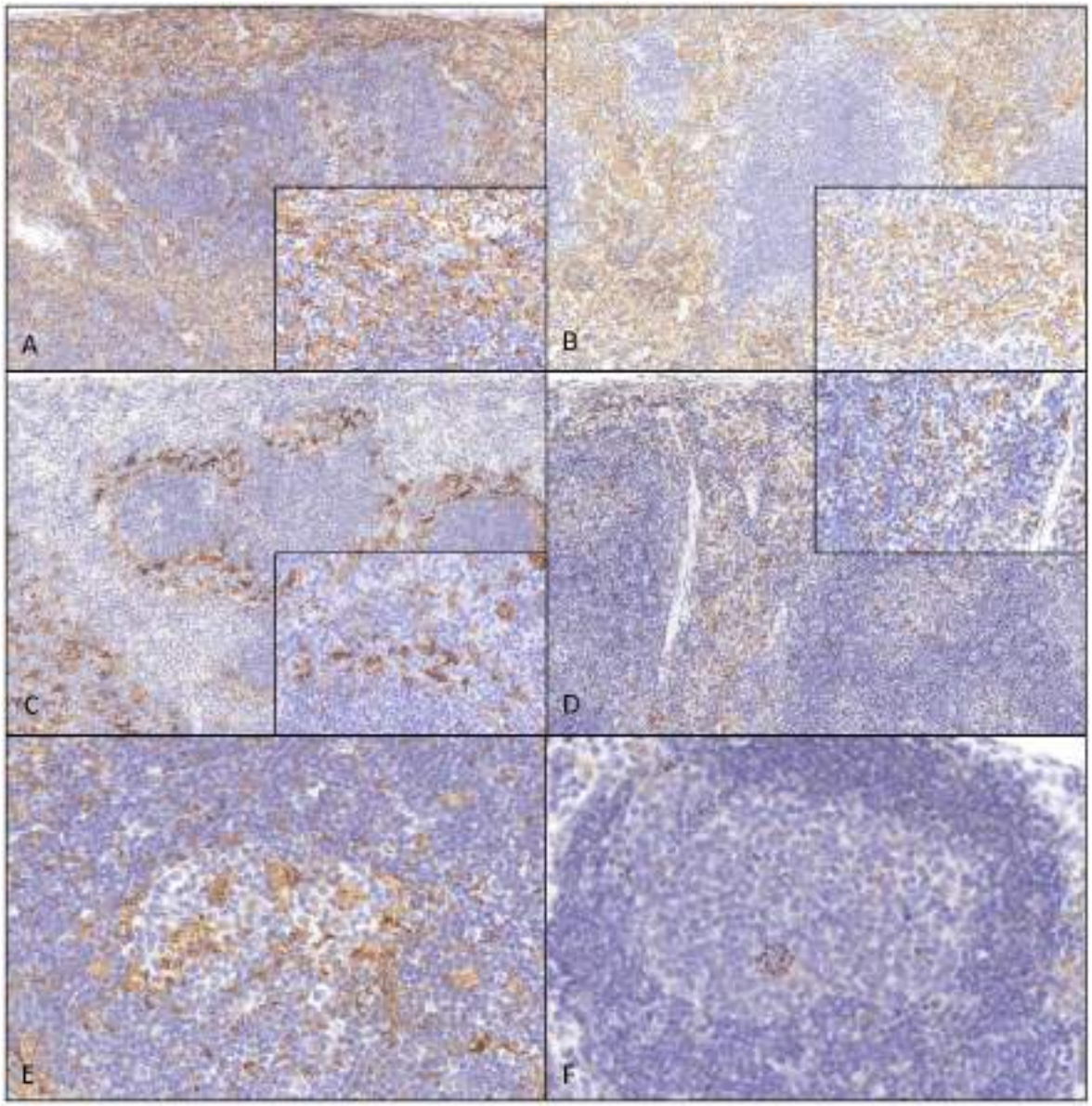

Figure 3. Spleen. A. Immunohistochemistry for Iba1, 20x. Numerous polymorphic Iba1+ RPMφs/DCs in the red pulp and numerous WPMφs comprising MoMφs/DCs in PALS, MMMφs and MZMφs in the white pulp marginal zone and numerous TBMs and FDCs in lymphoid follicles germinal centers were identified. **Inset**, 80x: Note the polymorphic shape of red pulp and marginal zone Iba1+ cells. **B.** Immunohistochemistry for F480, 20x. Numerous polymorphic F4/80+ RPMφs are visible in the red pulp. Only a few F4/80+ WPMφs could be appreciated in splenic PALS and lymphoid tissue. **Inset**, 80x**:** note the polymorphic morphology of F4/80+ RPMφs. **C.** Immunohistochemistry for MARCO, 20x. Numerous stellate MZMφs in the marginal zone outer layer are visible. **Inset**, 80x: MARCO+ MZMφs have a stellate morphology. **D.** Immunohistochemistry for HO-1, 20x Numerous polymorphic RPMφs in splenic red pulp, rare HO-1+ MoMφs in the marginal zone and a few to moderate round HO-1+ TBMφs and stellate FDCs in follicles germinal centers are visible. **Inset**, 80x: HO1+ RPMφs have a polymorphic morphology. **E.**

Immunohistochemistry for Iba1**,** 40x. Numerous stellate Iba1+ FDCs and round TBMφs can be appreciated in germinal centers, together with a moderate number of stellate Iba1+ cells in the mantle zone **F.** Immunohistochemistry for MHC-II, 40x. A round MHC-II+ TBMφ engulfing apoptotic debris is visible in a follicle germinal center. Note the weak positivity of stellate cells in the germinal center, interpreted as FDCs and in the mantle zone.

Lymph Node. Lymph nodes have a complex anatomical architecture, with different functional domains populated by several well-known subsets of mononuclear phagocytes specialized in lymph-borne antigen uptake and processing (Gray et al. 2012). Major populations are subcapsular sinus macrophages (SSMΦs) and medullary sinus macrophages (MSMΦs) in cortical and medullary sinuses respectively, medullary cord macrophages (MCMΦs) along medullary cords, interfollicular T zone macrophages (TZMΦs) a recently discovered resident population of macrophages involved in apoptotic debris clearance, DCs populating the paracortex and TBMΦs and FDCs in lymphoid germinal centers (Gray et al. 2012; Baratin et al 2017; Bellomo et al. 2018). The applied panel of antibodies allowed a clear distinction between cells populating the subcapsular and medullary sinuses and cells populating cortical and paracortical regions and medullary cords (Figure 4, A-F and Figure 5, A-D). In the sinuses we detected numerous round Iba1+, MARCO+, CD206+ and HO-1+ cells which were classified as either F4/80- subcapsular sinus macrophages (SSMΦ) or F4/80+ medullary sinus macrophages (MSMΦ) depending on the anatomical location (Figure 4, A-D; Figure 5, A, B, D). In the cortex, round Iba1+, MHC-II+ cells morphologically consistent with TBMΦ and stellate Iba1+, MHC-II+ cells consistent with FDCs were detected in reactive germinal centers, while in the mantle and marginal zones moderate number of stellate Iba1+ and rare MHC-II+ cells were detected and classified as MoDCs or cDCs, based on F4/80 negativity. In the paracortex, numerous Iba1+, MHC-II+ cells were classified as DCs or TZMΦ (Figure 4, A; Figure 5, B, C). (Baratin et al 2017; Bellomo et al. 2018). A moderate number of round Arginase 1+ cells were also detected in the paracortex together with a moderate number of round Ym1+ round cells mainly located at the cortico-medullary junction (Figure 4, E-F). Arginase 1 expression has been recognized in M2 macrophages as well as innate myeloid derived suppressors cells (MDSCs), but since MDSCs are not present in healthy murine lymph nodes, the stained cells most likely represent a population of M2 oriented Mφs, possibly involved in adaptive immune response regulation (Bronte et al. 2003; Mills et al. 2000; Gabrilovich et al. 2009; Tumino et al. 2023). We were, instead, unable to retrieve information about Ym1+ Mφs in lymph nodes; Ym1 has

been recognized as a marker of alternatively activated Mφs in the mouse, but, to the authors' knowledge, no report of a cortico-medullary localization exists in literature (Kang et al. 2022). In the medulla, numerous round to stellate Iba1+ and rarely MHC-II+ cells were detected along the medullary cords and classified accordingly as MCMΦ (Figure 4, A inset; Figure 5, C) (Bellomo et al. 2018). Notably, although TZMΦ and MCMΦ are reportedly F4/80+, we did not detect any F4/80+ cells in interfollicular T zones or along medullary cords in our samples (Figure 5, A) (Bellomo et al. 2018; Grey et al 2012).

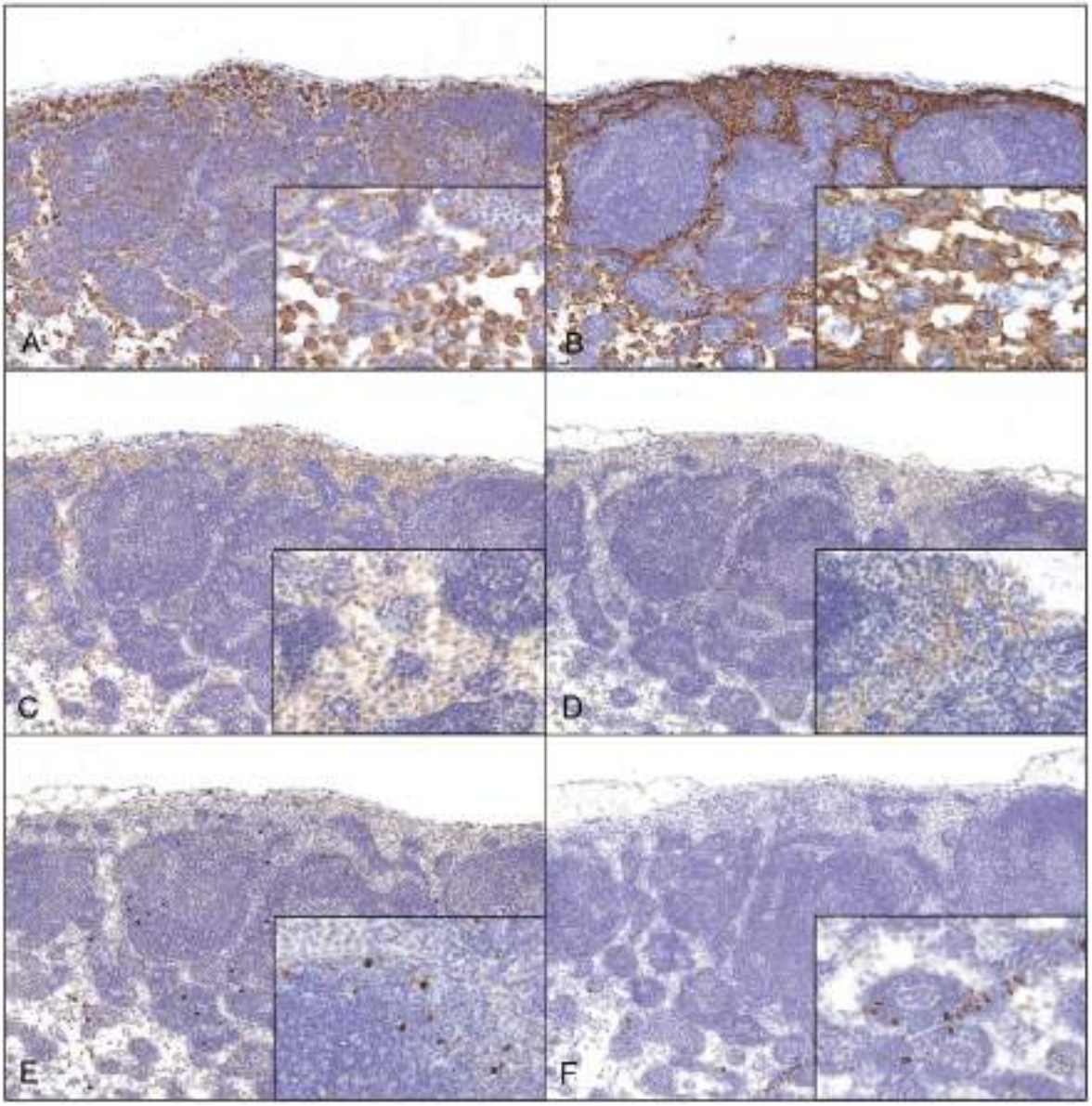

Figure 4. **Lymph node A**. Immunohistochemistry for Iba1, 20x. Numerous round Iba1+ SCSMΦs and MSMΦs were identified in the subcapsular and medullary sinuses respectively. Numerous stellate Iba1+ MoMΦs and TZMΦs in the paracortex and a moderate number of stellate Iba1+ MoMΦs/ DCs in the cortical tissue and of MCMΦs along medullary cords were detected. **Inset**, 80x: note the round morphology of Iba1+ MSMΦs and the stellate morphology of Iba1+ MCMΦs **B**. Immunohistochemistry for MARCO, 20x. **C**. Immunohistochemistry for CD206, 20x. **D** Immunohistochemistry for HO-1, 20x. **Insets**, 80x. Numerous round MARCO+, CD206+ and HO-1+ SCSMΦs and MSMΦs were stained, the latter cells more numerous with MARCO. No positive cells were observed in the cortical region and along medullary cords for all markers, except for rare, positive, round HO-1+ MoMΦs. At high magnification these cells have a round morphology **E.** Immunohistochemistry for Arginase 1, 20x. Rare Arginase 1+ round cells interpreted as M2 oriented MoMΦs were observed in the paracortical region as well as in the marginal and mantle zones. **Inset**, 80x: note the round morphology of arginase 1+ cells **F.** Immunohistochemistry for Ym1, 20x. A moderate number of round Ym1+ positive cells were detected along the cortico-medullary region, possibly representing M2 oriented MoMΦs. **Inset**, 80x: note the round morphology of Ym1+ cells at the cortico-medullary junction.

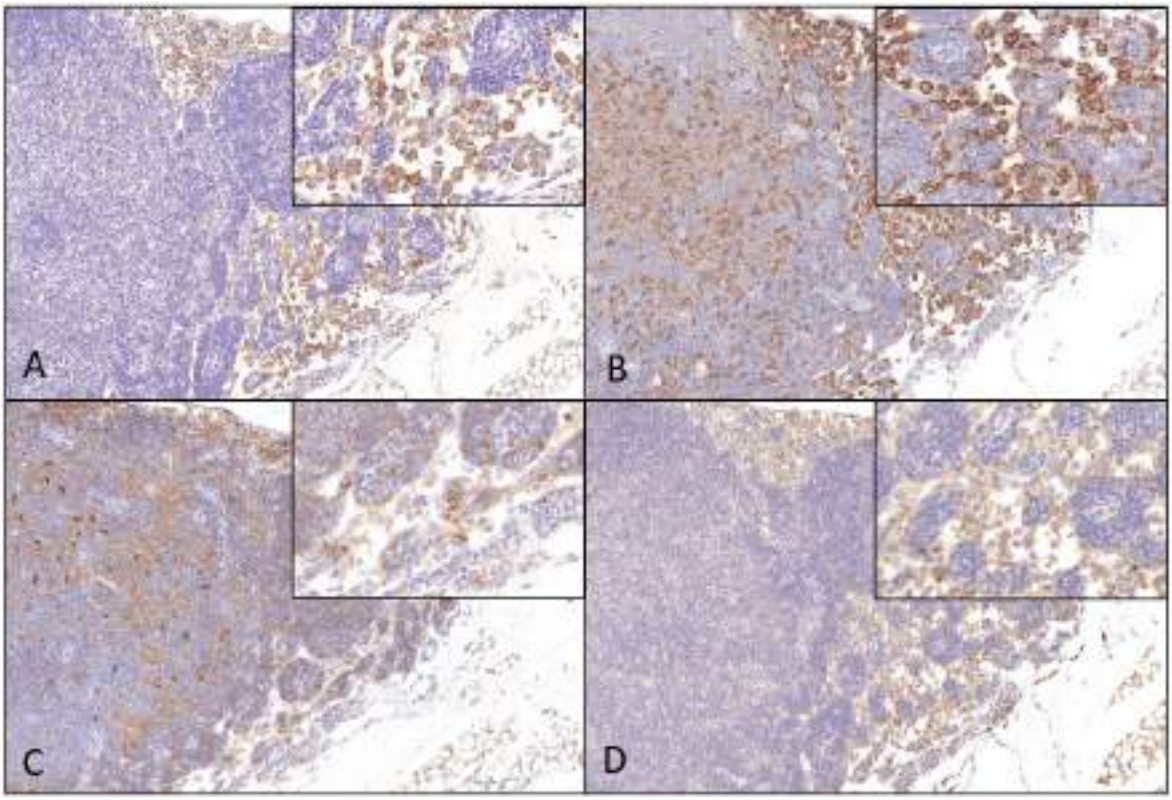

Figure 5. Lymph node. A. Immunohistochemistry for F4/80, 20x. Numerous round F4/80+ MSMΦs were stained. No positive cells are visible in the paracortical region and along the medullary cords. **Inset,** 80x: F4/80+ MSMΦs have a round morphology **B**. Immunohistochemistry for Iba1, 20x. Numerous round Iba1+ MSMΦ as well as numerous stellate Iba1+ TZMΦ /MoMΦs/ DCs in the paracortex and MCMΦs along medullary cords are visible. **Inset**, 80x: note the round morphology of Iba1+ MSMΦs **C**. Immunohistochemistry for MHC-II, 20x. Rare to moderate number of round MHC-II+ MSMΦ and moderate to numerous stellate MoMΦs /TZMΦ / DCs in the paracortex and MCMΦs along the medullary cords were identified. **Inset**, 80x: a moderate number of round MHC-II+ along medullary cords and rare round MHC-II+ MSMΦ**s** are visible**. D**. Immunohistochemistry for CD206, 20x. Numerous round CD206+ MSMΦs were stained. No to rare CD206+ cells were observed in the paracortical region, while no CD206+ cells were observed along medullary cords. **Inset**, 80x: round CD206+ MSMΦs are visible in medullary sinuses.

Thymus. Despite their importance in organ homeostasis, thymic mononuclear phagocytes have seldom been investigated, with existing reports mainly relying on flow-cytometry and transcriptomic data (Zhou et al. 2022; Guerri et al. 2013; Wood 1985; Wang et al 2022). In the cortex, we identified a moderate number of Iba1+ and HO-1+ stellate cells, with occasional expression of F4/80 and Ym1 (Figure 6, A, E, F). The lack of MHC-II expression suggests that these cells are most likely M2-oriented macrophages possibly involved in organ homeostasis and apoptotic debris clearance, hence classified as thymus resident macrophages (ThyMφs) or MoMφs (Figure 6, B) (Tsai et al. 2022; Zhou et al. 2022). In the medulla, numerous stellate Iba1+ and MHC-II+ cells were identified together with moderate number of Arginase 1+, Ym1+, HO-1+ and iNOS+ cells and rare MARCO+ and F4/80+, predominantly stellate cells (Figure 6, A-F). Most of these cells most likely represent cDCs or MoDCs as reported in thymic medulla and cortico-medullary regions (Kroger et al 2017; Zhou et al. 2022; Wang et al. 2022). This is further supported by the expression of iNOS, which was found in high amount in thymic antigen presenting cells. (Aiello et al. 2000). Despite this, a definitive distinction between DCs and ThyMφs/MoMφs with antigen-presenting function remains difficult also with flow-cytometric analysis since it has been demonstrated that both express dendritic markers such as MHC-II (Zhou et al. 2022).

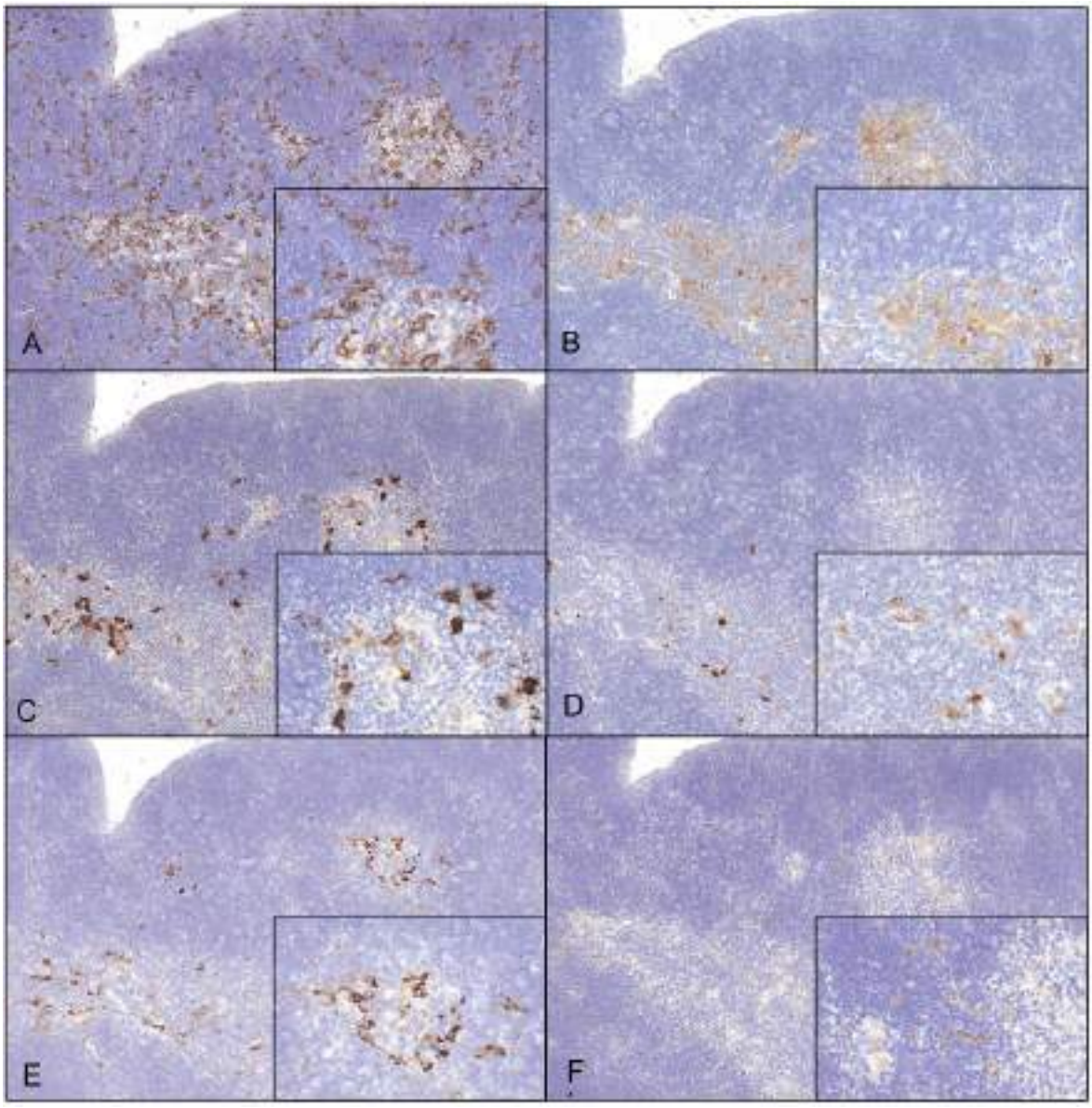

Figure 6. Thymus. **A.** Immunohistochemistry for Iba1, 20x. Moderate to numerous stellate Iba1+ MoMΦs/ThyMΦs in both the cortical and medullary regions and numerous Iba1+ stellate MoMΦs/ ThyMΦs/DCs in the medulla were identified. **Inset**, 80x: Iba1+ cells have a stellate morphology **B.** Immunohistochemistry for MHC-II, 20x. Numerous stellate MHC-II+ cells were observed in the medulla, representing either MoMΦs/ThyMΦs/ or DCs. **Inset**, 80x: MHC-II+ MoMΦs/ThyMΦs/DCs have a stellate morphology **C**. Immunohistochemistry for Arginase 1, 20x. **D.** Immunohistochemistry for iNOS, 20x. **E**. Immunohistochemistry for Ym1, 20x. **Insets**, 80x. A moderate number of round to stellate Arginase 1+, iNOS+ and Ym1+ MoMΦs / ThyMΦs are present in the thymic medullary region. In the insets, the round to stellate morphology of the positive cells can be appreciated **F**. Immunohistochemistry for HO-1, 20x. Rare stellate HO-1+ MoMΦs / ThyMΦs are present in both the medulla and cortex. **Inset**, 80x: note the stellate morphology of HO1+ cells.

Kidney. Although playing important functions in homeostasis and disease, the study of renal mononuclear phagocyte cells is still at an early stage (George et al. 2017). Our panel detected a moderate to rare number of spindle Iba1+, F4/80+ and CD206+ cells and rare to no Arginase 1+ cells in the capsule classified as MoMφs or renal resident macrophages (ReMφs). Rare arginase 1+ and Ym1+ spindle cells were also present along the capsule. These cells could possibly represent capsular MoMφs/ReMφs as well as monocytes circulating in stretched capsular vessels which could explain their spindle morphology. A moderate number of stellate Iba1+, F4/80+ and MHC-II+ cells, with rare expression of Arginase 1 and Ym1, were detected in close association to cortical and medullary tubules, while a moderate number of CD206+ round to stellate cells were identified around blood vessels (Figure 7, A-D). These cells were classified as either MoMφs, ReMφs or cDCs / MoDCs (Soos et al. 2006). Interestingly, CD206+ cells were also identified in the glomeruli as this marker is expressed by glomerular mesangial cells (Figure 7, C) (Linehan et al. 1972). According to flow cytometric data, the most common renal mononuclear phagocytes are F4/80+, MHC-II+ and CD11c+ cells often simultaneously expressing macrophagic and DCs markers even though molecular and functional data strongly suggest that only a minority of these are true dendritic cells (Gautier et al. 2012; Kawakami et al. 2013; George et al. 2017; Nelson et al. 2012). Furthermore, rare round Arginase 1+ and Ym1+ cells within the lumen of interstitial blood vessels were interpreted as circulating monocytes. Notably, in the renal papilla, only rare to moderate numbers of Iba1+ and CD206+ round to stellate cells were detected (Figure 7, E, F). Because molecular investigations on kidney macrophages highlighted specific transcriptomic profiles in renal papilla MPS cells, suggesting the existence of a specific population of mononuclear phagocytes in this location, the renal papilla could be populated by mononuclear cells expressing different markers than the ones tested (Cheung et al. 2022). In the renal pelvis, rare to moderate number of stellate and spindle Iba1+, F4/80+, MHC-II+, CD206+ and Arginase 1+ cells were identified in the lamina propria and classified as MoMφs / ReMφs or cDCs/ MoDCs, while round CD206+, Arginase1+ cells as MoMφs / ReMφs. Furthermore, rare perirenal Iba1+, F4/80+, CD206+ and Arginase1+ round to spindle cells were classified as white adipose tissue macrophages (WAT MΦs). These data are consistent with other reports and corroborate the anti-inflammatory M2 function of WAT MΦs in mice in steady state condition (Lumeng et al. 2007).

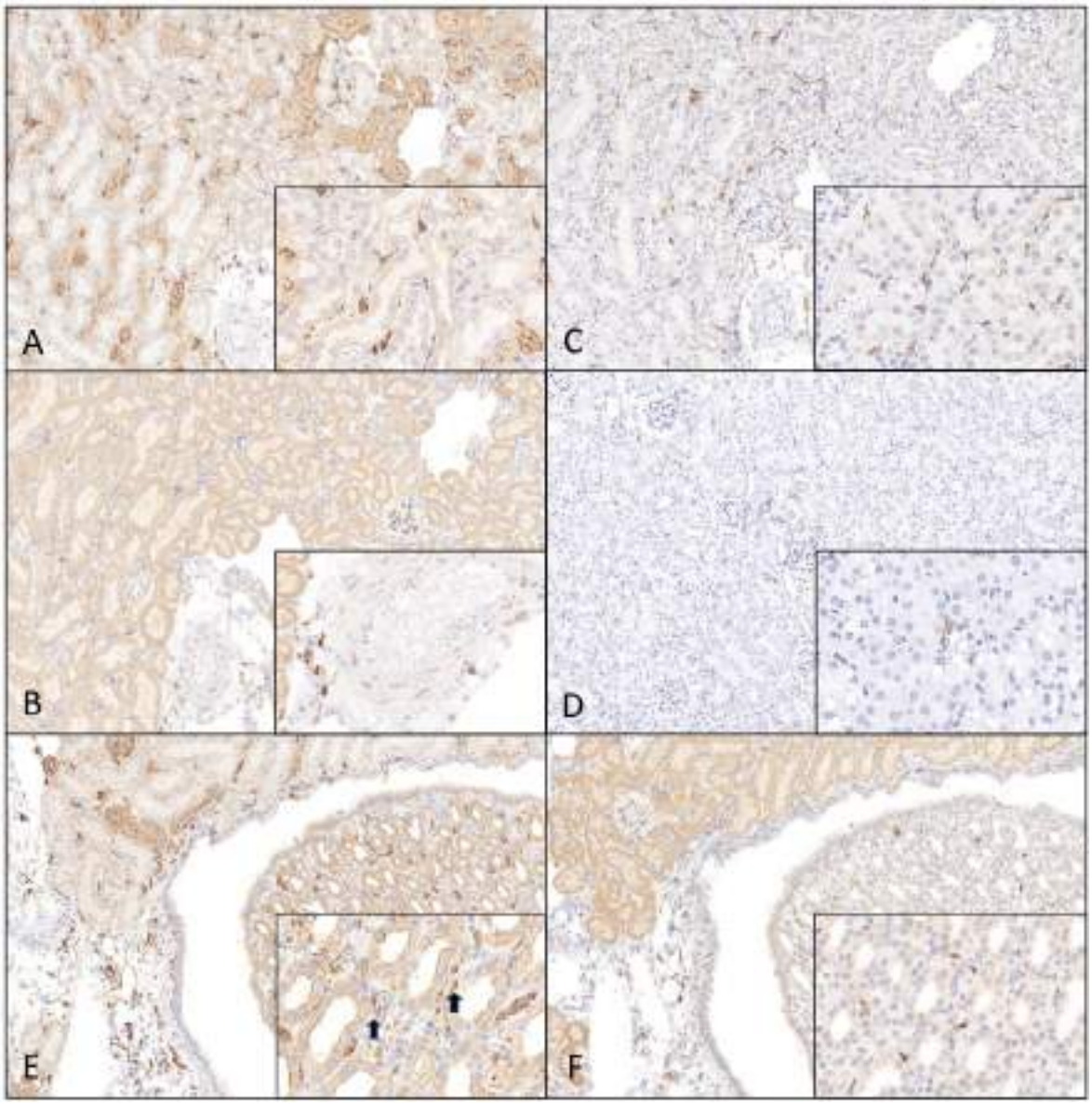

Figure 7. Kidney, cortical region. **A**. Immunohistochemistry for Iba1, 20x **B**. Immunohistochemistry for F4/80, 20x. **C**. Immunohistochemistry for CD206, 20x. **D**. Immunohistochemistry for MHC-II, 20x. A moderate number of stellate Iba1+ and F4/80+ and rare stellate MHC-II+ MoMφs/ ReMφs/ MoDCs/ cDCs were identified among tubules, in both the cortical and medullary interstitium. Moderate numbers of CD206+ MoMφs /ReMφs were present around medium caliber arterioles. **Insets,** 80x: Note the stellate morphology of Iba1+, F4/80+ and MHC-II+ cells among tubules and the round to stellate morphology of CD206+ cells around arterioles. **E-F**. **Kidney, pelvis, and renal papilla**. **E.** Immunohistochemistry for Iba1, 20x **F**. Immunohistochemistry for CD206, 20x. Rare to moderate numbers of stellate Iba1+ and CD206+ mononuclear phagocytes were observed in the renal papilla. Note the presence of stellate Iba1+ and CD206+ Mφs and DCs in the pelvis lamina propria. **Insets,** 80x**.** Spindle to stellate Iba1+ cells (arrows) and CD206+ cells are visible in the renal papilla interstitium.

Adrenals. Resident mononuclear phagocytes have been reported in the adrenal glands although a precise classification is lacking (Ozbek et al. 2006). A moderate number of Iba1+ stellate cells in all cortical regions, more numerous in the zona glomerulosa and rare MHC-II+ stellate cells in the zona glomerulosa were identified in the cortex while occasional Iba1+ and MHC-II+ stellate cells were noted in the medulla (Figure 8, A, C). Rare arginase 1+ round cells were also observed in the adrenal cortex, often in blood vessels hence classified as circulating monocytes (Figure 8, B). Based on the examined markers, most of these cells represent either resident adrenal MΦs (AdMΦs) or MoMφs intermixed to rare cDCs/MoDCs (Dolfi et al. 2022).

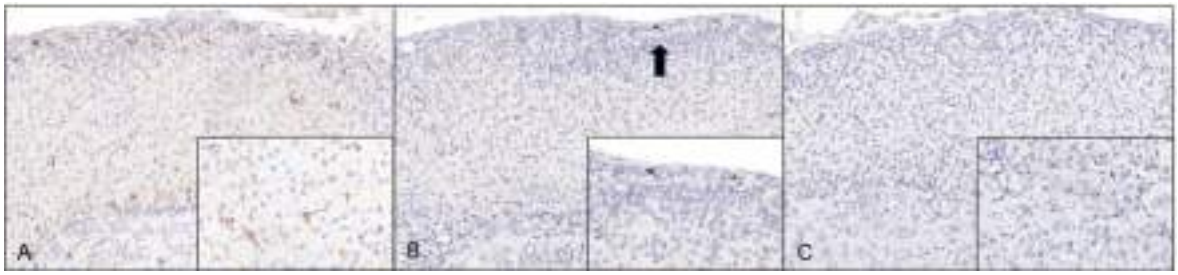

Figure 8. Adrenal gland. A. Immunohistochemistry for Iba1, 30x. Numerous stellate Iba1+ AdMΦs/ MoMΦs were present in both the medulla and the cortex, in the latter region more numerous in the zona glomerulosa. **Inset,** 80x**:** Iba1+ cells have a stellate morphology. **B.** Immunohistochemistry for Arginase 1, 30x. Rare round arginase 1+ cells are visible in the adrenal cortex, often within blood vessels (arrow). **Inset,** 80x**:** note the round morphology of arginase 1+ cells **C.** Immunohistochemistry for MHC-II, 30x. Rare stellate MHC-II+ cells representing MoDCs/ cDCs are visible in both cortex and medulla. **Inset**, 80x. Note the presence of stellate MHC-II+ cells in the adrenal medulla.

Small Intestine and Stomach. In steady state conditions, a population of continuously renewed MoMφs and MoDCs involved in gut protection against pathogens, immune tolerance towards luminal antigens as well as in gastro-intestinal motility and secretion is found along the gastro-intestinal system (Bain et al. 2018, Scott et al. 2020; Caer et al. 2020; Yip et al. 2021; Delfini et al. 2022). MPS cells were mainly detected in the intestinal mucosa and submucosa and in the gastric submucosa, both in the forestomach and glandular regions (Figure 9, A-D). In the intestinal mucosa lamina propria, there were numerous stellate to spindle Iba1+, F4/80+ cells, moderate number of stellate MHC-II+ cells and rare stellate CD206+ cells representing either MoMφs or MoDCs intermixed to less numerous round Iba1+, F4/80+, CD206+, Arginase1+, Ym1+, HO-1+, CD206+ cells and rare iNOS+ cells classified as MoMφs. Although highly phagocytic, intestinal mononuclear cells do not elicit overt inflammatory responses, as supported by expression of M2 markers, while iNOS expression has been related to smooth muscle relaxation more than inflammation (Smythies et al 2005; Bain 2018; Mori et al. 2014). MPS cells with a similar phenotype were observed in the stomach, particularly in the submucosa, although no Ym1+ and iNOS+ cells were identified. A few polymorphic Iba1+, F4/80+ and round and spindle CD206+ cells in the intestinal submucosa, classified as MoMφs and a few Iba1+, CD206+ round to spindle cells in tunica muscolaris and a few round to spindle Iba1+, Arginase1+, CD206+ cells on the serosa were detected in both stomach and intestine. These cells were classified as MoMφs and have been linked to submucosal vasculature integrity maintenance and to peristaltic activity regulation (Muller et al. 2014; De Schepper et al. 2018; Viola et al. 2020, Delfini et al. 2022). While no gastric associated lymphoid tissue was observed in our samples, lymphoid aggregates in the small intestine had moderate number of round Iba1+, MHC-II+ TBMs and stellate Iba1+, iNOS+, MHC-II+ FDCs in the germinal centers and moderate amount of stellate Iba1+, MHC-II+ (MoMφs/ DCs) and round Iba1+, iNOS+, Arginase1+ and rare HO-1+, Ym1+ cells (MoMφs) in the mantle zones (Hasui et al. 2000; Bonnardel et al. 2015).

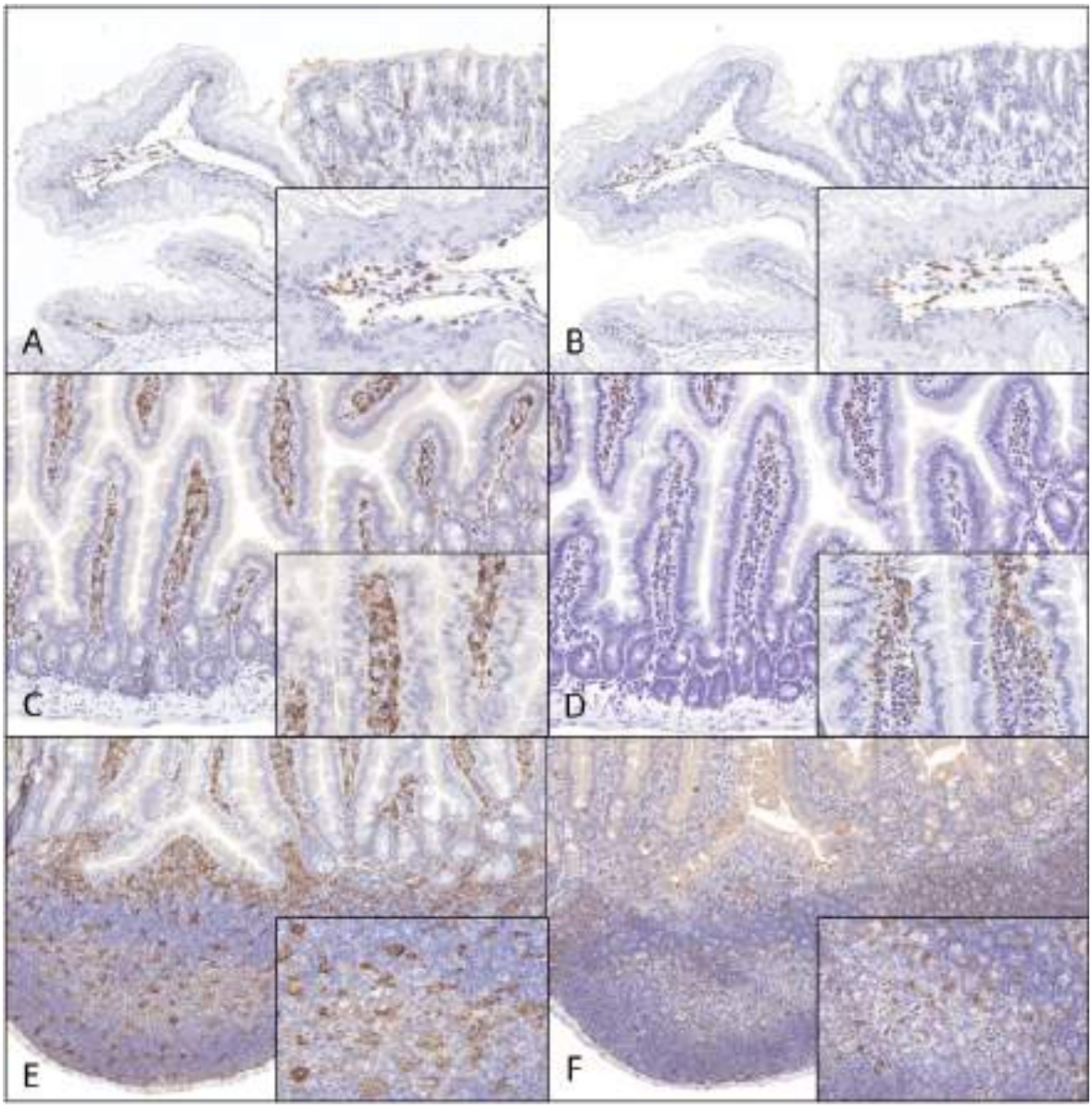

Figure 9. A, B. Forestomach, and glandular stomach. A. Immunohistochemistry for Iba1, 20x **B.** Immunohistochemistry for F4/80, 20x. A moderate number of round to spindle MoMφs/MoDCs are visible, particularly in the submucosa. **Inset,** 80x**:** Iba1+ , F4/80+ cells have a round to spindle morphology. **C, D. Small intestine. C.** Immunohistochemistry for Iba1, 20x **D.** Immunohistochemistry for F4/80, 20x. Numerous polymorphic MoMφs are visible along villi lamina propria. **Inset,** 80x**:** note the polymorphic shape of positive cells. **E, F. Peyer's Patches E.** Immunohistochemistry for Iba1, 20x **F.** Immunohistochemistry for iNOS, 20x. A moderate number of round Iba1+ TBMφs and of stellate Iba1+, iNOS+ FDCs in the germinal center zone and of stellate Iba1+, iNOS+ MoMφs in the mantle and marginal zones are visible. **Inset,** 80x: note the round, Iba1+ TBMφs engulfing basophilic apoptotic debris and the stellate morphology of iNOS+, Iba1+ FDCs and MoMφs.

Testis. Currently, two tissue-resident macrophagic populations are recognized in the testis: yolk-sack derived interstitial macrophages (IntMΦs) among Leydig cells and monocyte derived peri-tubular macrophages (PTMΦs), closely associated to peritubular myoid cells (Mossadegh-Keller et al. 2017; De Falco et al. 2014; Lokka et al. 2020). Together with DCs, they make up the testicular MPS (Da Silva et al. 2015; Bushan et al. 2020). Numerous Iba1+ and moderate number of polymorphic CD206+ and rare stellate F4/80+ in the testicular interstitium were classified as IntMΦs/ MoMΦs, while rare Iba1+ spindle cells closely associated to the tubular walls as PTMΦs (Figure 10, A-C). A recent publication highlighted that MPS cells in the testes, under physiological condition, exhibit immunosuppressive activity maintaining a local immune tolerance through cytokines production and MHC-II suppression (Shi et al 2022). Although their presence is reported in humans and other mammals, no MHC-II+ cells were identified in the testicular interstitium of the examined samples while moderate number of stellate MHC-II+ cells were stained in the epididymis (Pollanen et al. 1988; Guney saruhan et al. 2017; Bhushan et al. 2020).

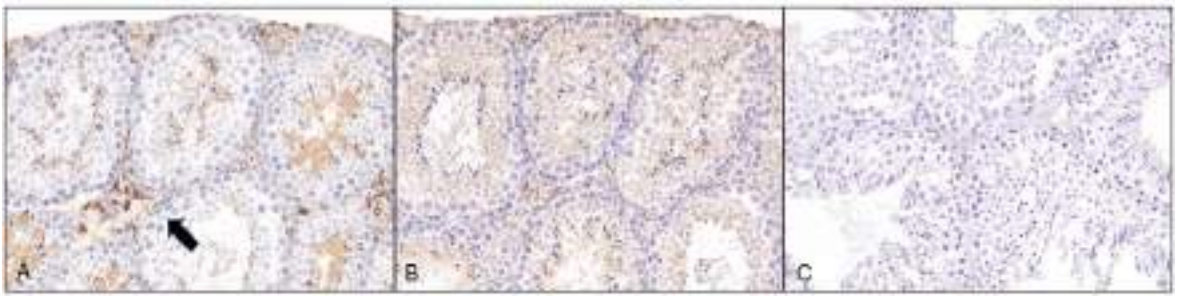

Figure 10. Testis. **A**. Immunohistochemistry for Iba1, 40x. Numerous stellate Iba1+ IntMΦs/ MoMΦs and rare spindle PTMΦs (arrow) were identified in the testis. **B**. Immunohistochemistry for CD206, 40x. Moderate number of stellate CD206+ IntMΦs/ MoMΦs populate the interstitium **C**. Immunohistochemistry for F4/80, 40x. Rare stellate F4/80+ IntMΦs/ MoMΦs among tubules are visible.

Heart. Resident embryo-derived cardiac macrophages (CaMΦs), MoMΦs and DCs, represent the primary resident immune cells in the heart, with a suggested role in cardiac immunity, homeostasis, and pathological conditions (Sanmarco et al. 2018; Sansonetti et al. 2020; Van der Borght et al. 2018). We identified rare, round to spindle, Iba1+ cells in the examined epicardium, myocardium and endocardium, mainly in the atria. Apart from the epicardium, these cells were F4/80 negative and variably expressed markers associated to M2 polarization, particularly CD206 in myocardium, hence classified as CaMΦs/ MoMΦs (Figure 11, A-C). (Revelo et al. 2021). Despite valvular pigmentation making it challenging to evaluate immunohistochemical positivity, rare round to spindle Iba1+ cells were identified in this region (Figure 11, D-F). Although DCs are reported in the heart, no MHC-II+ cells in myocardium endocardium and epicardium or valves were identified in the evaluated sections.

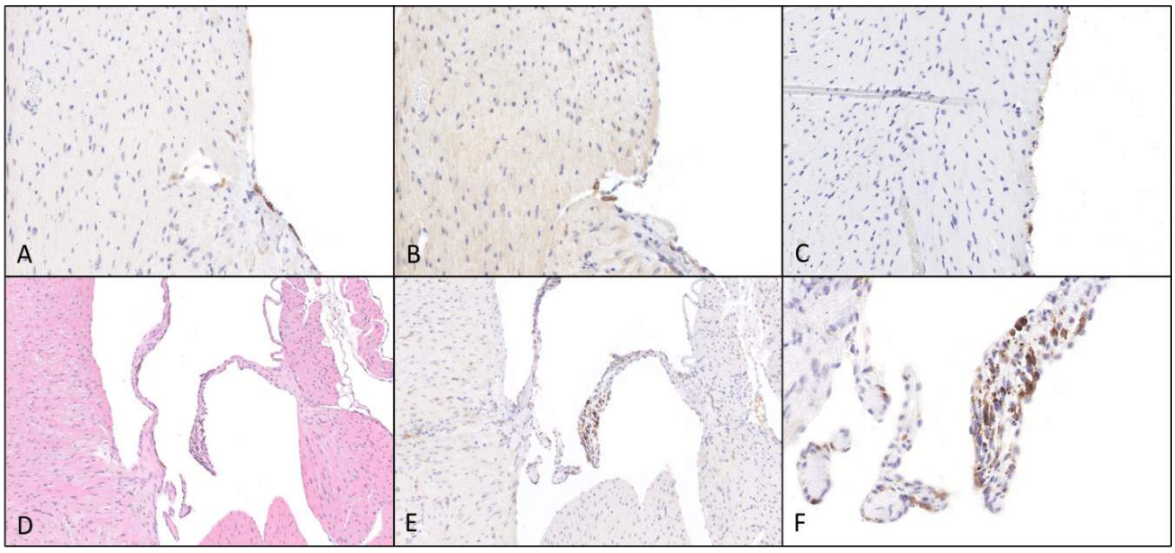

Figure 11. Heart. A. Immunohistochemistry for Iba1, 20x. **B.** Immunohistochemistry for CD206, 20x **C.** Immunohistochemistry for F4/80, 20x**.** Rare Iba1+, CD206+ and F4/80+ spindle CaMΦs/ MoMΦs along the epicaridial surface and rare myocardial Iba1+ cells are visible. **D. Mitral valve.** H&E, 20x **E. Mitral valve.** Immunohistochemistry for Iba1, 20x **F. mitral valve.** Immunohistochemistry for Iba1, 60x. Altough the presence of coarsely granular melanin pigment hampers immunohistochemical signal interpretation, a few Iba+ cells are present in the valvular stroma.

Lungs. In steady state, fetal liver-derived alveolar macrophages (AMΦs) in the alveolar spaces and bone-marrow derived interstitial macrophages (IMΦs), DCs and circulating monocytes in the pulmonary interstitium make up the pulmonary MPS (Misharin et al. 2013; Gibbings et al. 2017; Gibbins et al. 2018; Baharom et al. 2017). Numerous round MARCO+ and Ym1+ cells, a moderate number of round F4/80+ and rare CD206+, HO-1+ and MHC-II+ cells in the alveolar spaces and occasionally in the bronchiolar lumina were identified as AMΦs (Figure 12, B-E) (Misharin et al. 2013; Arredouani et al. 2004). Iba1 expression by AMΦs is controversial, and interestingly, we did not observe Iba1 expression by this population (Kohler et al 2007; Donovan et al. 2018). A moderate number of spindle to stellate Iba1+, F4/80+ and CD206+ cells and rare spindle to stellate MHC-II+, Ym1+, Arginase 1+ cells representing IMΦs/ MoDCs/ cDCs and rare Iba1+, F4/80+, Arginase 1+ round cells, classified as circulating monocytes were visible along the alveolar septa (Figure 12, A-F). In the peribronchial/perivascular tissue, numerous polymorphic Iba1+ cells, moderate number of polymorphic CD206+, moderate number of spindle to stellate MHC-II+ cells and rare F4/80+ and Ym1+ spindle to stellate cells were identified and classified as IMΦs/ MoMΦs/ MoDCs or cDCs (Figure 12, A-C, E).

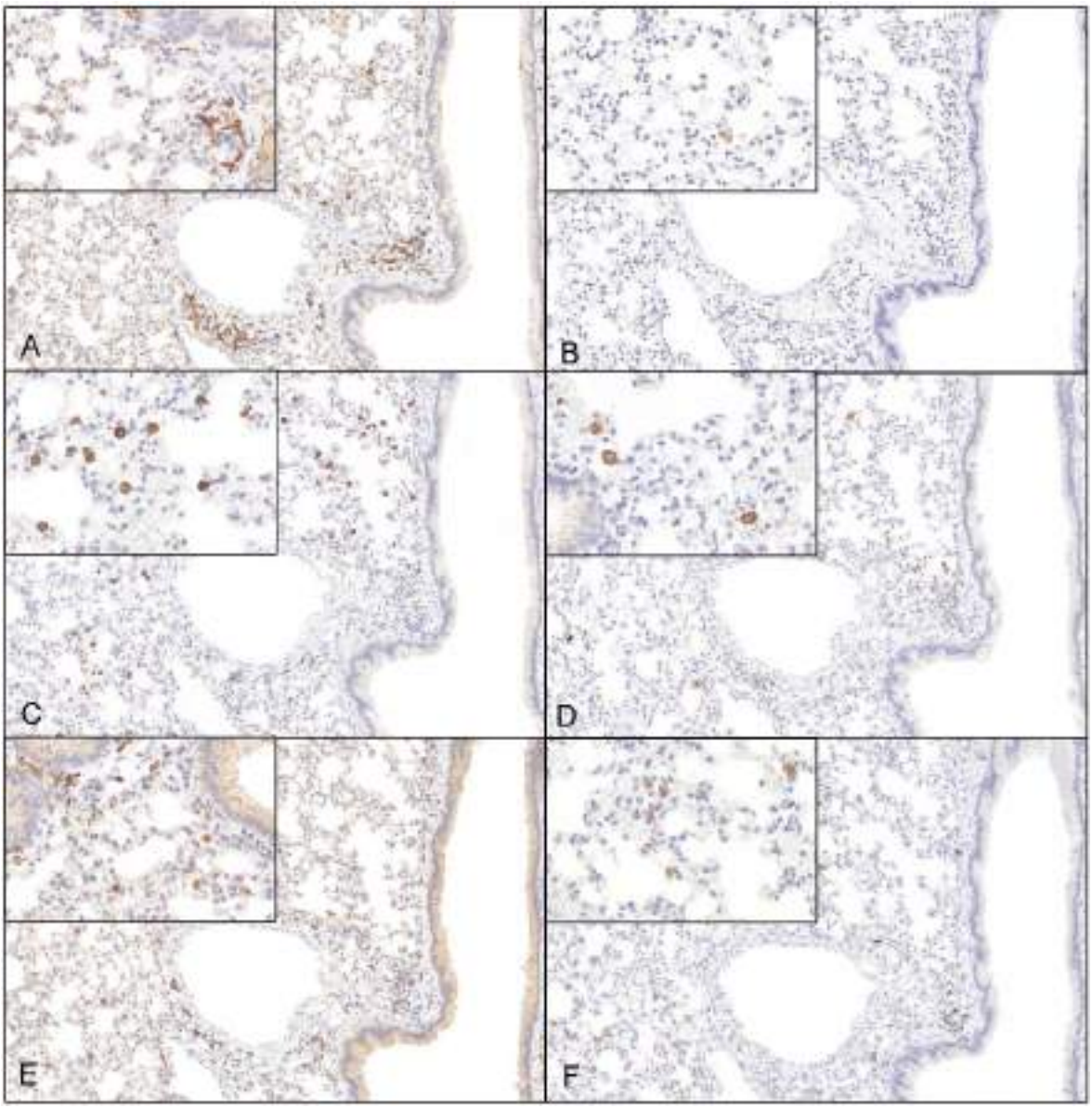
A
B
C
D
E
F

Figure 12. Lung. **A.** Immunohistochemistry for Iba1, 20x. Numerous perivascular and peribronchiolar polymorphic Iba1+ IMΦs, MoDCs and cDCs and occasional round to spindle Iba1+ IMΦs in the alveolar septa are visible. **Inset,** 80x**:** peribronchiolar and septal Iba1+ cells have a polymorphic morphology. **B** Immunohistochemistry for F4/80. Rare spindle to stellate F4/80+ perivascular and peribronchiolar IMΦs and a moderate number of round F4/80 AMΦs in the alveolar spaces are detected. **Inset,** 80x**:** round F4/80+ AMΦs and a round IMΦs in the alveolar septa are visible. **C**. Immunohistochemistry for Ym1, 20x. Numerous Ym1+ round AMΦs are visible in the alveolar spaces together with rare round to spindle IMΦs both in alveolar septa and perivascular and peribronchiolar space. **Inset,** 80x**:** note the round morphology of Ym1+ AMΦs and the presence or round to stellate IMΦs along the septa. **D** Immunohistochemistry for Marco, 20x. Moderate to numerous MARCO+ AMΦs were identified in pulmonary alveolar spaces. No positive cells were instead identified along alveolar septa or in peribronchiolar and perivascular space. **Inset,** 80x**:** round Marco+ AMΦs are visible. **E** Immunohistochemistry for CD206, 20x. Moderate to numerous polymorphic CD206+ perivascular and peribronchiolar IMΦs and rare CD206+ round AMΦs in alveolar spaces are visible. **Inset,** 80x**:** spindle to stellate CD206+ IMΦs around bronchioles and rare round AMΦs in the alveolar space are visible. **F** Immunohistochemistry for Arginase 1, 20x. A moderate number of round to spindle Arginase 1+ IMΦs in peribronchiolar and perivascular space and along alveolar septa are visible. **Inset,** 80x**:** note the presence of round to spindle cells in the alveolar septa interstitium.

Pancreas. The murine exocrine pancreas is populated by DCs and by two subsets of macrophages: yolk-sac derived resident pancreatic macrophages (PaMφs) scattered in the interstitium among acini and bone-marrow derived macrophages (MoMφs) mainly surrounding pancreatic ducts (Calderon et al. 2015). We identified rare spindle to stellate Iba1+, MHC-II+, F4/80- cells within the acinar interstitium, classified as PaMφs/ MoDCs/ cDCs (Figure 13, D-F). In the periductal interstitium, moderate number of spindle to stellate Iba1+ cells with occasional expression of F4/80+, CD206+, MHC-II+, were classified as MoMφs or MoDCs/ cDCs while round Arginase 1+, HO-1+ cells as MoMφs (Figure 13, G-I). Pancreatic islets were infiltrated by rare Iba1+, F4/80+ MHC-II+ stellate cells classified as Islet macrophages (IslMφs) (Figure 13, A-C). It has been demonstrated that islet-

associated phagocytes are distinct from DCs and are mainly resident yolk-sack derived macrophages (Zinselmeyer et al 2018), with regulatory functions on insulin release (Weitz et al. 2019; Calderon et al. 2015) although MHC-II+ stellate cells observed in pancreatic islets, could also represent islet-associated DCs. Finally, round to spindle Arginase 1+ cells at the islet periphery were also present. Based on negativity to other phagocyte markers tested, these cells most likely represent alpha and/or beta-cells, as arginase production has been reported in both cell types (Marselli et al. 2021).

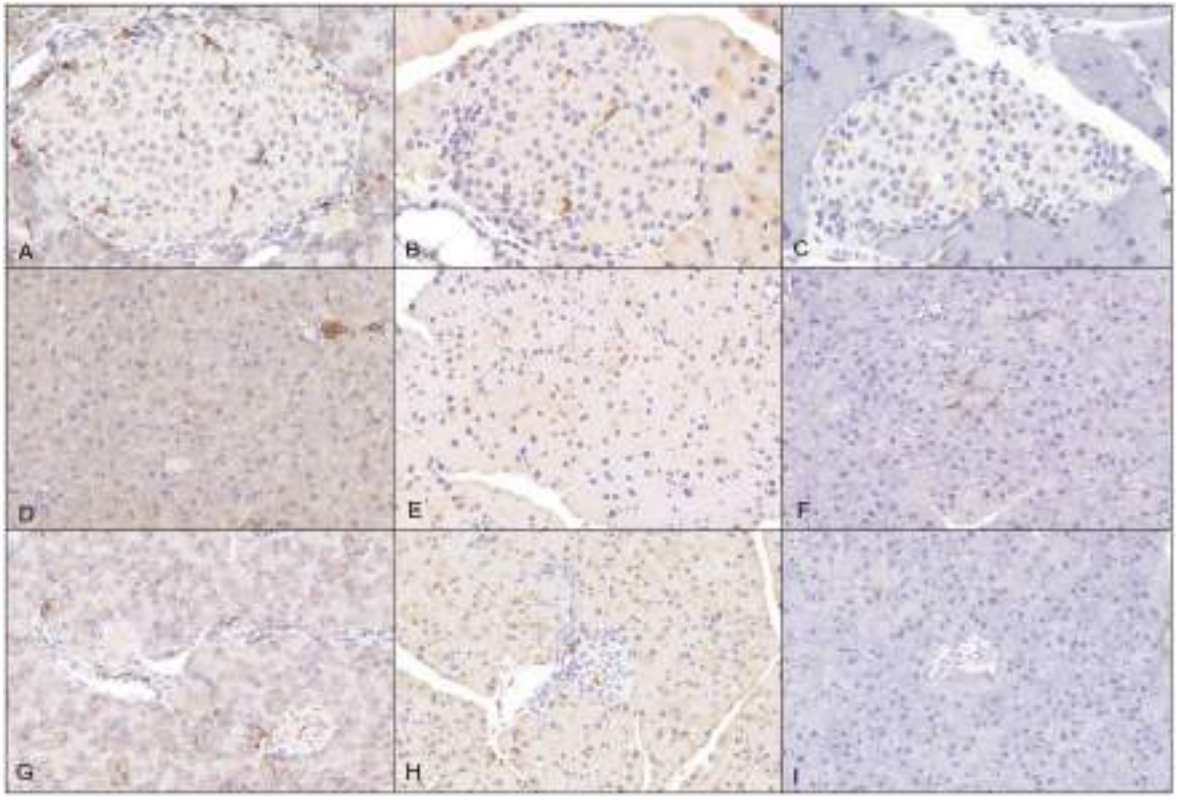

Figure 13. Pancreas, Islets of Langerhans . A. Immunohistochemistry for Iba1, 40x. **B.** Immunohistochemistry for F4/80, 40x. **C.** Immunohistochemistry for MHC-II, 40x. Rare spindle to stellate Iba1+, F4/80+ and MHC-II+ IslMφs/ MoDCs/ cDCs are visible among pancreatic endocrine cells. **Pancreas**, **exocrine tissue**. **D.** Immunohistochemistry for Iba1, 40x **E.** Immunohistochemistry for F4/80, 40x**. F.** Immunohistochemistry for MHC-II, 40x. Among pancreatic acini a few Iba1+ and MHC-II+ stellate PaMφs / MoDCs/ cDCs and no F4/80+ cells were identified. **Pancreas**, **Peritubular connective tissue**. **G.** Immunohistochemistry for Iba1, 40x **H.** Immunohistochemistry for F4/80, 40x**. I.** Immunohistochemistry for MHC-II, 40x. A moderate number of spindle to stellate Iba1+ and rare spindle to stellate F4/80+ and MHC-II+ MoMφs / MoDCs / cDCs are visible around blood vessels and pancreatic ducts connective tissue.

3.4.2. Pathological conditions.

The examination of a subset of pathological conditions allowed comparison with healthy organs. Since different strains were enrolled in the study, their different genetic and immune system background must be taken into consideration when interpreting the results, since their peculiar background could impact on MPS cells development, recruitment, and activation.

The case of necrosuppurative hepatitis was characterized by multiple nodular, coalescing foci with a central necrotic core surrounded by a rim of mixed inflammatory cells, mainly composed of degenerated neutrophils and mononuclear cells. Excluding the central necrotic area, where the signal was considered non-specific, immunohistochemical staining highlighted two distinct concentric regions of the inflammatory rim: a peri-necrotic inner layer, immediately adjacent to the necrotic core and a peripheral outer layer. Iba1 was expressed by a multitude of stellate cells both in the peri-necrotic and peripheral layers, as well as in the adjacent hepatic parenchyma. In the peri-necrotic layer, numerous MHC-II+, INOS+, Arginase 1+ cells, a moderate number of stellate MARCO+ and rare Ym1+ stellate cells were identified (Figure 14, A-H). Rare F4/80 expression and no Arginase 1 expression were noted in the peripheral layer (Figure 14, B, D). The cells of both layers were classified as infiltrating MoMΦs, with MHC-II+ cells representing either MoDCs or MHC-II-expressing MΦs with APC properties. It has been demonstrated that these cells are, in fact, recruited to necrotic liver lesions where they are able to evoke an inflammatory response and trigger a reparative process (Feng et al. 2023). Interestingly, particularly in the peri-necrotic area, there was co-expression of both M1 (MHC-II, iNOS) and M2 (Arginase 1, HO-1 and Ym1) markers. These findings may be interpreted considering lesion timing and MPS cells plasticity: these cells can, in fact, rapidly transform from M1-like macrophages with pro-inflammatory pathogen killing activity in the early phase of the lesions to their M2-like counterparts with anti-inflammatory and wound healing properties acting in later phases depending on the extracellular milieux (Ley, 2017; Tizard, 2018). Moreover, an increased number of Iba1+, F4/80+, MHC-II+ and MARCO+ intra-sinusoidal, plump, Kupffer cells were present in the unaffected adjacent hepatic parenchyma, compared to the healthy controls (Figure 15, A-F). Although some studies report difficulties in distinguishing reactive MoMΦs and Kupffer cells in pathological samples based on a flow-cytometric approach due to overlapping markers expression, the cellular morphology and the intra-sinusoidal localization prompted us to classify them as Kupffer cells (Guilliams and Van der Laar 2015; Ju et al. 2016). Nevertheless, the enhanced expression of MARCO and MHC-II indicates an increased antigen recognition, metabolization and presentation of Kupffer cells in the

inflammatory context as demonstrated in human hepatitis cases underlying, once more, the plasticity of the murine MPS (Chen et al. 2005; Ju et al. 2016; Pinto et al. 2018; Zhang et al. 2021; Zheng et al. 2023).

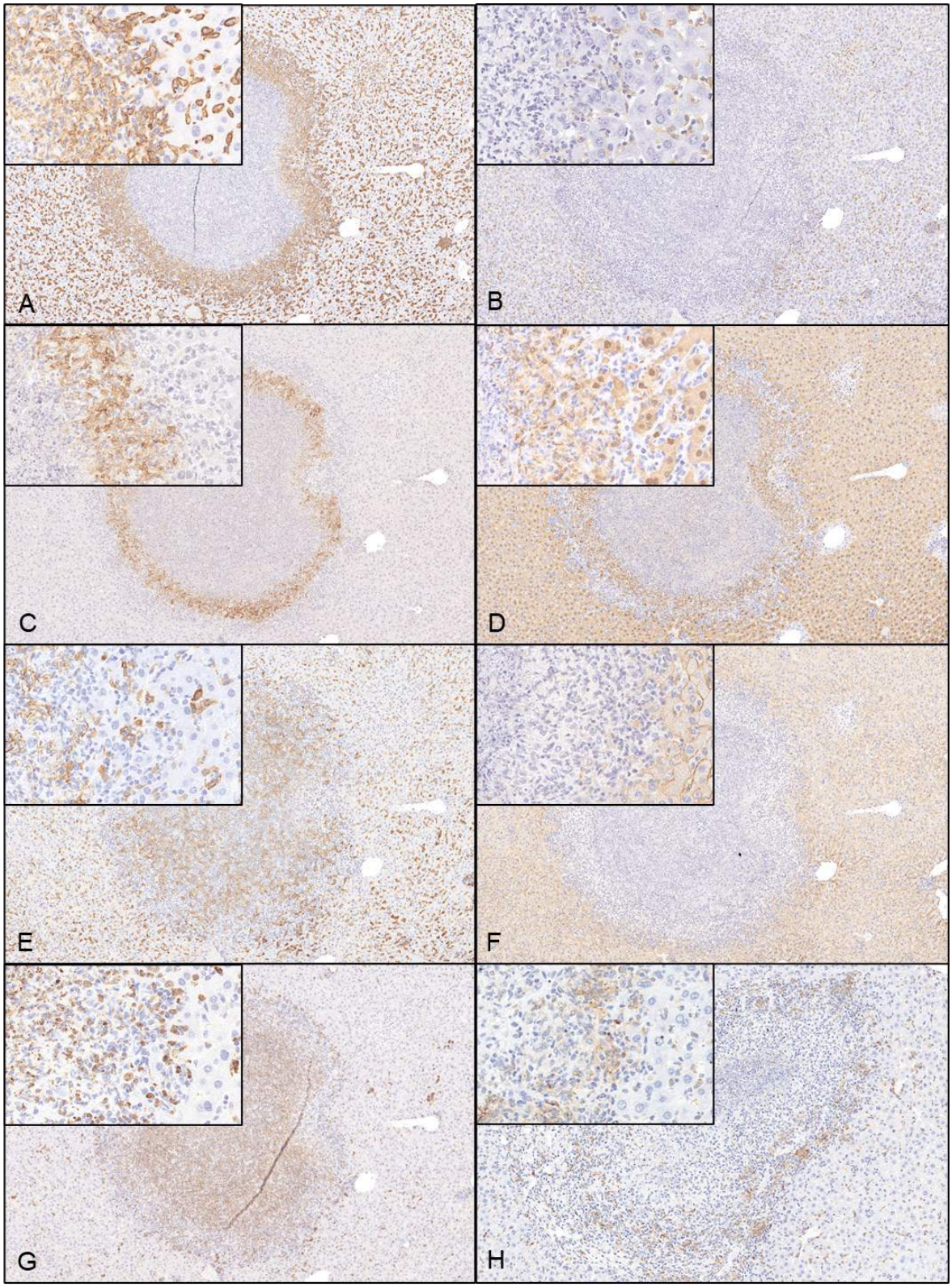

Figure 14. Necrosuppurative hepatitis A. Immunohistochemistry for Iba1, 10x. Numerous Iba1+ MoMΦs/ MoDCs/ cDCs are detected in both perinecrotic and peripheric layers. **Inset,** 80x: perinecrotic and peripheral Iba1+ cells have a stellate morphology. Note the plump Kupffer cells along sinusoids in the adjacent hepatic parenchyma. **B**. Immunohistochemistry for F4/80, 10x. Rare F4/80+ stellate MoMΦs were detected only in the peripheric layer while numerous Kupffer cells are visible along sinusoids. **Inset,** 80x: rare F4/80+ stellate cells in the peripheric layer and plump Kupffer cells are visible **C.** Immunohistochemistry for iNOS, 10x. **D** Immunohistochemistry for Arginase, 10x. Numerous stellate iNOS+ and Arginase 1+ cells were observed only in the perinecrotic layer. Note the absence of signal in the peripheric layer. **Insets,** 80x: at higher magnification, iNOS+ and Arginase 1+ cells have a stellate morphology **E.** Immunohistochemistry for MARCO, 10x. Excluding the central necrotic core signal, considered non-specific, a moderate number of stellate MARCO+ MoMΦs are visible in both the perinecrotic and peripheric layers. **Inset,** 80x: MARCO+ cells have a round to stellate morphology. **F.** Immunohistochemistry for CD206. No positive CD206+ cells are detected in either the perinecrotic or peripheral layer. **Inset,** 80x**:** no CD206+ cells are seen in either the perinecrotic or peripheric layers. **G.** Immunohistochemistry for Ym1, 10x. Rare Ym1+ stellate cells in the perinecrotic layer and a moderate number of Ym1+ stellate MoMΦs in the peripheric layer are visible. **Inset,** 80x: note the stellate morphology of Ym1+ cells **H.** Immunohistochemistry for MHC-II, 10x. Moderate number to numerous MHC-II+ stellate cells are visible in both the perinecrotic and peripheric layers. **Inset,** 80x: MHC-II+ cells have a stellate morphology.

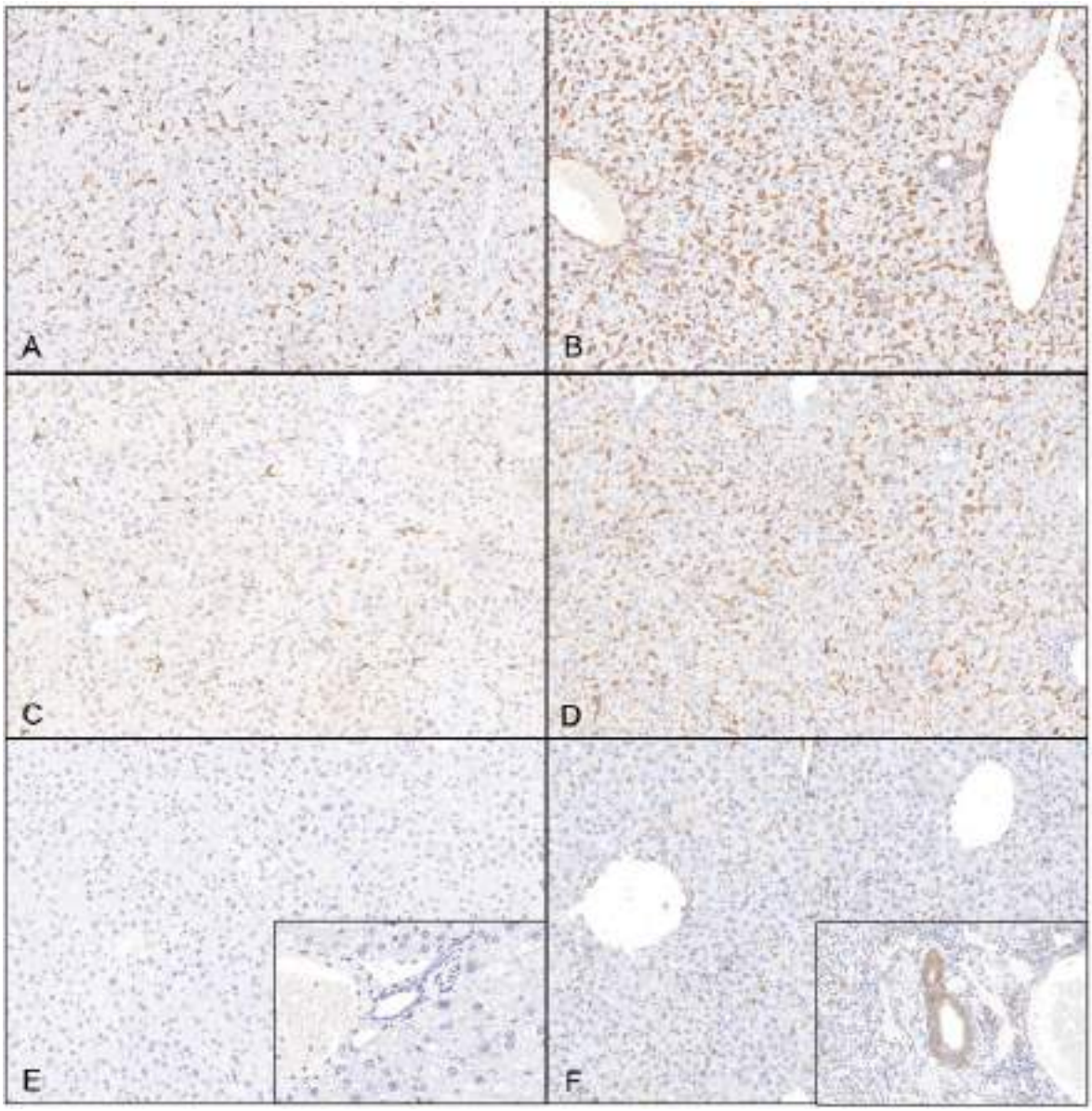

Figure 15. **Healthy liver** (**A, C, E**) **compared to necrosuppurative hepatitis** (**B, D, F**). **A-B**. Immunohistochemistry for Iba1, 20x. **C-D**. Immunohistochemistry for MARCO, 20x. **E-F**. Immunohistochemistry for MHC-II, 20x. An increase of stellate Iba1+, MARCO+, MHC-II+ cells, mostly representing hepatic Kupffer cells, is apparent among hepatic sinusoids. **E-F, insets, 50x**. Contrary to steady state bile ducts, MHC-II+ biliary ducts were found in periportal spaces of the necrosuppurative hepatitis case.

In the *Pneumocystis murina* experimental infection, the examined lungs were characterized by a severe, diffuse, histiocytic, interstitial pneumonia with intra-alveolar cyst forms associated to a concurrent eosinophilic crystalline pneumonia. Compared to the healthy lungs, an increased number of MHC-II+ cells in both the alveolar spaces and interstitium and an increase in interstitial Iba1+ cells were identified. Furthermore, in the

alveolar spaces, there was a higher number of Ym1+, Arginase1+, HO1+ cells, a marked decrease of MARCO+ cells and the appearance of numerous iNOS+ and Iba1+ intra-alveolar round cells, compared to the healthy controls (Figure 16, A-F; Figure 17 A-F). Most of the identified intra alveolar round cells most-likely represent monocyte-derived cells recruited by the inflammatory milieu intermixed to scatterer residual AMΦs as supported by Iba1 positivity of these cells and by the decreased number of MARCO+ cells in the alveolar spaces (Figure 17, E, F). Notably, concomitant expression of M2 and M1 markers was observed in this population. Although it must be noted that Ym1+ was also expressed by alveolar macrophages in steady state conditions, and that its expression was enhanced by the intra-histiocytic accumulation of Ym1 proteins in the context of the eosinophilic crystalline pneumonia, an M2-polarization of MPS cells can be hypothesized based on the increased number of arginase 1+ and HO1+ cells found in the infected lung compared to healthy controls. An adaptive immune response characterized by M2 macrophage polarization is, in fact, ultimately required for the effective clearance of pneumocystis pathogen in immunocompetent mice while immunocompromised animals usually mount a M1-skewed response (Nelson et al 2011; Nandakumar et al 2017). Interestingly, although the examined $CD40L^{-/-}$ strain is partially immunocompromised, we observed the presence of numerous reactive cells positive to M2 markers. Despite the absence of CD40, required for APCs-CD4+ T cells interaction, macrophage recruitment and polarization in these mice may not be affected by their genotype since it is dependent on cytokine production (Van Kooten and Banchereau 2000, Gordon and Martinez 2010, Tizard 2018).

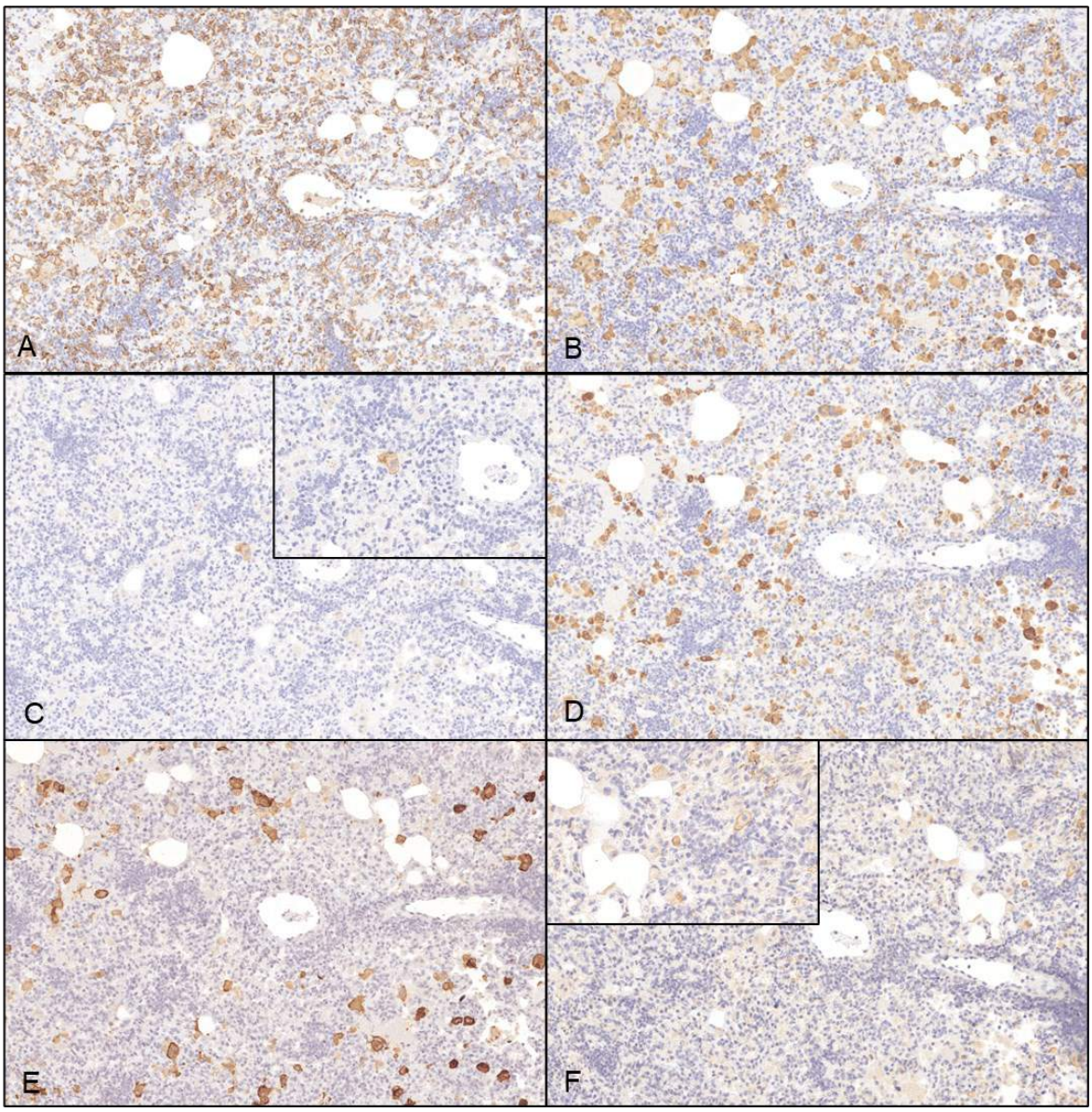

Figure 16. Lung with *Pneumocystis murina* infection. **A**. Immunohistochemistry for Iba1, 20x. Numerous polymorphic Iba1+ cells along alveolar septa and around blood vessels and bronchioles and numerous round Iba1+ MoMΦs/ DCs are visible. **B** Immunohistochemistry for Arginase 1, 20x. Rare to moderate stellate perivascular and peribronchiolar arginase 1+ IMΦs and numerous intra-alveolar arginase 1+ round MoMΦs are visible. **C.** Immunohistochemistry for MARCO, 20x. Only rare round MARCO+ cells could be appreciated in the pulmonary airways, interpreted as residual AMΦs. **Inset,** 60x: A MARCO+ AMΦ is apparent in an alveolar space **D.** Immunohistochemistry for Ym1, 20x. Rare spindle to stellate Ym1+ IMΦs in the perivascular and peribronchiolar tissue and numerous round Ym1+ MoMΦs / AMΦs are visible **E.** Immunohistochemistry for iNOS, 20x. Numerous round iNOS+ MoMΦs are visible in alveolar space **F.** Immunohistochemistry for CD206, 20x. Rare round CD206+ MoMΦs are detectable in

alveolar space. **Inset,** 40x: Higher magnification of rare CD206+ round MoMΦs in alveolar spaces.

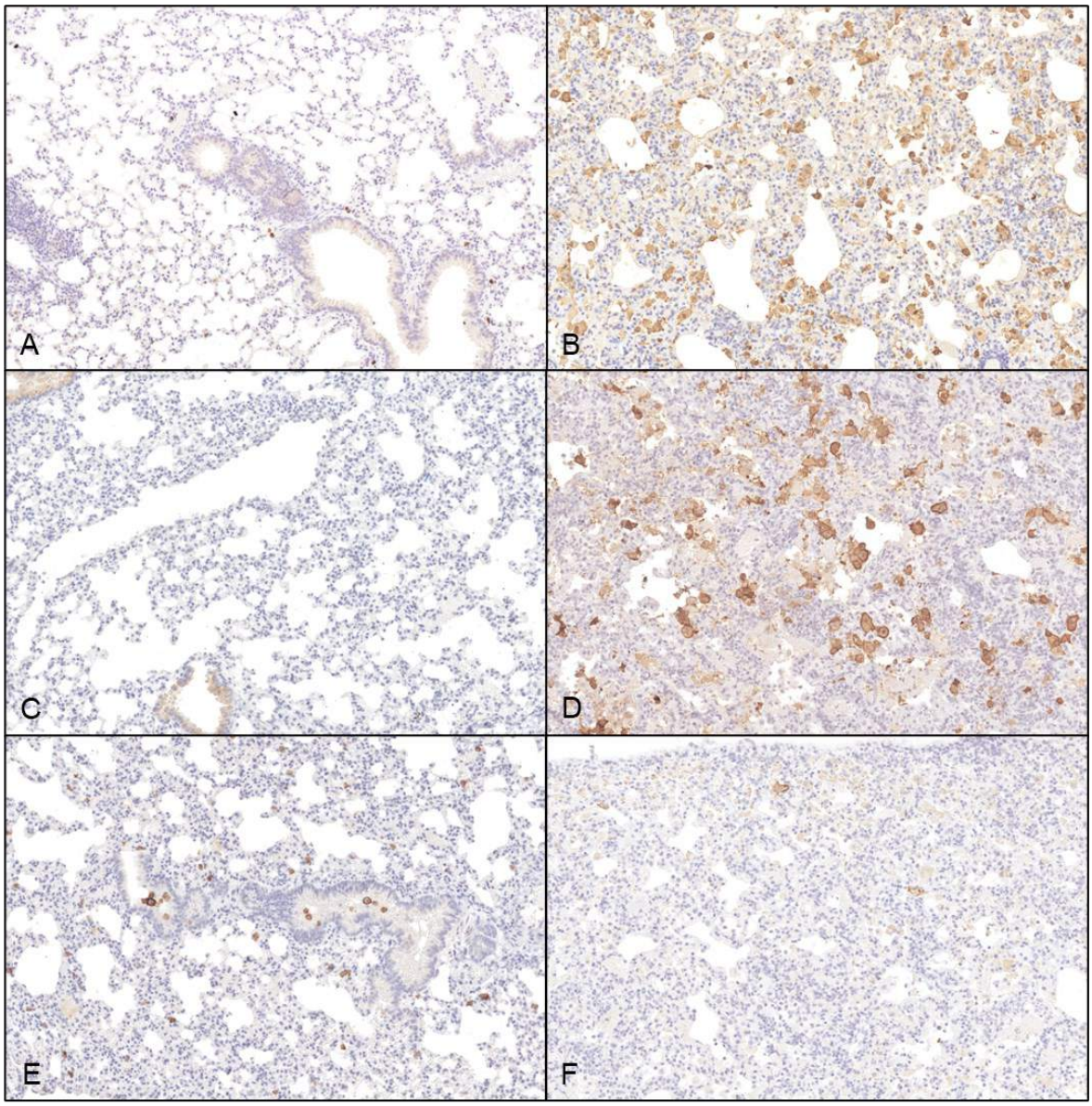

Figure 17. **Healthy lung (A, C, E) compared to *Pneumocystis murina* infection (B, D, F).** **A-B.** Immunohistochemistry for Arginase 1, 20x **C-D** Immunohistochemistry for iNOS, 20x. **E-F.** Immunohistochemistry for MARCO, 20x. Pneumocystis lungs are characterized by an increase of intra-alveolar Arginase 1+ and iNOS+ round MoMΦs and a decrease of MARCO+ round AMΦs.

Neoplastic conditions. Both the human synovial sarcoma xenograft and the fibrosarcoma syngraft were markedly infiltrated by MPS cells, mostly with overlapping results. Numerous

Iba1+ and F4/80+ classified as tumor associated macrophages (TAMs) were especially located in peri-necrotic intratumoral areas and at tumor periphery. F4/80 staining could not be evaluated in the murine fibrosarcoma syngraft due to over-fixation of the examined sample. Numerous spindle to polymorphic CD206+ cells, at tumor periphery and Arginase 1+ cells in the bulk of the tumor as well as variable amount of HO-1+ cells were observed in both conditions while no MHC-II+ cells and no to rare INOS+ cells were identified (Figure 18, A-F, Figure 19, A-F). Based on these results, both tumors were characterized by a tumor permissive microenvironment populated by numerous alternatively activated M2 macrophages and few pro-inflammatory M1 macrophages. Furthermore, Arginase 1 was expressed by round, spindle, and stellate cells with similar distribution to Iba1+ TAMs although they could represent Myeloid derived-suppressor cells (MDSCs) which are known to express Arginase 1 in the tumor microenvironment (Hirohashi and Sato, 2011).

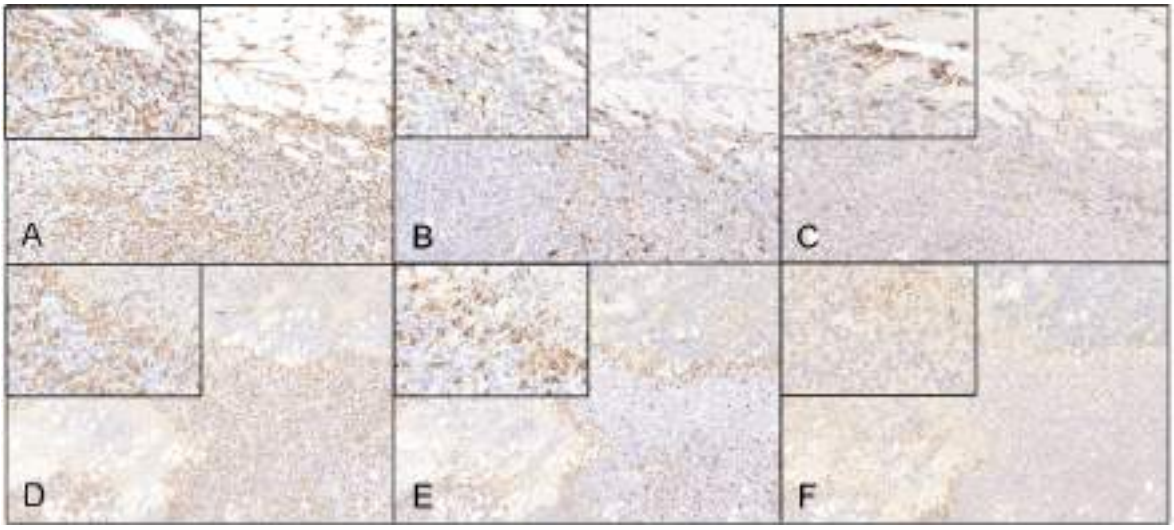

Figure 18. Murine fibrosarcoma syngraft. **A, B, C**. Tumor periphery. **D, E, F**. Tumor bulk and peri-necrotic areas. **A, D**. Immunohistochemistry for Iba1, 20x. **B, E.** Immunohistochemistry for Arginase 1, 20x **C. F.** Immunohistochemistry for CD206, 20x. **Insets**, 80x. Innumerable spindle to stellate Iba1+, numerous spindle CD206+ and Arginase 1+ M2 oriented MoMΦs at the periphery of the mass and innumerable Iba1+ polymorphic TAMΦs, numerous arginase 1+ stellate and rare stellate CD206+ TAMΦs in the bulk of the tumor and around necrotic areas are visible.

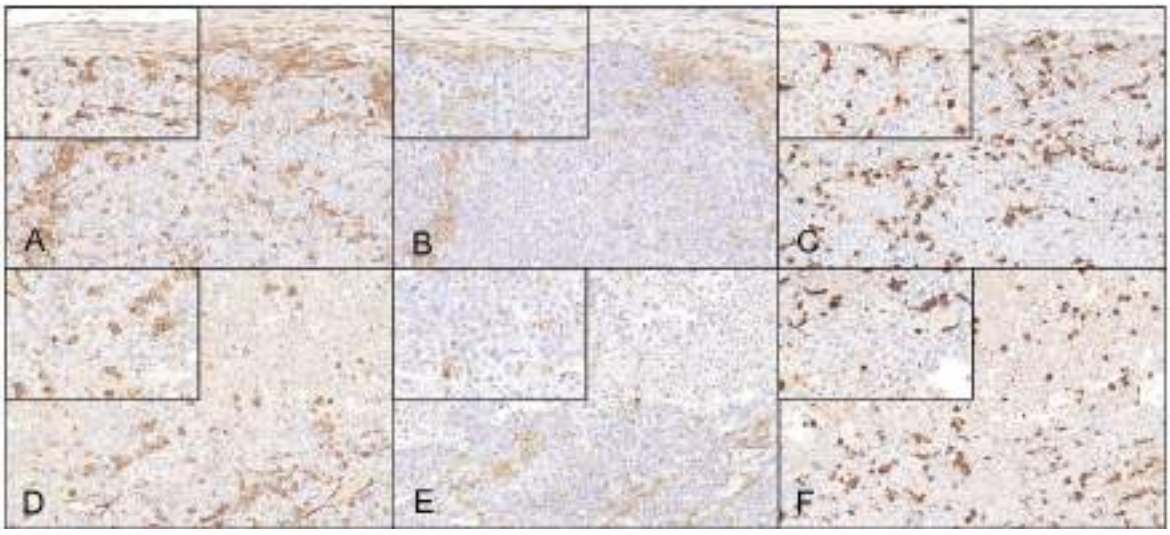

Figure 19. Human synovial sarcoma xenograft. A-F. Human synovial sarcoma xenograft. **A, B, C.** Tumor periphery **D, E, F.** Tumor bulk and peri-necrotic areas. **A, D**. Immunohistochemistry for Iba1, 20x. **B, E.** Immunohistochemistry for F4/80+, 20x **C. F.** Immunohistochemistry for Arginase 1. 20x. **Insets**, 80x. Innumerable Iba1+ spindle TAMΦs, numerous F4/80+ and moderate number of CD206+ polymorphic TAMΦs at the tumor periphery and numerous polymorphic Iba1+, F4/80+, Arginase 1+ cells are visible in the tumor bulk and perinecrotic areas. In the proximity of the necrotic tissue, positive cells tend to assume a round morphology.

3.4.3 MPS markers

Iba1 marked the highest number of MPS cells in almost all the examined tissues, occasionally more numerous than **F4/80**, the other pan-macrophagic marker, with the notable exception of alveolar macrophages, which were F4/80+/Iba1. Initially considered a microglia specific marker, Iba1 has been found useful to generally detect macrophage subpopulations in tissues (Kohler et al. 2007). More recently its expression has been detected also in cDCs and MoDCs, even though only CD11c was investigated as marker of DCs in these studies; since CD11c can also be expressed by monocytes and macrophages, there is still no definitive conclusion about the identification of DCs by Iba1 (Elizondo et al. 2017; Elizondo et al 2019;). Although F4/80 has been found expressed by a small fraction of DCs, DCs positivity could explain why Iba1 was able to detect more cells compared to F4/80 (Elizondo et al 2019; Vermaelen et al. 2004). Iba1 and F4/80 were able to identify numerous MPS cells in all pathological conditions, but it was not possible to evaluate F4/80 expression in the pneumocystis-infected lungs and in the murine fibrosarcoma syngraft, presumably due to over fixation of the samples. In fact, according to the authors' experience, despite the application of enzymatic epitope retrieval, F4/80 antigen is particularly affected by over-fixation. Furthermore, no peri-necrotic F4/80+ cells were observed in the hepatitis case (while F4/80+ Kupffer cells were present), possibly due to necrosis-related effects on F4/80 antigenicity.

MARCO, a class A scavenger receptor, was able to detect a subset of periportal and midzonal Kupffer cells, splenic MZMΦs, lymph nodal SCMΦs and MSMΦs, lung AMΦs and medullary ThyMΦs in steady state conditions. While MARCO+ Kupffer cells, splenic MZMΦs and alveolar MΦs are involved in blood-borne antigen clearance, MARCO+ lymph node subcapsular and medullary macrophages are specialized in lymph-borne antigen recognition (Arredouani et al 2004; Gray and Cyster, 2012). MARCO expression has been reported in the murine thymus but, to the author's knowledge, no immunohistochemical investigation has been carried out (Milne et al. 2005). MARCO+ ThyMφs or thymic MoMφs could be involved in apoptotic debris clearance. Interestingly we noted an increased number of MARCO+ Kupffer cells in sinusoids adjacent to the necro-suppurative foci in the hepatitis case and a reduction of MARCO+ AMΦs in the pneumocystis infection sample, suggesting an increase in antigens uptake in the liver and a decrease of AMΦs in the affected lung, possibly related to the recruitment of monocyte-derived MΦs or of pulmonary IMΦs with loss or substitution of the pre-existing AMΦs.

The enzyme **Arginase 1** is a marker of alternatively activated M2 macrophages, despite being also expressed by hepatocytes and cells of myeloid lineage, including neutrophils and myeloid-derived suppressor cells (MDSCs) (Yang and Ming 2014; Barron et al. 2017; Rodriguez et al 2013). Our study confirms the presence of Arginase 1+ hepatocytes and myeloid cells. Based on morphology it was possible to discriminate between granulocytes (i.e. small round cells with polylobate nuclei) and mononuclear phagocytes (i.e. large cells up to 20 μm in diameter with round to oval nuclei with variable morphology ranging from round to spindle/stellate). In general, Arginase 1+ large round cells were found in several organs and occasionally in blood vessels lumen representing MΦs and circulating monocytes respectively. Despite not being characteristic of any specific MPS subset, Arginase 1 positivity combined with cellular morphology, made it possible to speculate on the M2-like function of positive cells in the examined organs. Numerous stellate to polymorphic arginase 1+ cells both at the periphery and in the bulk of the examined tumors as well as numerous arginase 1+ round cells in the alveoli of the pneumocystis infected lungs and stellate cells in the peri-necrotic areas of the hepatitis case were detected, again reflecting their M2-oriented phenotype in these pathological conditions as well as, their possible role as MDSCs in the tumor microenvironment (Hirohashi and Sato, 2011).

Ym1 (Chil3), a rodent-specific chitinase-like protein, is constitutively expressed by some subsets of MΦs such as AMΦs and splenic macrophages and is induced in a vast range of pathological conditions including autoimmune diseases or fungal and parasitic infections (Roszer et al. 2005; Kang et al. 2022). In the mouse, it is considered a marker of M2 MΦs, but it is also expressed by monocytes and by mature and immature neutrophils (Shibuya et al. 2021; Kang et al. 2022). In general, we detected rare positive round monocytes in blood vessels and few positive round to spindle Ym1+ cells in most of the examined organs except for pancreas. As expected, Ym1 was expressed by splenic RPMΦs and by numerous myeloid precursors and by AMΦs in the lungs in steady state conditions. Numerous Ym1+ intra-alveolar macrophages were also found in the *Pneumocystis murina* infected lungs while only rare Ym1+ cells at the periphery or in the bulk of the examined tumors and occasional Ym1+cells in both the perinecrotic and peripheral layers in the hepatitis cases were detected.

CD206 also known as Macrophage Mannose Receptor (MMR), is a glycoprotein involved in pathogen phagocytosis expressed by MΦs, DCs, lymphatic and endothelial cells and glomerular mesangial cells and considered a marker of M2 polarization (Azad et al. 2014; Linehan et al. 1972, Tizard 2018). Our results highlighted the presence of round or stellate/spindle CD206+ cells in various organs representing either tissue resident or

MoMφs, most likely with M2 functions. CD206+ cells were abundant in neoplastic conditions, particularly at the periphery of the masses, and absent in the necro-suppurative hepatitis sample. In the lungs rare to moderate CD206+ were identified, with only minor differences between healthy and pathological conditions, particularly related to a higher number of CD206+ cells in peribronchial and perivascular regions of healthy lungs.

MHC-II is essential for antigen presentation to T cells and is expressed by antigen-presenting cells, namely DCs, MΦs, and B cells although in the mouse, its expression has been observed in T cells, keratinocytes, and endothelial cells in steady state conditions and in various epithelial and stromal cells in inflammatory conditions as well (Tizard 2018; Kambayashi et al. 2014). MHC-II+ stellate cells were observed in most of the examined organs except for the heart and testis. Notably, MHC-II+ cells were markedly increased in the hepatitis sample and there was an increase of MHC-II+ cells in the pulmonary interstitium in the pneumocystis infected lung, while, interestingly, no MHC-II+ cells were identified in the neoplastic samples, possibly supporting a M2 polarization of the investigated TAMs. Notably, in the hepatitis case, MHC-II expression was also found in biliary epithelial cells: epithelial cells can, in fact, express MHC-II capturing and processing antigens as a non-professional APC (Schrumpf et al. 2015).

HO-1 is an inducible enzyme involved in HEME metabolization with a critical role in inflammation and iron homeostasis expressed by MΦs, DCs, regulatory T cells as well as tumoral stromal and neoplastic cells and considered a marker of alternatively activated M2 macrophages (Pae et al. 2003; Chaveau et al. 2005; Vijayan et al. 2018). Round to spindle HO-1+ cells were observed in liver, spleen, thymus, pancreas, lung and lymph nodes (particularly sinuses). Rare HO-1+ peri necrotic cells in the hepatitis case, rare to moderate numbers of HO-1+ cells at the periphery and in the bulk of the examined tumors, and numerous round HO-1+ cells in the alveoli of the lungs with pneumocystis infection were found, representing M2 oriented macrophages in all pathologic conditions investigated.

iNOS is expressed by pro-inflammatory M1 macrophages although it has been found expressed also in mature DCs and plays a fundamental role in host defense against pathogens (Xue et al. 2018). In steady state condition no iNOS expression was noted in the majority of the examined organs apart from round to stellate cells in the thymus medulla where the iNOS expression has been associated to APCs activity and apoptosis induction (Aiello et al. 2000; Wallace 2018) In contrast to healthy samples, iNOS+ AMΦs in the pneumocystis-infected lung and more numerous iNOS+ cells in the hepatitis samples were observed, while only

rare iNOS+ cells were detected in the syngeneic fibrosarcoma sample, exclusively at the periphery of necrotic areas.

3.5. Conclusions

This study presents some limitations, primarily related to its retrospective nature. The use of FFPE samples introduces, for instance, pre-analytical variables pertaining to fixation times or sample processing protocols that can influence the outcome of the immunohistochemical staining. It is worth noting, furthermore, that the markers used in this thesis were restricted to those designed for use on FFPE tissues. Other markers commonly employed for MPS cells characterization in flow cytometry such as CD11b, CX3CR1, CD14, CD16, Ly6C1, CD64, are only applicable to fresh samples, thereby limiting their applicability for immunohistochemistry. Additionally, unlike flow cytometry, where multiple markers can be assessed simultaneously in a single cell, immunohistochemistry typically allows the evaluation of only one marker expression at a time. Nonetheless, unlike alternative techniques, immunohistochemistry permits the assessment of cellular morphology and considers the spatial arrangement of cells, providing crucial insights into their location within tissue and their interactions with neighboring cells, hence, offering valuable clues regarding their functions.

The investigated organs covered the main body systems, comprising the most frequently evaluated parenchymal organs (lung, liver, kidneys) as well as lymphoid organs (spleen, thymus, lymph nodes). The central nervous system and the female reproductive tract were, instead, excluded from the study since the anatomic complexity of the first and the marked variability of the second, based on hormonal influences and cycle activity, would require dedicated studies. Given their importance, an immunohistochemical characterization of MPS cells in these organs remains crucial and should be implemented in future studies.

The application of both pan-macrophagic and MPS subset-specific markers highlighted the extreme heterogeneity and plasticity of MPS in murine tissues in steady state condition and in selected pathological conditions. The combination of morphology, tissue localization and immunohistochemical positivity has made it possible to differentiate different MPS cells in the examined organs and, in specific cases, to precisely identify MPS subsets such as Kupffer cells in the liver or MZMΦ and MMMΦs in the spleen.

Our data highlighted the morphological and immunophenotypic heterogeneity of the cells composing the MPS of the mouse. The broad immunohistochemical panel applied

allowed to differentiate MPS populations based on their microanatomical location, cellular morphology and immunohistochemical positivity to specific MPS markers and occasionally to precisely identify specific MPS subsets, providing valuable data on MPS cells in the tissue context.

4. STUDY II. SEX-DEPENDENT MODULATION OF CAERULEIN-INDUCED ACUTE PANCREATITIS IN C57BL/6J MICE: HISTOPATHOLOGICAL AND IMMUNOHISTOCHEMICAL CHARACTERIZATION

This study was conducted in collaboration with the Department of Pharmacological and Biomolecular science of the University of Milan. Application SEED 2019 – Linea 3 of the University Project for Research Support. Project title: Peritoneal macrophages: sex-dependent modulation of transcoelomic migration and tissue repair in a model of acute pancreatitis (MACROGENDER).

4.1. Introduction

Acute pancreatitis (AP) is a sudden life-threatening condition caused by release and activation of acinar enzymes leading to glandular self-digestion and to potentially fatal systemic inflammatory states (Drake et al. 2021, Roberts et al. 2017). AP prevalence worldwide is increasing, and it has been linked to numerous risk factors and etiologies in human patients such as smoke, alcohol consumption, gallstones, hyperlipidemia, hypercalcemia, drug reactions and trauma (Munsell et al. 2010; Majidi et al. 2017; Zheng et al. 2021).

Biomedical research has mainly relied upon animal models, particularly mice and rats, to get insights on different features of normal and diseased pancreas (Yang et al. 2020). Different mechanical and chemical AP murine models have been developed with supramaximal caerulein-induced AP being one of the most used models to investigate pancreatic inflammatory conditions (Silva-Vaz et al. 2019, Yang et al. 2021). This cholecystokinin analogue oligopeptide induces pancreatic acinar enzymes release causing a self-limiting dose-dependent AP (Niederau et al. 1985; Shi-Ping et al. 2003).

Although the exact chain of events occurring after caerulein stimulation has not been fully elucidated yet, it has been demonstrated that this molecule causes pancreatic trypsinogen activation which rapidly leads to ROS formation, NF-kB and intrinsic apoptosis pathways activation, and DAMPs release with subsequent immune cells recruitment, immune cells PRRs-mediated activation, and cytokines production (Lerch et al. 2013, Kim et al. 2008; Watanabe et al. 2017). Both innate and adaptive immune cells play a role in pancreatitis pathogenesis and macrophages appear to be key players as they are involved in both the development of acute inflammation as classically activated (M1) macrophages and in the

reparative response as alternatively activated (M2) macrophages in more advanced phases of inflammation (Watanabe et al. 2017; Hu et al. 2020; Peng et al. 2021). The subsequent pancreatic regeneration is unique among the body organs and occurs through a process known as acinar to ductal metaplasia (ADM) in which damaged acinar cells de-differentiate into ductal like precursors expressing cytokeratin-19 (CK19), which are then capable of proliferation and differentiation to form new acini, re-establishing the normal pancreatic architecture (Murtaugh et al. 2015).

In the last decades, sex has been extensively recognized as an important biological variable modulating both physiological and pathological processes in different organs, including pancreas (Lopes Ramos et al. 2020; Gay et al. 2021; Wang et al. 2021). Although the overall incidence of pancreatitis seems not to differ significantly between sexes in humans, the rate of some forms of pancreatitis as well as pancreatic related mortality was reported to be higher in males compared to females, with estrogens proposed as potentially protective hormones in premenopausal women (Drake et al 2021, Wang et al. 2021). Studies investigating the role of sex in AP resulted in contrasting results, with some studies highlighting sex-dependent differences in pancreatitis extent and severity and others failing to detect such differences (Obafemi et al. 2018; Rao et al. 1982; Kubat et al 2013; Hagen et al. 2022; Diakopoulos et al. 2015). More investigations into the sex-related differences of AP and chronic pancreatitis are needed to improve prevention, clinical management, diagnostics, and therapeutics.

The aim of this study was, therefore, to investigate sex-dependent differences in pancreatitis development and subsequent resolution in a mouse model of caerulein-induced AP in C57BL6/J mice through a combination of clinical chemistry, histopathology, immunohistochemistry, and digital image analysis.

4.2. Materials and Methods

4.2.1. Animals

The use of animals in this study was approved by the internal organism for animal welfare of the University of Milan and by the Italian ministry of Health (authorization number 970/2020-PR). A total of 36 (19 females and 17 males) C57BL/6J mice of 4 months of age were purchased from Jackson laboratories (France) and housed at the animal facility of the Department of Pharmacological and Biomolecular Sciences at the University of Milan.

Animals were allowed to food and water access *ad libitum* and kept in temperature-controlled facilities on a 12-hours light and dark cycle.

4.2.2. Pancreatitis induction

Mice were injected intraperitoneally with PBS (vehicle) (14 mice) or 70 µg/kg of caerulein (Sigma-Aldrich C9026) (20 mice) every hour for 8 times a day, for 2 consecutive days. (Gitto et al. 2022) Mice were sacrificed 12 hours, 2 days, and 7 days after the last injection. After general anesthesia induction through xylazine and ketamine subcutaneous administration (6 and 78 mg/kg, respectively), blood was collected through intra-cardiac puncture using a 23 G needle. Mice were then sacrificed through cervical dislocation. Two non-manipulated control mice were also included in the study and sacrificed after 12 hours together with treated animals (Table 1). All mice were weighted daily before and after treatment until sacrifice.

Table 1. Summary of treatment group

TIME POINT	GROUP	M	F	TOTAL MICE
Not manipulated	Not manipulated	1	1	2
12 Hours	Vehicle (PBS)	3	3	6
	Caerulein	3	4	7
48 Hours	Vehicle (PBS)	2	2	4
	Caerulein	3	3	6
7 Days	Vehicle (PBS)	2	2	4
	Caerulein	3	4	7
TOTAL MICE	\	**17**	**19**	**36**

4.2.3. Clinical chemistry

Cardiac blood samples were collected in plain tubes (Eppendorf, Germany, Hamburg) and left to incubate for 30 minutes at room temperature to allow clot formation. Subsequently samples were centrifuged for 10 minutes at 2000 x *g at* 4°C (Eppendorf centrifuge 5415R, Eppendorf, Germany, Hamburg) and the harvested sera were then frozen at −20 °C until analysis. Glucose concentration (GOD-POD method) and amylase (CNP-G3 method) and lipase (DGGR method) activity were measured on sera with an automated spectrophotometer (BT3500, Biotecnica Instruments s.p.a. Rome, Italy) using reagents provided by the manufacturer of the instrument. Quality control procedures were performed before each

analysis with two levels of human based control sera (Control serum N and Control serum P) and with a human based calibrator (Multicalibrator) provided by the manufacturer of the instrument. To reduce the analytical variability of results, analyses were performed in batch within 10 days from sampling.

4.2.4. Histopathology

At sacrifice, pancreas was dissected from the duodenum, fixed in 10% neutral buffered formalin for 24 hours at room temperature, routinely processed for paraffin embedding, sectioned at 4 μm thickness, and stained with hematoxylin and eosin (H&E).

Pancreas sections were evaluated according to a newly designed semi-quantitative grading system reported in Supplemental Table 16. The examined findings included interstitial edema, interstitial inflammatory cell infiltration, acinar cell apoptosis, ADM, and pancreatitis extent, with a score ranging from 0 to 4 based on increasing severity.

A total pancreatitis histological score was then calculated by adding together the interstitial edema, interstitial inflammatory cell infiltration, and apoptosis scores and multiplying the sum by the pancreatitis extent score.

4.2.5. Immunohistochemistry

The following primary antibodies were applied: Iba1, F4/80, CD206, HO-1, MHC-II, B220, CD3ε, Ly6G, Cleaved-caspase 3 and CK19. Details on the applied antibodies is reported in supplemental Table 1. For all markers, except for F4/80, 4 μm sections of pancreas underwent deparaffinization and heat induced epitope retrieval (HIER) in a water bath for 40 min at 100°C (Dewax and HIER Buffer H, Thermo Scientific Lab Vision, cat. No. TA-999-DHBH). For F4/80 staining, slides were deparaffinized, rehydrated, rinsed in PBS, and unmasked with 1% trypsin (Sigma-Aldrich, T1426) for 30 minutes at 37°C. All slides were rinsed in PBS and placed in an autostainer (Lab Vision® Autostainer 480S-2D Thermo fischer scientific) after application of PAP pen (Liquid Daido Sangyo Co.,Ltd.). Endogenous peroxidase activity was blocked by incubating sections with 3% H_2O_2 for 10 minutes. Slides were rinsed, incubated with PBS containing 10% normal goat serum (IBA1, CD206, HO-1, Cleaved caspase-3, CK19) or 10% normal rabbit serum (F4/80, CD3e, B220, Ly6G, MHC-II), for 30 min at room temperature to prevent nonspecific background staining and subsequently incubated for 1 hour at room temperature with primary antibodies (supplemental Table 2). Sections were rinsed in PBS and incubated with a biotinylated

secondary antibody (goat anti-rabbit, Vector Laboratories, USA, cat. No. BA-1000 for Iba1, CD206, HO1, Cleaved caspase-3 and CK19; rabbit anti-rat, Vector Laboratories, USA, cat. No. BA-4001 for F4/80, B220, MHC-II and Ly6G; rabbit anti-goat Vector Laboratories, USA, cat. No. BA-5000 for CD3e) and labelled through avidin-biotin-peroxidase procedure (VECTASTAIN® Elite ABC-Peroxidase Kit Standard, Vector Laboratories, USA, cat. No.PK-6100). The immunoreaction was visualized with 3,3'-diaminobenzidine substrate (DAB, Peroxidase DAB Substrate Kit, Vector Laboratories, USA, cat. No. SK-4105). Sections were counterstained with Mayer's hematoxylin, dehydrated in a graded alcohol series and coverslipped with resinous mounting medium. Adequate positive controls were used for all markers.

All slides were digitalized in 40x high resolution mode (0.23 µm x pixel) through the NanoZoomer-XR Digital slide scanner (Hamamatsu, C12000) at the Unitech Nolimits facility (UNIMI, Milano) and were visualized using the NDP.view2 Viewing software (Hamamatsu, U12388-01).

4.2.6. Digital image analysis

The total pancreatic area and the pancreatitis area (i.e. area affected by pancreatitis) were manually outlined excluding peri-pancreatic adipose tissue, pancreatic lymph nodes and fat associated lymphoid clusters, using QuPath software (Bankhead et al. 2017). The percentage of pancreatitis area to total pancreas area was then calculated.

In sections immunostained with Iba1, F4/80, CD206, HO-1, MHC-II, B220, CD3ε and Ly6G, positive cells were detected using the positive cell detection function of QuPath, running a single threshold analysis after optimizing nucleus parameters, intensity parameters and reducing cellular fragmentation by modifying sigma and median filter radius parameters. Data were exported in excel and, for each marker, the number of positive cells per mm^2 of total pancreas area and the number of positive cells per mm^2 of pancreatitis area were calculated.

For cleaved caspase-3 and CK19, positive area was calculated after running a color deconvolution through the pixel classifier tool (create thresholder function). A threshold that could avoid non-specific signals was set and the positive area calculated. Data were exported in excel and the percentage of positive area per total pancreatic area and positive area per pancreatitis area for each marker was calculated.

4.2.7. Statistical analysis

Data were analyzed using Graph Pad Prism version 9.0 (GraphPad Software, San Diego, CA, USA). Non-manipulated and PBS (vehicle) treated animals were considered together as controls in the analysis since no differences were identified between the two groups. Shapiro-Wilk Normality test was performed to assess data distribution. Comparisons between the groups were performed using Mann–Whitney U test. P-values < 0.05 were considered statistically significant.

4.3. Results

4.3.1. Body Weight and clinical data

After the first day of injections, caerulein-treated animals showed moderate manifestations of pain, as demonstrated by orbital tightening, nose bulge, changed ear position and scruffy coat. Caerulein-treated mice were also less active compared to vehicle-treated animals. All these signs of pain were exacerbated following the second day of injections, at 12 hours; animal behavior was restored at 48 hours. No differences in pain levels and manifestation were observed between males and females.

A significative reduction in body weight was observed in both caerulein-treated male and female mice after the first day of injections compared to vehicle-treated and non-manipulated control mice. The body weight of caerulein-treated female mice returned to basal levels three days after the last caerulein injection, while the body weight of caerulein-treated male mice took longer to return to basal levels (6 days) (Figure 1). No significant changes were detected in the body weight of vehicle-treated and non-manipulated control animals at all the time points analyzed.

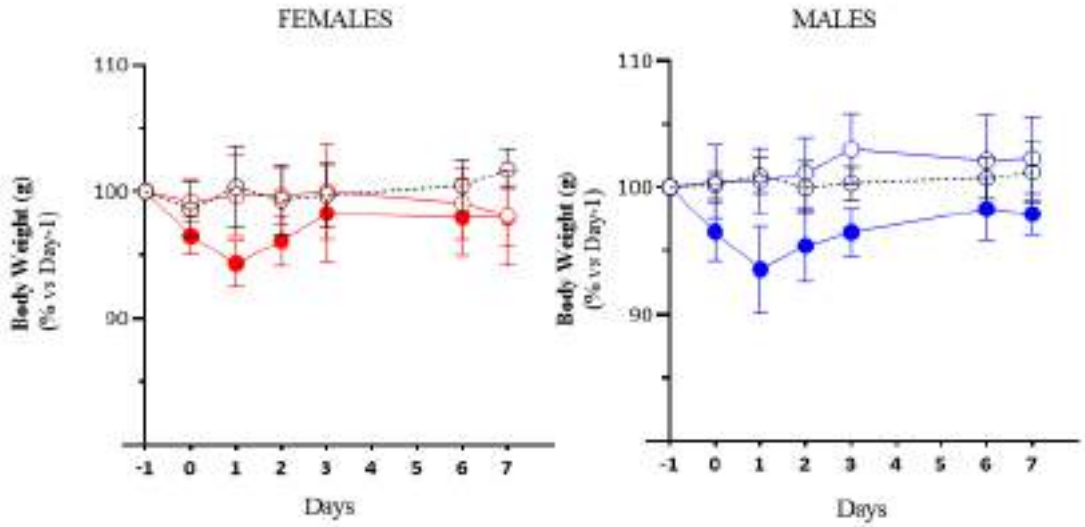

Figure 1. Female and male mice body weights expressed in % compared to day-1 weights.

4.3.2. Clinical chemistry

No significant differences were observed between male and female mice in glucose concentration and amylase and lipase activity. Pancreatic amylases were highest at 12 hours in both sexes as compared to vehicle-treated animals with a progressive return to basal levels at 48 hours and day 7.. No other significant differences were observed among time points and between treated and control mice (Figure 2).

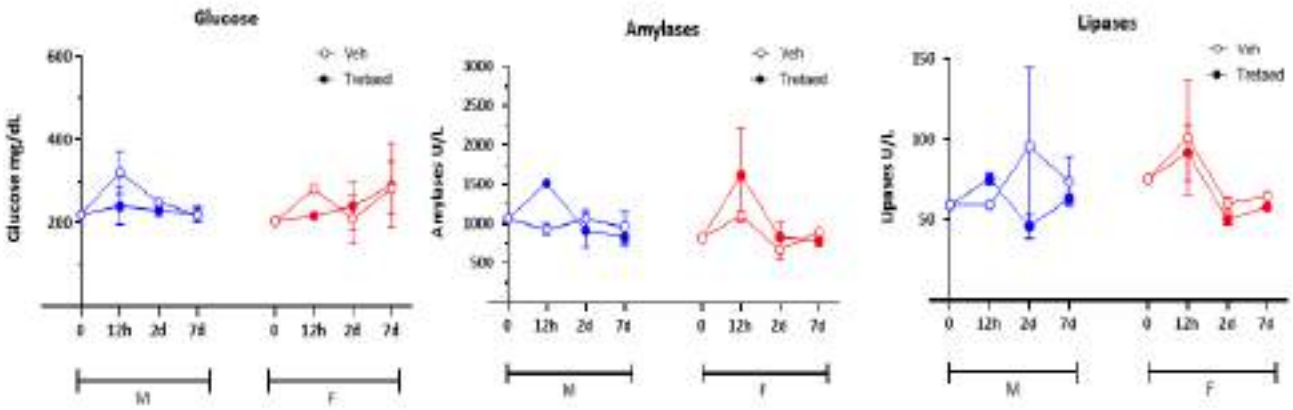

Figure 2. Glucose concentration and amylases and lipases activity in male and female mice.

4.3.3. Histopathology

Results of the histopathological evaluation are summarized in Table 3 and in Figure 4. Raw data is reported in Supplemental Table 17.

Lesions were identified in the pancreas of 20 out of 20 (100%) caerulein-treated mice at all examined time points (12 hours, 48 hours, 7 days), involving exocrine pancreas and interstitium but sparing the endocrine pancreas and ducts. No lesions were observed in non-manipulated control mice or vehicle treated mice.

Overall, pancreatitis was characterized by interstitial edema, interstitial infiltration of inflammatory cells, apoptosis of acinar cells and presence, particularly in later time points, of tubular-like structures resembling pancreatic ducts (consistent with ADM).

At 12 hours, in both sexes, there was moderate to severe interstitial edema with frequent individualization of pancreatic acini, interstitial infiltration of inflammatory cells mainly composed of macrophages and neutrophils admixed with rare lymphocytes and plasma cells, and rare apoptotic acinar cells. The extent of pancreatitis was higher in female mice than in male mice.

Table 2. Summary of semi-quantitative pancreatitis evaluation. Results are expressed as median values. N: neutrophils, M:macrophages, L: lymphocytes, P: plasma cells. Total pancreatitis histological score was calculated as the sum of Edema, Interstitial infiltrates and Apoptosis scores multiplied per the Extent score. ADM was not used to calculate total score since it was considered part of the healing process.

Group	Time Point	Number	Sex	Edema	Interstitial Infiltrates	Inflammatory Cell types	Apoptosis	ADM	Extent	Total pancreatitis Histology Score
Not Manipulated	12 hours	1	M	0	0	n/a	0	0	0	0
		1	F	0	0	n/a	0	0	0	0
Control	12 hours	3	M	0	0	n/a	0	0	0	0
		3	F	0	0	n/a	0	0	0	0
	48 hours	2	M	0	0	n/a	0	0	0	0
		2	F	0	0	n/a	0	0	0	0
	7 days	2	M	0	0	n/a	0	0	0	0
		2	F	0	0	n/a	0	0	0	0
Caerulein	12 hours	3	M	3	3	N, M, rare L and P	1	0	2	14
		4	F	2.5	3.5	N, M, rare L and P	0	0	3.5	21.5
	48 hours	3	M	2	3	N, M, rare L and P	4	2	2	18
		3	F	1	2	N, M, rare L and P	2	2	1	5
	7 days	3	M	0	1	M, L, P and rare N	3	3	1	4
		4	F	0	1	M, L, P and rare N	0.5	2	1	1.5

At 48 hours, interstitial edema decreased in both sexes, interstitial inflammatory cells and more numerous apoptotic figures involving both pancreatic acinar cells and recruited inflammatory cells, more numerous in males compared to females and early ADM were found (Figure 5, A, B and Figure 6, A, B)

At day 7 there was an almost complete recovery in both sexes with only residual scattered, patchy areas of pancreatitis characterized by fibroplasia, inflammatory mononuclear infiltration, residual apoptoses, (higher in males than in females) and, in the residual affected areas, presence of well- defined, neo-formed pancreatic ducts, slightly higher in males than female mice, indicative of ADM. (Figure 4 E, F, Figure 6, C, D)

Based on the total pancreatitis histological score, females reached a peak of pancreatitis severity at 12 hours followed by a progressive decrease at later time points and almost complete resolution at day 7, while, in males the peak of pancreatitis severity was delayed at 48 hours with residual lesions (mainly in terms of apoptosis) still detectable at day 7 (Figure 3 A).

Digital image analysis of the extent of pancreatitis confirmed that, at 12 hours, the % of pancreatitis area was increased in females compared to males (64% in females and 33% in males), while, at 48 hours, the extent of pancreatitis was higher in males compared to females (mean of 24% in males and 8% in females). No differences were identified at day 7 (2.70% in males and 2.53% in females) (Figure 3 B).

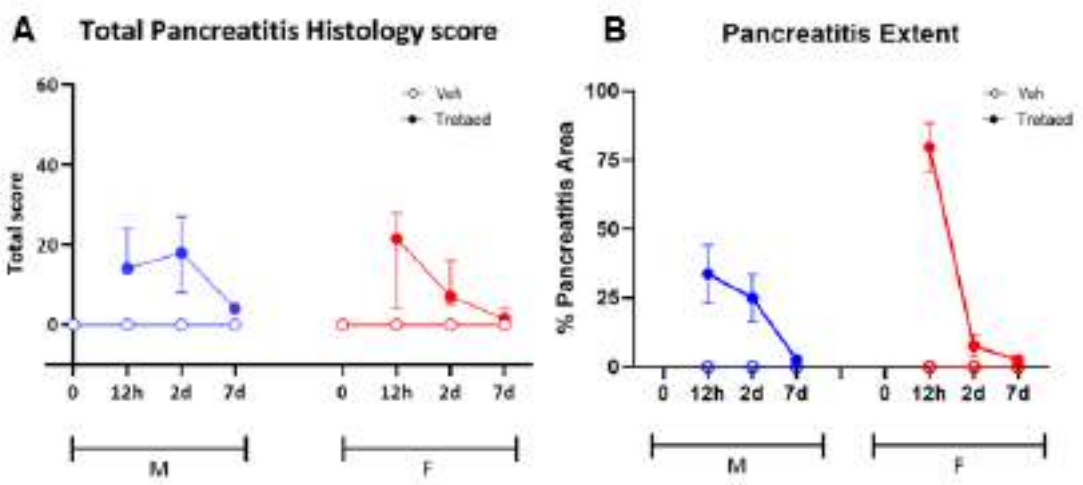

Figure 3. A. Total pancreatitis histology score B. pancreatitis extent (digital image analysis) in male and female mice. In male mice, the peak of pancreatitis was delayed as compared to female mice (48h and 12h, respectively). Digital image analysis revealed a higher pancreatis extent in female mice at 12 hours and a higher pancreatitis extent in males at 48 hours.

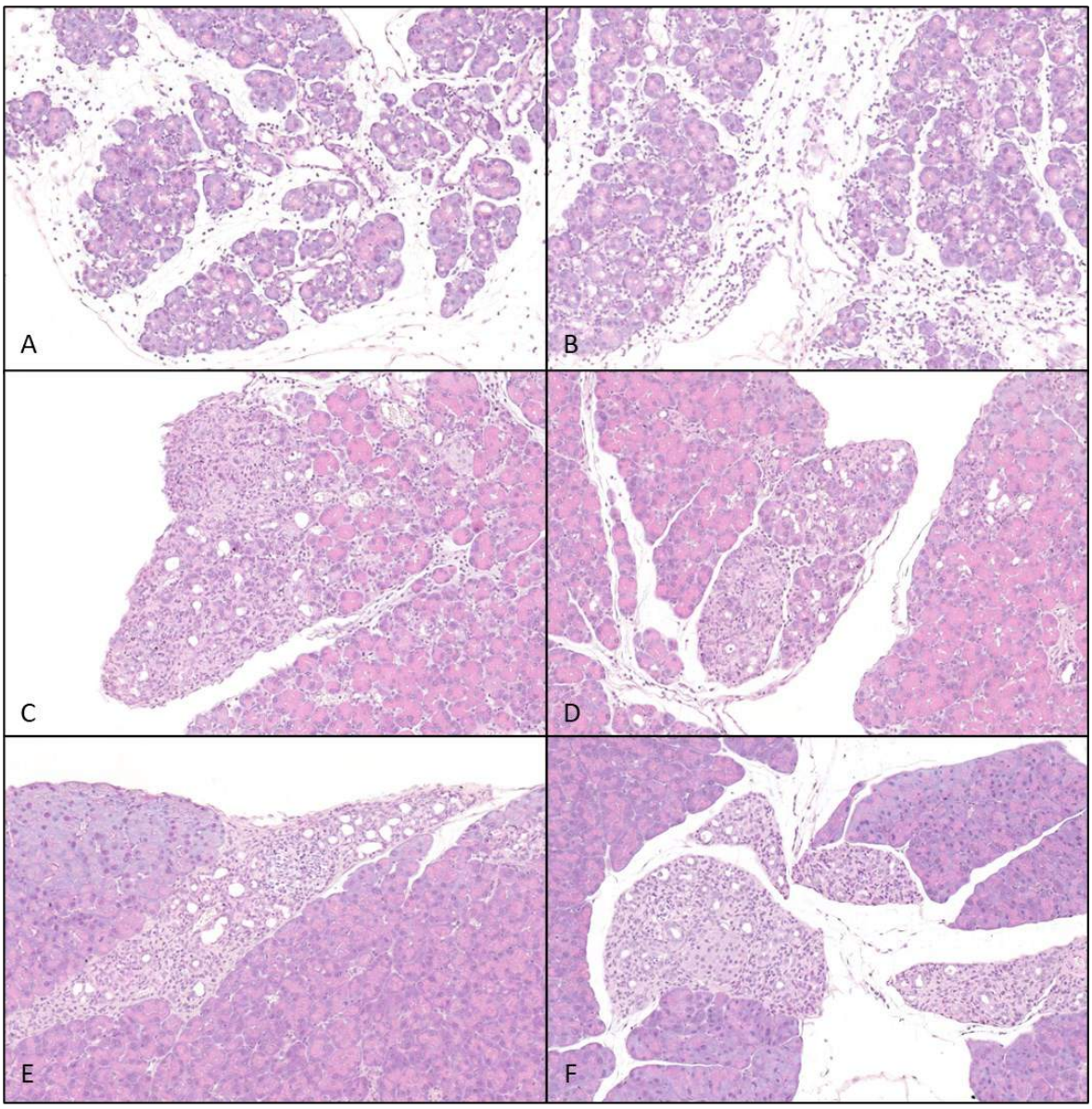

Figure 4. Caerulein-induce acute pancreatitis, mouse, Hematoxylin, and eosin (HE), 20x. **A, B.** Acute pancreatitis 12 hours after last caerulein treatment. Male mice (**A**) were characterized by lower interstitial inflammatory cells compared to female mice (**B**). **C, D.** Acute pancreatitis 48 hours after last caerulein treatment. Male mice had more extensive pancreatitis areas (**C**) compared to female mice (**D**). **E, F.** Acute pancreatitis 7 days after last caerulein treatment. residual areas of pancreatitis, characterized by fibroplasia and mononuclear inflammation were seen in both males (**E**) and females (**F**).

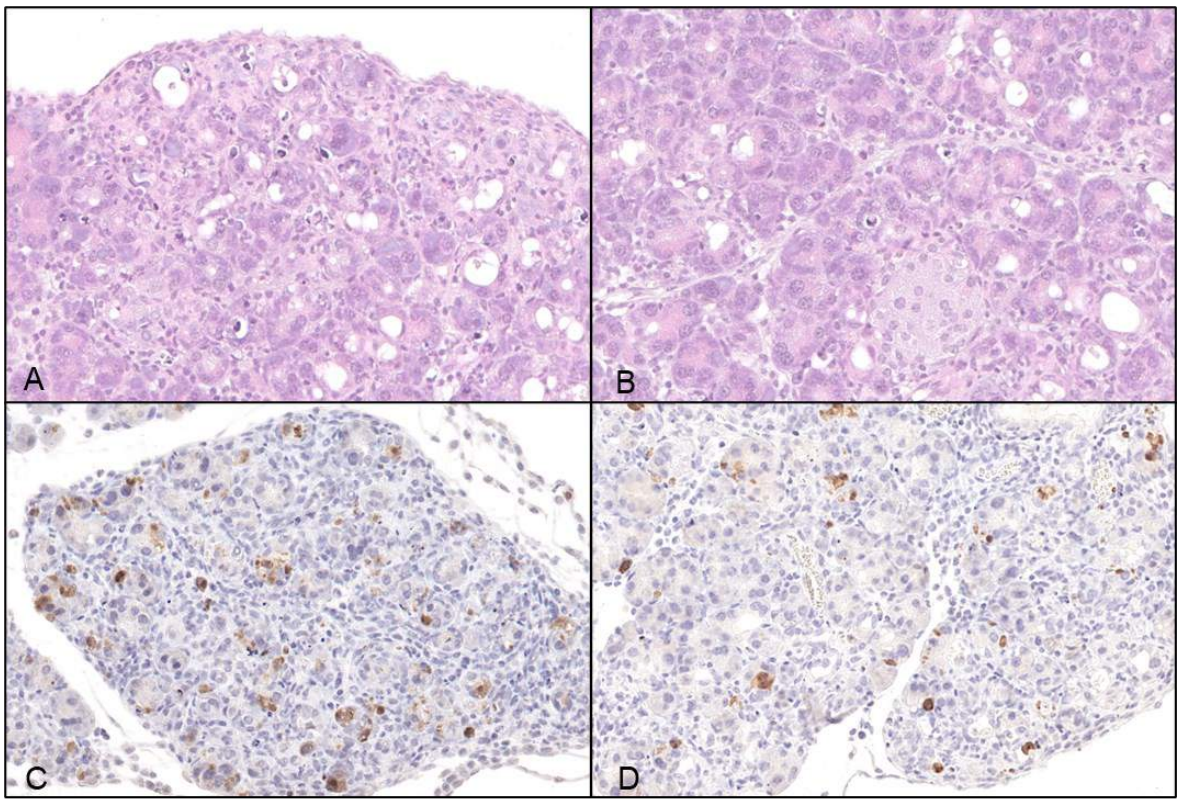

Figure 5. Caerulein-induced acute pancreatitis, mouse. **A, B.** Hematoxylin, and eosin (HE) **C-D**. Immunohistochemistry for cleaved caspase-3. More numerous apoptotic cells and cleaved caspase-3 positive cells were observed in males (**A, C**) compared to females (**B, D**) at 48 hours after last caerulein treatment.

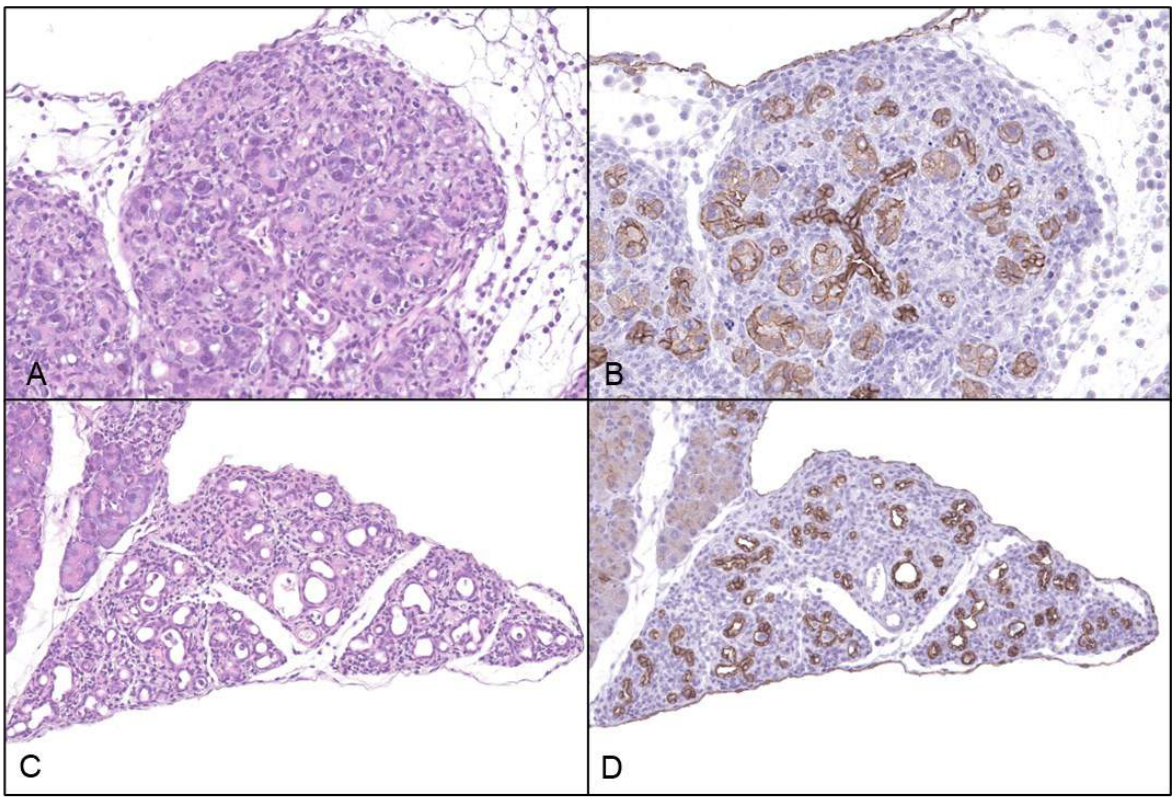

Figure 6. Caerulein-induced acute pancreatitis, mouse. **A, C.** Hematoxylin and eosin (HE). **B, D.** Immunohistochemistry for cytokeratin-19 (CK19). 48 hours after the last caerulein treatment, ill-defined ducts still resembling pancreatic acini and characterized by a mild expression of CK19 were evident (**A, B**). 7 days after the last caerulein treatment well defined, CK19 positive ducts, morphologically indistinguishable from normal intra and interlobular ducts were present (**C, D**).

4.3.4. Immunohistochemistry

Results of quantification by digital image analysis of immune cells, ADM (identified by CK19) and apoptosis (identified by cleaved caspase 3) performed on pancreatitis area and total pancreatic area are reported in Figures 7 and 8. Representative images are shown in Figures 5, 6, 9, 10 and 11.

The immunohistochemical analysis revealed that Iba1+ and F4/80+ macrophages were the most prominent inflammatory cell population in the pancreas of treated animals at all examined time points, infiltrating the pancreatic interstitium at 12 hours, 48 hours, and day 7. Rare CD3ε+ T cells and B220+ B cells were scattered in the interstitium at 12 hours and progressively increased at 48 hours and at 7 days in both sexes. Ly6G+ cells were rare in all time points in both sexes and showed a progressive decrease from 12 hours to day 7 (Figure 9).

Iba1+ and F4/80+ cells progressively increased from 12 hours to day 7 in pancreatitis areas with no statistically significant differences between sexes. When considering Iba1+ and F4/80+ positive cells on total pancreatic area, positive cells were characterized by a progressive decrease from 12 hours to day 7 and were higher at 48 hours in males compared to females although failing to reach a significant P value for both Iba1 and F4/80 (Figure 10).

CD206+ macrophages progressively increased from 12 hours to day 7 in males and increased at 48 hours followed by a mild decrease at day 7 in females, with males having higher CD206+ cells at 48 hours and day 7 (Figures 10 and 11). When considering CD206+ cells on the total pancreatic area a progressive decrease in both sexes were present with males having more CD206+ cells than females at 48 hours similarly to what observed for Iba1+ and F4/80+ cells, and at day 7

HO1+ macrophages in pancreatitis areas exhibited a different trend compared to CD206+ cells, with a progressive decrease of HO1+ cells from 12 hours to day 7 in males and a decrease at 48 hours followed by an increase at day 7 in females, without differences between sexes. When considering HO1+ cells on the total pancreatic area a progressive decrease of positive cells was observed in both sexes with males exhibiting more HO1+ cells at 48 hours compared to females.

MHC-II+ cells progressively increased from 12 hours to day 7 in both sexes, with a marked increase in males and a mild increase in females at day 7 (Figure 11). When considering the MHC-II+ cells on the total pancreatic area males were characterized by a

progressive increase from 12 hours to day 7 while females showed a progressive decrease of MHC-II+ cells.

CD3ε+ cells increased in both sexes from 12 hours to day 7 (Figure 9). When considering CD3ε+ cells on the total pancreatic area, females had higher T cell infiltration compared to males at 12 hours even though not statistically significant, and there was a progressive decrease at 48 hours and day 7 in males and a decrease at 48 hours followed by a mild increase in females at day 7, with no differences between sexes.

B220+ cells in pancreatitis area increased in both sexes from 12 hours to day 7, with slightly higher B220+ cells in females compared to males at day 7 (Figure 9). When considering the number of B220+ cells on the total pancreatic area, males were characterized by a mild increase at 48 hours followed by a decrease at day 7, while females were characterized by a higher concentration at 12 hours followed by a decrease at 48 hours and subsequent increase at day 7.

Ly6G+ cells decreased from 12 hours to day 7 in both sexes, with higher Ly6G+ cells in males compared to females at 48 hours (Figure 9). When considering the Ly6G positive cells on the total pancreatic area there was a progressive decrease from 12 hours to day 7, with males showing higher Ly6G+ cells compared to females at 48 hours. Interestingly, a moderate number of polymorphonucleated cells, morphologically consistent with neutrophils, were not stained by Ly6G marker.

Cleaved Caspase-3+ area increased at 48 hours and subsequently decreased at day 7 in both sexes with higher positive area in females at 12 hours and higher positive area in males at 48 hours and day 7. When considering cleaved caspase 3 positive area on total pancreatic area, females had higher % of positive area compared to males at 12 hours while males had higher positive area at 48 hours. No overt differences were observed at day 7 in both sexes.

Different patterns of CK19 expression were identified at 12 hours, 48 hours, and day 7 in treated animals. At 12 hours there was a diffuse cytoplasmic staining of mild intensity of pancreatic acinar cells with a higher % of positive area on total pancreas area and pancreatitis area in females compared to males. At 48 hours, CK19 was expressed by multiple, tubular-like structures resembling pancreatic ducts but lined by plumper cells and less intensely stained compared to normal intra and interlobular pancreatic ducts (Figure 6, B). There was a slightly higher % of CK19 positive area in females compared to males in pancreatitis area and higher CK19 positive area in males compared to females on total

pancreatic area. On day 7, CK19 stained numerous newly formed ducts indistinguishable from intra and interlobular pancreatic ducts, for morphology and staining intensity. There was a higher % of CK positive area on pancreatitis area in males compared to females, while no differences could be identified between sexes regarding % of positive area on total pancreatic area.

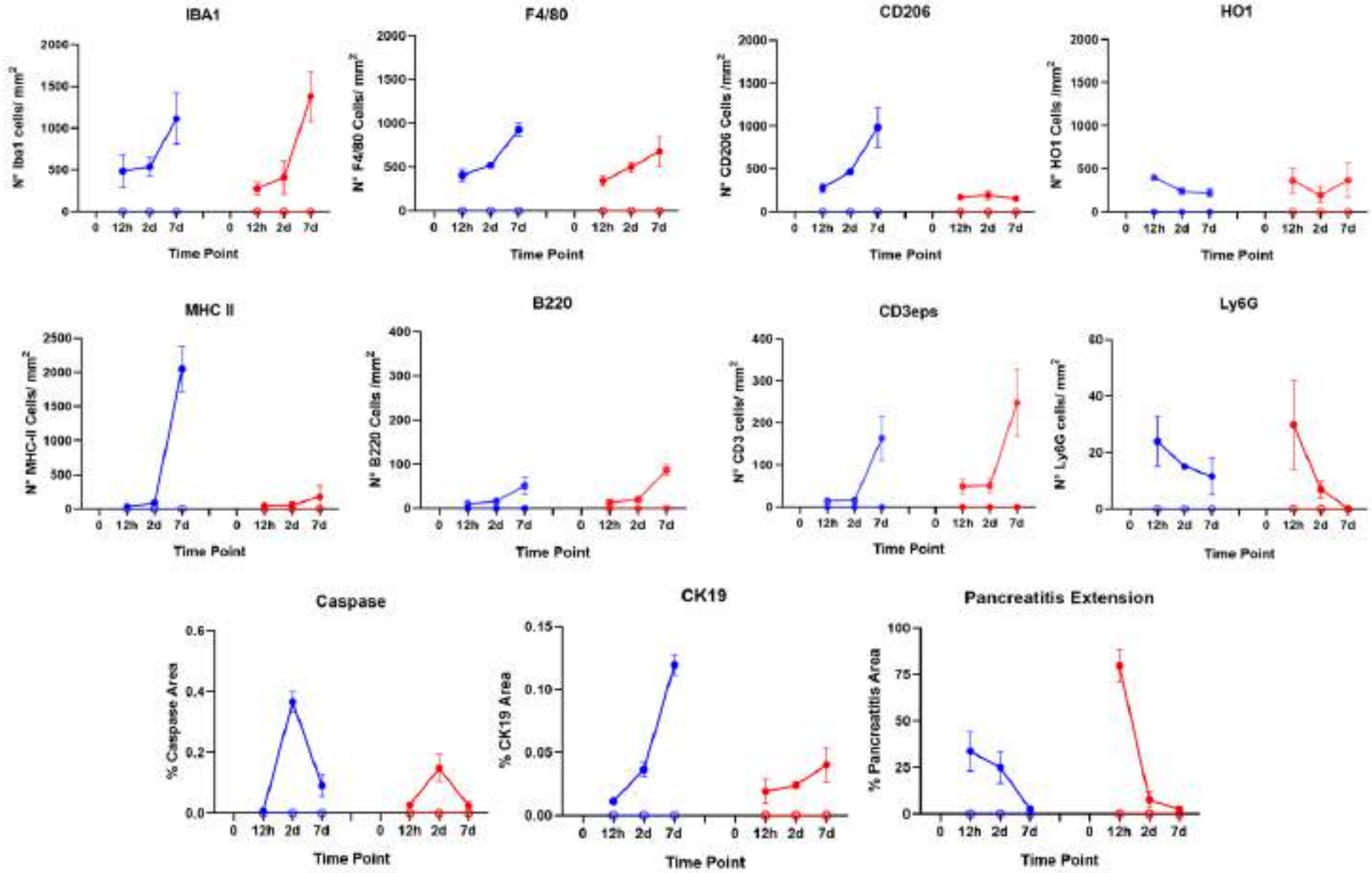

Figure 7. Graphs of positive cells and % of positive area on pancreatitis area.

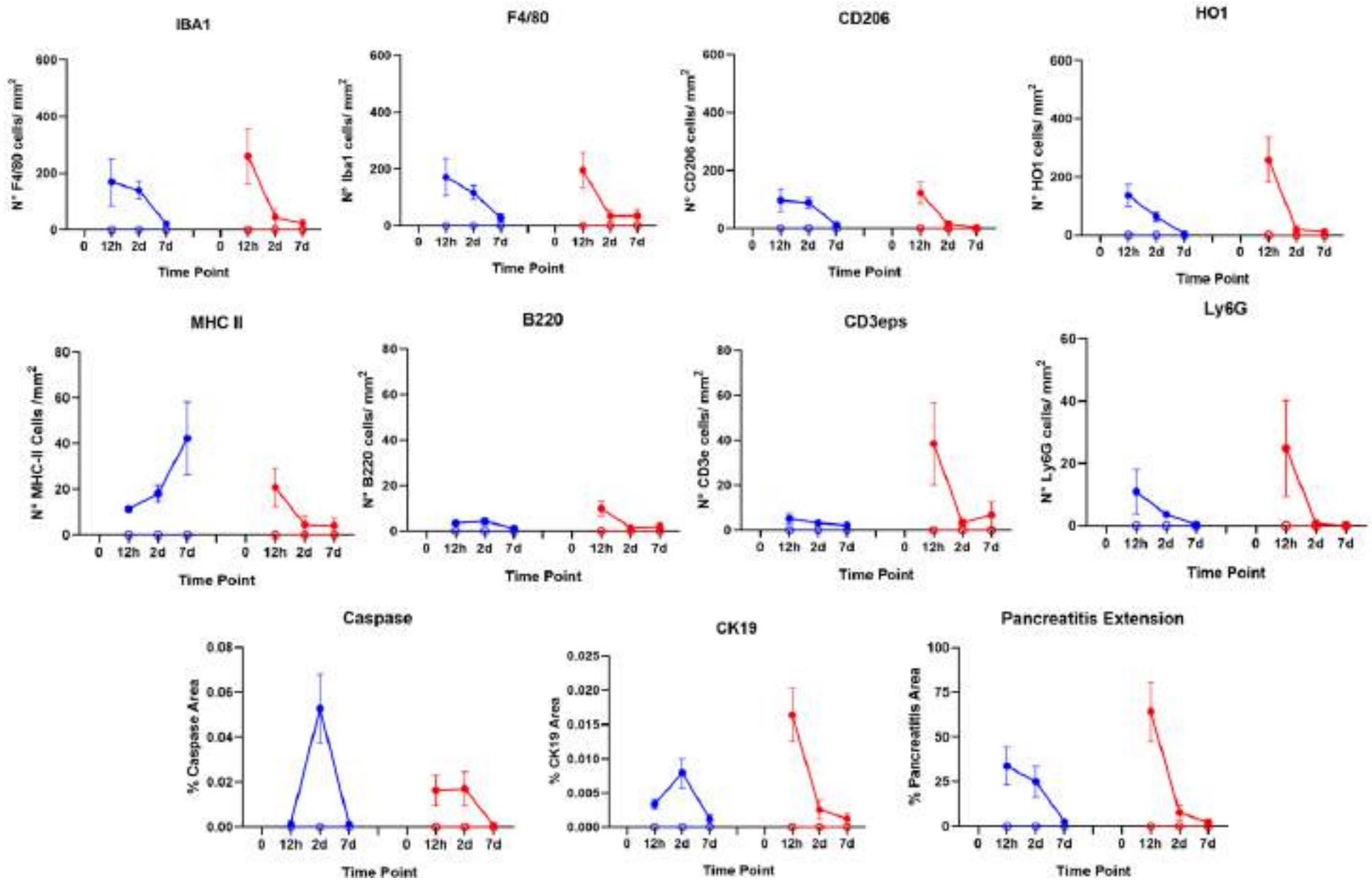

Figure 8. Graphs of positive cells and % of positive area on total pancreatic area.

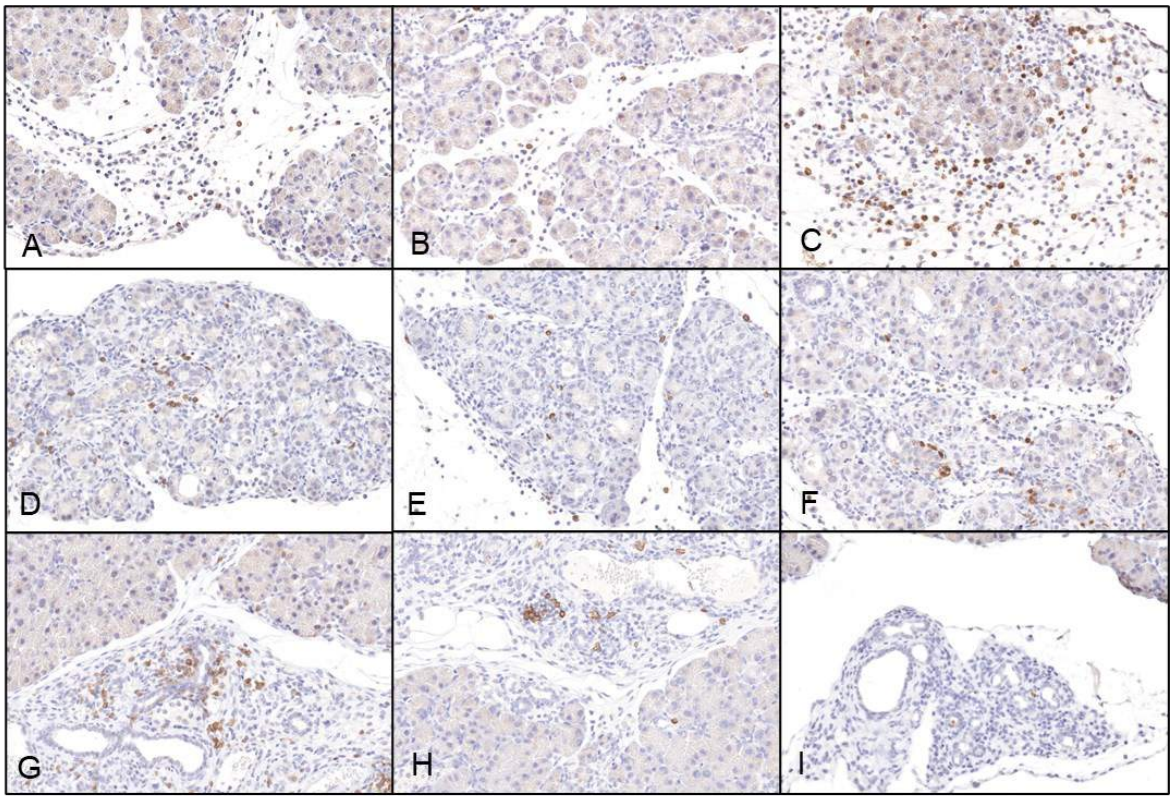

Figure 9. Caerulein-induced acute pancreatitis, mouse, immunohistochemistry for CD3ε (**A, D, G**), B220 (**B, E, H**) and Ly6G (**C, F, I**). T lymphocytes and B lymphocytes progressively increased from 12 hours to 7 days after last caerulein treatment. Neutrophils progressively decreased from 12 hours to 7 days after the last caerulein treatment.

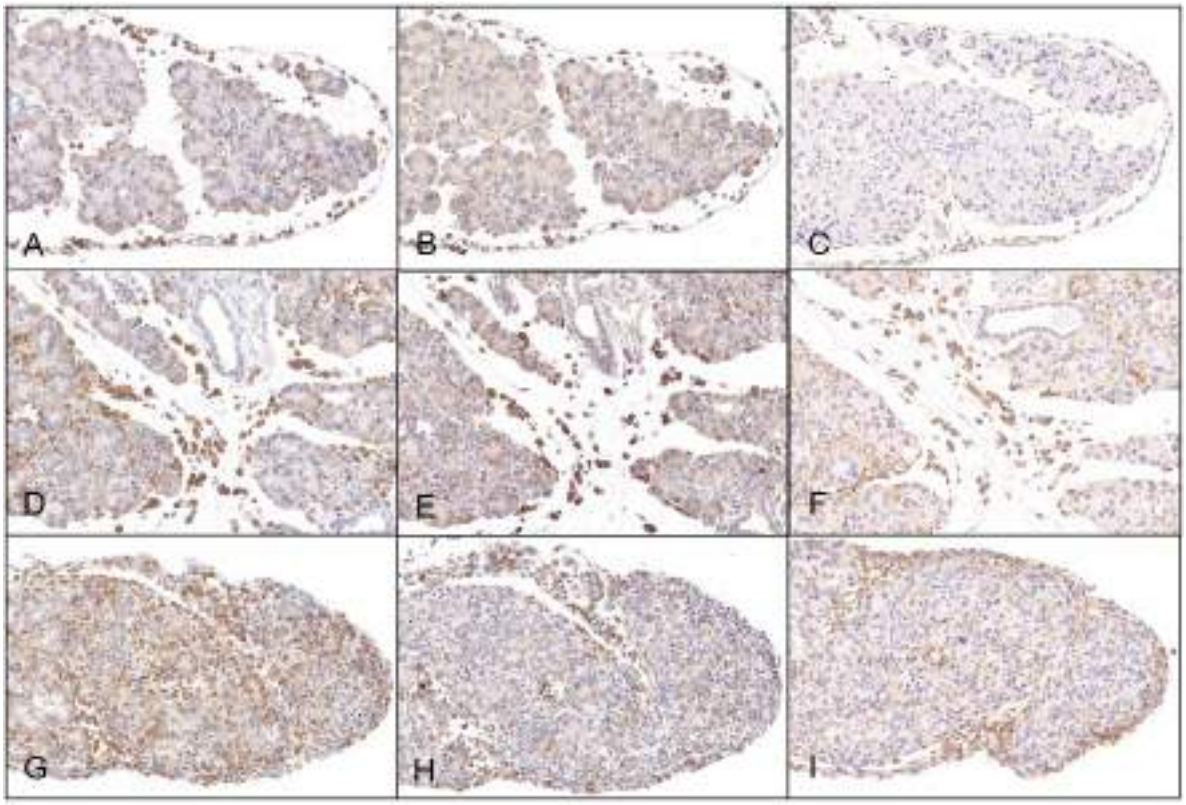

Figure 10. Caerulein-induced acute pancreatitis, mouse, immunohistochemistry for Iba1 (**A, D, G**), CD206 (**B, E, H**) and F4/80 (**C, F, I**). Iba1+, CD206+ and F4/80+ macrophages progressively increased from 12 hours to 7 days after the last caerulein treatment.

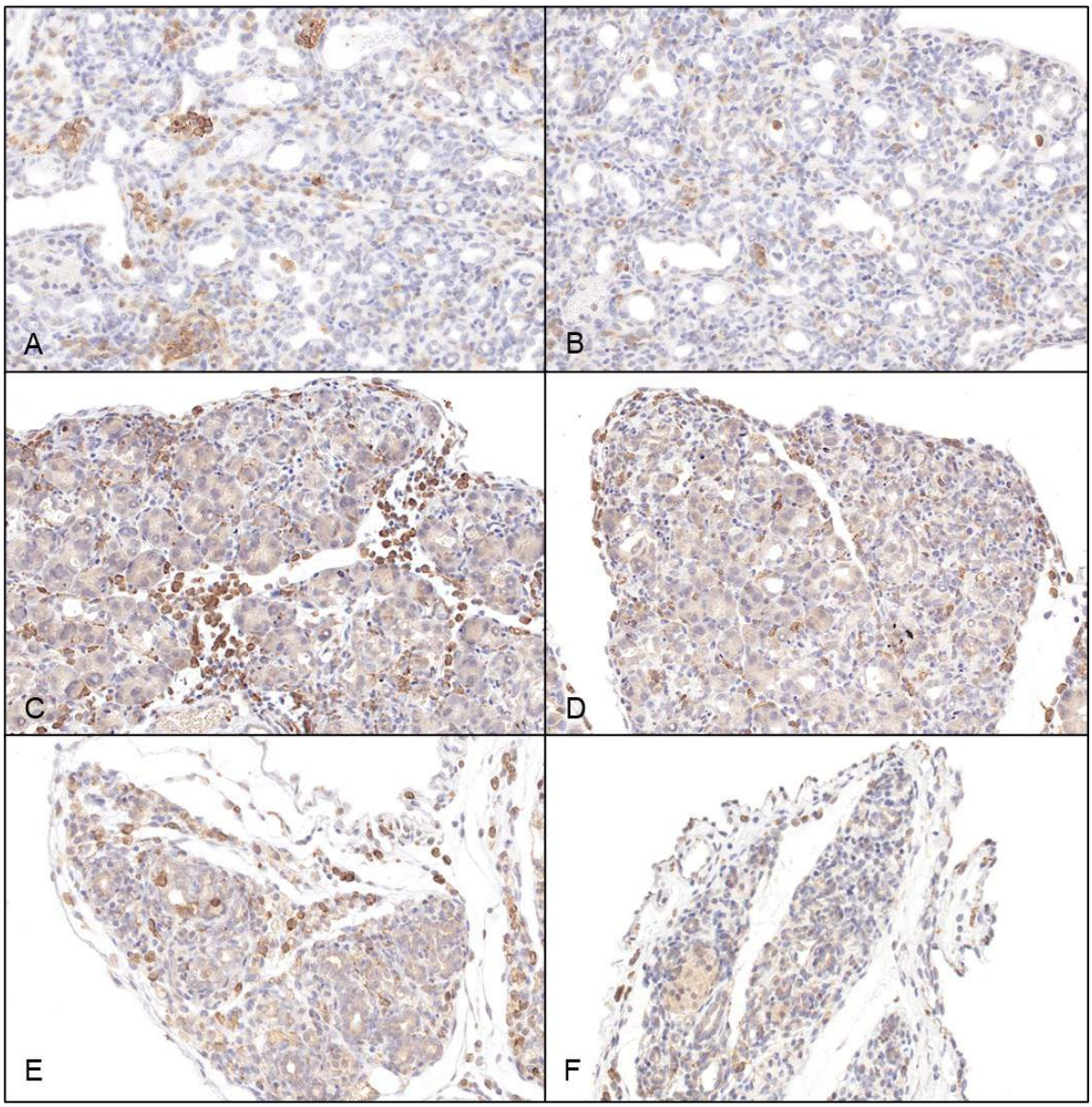

Figure 11. Caerulein-induced acute pancreatitis, mouse, immunohistochemistry for MHC-II (**A, B**) and CD206 (**C-F**). At 7 days after last caerulein treatment, male mice had more numerous MHC-II positive cells (**A**) compared to female mice (**B**). At both 48 hours (**C, D**) and 7 days (**E, F**) male mice had more numerous CD206+ macrophages (**C, E**) compared to females (**D, F**).

4.4. Discussion

The aim of the study was to investigate the role of gender in acute pancreatitis development and resolution through the application of clinical chemistry, histology, and immunohistochemistry in a murine caerulein-induced pancreatitis model.

Both clinical chemistry and histopathologic results were indicative of an acute pancreatic inflammatory process followed by a quick, almost complete resolution in a 7-day interval in both male and female mice. Peak of pancreatic amylases at 12 hours with return to baseline levels after 48 hours, similarly to previous reports, highlighted a very fast pancreatic damage followed by a quick resolution without sex-related differences (Altavilla et al. 2003; Norkina et al. 2006; Hashimoto et al. 2008). No significant differences were observed in glucose concentration between control and treated animals in both sexes, indicating a minimal impact of pancreatitis on glucose metabolism. The slight and transitory reduction of glucose concentration observed at 12 hours both in male and female treated animals could be a direct effect of caerulein on pancreatic endocrine activity, with enhanced insulin release, as previously reported in rodent's pancreas (Nielsen et al. 1981; Sakamoto et al. 1985).

Caerulein administration was previously demonstrated to cause a dose-related, time-dependent, self-limiting pancreatitis, histologically characterized by variable interstitial edema, interstitial neutrophilic and mononuclear cells infiltration, pancreatic acinar disarray, degeneration, apoptosis and ADM. Although differences in caerulein doses, administration protocols and evaluated time points exist in literature, lesions observed in our study are consistent with other published reports (Willemer et al. 1993; Norkina et al. 2006; Zhang et al. 2014).

Pancreatitis histological score in female mice resulted increased at 12 hours and decreased at 48 hours and day 7 compared to male mice, suggesting a faster onset and a faster resolution of pancreatitis in female mice. This is further supported by the higher expression of CK19 in females at early time points, indicative of a quicker or more efficient reparative process compared to males and by a lower presence of ADM in later time points, suggestive of an advanced reparative process in females compared to males. At day 7, both male and female mice in our study had residual pancreatic lesions in the form of acinar atrophy and macrophagic and lymphocytic inflammation. Although numerous studies on the caerulein induce model report a complete recovery of pancreatic architecture, residual lesions at day 7 have been reported by some authors and could be attributed to differences

in caerulein administration protocols and doses, caerulein commercial product specificities or even mouse strain used since strain-dependent susceptibility to caerulein effects has been recognized (Lugea et al. 2006; Norkina et al. 2006; Hashimoto et al. 2008; Hagen et al. 2022; Wang et al. 2010; Zhang et al 2017).

Few studies comparing male and female mice in caerulein-induced AP exist in literature, often focusing on knockout mice strains in specific experimental settings (Kubat et al. 2013; Hagen et al. 2022). A study comparing caerulein-treated male and female corticotropin-releasing factor receptor 2–deficient ($Crhr2^{-/-}$) mice showed that necrosis, polymorphonuclear cell infiltration and zymogen depletion were significantly increased in male $Crhr2^{-/-}$ mice, whereas only necrosis and acinar vacuolization were significantly increased in females compared to sex-matched wild type controls, thus hypothesizing a sex modulating role in pancreatitis pathogenesis (Kubat et al 2013). Hagen and colleagues demonstrated that female mice deficient in LAT1, an amino acid transporter involved in pancreatic metabolism, had delayed regeneration compared to male LAT1 deficient mice, hypothesizing a sexual influence on pancreatic amino acid metabolism (Hagen et al. 2022). A study using autophagy deficient Ptf1aCreex1;Atg5F/F mice demonstrated a lower incidence and severity of chronic pancreatitis in females compared to males, attributed to a higher efficacy of steroid-dependent ROS metabolism in female mice (Diakopoulos et al. 2015). Nevertheless, it is worth mentioning that a study investigating sex differences in a caerulein induced model of chronic pancreatitis in wild type C57BL/6 mice failed to detect differences in male and female mice regarding both disease severity and recovery (Obafemi et al. 2018).

Apoptosis has been recognized as an important protective mechanism against pancreatic oxidative stress-induced necrosis in the caerulein-induced pancreatitis model (Mareninova et al. 2006; Lugea et al. 2006; Kim et al. 2008; Boonchan et al. 2021). In our study, apoptosis of both acinar cells and interstitial inflammatory cells increased at 48 hours and subsequently decreased at day 7 in both sexes as reported in other studies (Zhang et al. 2017). However, our results revealed that males had more apoptosis than females at both 48h and day 7, suggesting a sex-modulation of apoptosis. An estrogen receptor-mediated inhibitory influence of estrogens on apoptosis pathways has been recognized in both acinar and innate and adaptive immune cells (Hilgendorf et al. 2001; Lewis-Wambi et al. 2009; Kovats 2015).

As pancreatic regeneration occurs through ADM, CK19, a marker of ductal differentiation, has been proven useful in the investigation of pancreatic regeneration and

post-inflammatory recovery (Storz 2017). At 12 hours, pancreatic acinar cells of both male and female mice were characterized by a diffuse slight cytoplasmic CK19+ staining. Since in controls no CK19 staining was observed at the level of acinar cells and CK19 mRNA expression was previously detected as soon as 12 hours after caerulein administration, the diffuse slight staining observed in pancreatic acinar cells was interpreted as an early CK19 expression by acinar cells (Hagen et al. 2022). Females showed higher CK19 expression compared to males, potentially suggesting a quicker or more efficient regenerative response. At 48 hours CK19 positive ill-defined ducts interpreted as acinar cells phenotypically transitioning to pancreatic ducts were stained, consistent with ADM, without relevant differences between sexes. At day 7, in the residual affected areas, CK19 stained numerous well-differentiated ducts resembling normal intra and interlobular ducts, and the % of CK19 positive area on pancreatitis area was higher in males compared to females, potentially suggesting a protracted pancreatic regeneration in males compared to females. Overall data support a quicker onset and more efficient reparative response in female C57BL/6J mice compared to males.

The two pan macrophagic markers Iba1 and F4/80 showed a similar trend of positivity in treated male and female mice, with Iba1 detecting more numerous cells than F4/80, possibly because of its ability to mark other mononuclear phagocytes such as various subsets of dendritic cells (Elizondo et al. 2019). Iba1+ and F4/80+ macrophages represented the predominant inflammatory population observed in the pancreas of both treaded male and female mice, with increasing concentration in pancreatitis areas and decreasing concentration in the overall pancreatic tissue from 12 hours to day 7 and with more numerous Iba1+ and F4/80+ positive cells in males in the total pancreatic area at 48 hours, reflecting the larger area of pancreas involved by pancreatitis in males compared to females in this time point. Although quantification methods of immune cells hugely vary among studies, our data are consistent with what reported in literature where on the total pancreas, F4/80+ macrophages were observed to increase in the very acute phases and progressively decrease over time (Folias et al. 2014; Wu et al. 2020; Lu et al 2021). CD206+ macrophages were found higher in males compared to females at both 48 hours and day 7 in both pancreatitis and total pancreatic areas. Wu and colleagues, using both Balb/c and C57BL/6 mice showed that CD206+ cells reached a peak at day 3 after caerulein administration, followed by a progressive decrease in other time points as observed in males in our study and correlated CD206 cells infiltration to a pro-resolving anti-inflammatory response. Male mice in our study had larger areas of pancreatitis and more CD206+ M2 anti-inflammatory macrophages compared to females at day 2, which, on the contrary, had less pancreatis areas and

decreasing CD206+ cells, thus supporting a more severe and ongoing reparative response in males and a partially resolved response in females.

Heme oxygenase 1 (HO-1) is an anti-inflammatory and antioxidant enzyme expressed by M2 macrophages and modulated according to specific pathophysiologic conditions such as presence of hemorrhages and ROS (Vijayan et al. 2018). Although both considered markers of M2 differentiation, CD206 and HO1 in our study yielded different results suggesting the existence of different subsets of alternatively activated macrophages differentially expressing CD206 and HO1 markers. This differential expression was demonstrated in other murine studies, where CD206+ cells expressing HO-1 were mainly involved in ROS clearance (Choi et al. 2010; Rossi et al. 2021).

Although numerous studies demonstrated the predominant role of M1, classically activated, pro-inflammatory macrophages in the first phases of inflammation (Wu et al. 2020; Shrivastava et al. 2010) our study revealed a peak of MHC-II in males at day 7. This is consistent with other reports demonstrating mild to no increase of MHC-II+ cells at the 12 hours-2-day interval and a peak at day 3 in a caerulein-induced model and at day 7 in a pancreatic duct ligation model (Bedrosian et al. 2011; Van Gassen et al. 2015). While, in females, there was a progressive decrease of MHC-II+ cells, in males, MHC-II+ cells were characterized by a progressive increase, reaching a peak at day 7 with higher number compared to females. The marked difference at day 7 could be related to the presence of residual M1 pro-inflammatory macrophages in pancreatitis areas or to an increase of dendritic cells or other professional APCs such as B lymphocytes involved in both T helper activation and immunotolerance in male mice (Adler et al. 2017).

B220+ cells and CD3ε+ cells were rare and characterized by a progressive increase in both sexes in the pancreatitis areas and a progressive decrease in the total pancreatic area. Although lymphocytes are thought to play a marginal role in pancreatitis immunopathogenesis and are, thus, seldomly investigated in caerulein-induced models of pancreatitis, a study using $Rag^{-/-}$ mice, deficient of both T and B lymphocytes, demonstrated the development of an atypical pancreatic inflammation characterized by increase pancreatic damage and M1 macrophagic infiltration in acute phases compared to wild type mice, demonstrating a role of B and T cells in inflammatory modulation of pancreatitis (Folias et al. 2014). Nevertheless, our data seem to support a marginal role of these cells in AP of wild type mice, with no differences between sexes.

Ly6G+ cells were rare and characterized by a progressive decrease in both pancreatitis area and total pancreatic area in both sexes, with males showing higher Ly6G+ cells on total pancreatic area compared to females at 48 hours reflecting, once more, a more intense inflammation in male mice. Our results detected an unexpectedly low number of Ly6G+ cells although consistent with other reports highlighting higher neutrophilic concentration in early phases of pancreatitis followed by a progressive decrease (Norkina et al. 2006; Sendler et al. 2018). The recruited neutrophils observed in our cases, could represent an immature pool of newly recruited neutrophils, which are characterized by a low expression of Ly6G (Mackey et al. 2019; Deniset et al. 2017).

In conclusion, the results of this study revealed a faster onset and resolution of pancreatitis in female mice compared to male mice. Male mice were characterized by higher CD206+ cells at 48 hours and day 7, higher MHC-II cells at day 7, more prominent ADM at day 7, and more numerous apoptoses at 48h and day 7 than females suggesting a protracted damage or a delayed reparative response in males. Data presented in this study support a sex-dependent effect on pancreatitis severity, apoptosis, and innate and adaptive immune cell infiltration in a caerulein-induced model of AP.

5. STUDY III. A COMPARISON BETWEEN HOT SPOT FIELDS AND WHOLE SLIDE IMAGE ANALYSIS FOR IMMUNE CELL INFILTRATES INVESTIGATION IN A MURINE MODEL OF CAERULEIN-INDUCED ACUTE PANCREATITIS.

5.1. Introduction

Digital image analysis (DIA) is increasingly used in histopathology to obtain quantitative results from histological and immunohistochemical slides. DIA provides, in fact, numerous advantages compared to a traditional semi-quantitative analysis minimizing evaluator-dependent subjectivity, improving study reproducibility, and increasing statistical analysis efficiency allowing to obtain numerical, quantitative data instead of qualitative data (Aeffner et al. 2019).

DIA performed on conventional pictures or scanned slides is often based on color deconvolution, a process in which color images, representing a combination of red, green, and blue colors are split into different grayscale images, each representing the intensity of a single stain of the original image (Alsubaie et al. 2017). These pictures are then analyzed setting threshold values that highlight pixels with the desired staining intensity opposed to the background.

Quantitative results from stained slides can be obtained either from pictures taken randomly from an examined specimen or from the most positive fields of the samples (hot spot fields) or evaluating all the available tissue or a large, manually, or automatically detected, region of interest (ROI), the latter method requiring slide digitalization (whole slide image) (Nofallah et al. 2022; Kunz et al. 2014). Both types of analysis are performed with dedicated DIA software, each with different specificities, properties, interfaces, and costs. Examples of free software are ImageJ or QuPath (Schneider et al. 2012; Bankhead et al. 2017).

Although DIA software and histopathologic slide digitalization are becoming increasingly affordable, thus making whole slide DIA more appealing, selected hot spot analyses are still applied successfully by researchers and diagnostic pathologists for a number of reasons: lack of technical equipment or expertise in DIA software use, familiarity with selected field analysis, high storage requirements for digital slides or use of diagnostic cut offs based on selected fields such as mitotic counts evaluated in 10 high power fields in several canine tumors comprising mast cell tumors, soft tissue sarcomas, pulmonary

carcinoma and osteosarcoma (Flores et al. 2022; Barboza et al. 2023; Brugmann et al. 2012; Avallone et al. 2021). Although the two approaches (hot spot field analysis and whole slide analysis) have been and still are applied in both human and veterinary medicine, direct comparisons between the two methods for histological specimens' analysis have been rarely performed (McIntire et al. 2018; Cizkova et al. 2021; Luchian et al. 2023; Apaolaoza et al. 2021).

The aim of the study was, therefore, to compare the concordance of hot spot fields analysis and whole slide image analysis on inflammatory cell infiltrates quantification in a mouse model of caerulein-induced acute pancreatitis.

5.2. Materials and methods

A total of 20 pancreas from mice with pancreatitis, collected at 12 hours, 48 hours, and 7 days after last caerulein administration were routinely processed and immunohistochemically stained with markers directed towards Iba1 and F4/80 (macrophages), HO-1 and CD206 (M2 polarized macrophages), MHC-II (M1 macrophages/ antigen presenting cells), B220 (B cells), CD3e (T cells) and Cleaved caspase 3 (apoptotic cells). Slides were digitalized in 40x high resolution mode (0.23 µm x pixel) through the NanoZoomer-XR digital slide scanner (Hamamatsu, C12000) at the Unitech Nolimits facility (UNIMI, Milan). More technical details on the immunohistochemical staining can be found in the material and methods section of study II (Chapter 3.2.5.).

Hot spot fields analysis. Three 20x, hot spot fields (corresponding to a total area of 1.84 mm^2) were taken from each immunostained slide using NDP.view2 software (Figure 1, A). Each acquired image was uploaded in ImageJ and split into 3 greyscale images using the "split channels" function (color deconvolution). The channel with the highest contrast between the immunohistochemical positive signal and the non-specific background staining (blue channel) was selected. For each marker, a threshold value that could detect positive signal avoiding non-specific background stain was selected and the % of positive area per field calculated (Image 1, C, D, F, G, I, L).

Whole slide image analysis. The same digital slides were uploaded in QuPath software, setting all slides as brightfield hematoxylin-DAB type. Because pancreatitis was not a diffuse process, but multifocally affected pancreatic tissue, the areas of pancreatitis were manually outlined in each sample, and, in these areas, positive pixels were classified through

the classify → pixel classification → create thresholder commands, using very high-resolution input (0.44 µm /pixel) and the % of positive area per pancreatitis area calculated.

Results were analyzed with GraphPad version 9.0 (GraphPad Software, San Diego, CA, USA). Shapiro-Wilk Normality test was performed to assess data distribution. Bland-Altman test was used to evaluate concordance between the two methods measurements and the Pearson correlation test was used to evaluate the linear correlation between the measurements. Pearson correlation coefficients (r) greater that 0.6 were considered index of strong correlation, while coefficients between 0.6 and 0.4 and between 0.4 and 0 were considered index of moderate and low correlation respectively (Obilor et al. 2018).

5.3. Results

% of positive areas measured with QuPath (whole slide analysis) and ImageJ (hot spot field analysis) are summarized in Table 1. All measurements obtained can be found in Supplemental Tables 23 and 24.

ImageJ (Hot spot fields) and QuPath (whole slide) % of positive areas showed strong linear correlation for all the evaluated markers (**Iba1** r = 0.859; **F4/80** r = 0.672; **HO1** r= 0.754; **CD206** r = 0.789; **MHC-II** r = 0.9449; **B220** r = 0.690; **CD3e** = 0.739; **Cleaved caspase 3** r = 0.973) (Figure 2).

More than 95% of the measurements obtained with ImageJ and QuPath for each marker fell within the confidence interval, as revealed by the Bland-Altmann test (Figure 3).

Table 1. Mean % of positive areas and standard deviation measured by QuPath and ImageJ.

	QuPath (whole slide)	ImageJ (hot spot)
IBA1	0.07028 ± 0.038	0.06218 ± 0.029
F4/80	0.01949 ± 0.011	0.01977 ± 0.008
HO1	0.01508 ± 0.008	0.00842 ± 0.008
CD206	0.00842 ± 0.007	0.01751 ± 0.008
MHC-II	0.00326 ± 0.005	0.00299 ± 0.003
B220	0.00096 ± 0.001	0.00156 ± 0.001
CD3e	0.00243 ± 0.003	0.00280 ± 0.002
Caspase	0.10674 ± 0.131	0.20308 ± 0.252

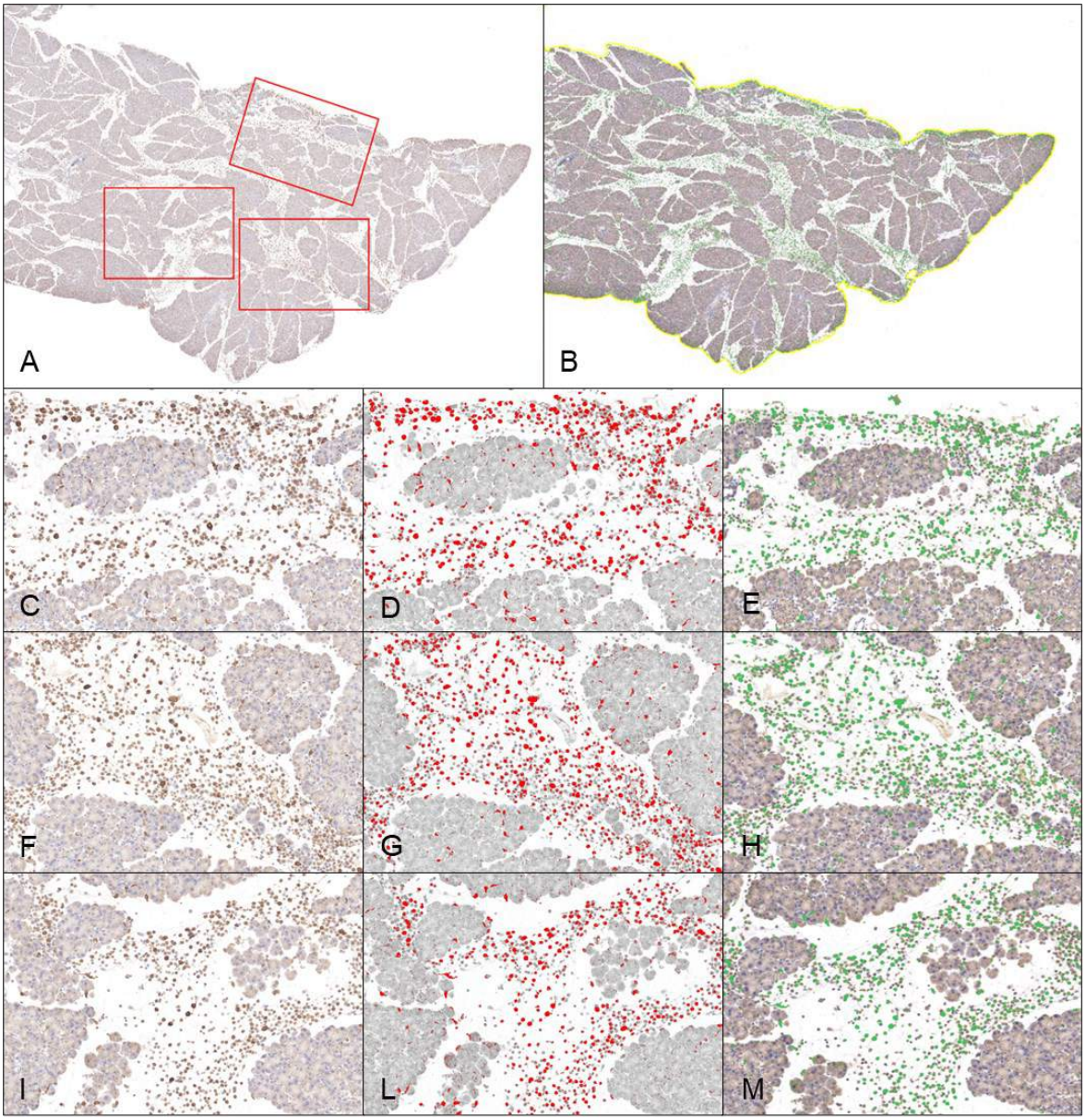

Figure 1. Iba1 immunohistochemical staining. **A**. Hot spot fields selection for ImageJ analysis. **B**. The pancreatitis area was manually selected in QuPath and a threshold detecting positive signal applied (green signal). In the pictures below, the three selected hot spot fields (**C, F, I**) can be seen together with ImageJ threshold application outcome (red signal) (**D, G, L**) and with QuPath threshold application outcome (green signal) (**E, H, M**).

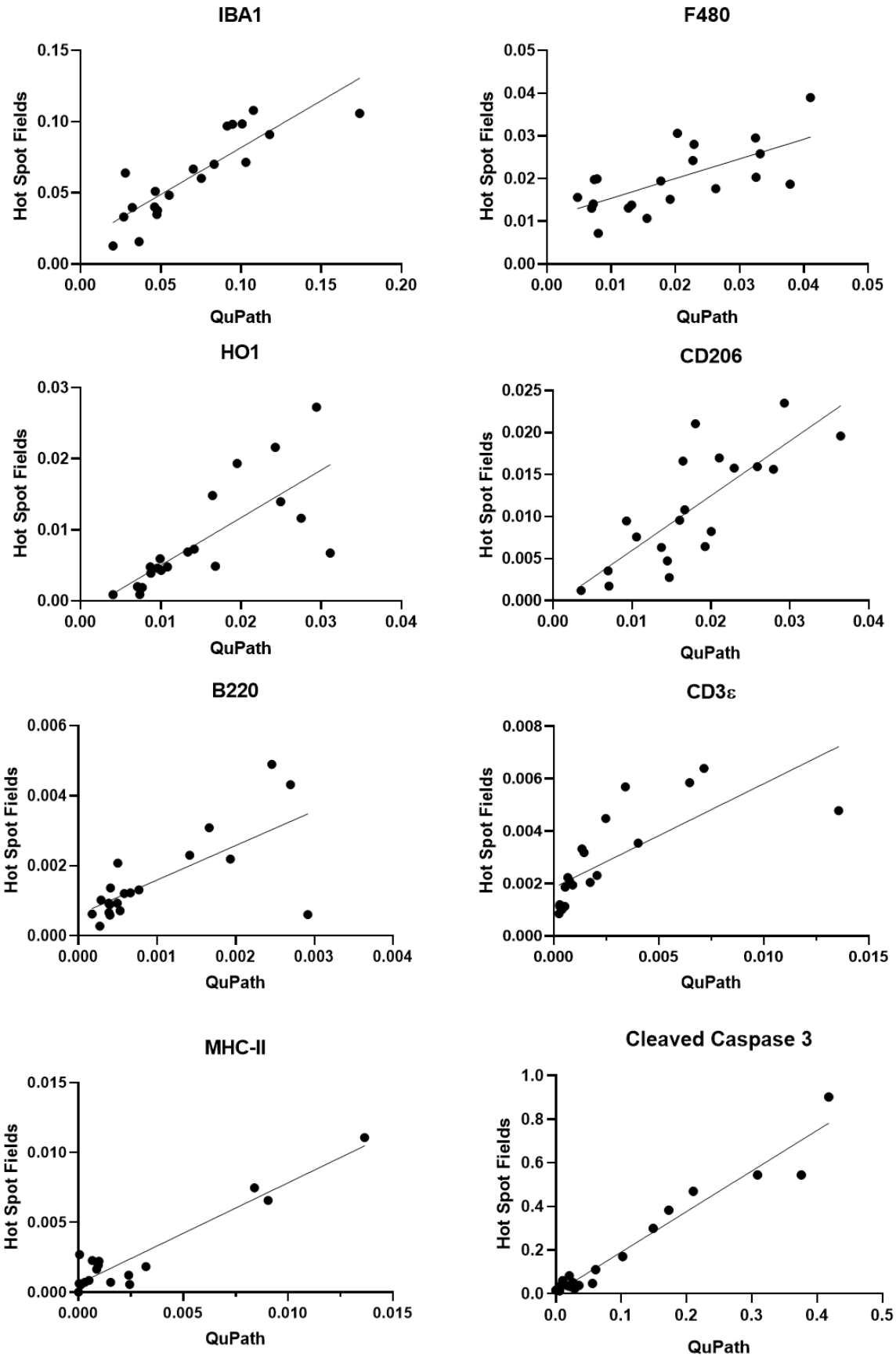

Figure 2. Pearson correlation test. For all evaluated markers a strong correlation between ImageJ values (hot spot) and QuPath measured values (whole slide) was obtained.

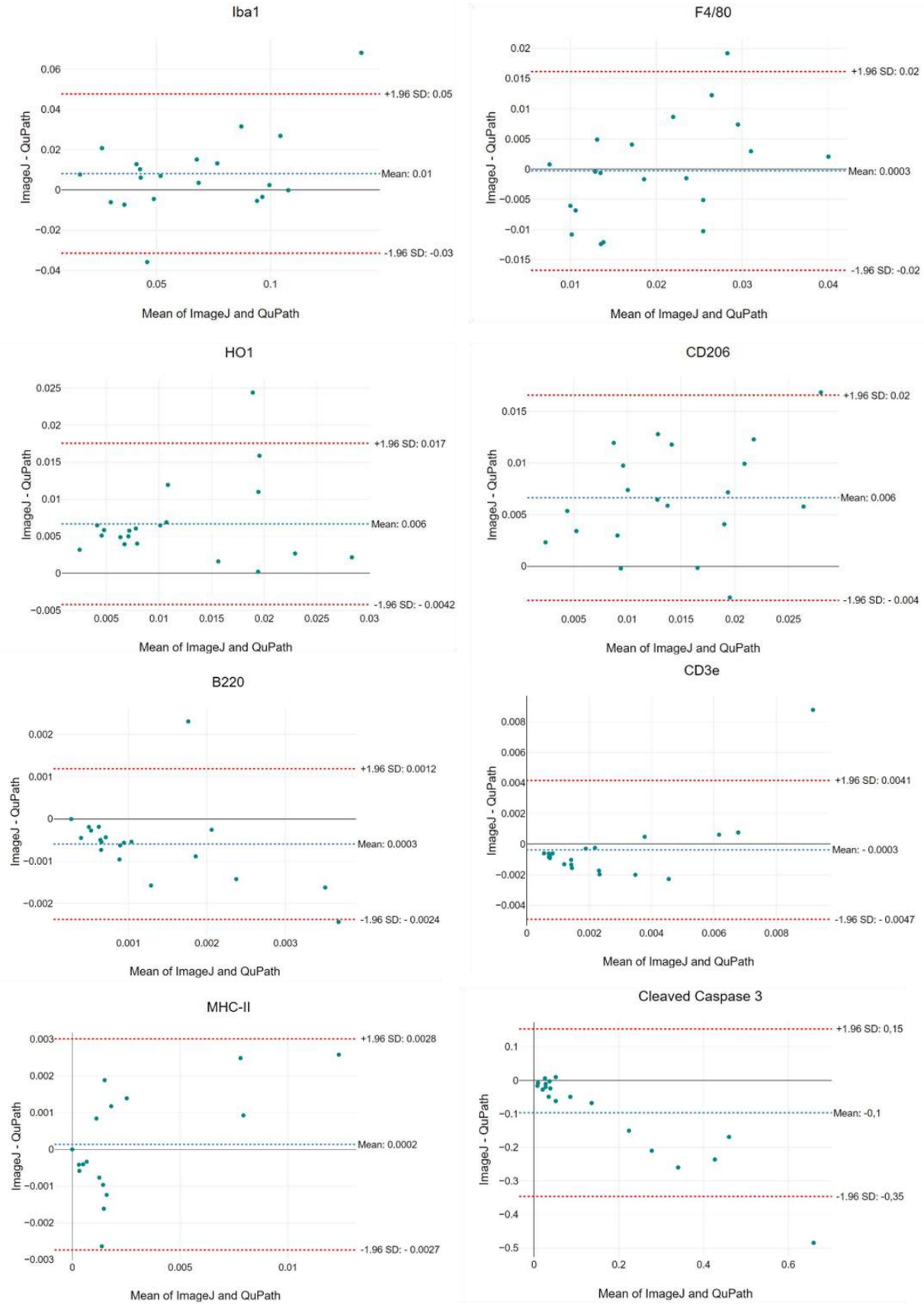

Figure 3. Bland-Altman test. For all evaluated markers, more than 95% of the values fell within the confidence interval, highlighting a high concordance between the measurements.

5.4. Discussion

Our results highlighted a strong linear correlation between the % of positive area measured with a hot spot field and whole slide approach for all markers. A strong linear correlation indicates that the measurements obtained with the two methods are related, since they vary in values proportionally, but does not imply agreement between values: in other words, strong linear correlation does not stand for numerically similar values. For this reason, Bland-Altman test was applied, revealing a good agreement among measurements: thus indicating that obtained measurements were numerically similar and demonstrating that, despite deploying a different algorithm and applying different threshold levels for pixel quantification, with a tendency to systematically over or underestimate the values depending on the marker, both software effectively and similarly measure positive area on immunohistochemical stained slides.

Although DIA is extensively applied in research and diagnostics worldwide, only a few studies directly compared hot spot and whole slide approaches for area quantification. In a study measuring CD31+ area in xenograft samples, the hot spot analysis yielded a higher positive area compared to the whole-slide analysis. This result is expected when the immunohistochemical positive signal is not evenly distributed in the slide or when there is high discrepancy between the hot spot area and total area examined. In these cases hot spot fields tend, in fact, to overestimate positive areas (Chantrain et al. 2003; Kunz et al. 2014). Discrepancies between hot spot and whole slide measurements are often related to fields selection, which is often an evaluator-dependent process prone to inter-observer variability (Van der Laak et al. 1998; Chantrain et al. 2003). When applied to the same test images, hot spot and whole-slide analysis have been found to give similar results with ImageJ and QuPath software used to quantify positive signals of target placental cells or renal fibrosis on Masson's trichrome stain or even to measure microanatomical structures such as glomerular width or tubular diameter, with high agreement (Cizkova et al. 2021; Sanchez-Jaramillo et al. 2022; Brahmadi et al. 2023).

ImageJ and QuPath are not only limited to area measurement but allow counting of cells or target histologic structures, with variable agreements depending on the target. ImageJ automated counts of adipocytes on selected micrographs identified statistically less adipocytes compared to QuPath, taken an equivalent area (Maguire et al. 2020). QuPath and ImageJ mitotic counts in 40 high magnification images reached a good agreement (Ibrahim et al. 2022) while in a study comparing QuPath and ImageJ efficiency in axons quantification

in rat optic nerve samples, QuPath outperformed Axon J on axons quantification (Mysona et al. 2020).

Since ImageJ software has proven to be inaccurate in the detection of positive cells, particularly of cells with dendritic/ stellate morphology, in the present study only positive area data were obtained with the two software and compared. Concerning positive areas, the hot spot fields selected for the ImageJ analysis were, in most cases, highly representative of all the examined pancreatitis tissue and positive cells and cleaved caspase 3 signal were evenly distributed in the pancreatitis tissue, thus avoiding hot-spot related bias of overestimation. As supported by literature data, these factors (selection of representative areas for the analysis and staining uniformity) explain the high agreement among measures obtained with ImageJ and QuPath (Kunz et al. 2014; McIntire et al. 2019).

In conclusion, data obtained from our cases suggests that both a whole-slide field and hot spot approach could be efficiently applied for immunohistochemical positive area measurement of immune cell infiltrate and apoptoses.

6. STUDY IV- IMPORTANT FUNCTIONAL ROLE OF THE PROTEIN OSTEOPONTIN IN THE PROGRESSION OF MALIGNANT PLEURAL MESOTHELIOMA.

This study was conducted in collaboration with Humanitas Research Hospital, Rozzano, Milan and was in part published, on Frontiers in Immunology.[1]

6.1. Introduction

Malignant Pleural Mesothelioma (MPM) is a malignant neoplasm arising from the pleural mesothelial lining of the lungs strongly associated, in humans, with long-lasting inflammation induced by inhaled, non-degradable asbestos fibers (Mott 2012). MPM typically carries a poor prognosis due to its aggressive behavior, the absence of useful early diagnostic biomarkers, its tendency to grow with a diffuse, infiltrative pattern instead of forming discrete masses and its chemotherapy resistance (Remon et al. 2012).

Three main histological subtypes of MPM have been recognized: epithelioid mesotheliomas, the most common subtype, sarcomatous mesotheliomas associated to the worst prognosis, and intermediate mesotheliomas, characterized by a combination of both epithelioid and sarcomatous appearance (Brcic et al. 2012).

Over the last decades the pathogenetic mechanisms giving rise to this neoplasm have been elucidated: after inhalation, asbestos fibers reach the pleura through lymphatics and induce chronic inflammation with release of reactive oxygen and nitrogen species causing DNA damage and progressive accumulation of DNA mutations initiating cancer development (Xu et al. 2002; Bueno et al. 2016; Gogou et al. 2022).

Previous studies carried out by our research group into MPM tumor-promoting inflammatory mechanisms highlighted a high expression, in human tumor samples, of the *Spp1* gene, coding for the protein osteopontin (OPN). OPN is a highly phosphorylated protein produced by macrophages, mesenchymal and epithelial cells. OPN interacts with the transmembrane protein CD44 on target cells, regulating cellular motility, immune response, and apoptosis with a pro-tumoral function (Scatena et al. 2007; Hattori et al. 2021). Although OPN has already been investigated in MPM as a prognostic marker, with higher levels of

[1] Digifico E, et al. Important functional role of the protein osteopontin in the progression of malignant pleural mesothelioma. *Front Immunol*. 2023. 14:1116430.

serum OPN associated to worst prognostic outcome in human patients, studies investigating the functional role of OPN in MPM progression are lacking (Schilebeecx et al. 2021; Hollovoet et al. 2011).

Another important molecule that gained the attention of our research group was the glycoprotein non metastatic B protein (GPNMB). Previous investigations highlighted that soluble forms of GPNMB, mainly produced by tumor associated macrophages (TAMs), interact with CD44 receptor on cancer cells decreasing pro-inflammatory cytokines production, promoting angiogenesis and inducing IL-33 production, the latter promoting expansion of cancer stem cells and favouring the acquisition of metastatic phenotype in murine tumor models of pancreatic carcinoma, mammary carcinoma and fibrosarcoma (Grigoriu et al. 2007; Rose et al. 2010; Hu et al. 2013; Liguori et al. 2021)

The aim of the study was, therefore, to investigate OPN and GPNMB role in mesotheliomas development using a murine transgenic orthotopic model of MPM in combination with CD44 receptor blockage. Additionally, immunohistochemical characterization and quantification of intra-tumoral blood vessels and of TAMs and tumor infiltrating lymphocytes (TILs) was carried out to investigate OPN and GPNMB effects on tumor immune cells recruitment and angiogenesis.

6.2. Materials and Methods

In this study, we mainly focused on the histopathologic and immunohistochemical analysis of samples received from the Humanitas Research Hospital (Rozzano, Milan). For completeness, details on mesothelioma cell lines generation and on *in vivo* procedures performed are provided below.

6.2.1. Osteopontin-silenced Murine Mesothelioma Cell Lines Generation

A murine MPM sarcomatous cell line (AB1) and a murine MPM epithelioid cell line (AB22) were generated in BALB/c mice through intraperitoneal injection of crocidolite asbestos fibers according to previously published procedures (Davis et al. 2012). Cell lines were cultured in RPMI 1640 (Lonza) supplemented with 10% FBS (Sigma), 2mM L-glutamine, 100 U/mL penicillin and 100 µg/mL streptomycin (Life Technologies Inc.) at 37°C and 5% CO2. To silence the *Spp1* gene coding for osteopontin, AB1 and AB22 cells were stably transduced with the lentiviral vector MISSION shRNA (SHCLNG, 10041725MN, SIGMA). Viral particles were generated in HEK293T cells transfected with Lipofectamine2000 (ThermoFisher Scientific) according to manufacturer's instruction. Selection of transduced cells was performed using Puromycin (2 ug/ml for three days after each defrosting). A non-

targeting shRNA (scrambled) was used to transduce the control cell lines. All cell types were routinely checked for Mycoplasma contamination.

6.2.2. AB22 Mesothelioma Cell Lines *in vivo* Inoculation

Mice were used in compliance with national (D. L. N. 26, G.U. March 4, 2014) and international law and policies (EEC Council Directive 2010/63/EU, OJ L 276/33, 22-09-2010; National Institutes of Health Guide for the Care and Use of Laboratory Animals, (authorization N° 296/2020-PR), and US National Research Council, 2011). 8 weeks old BALB/c mice were purchased from Charles River. The procedures for the syngeneic orthotopic mouse model have been previously described (Digifico et al. 2020). Since the *in vitro* characterization of the engineered cells revealed that OPN silencing had no effect on AB1 cells proliferation, the *in vivo* experiment was carried out only with engineered AB22 cells. Mice were anesthetized with ketamine/xylazine and positioned on left lateral decubitus. The thoracic area was shaved and sterilized with 70% ethanol. An 8-10 mm skin incision was performed on the right thorax (close to the axillary region) and $5x10^4$ cells resuspended in 50 µl saline solution were injected between the third and the fourth costal space, with the needle perpendicularly oriented on the rib cage (29-gauge needle of a 500 ul syringe U100, BD Becton, Dickinson). To standardize the injection and avoid lung perforation, the needle was overmounted by a 200ul tip, properly cut to expose the needle of 3 mm only. After cell injection, mice were sutured and kept under a heating lamp to recover from the anesthesia.

Two separate experiments were carried out:

6.2.3. Experiment 1: Role of OPN in Murine MPM Growth

Fifteen Balb/c mice were inoculated with engineered AB22 mesothelioma cells: 10 with OPN silenced cells (shOPN) and 5 with control cells (shSCRB). 5 shOPN and 5 shSCRB mice were sacrificed at day 17 while 5 shOPN were additionally sacrificed at a later time point, at day 59. Lungs and intra-thoracic masses were collected, fixed in 10% buffered formalin, routinely processed for histopathology, cut at 4 µm thickness, and stained with hematoxylin and eosin. Digital slides were obtained from hematoxylin and eosin-stained sections using the NanoZoomer S60 Digital slide scanner (Hamamatsu, C13210-01) at 40x resolution and visualized by NDP.view2 Viewing software (Hamamatsu, U12388-01). For each case, pulmonary nodules were progressively numbered form the biggest to smallest and were, subsequently, manually outlined using the free hand selection tool, obtaining the mass area expressed in mm^2. For each nodule, areas of lytic and coagulative necrosis as well as

areas of blood vessels dilation (angiectasia) were additionally manually outlined obtaining the corresponding area in mm^2. For each mouse, the mean tumors number, mean tumoral area of each mass, the total tumor area, area of necrosis per tumor area, % of tumors with necrosis, area of angiectasia per tumor area and % of tumors with angiectasia were obtained.

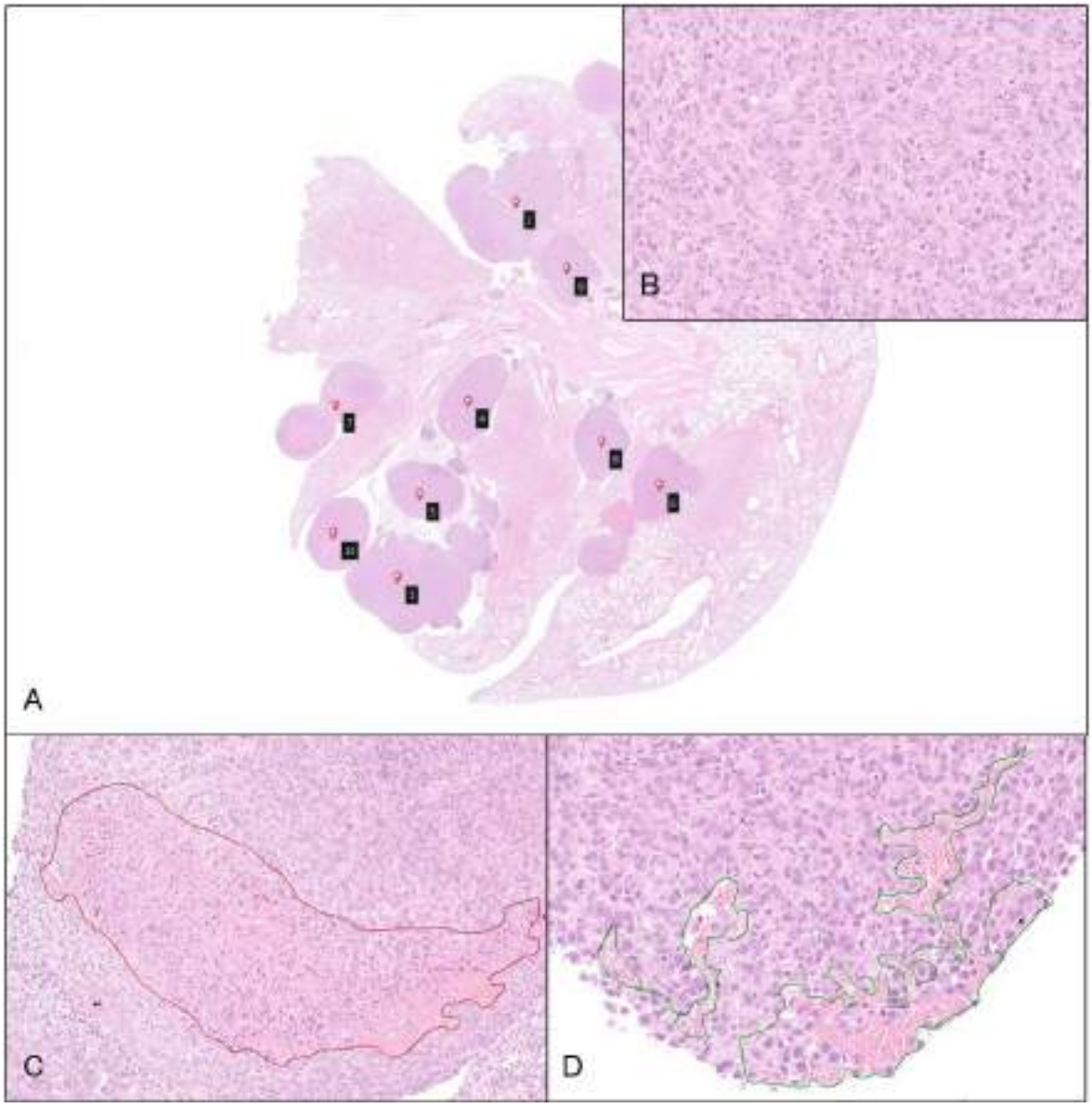

Figure 1. Lung with multiple MPMs, HE. **A.** MPMs were enumerated from the largest to the smallest mass. 1x. **B.** Higher magnification of MPM cells exhibiting an epithelioid morphology, 40x. **C.** Areas of necrosis, characterized by clumps of amorphous eosinophilic material intermixed to basophilic karyorrhectic debris were manually outlined, 20x **D.** Areas of angiectasia, characterized by dilated, blood-filled, lacunae were manually outlined, 40x.

A 4 µm section underwent deparaffinization and heat induced epitope retrieval (HIER) in a water bath for 40 min at 100°C (Dewax and HIER Buffer H, Thermo Scientific Lab Vision, cat. No. TA-999-DHBH). The slides were rinsed in PBS and placed in an autostainer (Lab Vision® Autostainer 480S-2D Thermo Fischer scientific) after application of PapPen (Liquid Daido Sangyo Co. Ltd.). Endogenous peroxidase activity was blocked by incubating sections with 3% H_2O_2 for 10 minutes. Slides were rinsed, incubated with PBS containing 10% or normal goat serum for 30 min at room temperature to prevent nonspecific background staining and then incubated for 1 hour at room temperature with a primary anti-OPN antibody. Sections were subsequently rinsed in PBS and incubated with a biotinylated secondary antibody (goat anti-rabbit, Vector Laboratories, USA, cat. NO. BA-4000) and labelled through avidin-biotin-peroxidase procedure (VECTASTAIN® Elite ABC-Peroxidase Kit Standard, Vector Laboratories, USA, cat. No.PK-6100). The immunoreaction was visualized with 3,3'-diaminobenzidine substrate (DAB, Peroxidase DAB Substrate Kit, Vector Laboratories, USA, cat. No. SK-4105). Sections were counterstained with Mayer's hematoxylin, dehydrated in a graded alcohol series and coverslipped with resinous mounting medium.

Slides were digitalized using the NanoZoomer S60 Digital slide scanner at 40x resolution (Hamamatsu, C13210-01) and visualized by NDP.view2 Viewing software (Hamamatsu, U12388-01). For each case, pulmonary nodules were progressively numbered form the biggest to the smallest and 1, hot spot field at 20x magnification, was taken from each of the biggest 10 masses, corresponding to fields with the highest density of positive cells. Regions with necrotic tissue and cut/staining artifacts were carefully avoided. Images were, then, processed in ImageJ software (http://rsb.info.nih.gov/ij/). After color splitting of original images into 3 greyscale images corresponding to the red, green and blue channels, the blue channel was selected as the most appropriate to distinguish positive signal against background. A threshold value that could avoid non-specific signals was selected and applied to each hot-spot field to calculate the positive area/total area ratio expressed in percentage.

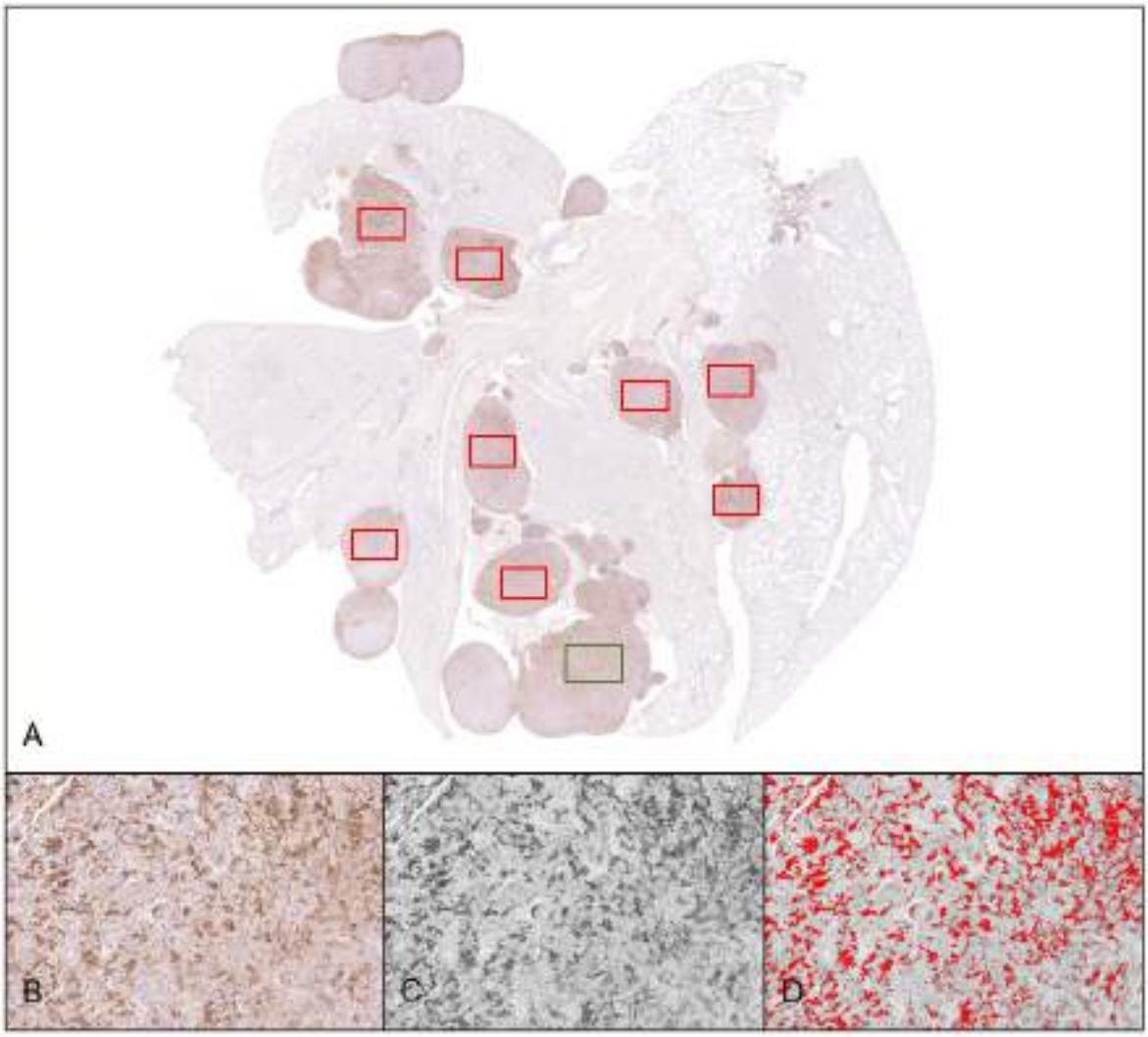

Figure 2. Lungs with multiple MPMs. Immunohistochemistry for Iba1. **A.** A single, 20x, hot spot field was taken from each of the biggest 10 masses. **B.** Original images were split into greyscale images and the blue channel (**C**) was selected as the most appropriate for the positive area measurement after the application of a proper Threshold (**D**) with ImageJ software.

6.2.4. Experiment 2: Inhibition of OPN Signaling Through CD44 Receptor Blockage

Ten Balb/c mice were inoculated with engineered shSCRB AB22 mesothelioma cells on day 0. Five animals were treated intra-peritoneally with anti-CD44 mAb (BioXcell, BE0039, 10 mg/kg), while 5 were treated with an anti-irrelevant antibody at days 7, 12, 16 and 19 post tumor injection and sacrificed at day 33. Tumor samples were collected and processed for histopathology as described in experiment 1.

Serial sections of 4 µm were additionally obtained for each case and immunostained with primary antibodies marking different TILs subsets (CD3ε, CD4, CD8, FoxP3), TAMs (Iba1), OPN, GPNMB and blood vessels (CD31). Details on primary antibodies used in the study can be found in supplementary Table 1.

4 µm sections underwent deparaffinization and heat induced epitope retrieval (HIER) in a water bath for 40 min at 100°C (Dewax and HIER Buffer H, Thermo Scientific Lab Vision, cat. No. TA-999-DHBH). The slides were rinsed in PBS and placed in an autostainer (Lab Vision® Autostainer 480S-2D Thermo fischer scientific) after application of PapPen (Liquid Daido Sangyo Co. Ltd.). Endogenous peroxidase activity was blocked by incubating sections with 3% H_2O_2 for 10 minutes. Slides were rinsed, incubated with PBS containing 10% or normal goat serum (IBA1, CD31, OPN), normal rabbit serum (CD3e, CD4, CD8, FoxP3, GPNMB) for 30 min at room temperature to prevent nonspecific background staining and then incubated for 1 hour at room temperature with primary antibodies. Sections were subsequently rinsed in PBS and incubated with a biotinylated secondary antibody (goat anti-rabbit, Vector Laboratories, USA, cat. NO. BA-4000, rabbit anti-rat, Vector Laboratories, USA, cat. No. BA-4001, rabbit anti-goat, Vector Laboratories, USA, cat. No BA-5000) and labelled through avidin-biotin-peroxidase procedure (VECTASTAIN® Elite ABC-Peroxidase Kit Standard, Vector Laboratories, USA, cat. No.PK-6100). The immunoreaction was visualized with 3,3'-diaminobenzidine substrate (DAB, Peroxidase DAB Substrate Kit, Vector Laboratories, USA, cat. No. SK-4105). Sections were counterstained with Mayer's hematoxylin, dehydrated in a graded alcohol series and coverslipped with resinous mounting medium. For all markers adequate positive controls (murine lymphoid tissues) and negative controls (omission of primary antibody) were used.

Slides were digitalized using the NanoZoomer S60 Digital slide scanner (Hamamatsu, C13210-01) at 40x magnification and visualized by NDP.view2 Viewing software (Hamamatsu, U12388-01). For each case, all tumors, intratumoral areas of necrosis and intratumoral areas of angiectasia were manually outlined using NDP.view2 Viewing software obtaining the respective areas expressed in mm^2. The total tumor area, the total necrosis area and the total angiectasia area were divided per the number of tumors obtaining the mean tumor area, the mean necrosis and the mean angiectasia area. Pulmonary nodules were then progressively numbered from the largest to the smallest and 1, 20x magnification, hot spot field was taken from each of the biggest 10 masses for every evaluated marker, corresponding to fields with the highest density of positive cells. Regions with necrotic tissue and cut/staining artifacts were carefully avoided for image analysis. Images were then processed in ImageJ software (http://rsb.info.nih.gov/ij/). After color splitting the original

images into 3 greyscale images corresponding to the red, green, and blue channels, the blue channel was selected as the most appropriate to distinguish positive signal against background. A threshold value that could avoid non-specific signals was selected and applied to each hot-spot field to calculate the positive area/total area ratio expressed in percentage.

6.2.5. Statistical analysis

Data were analyzed using Graph Pad Prism version 9.0 (GraphPad Software, San Diego, CA). Data distribution was assessed with Shapiro-Wilk test. Statistical analyses of the results were performed using the Mann-Whitney U test and the Kruskal-Wallis test. P-values < 0.05 were considered statistically significant. In both experiments, animals with no tumors or identified as outliers by the statistical analysis software were excluded from the analysis. Regarding digital image analysis, the analysis was performed both considering a mouse as a statistical unit or considering each individual tumors as the statistical unit.

6.3. Results

6.3.1. Experiment 1

Results are summarized in Table 1.

ShOPN AB22 cells had a lower growth compared to the control shSCRB AB22 cells at day 17, with statistically significant less numerous tumors ($P < 0.0179$) and lower total tumor area ($P < 0.0357$). At the same time point, lower total angiectasia areas ($P < 0.0357$) and lower mean angiectasia per tumor ($P < 0.0357$) were observed in shOPN AB22 group compared to shSCRB AB22 cells. The 5 mice treated with shOPN AB22 cells and sacrificed at day 59, had higher tumor area and more numerous tumors compared to shOPN AB22 treated animals sacrificed at 17 days, but still less numerous than shSCRB AB22 treated animals, sacrificed at 17 days, although not statistically significant (Table. 1).

OPN expression was mainly detected in neoplastic cells and in macrophage cytoplasms together with few scattered dots in the extracellular space, consistent with OPN extracellular granules. No differences in OPN positive area were detected among the groups.

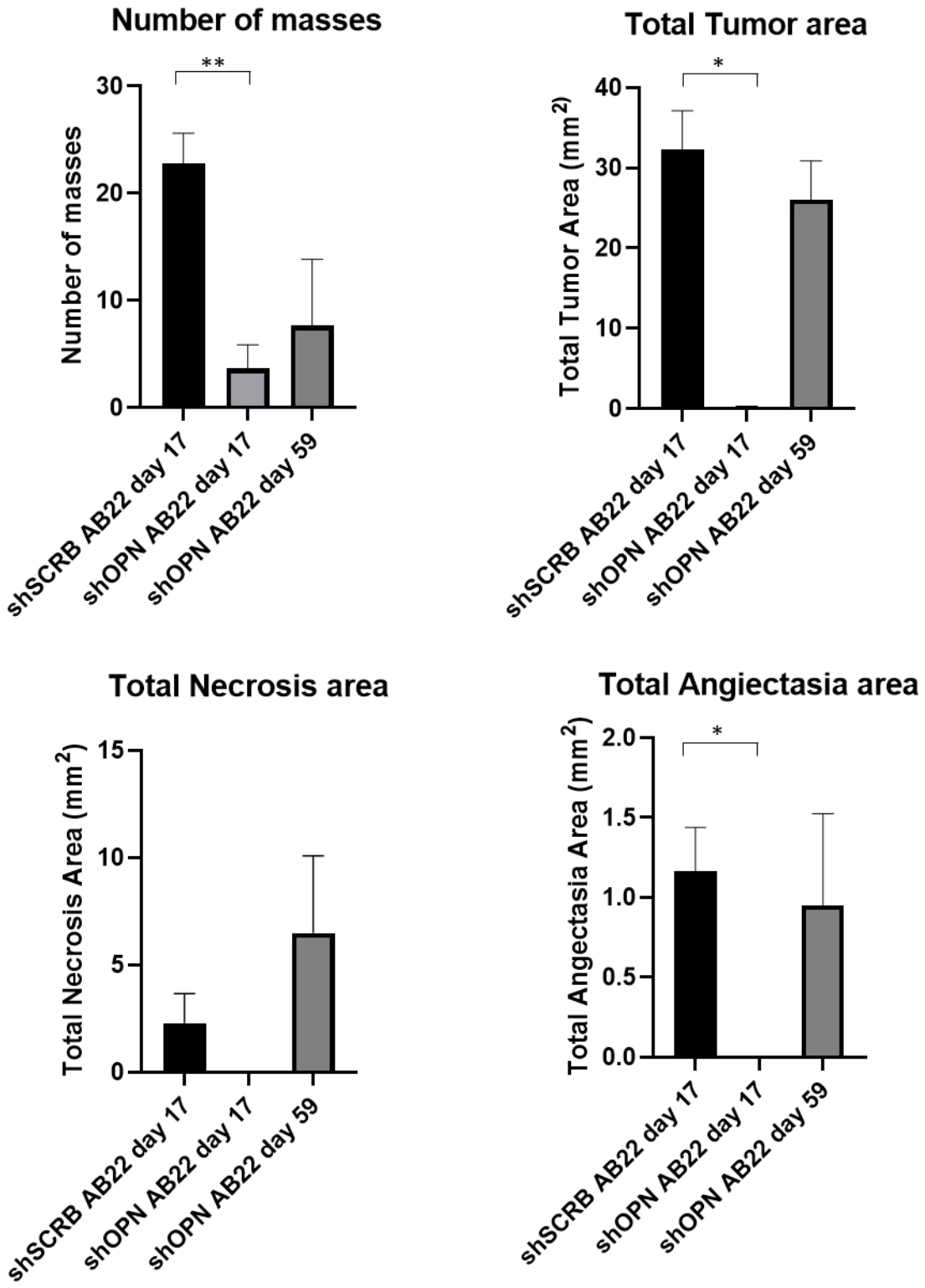

Figure 3. Graphs of number of masses, Total tumor area, Total necrosis area and Total angiectasia area in shSCRB AB22 and shOPN AB22 mice sacrificed at day 17 and shOPN AB22 mice sacrificed at day 59. * P value < 0.05.

Table 1. Results summary of experiment 1.

Group	Sacrifice	Mouse ID	No. of Tumors	Total Tumor Area	Mean Tumor Area	Total Necrosis Area	Mean Necrosis Area	% Tumors with necrosis	Total Angiectasia Area	Mean Angiectasia Area	% Tumors with Angiectasia
AB22 shSCRB	Day 17	6AD	26	24.69	0.95	7.57	0.12	19%	1.37	0.06	31%
		6AS	32	49.24	1.54	1.70	0.04	22%	2.11	0.11	34%
		6BD	16	37.09	2.32	2.00	0.04	25%	0.77	0.05	25%
		6BS	20	26.86	1.34	0.00	0.00	0%	0.55	0.04	25%
		60	20	23.30	1.16	0.23	0.01	15%	1.03	0.05	35%
		Mean	22.80	32.23	1.46	2.30	0.04	16%	1.17	0.06	30%
AB22 shOPN	Day 17	8AD	8	0.1931	0.02	0.00	0	0%	0.00	0.00	0%
		8AS	0	0	\	\	\	\	\	\	\
		8BD	2	0.387	0.19	0.00	0	0%	0.00	0.00	0%
		8BS	0	0	\	0.00	\	\	0.00	\	\
		80	1	0.0118	0.01	\	0	0%	\	0.00	0%
		Mean	2.20	0.12	0.07	0.00	0.00	0%	0	0.00	0%
		Mean w/o 8AS 8BS	3.67	0.20	0.07	0.00	0.00	0%	0	0.00	0%
AB22 shOPN	Day 59	7AD	20	34.17	1.71	5.04	0.05	30%	0.88	0.04	25%
		7AS	0	0.00	\	\	\	\	\	\	\
		7BD	1	26.60	26.60	13.3	0.50	100%	1.98	0.07	100%
		7BS	2	17.28	8.64	1.11	0.07	100%	0.00	0.00	0%
		70	0	0.00	\	\	\	\	\	\	\
		Mean	4.60	15.61	12.32	6.48	0.21	77%	0.95	0.04	42%
		Mean w/o 7AS 70	7.67	26.02	12.32	6.48	0.21	77%	0.95	0.04	42%

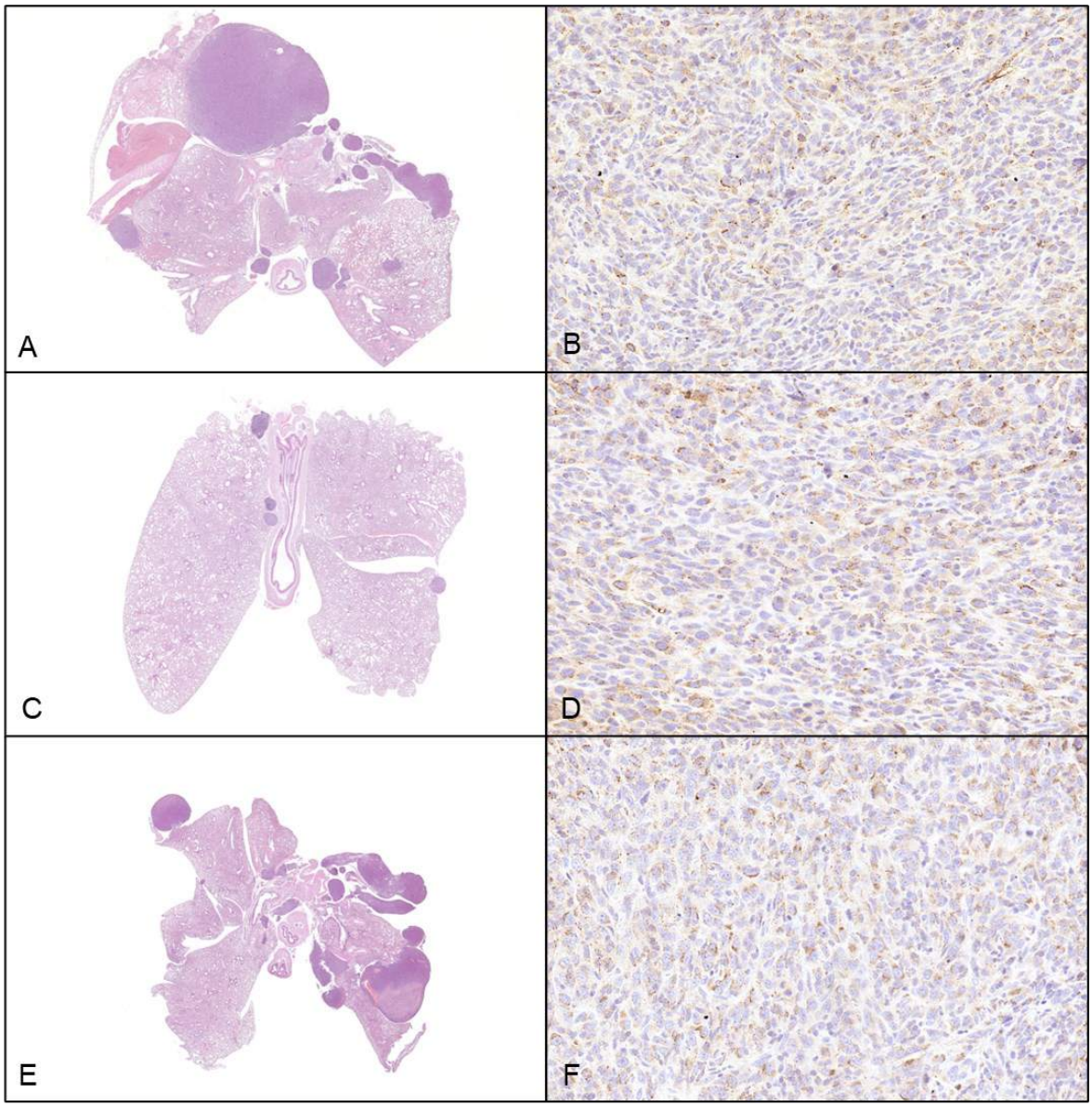

Figure 4. **Lungs with MPMs**, HE, 1x (**A, C, E**) shSCRB mice (**A**) had more numerous tumors and higher tumor area compared to both shOPN mice sacrified at day 17 (**C**) and day 59 (**E**). **MPM,** Immunohistochestry for OPN, 20x (**B, D, F**). No differences in OPN expression was detected among shSCRB mice (**B**), shOPN mice sacrified at day 17 (**D**) and shOPN mice sacrified at day 59 (**F**).

6.3.2. Experiment 2

Results are summarized in Table 2.

No statistically significant differences between the two groups regarding number of tumors, tumor area, tumoral necrosis area or tumoral angiectasia area were detected although anti-CD44 treated mice had lower number of tumors and lower tumoral necrosis and angiectasia areas compared to anti-irrelevant treated mice. Anti CD-44 treated group had more CD3+ T cells, CD4+ T cells and less Foxp3+ cells infiltration, higher CD31+ area and lower GPNMB+ area compared to control group. When considering each individual tumor as statistical unit these differences resulted statistically significant: CD3 ($P< 0.0085$), CD4+ ($P < 0.0221$), FoxP3+ ($P < 0.0016$), CD31 ($P < 0.0421$), GPNMB ($P < 0.0090$). No differences in Iba1+ cells, CD8+ cells and OPN positive area were detected through DIA between the two groups.

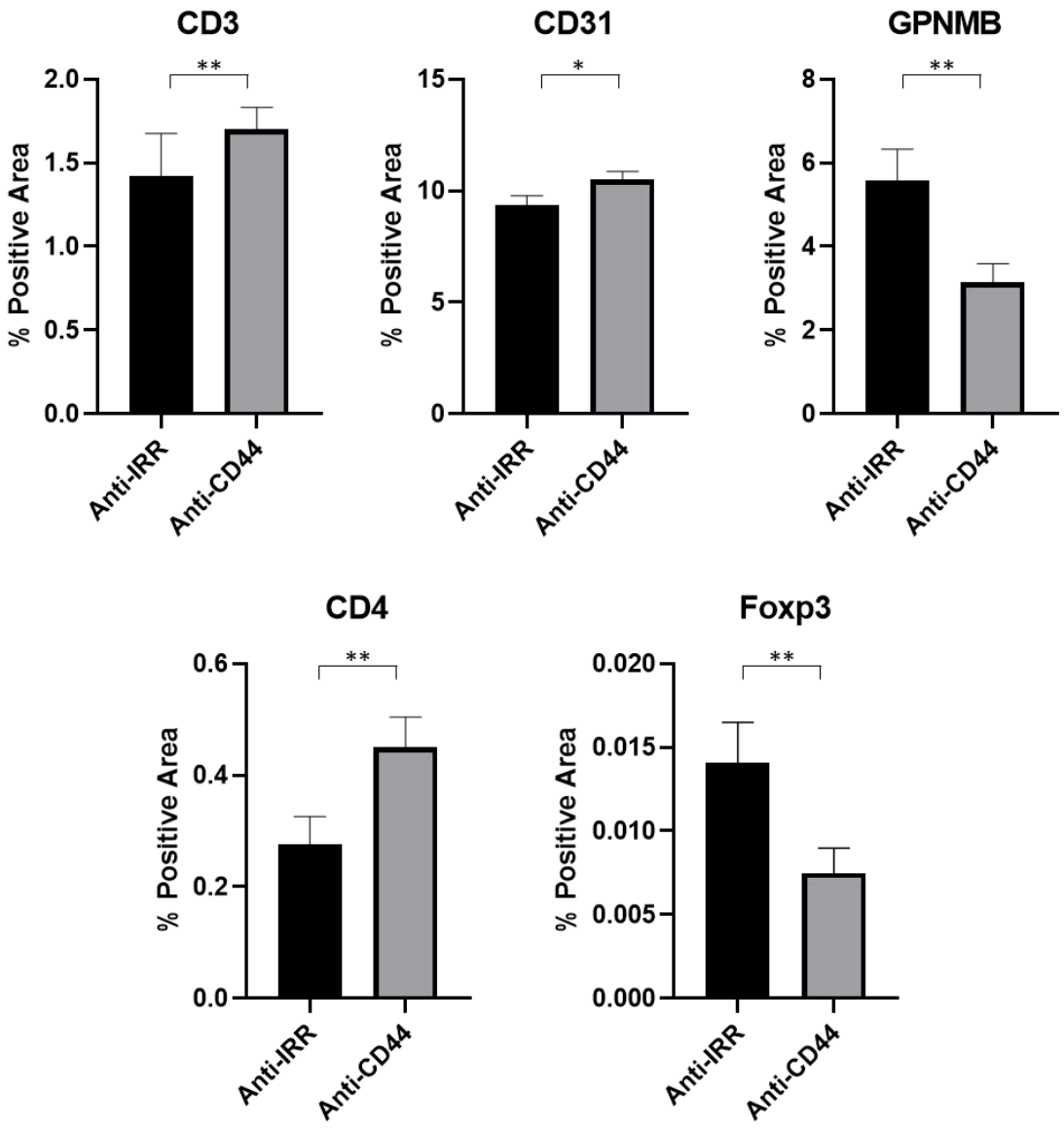

Figure 5. Graphics of CD3, CD4, FoxP3 and CD31 % of positive area

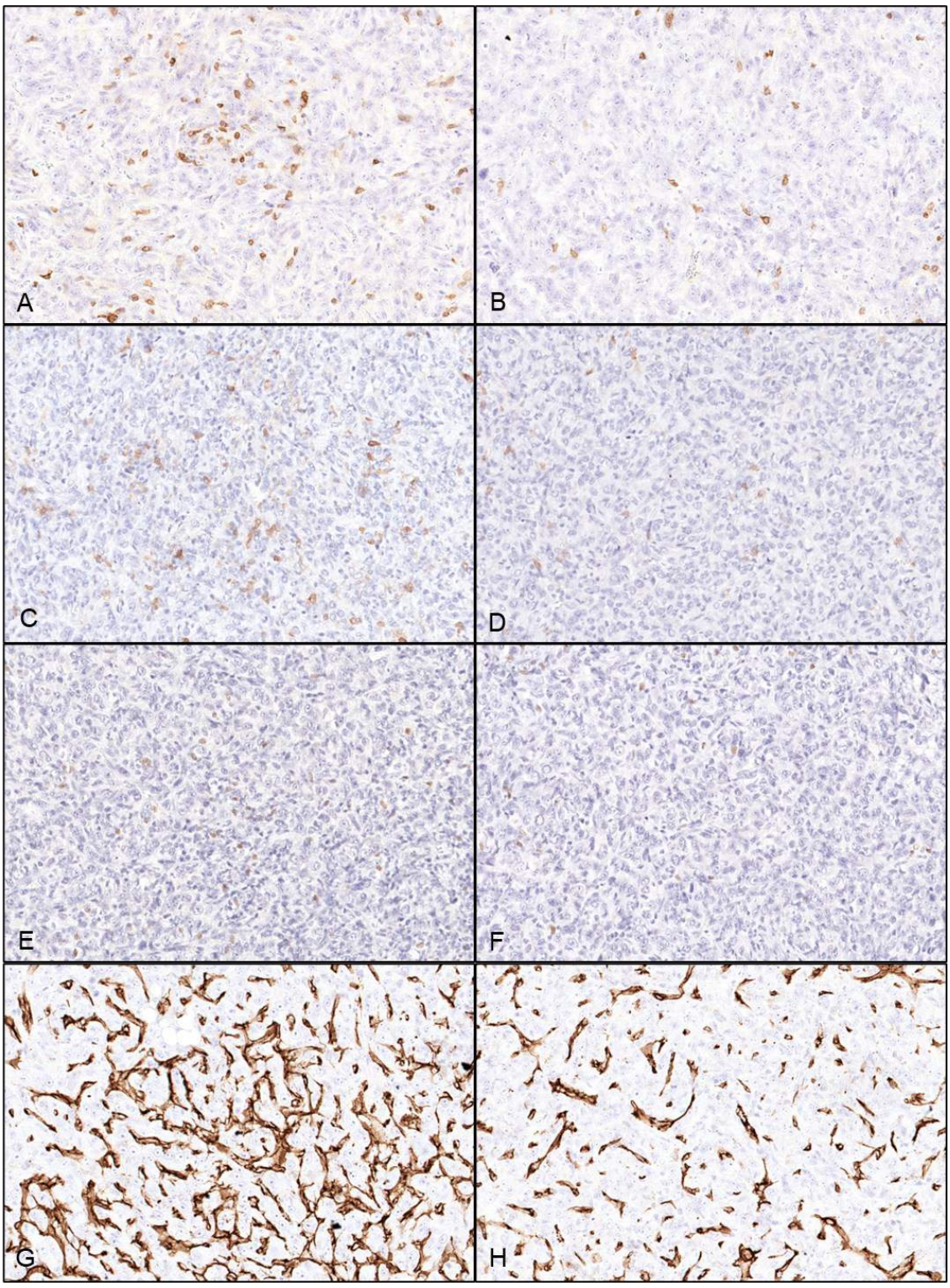

Figure 6. **MPMs**. Immunohistochemistry for CD3 (**A, B**), CD4 (**C, D**), FoxP3 (**E, F**) and CD31 (**G, H**). Anti CD-44 treated mice had more intratumoral CD3+ (**A**), CD4+ (**C**), FoxP3+ (**E**) infiltrating cells and more blood vessels (**G**) compared to anti-irrelevant mice (**B, D, F, H** respectively).

Table 2. Results summary of experiment 2.

Group	Mouse ID	No. of Tumors	Total Tumor Area	Mean Tumor Area	Total Necrosis Area	Mean Necrosis Area	% Tumors with necrosis	Total Angiectaisa Area	Mean Angiectasia Area	% Tumors with Angectasia/ Hemorrhage
shSCRB anti-Irrelevante	2AD	32	31.12	0.97	0.772	0.010	3%	0.65	0.062	28%
	2AS	40	57.65	1.44	3.21	0.035	10%	1.25	0.021	15%
	2BD	0	0.00	0.00	0.00	0.000	0%	0.00	0.000	0%
	2BS	22	28.87	1.31	1.43	0.044	32%	2.12	0.103	55%
	20	37	65.04	1.76	4.90	0.035	22%	3.02	0.047	35%
	Mean	26.20	36.53	1.10	2.06	0.025	13%	1.41	0.05	27%
	Mean w/o 2BD	32.75	45.67	1.37	2.58	0.03	17%	1.76	0.06	33%
shSCRB anti-CD44	3AD	26	27.67	1.06	2.39	0.048	12%	0.54	0.024	15%
	3AS	16	17.25	1.08	0.00	0.000	0%	1.29	0.086	44%
	3BD	32	71.35	2.23	0.38	0.015	13%	4.17	0.073	30%
	3BS	24	21.64	0.87	0.26	0.013	8%	0.52	0.055	20%
	30	5	2.69	0.54	0.00	0.000	0%	0.05	0.034	33%
	Mean	20.60	28.12	1.16	0.60	0.02	7%	1.31	0.05	28%
	Mean w/o 30	24.50	34.48	1.31	0.76	0.02	8%	1.63	0.06	27%

6.4. Discussion

This study investigated the role of OPN expression in a murine orthotopic model of MPM and its relationship with neoplastic growth and immune cell infiltration. Although OPN has already been investigated as a prognostic marker in humans, studies on the functional role of OPN in MPM development and progression were lacking (Grigoriu et al. 2007; Rangaswami et al. 2006). OPN silencing of AB22 mesothelioma cells resulted in decreased tumors number and decreased tumor area in mice sacrificed at both day 17 and day 59 post tumoral cells injection, compared to control not-OPN silenced mice, supporting an OPN pro-tumoral role in MPM development. Elevated OPN levels have, in fact, been detected in several malignancies including breast, prostate, colorectal and lung carcinomas and melanoma and have been associated to tumor progression (Irby et al. 2004; Thalmann et al. 1999; Zhou et al. 2005; Chambers et al. 1996; Cook et al. 2005). OPN tumor-promoting functions are achieved through different mechanisms: by binding to CD44 membrane receptor triggering an intracellular pathway which favors cancer cell survival, by activating MMPs leading to extracellular matrix remodeling and tumor invasion enhancement and by PI3K/Akt pathway activation with promotion of tumor angiogenesis (Rangaswami et al. 2006; Kariya et al. 2022). Interestingly, OPN expression was immunohistochemically detected both in the cytoplasm of cells and extracellular space, in its secreted form, without statistically significant differences among groups. This could be attributable to OPN expression by tumor-associated macrophages, since these cells can express OPN.

The blocking of CD44 in OPN producing MPM cells, although not statistically significant, resulted in decreased tumoral growth, thus suggesting that the CD44/IL-33 pathway could be involved in MPM development. CD44 has in fact been related to cancer cells proliferation, epithelial–mesenchymal transition and metastasis in several human cancers, comprising gallbladder (He et al. 2018), prostate (Carneiro et al. 2019), and ovarian carcinomas, (Mishra et al. 2019) oral squamous cell carcinomas (Yuan et al 2022) and melanomas (Dzobo et al. 2021). The immunohistochemical analysis revealed that intra tumoral CD3+ T cells, CD4+ T cells and CD31+ blood vessels were increased in anti-CD44 treated mice while FoxP3+ T regulatory cells were decreased compared to anti-irrelevant treated mice. CD44 expression has, in fact, been correlated to M2 TAMs and T helper cells tumor-immune cell infiltration (Liu S et al 2023) and CD44 expression additionally promotes the expression of FoxP3 and T regulatory cells survival, thus,

inducing cancer immunosuppression (Liu et al. 2009; Bollyky et al. 2009). These findings suggest that the OPN-CD44 axis could impact immune cell recruitment in MPMs, modulating the immune microenvironment.

Interestingly, anti-CD44 treated animals also had lower GPNMB expression, another molecule interacting with CD44 receptor and associated with cancer immunosuppression. GPNMB, in fact, promotes M2 macrophage infiltration and suppresses pro-inflammatory cytokines. (Lazaratos et al. 2022). The lower expression of this marker highlights how blockage of its receptor CD44 could lead to a decrease of GPNMB.

Even with a higher vascular density, anti CD44 mice had lower tumor burden compared to anti-irrelevant mice. This could be attributed to the lower immunosuppressive presence of FoxP3+ cells or to others, not investigated, mechanisms. CD44/IL33 inhibition, could have led, for instance, to decrease activation of other tumor-promoting pathways such as STAT3 or PI3K/Akt pathways leading to decreased growth factors production or even to an increase in P53 activity with enhanced tumor apoptosis (Bonelli et al. 2020; Huang et al. 2021).

In conclusion this study highlighted the pivotal role of OPN and of CD44 in MPM development and growth. The silencing of OPN and the blockage of CD44 influenced tumor growth and modulated tumor-immune system infiltrates and GPNMB expression providing valuable data on OPN and CD44 as potential prognostic and therapeutic targets in MPM patients.

7. CONCLUSIONS

This thesis characterizes murine immune system cells across various physiological and pathological conditions.

The first study characterized healthy tissue mononuclear phagocytes through a combination of cellular morphology, tissue localization, and immunohistochemical analysis. For each organ, a synoptic Table summarizing the findings has been provided, to facilitate data consultation (supplemental Tables 2-19). This work serves as a valuable resource for researchers employing histopathological and immunohistochemical techniques as well as flow cytometry and molecular techniques, which provide data without considering tissue context and cellular morphology.

The second study investigated potential sex-related differences in an inflammatory model of caerulein-induced acute pancreatitis through a combination of histopathology and clinical chemistry and focused on the characterization and quantification of macrophages, T and B lymphocytes and neutrophils through digital image analysis. This study highlighted a sex-related modulation of pancreatitis severity, apoptosis, regeneration as well as of M1 and M2 macrophages recruitment.

The third study compared two methods of digital image analysis (DIA) on pancreatitis samples, a whole slide approach and a hot spot field approach, aimed at immune cells quantification. Given the increasing prevalence of image analysis in histopathology, as evidenced by the high number of recent publications in the literature, and the lack of direct comparisons among different analysis methods, a comparative analysis between whole-slide and hot spot field approaches has been performed, discussing advantages and disadvantages of each technique.

Lastly, in the fourth study, tumor infiltrating lymphocytes and tumor-associated macrophages were studied and quantified in an orthotopic model of pleural malignant mesothelioma, revealing an Osteopontin and a CD44 modulation on tumor growth, vascularization, and T cells infiltration.

Overall, the data presented in this thesis significantly contributes to the understanding of murine immune system dynamics in physiological, inflammatory, and neoplastic conditions, providing valuable insights on immune system cells activity and recruitment and presenting valuable observations for future investigations in murine immunopathology.

8. REFERENCES

1. Adler LN, Jiang W, Bhamidipati K et al. The other function: class II-restricted antigen presentation by B cells. *Front Immunol*. 2017. 8:319.
2. Aeffner F, Zarella MD, Buchbinder N et al. Introduction to Digital Image Analysis in Whole-slide Imaging: A White Paper from the Digital Pathology Association. *J Pathol Inform*. 2019. 10:9-15.
3. Aiello S, Noris M, Piccinini G et al. Thymic dendritic cells express inducible nitric oxide synthase and generate nitric oxide in response to self- and alloantigens. *J Immunol*. 2000. 164(9):4649-58.
4. Alliot F, Godin I, Pessac B. Microglia derives from progenitors, originating from the yolk sac, and which proliferate in the brain. *Brain Res Dev Brain Res*. 1999. *117*(2):145–152.
5. Allavena P, Sica A, Solinas G, Porta C, Mantovani A. The inflammatory micro-environment in tumor progression: the role of tumor-associated macrophages. *Crit Rev Oncol Hematol*. 2008. 66(1):1-9.
6. Allman D, Wilmore JR, Gaudette BT. The continuing story of T-cell independent antibodies. *Immunol Rev*. 2019. 288(1):128-135.
7. Alsubaie N, Trahearn N, Raza SE, Snead D, Rajpoot NM. Stain Deconvolution Using Statistical Analysis of Multi-Resolution Stain Colour Representation. *PLoS One*. 2017. 12(1):e0169875.
8. Altavilla D, Famulari C, Passaniti M, Galeano M, Macrì A, Seminara P et al. Attenuated Caerulein-Induced Pancreatitis in Nuclear Factor–kB–Deficient Mice. *Lab Invest*. 2003. 83(12):1723-1732.
9. Antonangeli F, Grimsholm O, Rossi MN, Velotti F. Editorial: Cellular Stress and Inflammation: How the Immune System Drives Tissue Homeostasis. *Front Immunol*. 2021. 12:668876.
10. Apaolaza PS, Petropoulou PI, Rodriguez-Calvo T. Whole-Slide Image Analysis of Human Pancreas Samples to Elucidate the Immunopathogenesis of Type 1 Diabetes Using the QuPath Software. *Front Mol Biosci*. 2021. 8:689799.
11. Aristizabal B, Gonzalez A. *Innate immune system*. In: Anaya JM, Shoenfeld Y, Rojas-Villarraga A, et al. *Autoimmunity: from Bench to Bedside*. El Rosario University Press, 2013.
12. Arredouani M, Yang Z, Ning Y et al. The scavenger receptor MARCO is required for lung defense against pneumococcal pneumonia and inhaled particles. *J Exp Med*. 2004. 200(2):267-72.
13. Avallone G, Rasotto R, Chambers JK et al. Review of Histological Grading Systems in Veterinary Medicine. *Vet Pathol*. 2021. (5):809-828.
14. Avota E, Koethe S, Schneider-Schaulies S. Membrane dynamics and interactions in measles virus dendritic cell infections. *Cell Microbiol*. 2013. 15(2):161-9.
15. Axelrod ML, Cook RS, Johnson DB, Balko JM. Biological Consequences of MHC-II Expression by Tumor Cells in Cancer. *Clin Cancer Res*. 2019. 15;25(8):2392-2402.
16. Azad AK, Rajaram MV, Schlesinger LS. Exploitation of the Macrophage Mannose Receptor (CD206) in Infectious Disease Diagnostics and Therapeutics. *J Cytol Mol Biol*. 2014. 1(1):1000003.
17. Bailey M, Christoforidou Z, Lewis MC. The evolutionary basis for differences between the immune systems of man, mouse, pig and ruminants. *Vet Immunol Immunopathol*. 2013. 152(1-2):13-9.
18. Bain CC, Schridde A. Origin, Differentiation, and Function of Intestinal Macrophages. *Front Immunol*. 9:2733, 2018.
19. Baharom F, Rankin G, Blomberg A et al. Human Lung Mononuclear Phagocytes in Health and Disease. *Front Immunol*. 2017. 8:499.
20. Balan S, Saxena M, Bhardwaj N. Dendritic cell subsets and locations. *Int Rev Cell Mol Biol*. 2019. 348:1-68.
21. Bankhead P, Loughrey MB, Fernández JA et al. QuPath: Open-source software for digital pathology image analysis. *Sci Rep*. 2017. 7(1):16878.

22. Baratin M, Simon L, Jorquera A et al. T Cell Zone Resident Macrophages Silently Dispose of Apoptotic Cells in the Lymph Node. *Immunity*. 2017. 15;47(2):349-362.
23. Barboza T, Beaufrère H, Reavill D, Susta L. Morphological features of hepatic lipid changes in bearded dragons (*Pogona vitticeps*) and a proposed grading system. *Vet Pathol.* 2023. 60(1):123-132.
24. Barnaba V, Watts C, de Boer M, Lane P, Lanzavecchia A. Professional presentation of antigen by activated human T cells. *Eur J Immunol*. 1994. 24(1):71-5.
25. Barron L, Smith AM, El Kasmi KC et al. Role of arginase 1 from myeloid cells in th2-dominated lung inflammation. *PloS One*. 2013. 8(4):e61961.
26. Baumgart M, Moos V, Schuhbauer D, Müller B. Differential expression of major histocompatibility complex class II genes on murine macrophages associated with T cell cytokine profile and protective/suppressive effects. *Proc Natl Acad Sci U S A.* 1998. 9;95(12):6936-40.
27. Bedrosian AS, Nguyen AHm Hackman M. Dendritic cells promote pancreatic viability in mice with acute pancreatitis. *Gastroenterology.* 2011. 141(5): 1915-1926.
28. Bellomo A, Gentek R, Bajénoff M et al. Lymph node macrophages: Scavengers, immune sentinels and trophic effectors. *Cell Immunol*. 2018. 330:168-174.
29. Bhushan S, Theas MS, Guazzone VA et al. Immune Cell Subtypes and Their Function in the Testis. *Front Immunol*. 2020. 11:583304.
30. Björkström NK. Immunobiology of the biliary tract system. *J Hepatol*. 2022. 77(6):1657-1669.
31. Bjornson-Hooper ZB, Fragiadakis GK, Spitzer MH et al. A Comprehensive Atlas of Immunological Differences Between Humans, Mice, and Non-Human Primates. *Front Immunol*. 2022 Mar 11;13:867015.
32. Bleesing JJ, Fleisher TA. Human B cells express a CD45 isoform that is similar to murine B220 and is downregulated with acquisition of the memory B-cell marker CD27. *Cytometry B Clin Cytom*. 2003. 51(1):1-8.
33. Blériot C, Ginhoux F. Understanding the Heterogeneity of Resident Liver Macrophages. *Front Immunol*. 2019, 10:2694.
34. Bollyky PL, Falk BA, Long SA et al. CD44 stimulation promotes FoxP3+ regulatory T cell persistence and function via production of IL-2, IL-10, and TGF-beta. *J Immunol*. 2009.183(4):2232-41.
35. Bonelli M, Terenziani R, Zoppi S et al. Dual Inhibition of CDK4/6 and PI3K/AKT/mTOR Signaling Impairs Energy Metabolism in MPM Cancer Cells. *Int J Mol Sci*. 2020. 21(14):5165.
36. Bonnardel J, Da Silva C, Henri S et al. Innate and adaptive immune functions of Peyer's patch monocyte-derived cells. 2015. *Cell Rep*. 11(5):770-84.
37. Boonchan M, Arimochi I, Otsuka K et al. Necroptosis protects against exacerbation of acute pancreatitis. *Cell Death Dis*. 2021. 12 (6):60.
38. Borges da Silva H, Fonseca R, Pereira RM. Splenic macrophage subsets and their function during blood-borne infections. *Front Immunol*. 2015. 6:480.
39. Boshtam M, Asgary S, Kouhpayeh S, Shariati L, Khanahmad H. Aptamers Against Pro- and Anti-Inflammatory Cytokines: A Review. *Inflammation*. 2017. 40(1):340-349.
40. Bosma GC, Custer RP, Bosma MJ. A severe combined immunodeficiency mutation in the mouse. *Nature*. 1983;301:527–530.
41. Brahmadi A, Ningrom IC. Comparative analysis of Kidney Histomormophetry utilizing two distinct image processing software. *J Biomed Trasl Med*. 2023. 9 (3): 104-110.
42. Brcic L, Kern I. Clinical significance of histologic subtyping of malignant pleural mesothelioma. *Transl Lung Cancer Res*. 9(3):924-933, 2020.
43. Brestoff JR, Kim BS, Saenz SA et al. Group 2 innate lymphoid cells promote beiging of white adipose tissue and limit obesity. *Nature*. 2015. 519(7542):242-6.
44. Bronte V, Serafini P, De Santo C et al. IL-4-induced arginase 1 suppresses alloreactive T cells in tumor-bearing mice. *J Immunol*. 2003. 170(1):270-8,
45. Brügmann A, Eld M, Lelkaitis G. Digital image analysis of membrane connectivity is a robust measure of HER2 immunostains. *Breast Cancer Res Treat.* 2012. 132(1):41-9.

46. Bueno R, Stawiski EW, Goldstein LD et al. Comprehensive genomic analysis of malignant pleural mesothelioma identifies recurrent mutations, gene fusions and splicing alterations. *Nat Genet*. 48(4):407-16, 2016.
47. Caër C and Wick MJ. Human Intestinal Mononuclear Phagocytes in Health and Inflammatory Bowel Disease. *Front Immunol*. 2020. 11:410, 2020.
48. Calderon B, Carrero JA, Ferris ST et al. The pancreas anatomy conditions the origin and properties of resident macrophages. *J Exp Med*. 2015; 212(10):1497-512.
49. Cano RLE, Lopera DE. Introduction to B and T lymphocytes. In: Anaya JM, Shoenfeld Y, Rojas-Villarraga A, et al. Autoimmunity: from Bench to Bedside. El Rosario University Press, 2013.
50. Cariappa A, Chase C, Liu H, Russell P, Pillai S. Naive recirculating B cells mature simultaneously in the spleen and bone marrow. *Blood*. 2007. 109(6):2339-45.
51. Carlin LM, Stamatiades EG, Auffray C, Hanna RN, Glover L, Vizcay-Barrena G et al. Nr4a1-dependent Ly6C(low) monocytes monitor endothelial cells and orchestrate their disposal. *Cell*. 2013. *153*(2): 362–375.
52. Cassado A. F4/80 as a Major Macrophage Marker: The Case of the Peritoneum and Spleen. *Results Probl Cell Differ*. 2017;62:161-179.
53. Castelo-Branco C, Soveral I. The immune system and aging: a review. *Gynecol Endocrinol*. 2014. 30(1):16-22.
54. Cerutti A, Cols M, Puga I. Marginal zone B cells: virtues of innate-like antibody-producing lymphocytes. *Nat Rev Immunol*. 2013. 13(2):118-32.
55. Cesta MF. Normal structure, function and histology of the spleen. *Toxicol Pathol*. 2006. 34(5):455-465.
56. Chambers AF, Wilson SM, Kerkvliet N, O'Malley FP, Harris JF, Casson AG. Osteopontin expression in lung cancer. *Lung Cancer*. 1996. 15(3):311-23.
57. Chantrain CF, DeClerck YA, Groshen S, McNamara G. Computerized quantification of tissue vascularization using high-resolution slide scanning of whole tumor sections. *J Histochem Cytochem*. 2003. 51(2):151-8.
58. Chaplin DD. Overview of the immune response. *J Allergy Clin Immunol*. 2010, 125(2 Suppl 2):S3-23.
59. Charnetski CJ, Brennan FX. Sexual frequency and salivary immunoglobulin A (IgA). *Psychol Rep*. 2004. 94(3 Pt 1):839-44.
60. Chauveau C, Rémy S, Royer PJ et al. Heme oxygenase-1 expression inhibits dendritic cell maturation and proinflammatory function but conserves IL-10 expression. *Blood*. 2005. 106(5):1694-702.
61. Chen J, Wright K, Davis JM, Jeraldo P, Marietta EV, Murray J et al. An expansion of rare lineage intestinal microbes characterizes rheumatoid arthritis. *Genome Med*. 2016. 8(1):43.
62. Chen M, Tabaczewski P, Truscott SM et al. Hepatocytes express abundant surface class I MHC and efficiently use transporter associated with antigen processing, tapasin, and low molecular weight polypeptide proteasome subunit components of antigen processing and presentation pathway. *J Immunol*. 2005. 175(2): 1047-1055.
63. Chen Y, Hwang SL, Chan VS et al. Binding of HIV-1 gp120 to DC-SIGN promotes ASK-1-dependent activation-induced apoptosis of human dendritic cells. *PLoS Pathog*. 2013. 9(1):e1003100.
64. Cheung MD, Erman EN, Moore KH et al. Resident macrophage subpopulations occupy distinct microenvironments in the kidney. *JCI Insight*. 2022. 7(20):e161078.
65. Chirumbolo S, Bjørklund G, Sboarina A, Vella A. The role of basophils as innate immune regulatory cells in allergy and immunotherapy. *Hum Vaccin Immunother*. 2018. 14(4):815-831.
66. Choi KM, Kashyap PC, Dutta M. CD206-Positive M2 Macrophages That Express Heme Oxygenase-1 Protect Against Diabetic Gastroparesis in Mice. *Gastroenterology*. 2010. 138:2399–2409.
67. Chorro L, Sarde A, Li M, Woollard KJ, Chambon P, Malissen B. et al. Langerhans cell (LC) proliferation mediates neonatal development, homeostasis, and inflammation-associated expansion of the epidermal LC network. *J Exp Med*. 2009. 206(13): 3089–3100.

68. Chow A, Brown BD, Merad M. Studying the mononuclear phagocyte system in the molecular age. *Nat Rev Immunol.* 2011. 11(11):788-798.
69. Cinelli MA, Do HT, Miley GP, Silverman RB. Inducible nitric oxide synthase: Regulation, structure, and inhibition. *Med Res Rev*. 40(1):158-189, 2020.
70. Cizkova K, Foltynkova T, Gachechiladze M, Tauber Z. Comparative Analysis of Immunohistochemical Staining Intensity Determined by Light Microscopy, ImageJ and QuPath in Placental Hofbauer Cells. *Acta Histochem Cytochem*. 2021. 25;54(1):21-29..
71. Clever S, Volz A. Mouse models in COVID-19 research analyzing the adaptive immune response. *Med Microbiol Immunol*. 2023. 212(2):165-183.
72. Constant DA, Nice TJ, Rauch I. Innate immune sensing by epithelial barriers. *Curr Opin Immunol*. 2021. 73:1-8.
73. Cook AC, Tuck AB, McCarthy S et al. Osteopontin induces multiple changes in gene expression that reflect the six "hallmarks of cancer" in a model of breast cancer progression. *Mol Carcinog*. 2005. 43(4):225-36.
74. Correa RG, Milutinovic S, Reed JC. Roles of NOD1 (NLRC1) and NOD2 (NLRC2) in innate immunity and inflammatory diseases. Biosci Rep. 2012 Dec;32(6):597-608.
75. Cox MA, Kahan SM, Zajac AJ. Anti-viral CD8 T cells and the cytokines that they love. *Virology*. 2013. 435(1):157-69.
76. Crotty S, Felgner P, Davies H, Glidewell J, Villarreal L, Ahmed R. Cutting edge: long-term B cell memory in humans after smallpox vaccination. *J Immunol*. 2003. 171(10):4969-73.
77. Da Silva N, Barton CR. Macrophages and dendritic cells in the post-testicular environment. 2016. *Cell Tissue Res*. 363(1):97-104.
78. Davies LC, Jenkins SJ, Allen JE, Taylor PR. Tissue-resident macrophages. *Nat Immunol.* 2013. *14*(10): 986–995.
79. Davis MR, Manning LS, Whitaker D, Garlepp MJ, Robinson BW. Establishment of a murine model of malignant mesothelioma. *Int J Cancer*. 52(6):881-6, 1992.
80. DeFalco T, Bhattacharya I, Williams AV et al. Yolk-sac-derived macrophages regulate fetal testis vascularization and morphogenesis. *Proc Natl Acad Sci U S A*. 2014. 10;111(23):E2384-93.
81. De Schepper S, Verheijden S, Aguilera-Lizarraga J et al. Self-Maintaining Gut Macrophages Are Essential for Intestinal Homeostasis. 2018. *Cell*. 175(2):400-415.
82. Delfini M, Stakenborg N, Viola MF et al. Macrophages in the gut: Masters in multitasking. *Immunity*. 2022. 55(9):1530-1548.
83. Dempsey PW, Allison ME, Akkaraju S, Goodnow CC, Fearon DT. C3d of complement as a molecular adjuvant: bridging innate and acquired immunity. *Science*. 1996. 271(5247):348-50.
84. Deniset JF, Surewaard BG, Lee WY, Kubes P. Splenic $Ly6G^{high}$ mature and $Ly6G^{int}$ immature neutrophils contribute to eradication of *S. pneumoniae*. *J Exp Med*. 2017. 214(5):1333-1350.
85. Devey L, Ferenbach D, Mohr E et al. Tissue-resident macrophages protect the liver from ischemia reperfusion injury via a heme oxygenase-1 dependent mechanism. *Mol Ther*. 2009.17(1):65-72.
86. Dhatchinamoorthy K, Colbert JD, Rock KL. Cancer Immune Evasion Through Loss of MHC Class I Antigen Presentation. *Front Immunol*. 2021. 12:636568.
87. Diakopoulos KN, Lesina M, Wormann S, Song L, Aichler M, Shild L et al. Impaired autophagy induced chronic atrophic pancreatitis in mice via sex and nutrition-dependent process. *Gastroenterology*. 2015. 148:626-638.
88. Digifico E, Erreni M, Colombo FS, Recordati C, Migliore R, Frapolli R et al. Optimization of a Luciferase-Expressing Non-Invasive Intrapleural Model of Malignant Mesothelioma in Immunocompetent Mice. *Cancers (Basel).* 12(8):2136, 2020.
89. Doeing DC, Borowicz JL, Crockett ET. Gender dimorphism in differential peripheral blood leukocyte counts in mice using cardiac, tail, foot, and saphenous vein puncture methods. *BMC Clin Pathol.* 2003. 3(1):3.
90. Doener F, Michel A, Reuter S et al. Mast cell-derived mediators promote murine neutrophil effector functions. *Int Immunol*. 2013. 25(10):553-61.

91. Dolfi B, Gallerand A, Firulyova MM et al. Unravelling the sex-specific diversity and functions of adrenal gland macrophages. *Cell Rep*. 2022. 14;39(11):110949.
92. Donovan KM, Leidinger MR, McQuillen LP et al. Allograft Inflammatory Factor 1 as an Immunohistochemical Marker for Macrophages in Multiple Tissues and Laboratory Animal Species. *Comp Med*. 2018. 68(5):341-348.
93. Drake M, Dodwad SJM, Davis J, Kao LS, Cao Y, Ko TC. Sex related differences of acute and chronic pancreatitis in adults. *J. Clin. Med*. 2021. 10, 300.
94. Duffy EB, Drake JR, Harton JA. Evolving Insights for MHC Class II Antigen Processing and Presentation in Health and Disease. *Curr Pharmacol Rep* . 2017. 3: 213–220.
95. Dunkelberger JR, Song WC. Complement and its role in innate and adaptive immune responses. *Cell Res*. 2010. 20(1):34-50.
96. Dzobo K, Sinkala M. Cancer Stem Cell Marker CD44 Plays Multiple Key Roles in Human Cancers: Immune Suppression/Evasion, Drug Resistance, Epithelial-Mesenchymal Transition, and Metastasis. *OMICS*. 2021. 25(5):313-332.
97. Katsoulis-Dimitriou K, Kotrba J, Voss M, Dudeck J, Dudeck A. Mast Cell Functions Linking Innate Sensing to Adaptive Immunity. *Cells*. 2020. 9(12):2538.
98. Eberl G, Colonna M, Di Santo JP, McKenzie AN. Innate lymphoid cells: a new paradigm in immunology. *Science*. 22;348(6237), 2015.
99. English K, Tan SY, Kwan R et al. The liver contains distinct interconnected networks of $CX3CR1^{+}$ macrophages, $XCR1^{+}$ type 1 and $CD301a^{+}$ type 2 conventional dendritic cells embedded within portal tracts. *Immunol Cell Biol*. 2022. 200(6):394-408.
100. Eiz-Vesper B, Schmetzer HM. Antigen-Presenting Cells: Potential of Proven und New Players in Immune Therapies. Transfus Med Hemother. 2020 Dec;47(6):429-431.
101. Elizondo DM, Andargie TE, Yang D et al. Inhibition of Allograft Inflammatory Factor-1 in Dendritic Cells Restrains CD4+ T Cell Effector Responses and Induces CD25+Foxp3+ T Regulatory Subsets. *Front. Immunol*. 2017. 8:1502.
102. Elizondo DM, Brandy NZD, da Silva RLL et al. Allograft Inflammatory Factor-1 Governs Hematopoietic Stem Cell Differentiation Into cDC1 and Monocyte-Derived Dendritic Cells Through IRF8 and RelB in vitro. *Front. Immunol*. 2019. 10:173.
103. Eloranta ML, Alm GV. Splenic marginal metallophilic macrophages and marginal zone macrophages are the major interferon-alpha/beta producers in mice upon intravenous challenge with herpes simplex virus. *Scand J Immunol*. 1999. 49(4):391-4.
104. Esensten JH, Helou YA, Chopra G, Weiss A, Bluestone JA. CD28 Costimulation: From Mechanism to Therapy. *Immunity*. 2016. 44(5):973-88.
105. Eu wide animal research statistics, 2020. Accessed November 15, 2023. https://www.understandinganimalresearch.org.uk/news/eu-wide-animal-research-statistics-2020.
106. Eyerich S, Eyerich K, Pennino D et al. Th22 cells represent a distinct human T cell subset involved in epidermal immunity and remodeling. *J Clin Invest*. 2009. 119(12):3573-85.
107. Evren E, Ringqvist E, Willinger T. Origin and ontogeny of lung macrophages: from mice to humans. *Immunology*. 2020 Jun;160(2):126-138.
108. Feng D, Xiang X, Guan Y et al. Monocyte-derived macrophages orchestrate multiple cell-type interactions to repair necrotic liver lesions in disease models. *J Clin Invest*. 133,15:e166954, 2023.
109. Feyaerts D, Urbschat C, Gaudillière B, Stelzer IA. Establishment of tissue-resident immune populations in the fetus. *Semin Immunopathol*. 2022. 44(6):747-766.
110. Folias E. Peneranda C, Su AL. Aberrant Innate Immune Activation following Tissue Injury Impairs Pancreatic Regeneration Alexandra. *PLoS One*. 9(7):e102125, 2014.
111. Filippi MD. Mechanism of Diapedesis: Importance of the Transcellular Route. *Adv Immunol*. 2016. 129:25-53.
112. Flores AR, Rêma A, Mesquita JR et al. Vimentin and Ki-67 immunolabeling in canine gastric carcinomas and their prognostic value. *Vet Pathol*. 2022. 59(6):903-914.
113. Franchi L, Warner N, Viani K, Nuñez G. Function of Nod-like receptors in microbial recognition and host defense. *Immunol Rev*. 2009. 227(1):106-28.

114. Frauwirth KA, Thompson CB. Activation and inhibition of lymphocytes by costimulation. *J Clin Invest*. 2002. 109(3):295-9.
115. Fujiyama S, Nakahashi-Oda C, Abe F. Identification and isolation of splenic tissue-resident macrophage sub-populations by flow cytometry. *Int Immunol*. 2019. 31(1):51-56.
116. Fukaya T, Murakami R, Takagi H et al. Conditional ablation of CD205+ conventional dendritic cells impacts the regulation of T-cell immunity and homeostasis in vivo. *Proc Natl Acad Sci U S A*. 2012. 109(28):11288-93.
117. Gabrilovich DI, Nagaraj S. Myeloid-derived suppressor cells as regulators of the immune system. *Nat Rev Immunol*. 2009. 9(3):162-74.
118. Gautier EL, Shay T, Miller J. Gene-expression profiles and transcriptional regulatory pathways that underlie the identity and diversity of mouse tissue macrophages. *Nat Immunol*. 2012. 13(11):1118-1128.
119. Gay L, Melenotte C, Lakbar I, Mezouar S, Devaux C, Raoult D et al. Sexual dimorphism and gender in infectious diseases. *Front Immunol*. 2021. 12:698121.
120. Geddes K, Magalhães JG, Girardin SE. Unleashing the therapeutic potential of NOD-like receptors. *Nat Rev Drug Discov*. 2009. 8(6):465-79.
121. George JF, Lever JM, Agarwal A. Mononuclear phagocyte subpopulations in the mouse kidney. *Am J Physiol Renal Physiol*. 2017. 312(4):640-646.
122. Gibbings SL, Jakubzick CV. Isolation and Characterization of Mononuclear Phagocytes in the Mouse Lung and Lymph Nodes. *Methods Mol Biol*. 2018. 1809:33-44.
123. Gibbings SL, Thomas SM, Atif SM et al. Three Unique Interstitial Macrophages in the Murine Lung at Steady State. *Am J Respir Cell Mol Biol*. 2017. 57(1):66-76.
124. Ginhoux F, Greter M, Leboeuf M et al. Fate mapping analysis reveals that adult microglia derive from primitive macrophages. *Science*. 2010. 330(6005):841-5.
125. Girardin SE, Boneca IG, Viala J, Chamaillard M, Labigne A, Thomas G, Philpott DJ, Sansonetti PJ. Nod2 is a general sensor of peptidoglycan through muramyl dipeptide (MDP) detection. *J Biol Chem*. 2003. 278(11):8869-72.
126. Gitto SB, Nakkina SP, Beardsley JM, Altomare DA. *Induction of pancreatitis in mice with susceptibility to pancreatic cancer*. In: *Experimental Models of Infection, Inflammation, and Injury*. Methods in Cell Biology, Volume 168,1st edition, Academic Press.
127. Godwin JW, Pinto AR, Rosenthal NA. Chasing the recipe for a pro-regenerative immune system. *Semin Cell Dev Biol*. 2017. 61:71-79.
128. Gogou E, Zarogiannis SG, Siachpazidou D, Hatzoglou C and Gourgoulianis KI. Causes and Pathogenesis of Malignant Mesothelioma. In *Mesothelioma*. IntechOpen; 2022.
129. Gomes-Solecki M, Santecchia I, Werts C. Animal Models of Leptospirosis: Of Mice and Hamsters. *Front Immunol*. 2017. 21;8:58.
130. Gondek DC, Lu LF, Quezada SA, Sakaguchi S, Noelle RJ. Cutting edge: contact-mediated suppression by CD4+CD25+ regulatory cells involves a granzyme B-dependent, perforin-independent mechanism. *J Immunol*. 2005. 174(4):1783-6.
131. Gordon S and Pluddemann A. The mononuclear phagocytic system. Generation of diversity. *Front Immunol*. 10:1893, 2019.
132. Gordon S and Martinez FO. Alternative activation of macrophages: mechanism and functions. *Immunity*. 2010. 32(5):593-604.
133. Goudot C, Coillard A, Villani AC, Gueguen P, Cros A. Sarkizova S et al. Aryl Hydrocarbon Receptor Controls Monocyte Differentiation into Dendritic Cells versus Macrophages. *Immunity*. 2017. 47(3): 582–596.
134. Gray EE, Cyster JG. Lymph node macrophages. *J Innate Immun*. 2012. 4(56):424-436.
135. Grigoriu BD, Scherpereel A, Devos P et al. Utility of osteopontin and serum mesothelin in malignant pleural mesothelioma diagnosis and prognosis assessment. *Clin Cancer Res*. 2007. 13(10):2928-35.
136. Gu X, Li SY, DeFalco T. Immune and vascular contributions to organogenesis of the testis and ovary. *FEBS J*. 2022. 289(9):2386-2408.

137. Guarino MP, Carotti S, Morini S et al. Decreased number of activated macrophages in gallbladder muscle layer of cholesterol gallstone patients following ursodeoxycholic acid. *Gut*. 2008. 57(12):1740-1741.
138. Gubin MM, Vesely MD. Cancer Immunoediting in the Era of Immuno-oncology. *Clin Cancer Res*. 2022. 28(18):3917-3928.
139. Guerri L, Peguillet I, Geraldo Y et al. Analysis of APC types involved in CD4 tolerance and regulatory T cell generation using reaggregated thymic organ cultures. *J Immunol*. 2013. 190(5):2102-2110.
140. Guilliams M, Ginhoux F, Jakubzick C et al. Dendritic cells, monocytes and macrophages: a unified nomenclature based on ontogeny. *Nat Rev Immunol*. 2014. 4(8):571-8.
141. Guilliams M, Mildner A, Yona S. Developmental and Functional Heterogeneity of Monocytes. *Immunity*. 2018. 49(4):595-613.
142. Guilliams M, Van de Laar L. A hitchhiker's guide to myeloid cell subsets: practical implementation of a novel mononuclear phagocyte system. *Front Immunol*. 6:406, 2015.
143. Güney Saruhan B, Sağsöz H, Akbalık E et al. Distribution of CD68-, CD8-, MHCI- and MHCII-positive cells in the bull and ram testis and epididymis. 2017. *Anat Histol Embryol*. 47(4):313-321.
144. Hagen CM, Roth E, Graf TR, Verrey F, Graf R, Gupta A et al. Loss of LAT1 sex-dependently delays recovery after caerulein induced acute pancreatitis. *Word J Gastroenterol*. 2022. 28(10):1024-1054.
145. Haley PJ. Species differences in the structure and function of the immune system. *Toxicology*. 2003. 188(1):49-71.
146. Han Y, Liu D, Li L. PD-1/PD-L1 pathway: current researches in cancer. *Am J Cancer Res*. 2020. 10(3):727-742.
147. Han J, Gallerand A, Erlich EC et al. Human serous cavity macrophages and dendritic cells possess counterparts in the mouse with a distinct distribution between species. *Nat Immunol*. 2024 Jan;25(1):155-165.
148. Hansen JD, Vojtech LN, Laing KJ. Sensing disease and danger: a survey of vertebrate PRRs and their origins. *Dev Comp Immunol*. 201. 35(9):886-97.
149. Harman AN, Kim M, Nasr N, Sandgren KJ, Cameron PU. Tissue dendritic cells as portals for HIV entry. *Rev Med Virol*. 2013. 23(5):319-33.
150. Hashimoto D, Ohmuraya M, Hirota M, tamamoto A, Suyama K, Ida S et al. Involvement of autophagy in trypsinogen activation within the pancreatic acinar cells. *J Cell Biol*. 2008. 181 (7): 1065-1072.
151. Hasui K, Nakamura T, Sato E, Izumo S. Expression of inducible nitric oxide synthase in epithelial cells, mucosa-associated lymphoid tissue, and regional lymph nodes of the stomach with Helicobacter pylori-associated peptic ulcer. *Dendric cells*. 2000. 10:5-9.
152. Hattori T, Iwasaki-Hozumi H, Bai G, Chagan-Yasutan H, Shete A, Telan EF et al. Both Full-Length and Protease-Cleaved Products of Osteopontin Are Elevated in Infectious Diseases. *Biomedicines*. 13;9(8):1006, 2021.
153. He Y, Xue C, Yu Y et al. CD44 is overexpressed and correlated with tumor progression in gallbladder cancer. *Cancer Manag Res.* 2018. 10:3857-3865.
154. Herzog S, Reth M, Jumaa H. Regulation of B-cell proliferation, and differentiation by pre-B-cell receptor signalling. *Nat Rev Immunol*. 2009. 9(3):195-205.
155. Hettinger J, Richards DM, Hansson J, Barra MM, Joschko AC, Krijgsveld J, Feuerer M. Origin of monocytes and macrophages in a committed progenitor. *Nat Immunol*. 2013. 14(8):821-30.
156. Hey YY, O'Neill HC. Murine spleen contains a diversity of myeloid and dendritic cells distinct in antigen presenting function. *J Cell Mol Med*. 2012. 16(11):2611-2619.
157. Hilgendorf I, Gellersen O, Emmrich J, Mikkat U, Krammer HJ, Muller PK et al. Estradiol Has a Direct Impact on the Exocrine Pancreas as Demonstrated by Enzyme and Vigilin Expression. *Pancreatol*. 2011. 1:24-29.

158. Hirohashi Y and Sato N. Tumor-associated dendritic cells: molecular mechanisms to suppress antitumor immunity. *Immunotherapy*. 2011. 3(8):945-947.
159. Hoeffel G, Chen K, Lavin Y, Low D, Almeida FF, See P et al. C-Myb(+) 131rythron-myeloid progenitor-derived fetal monocytes give rise to adult tissue-resident macrophages. *Immunity*. 2015. *42*(4), 665–678.
160. Hoeffel G, Ginhoux F. Fetal monocytes and the origins of tissue-resident macrophages. *Cell Immunol*. 2018. 330:5-15.
161. Hoeffel G, Wang Y, Greter M et al. Adult Langerhans cells derive predominantly from embryonic fetal liver monocytes with a minor contribution of yolk sac-derived macrophages. *J Exp Med*. 2012. 209(6):1167-81.
162. Hollevoet K, Nackaerts K, Gosselin R, De Wever W, Bosquée L, De Vuyst P et al. Soluble mesothelin, megakaryocyte potentiating factor, and osteopontin as markers of patient response and outcome in mesothelioma. *J Thorac Oncol*. 6(11):1930-7, 2011.
163. Hoving JC, Wilson GJ, Brown GD. Signalling C-type lectin receptors, microbial recognition, and immunity. *Cell Microbiol*. 2014. 16(2):185-94.
164. Hu F, Lou N, Jiao J, Guo F, Xiang H, Shang D. Macrophages in pancreatitis: mechanism and therapeutic potential. *Biomed Pharmacother.* 2020. 131:110693.
165. Huang YJ, Boushey HA. The microbiome in asthma. *J Allergy Clin Immunol*. 2015. 135(1):25-30.
166. Huang N, Cui X, Li W, Zhang C, Liu L, Li J. IL-33/ST2 promotes the malignant progression of gastric cancer via the MAPK pathway. *Mol Med Rep*. 2021. 23(5):361.
167. Hudson I, Hopwood D. Macrophages and mast cells in chronic cholecystitis and normal gallbladders. *J Clin Pathol*. 1986. 39(19):1082-1087.
168. Hulsmans M, Clauss S, Xiao L et al. Macrophages Facilitate Electrical Conduction in the Heart. *Cell*. 2017. 169(3):510-522.e20.
169. Hume DA, Perry VH, Gordon S. The mononuclear phagocyte system of the mouse defined by immunohistochemical localization of antigen F4/80: macrophages associated with epithelia. *Anat Rec*. 1984. 210(3):503-512.
170. Hume DA, Robinson AP, MacPherson GG, Gordon S. The mononuclear phagocyte system of the mouse defined by immunohistochemical localization of antigen F4/80. Relationship between macrophages, Langerhans cells, reticular cells, and dendritic cells in lymphoid and hematopoietic organs. *J Exp Med.* 1983. 158(5):1522-1536.
171. Ibrahim A, Toss MS, Makhlouf S, Miligy IM, Minhas F, Rakha EA. Improving mitotic cell counting accuracy and efficiency using phosphohistone-H3 (PHH3) antibody counterstained with haematoxylin and eosin as part of breast cancer grading. *Histopathology*. 2023. 82(3):393-406.
172. Inoue T, Kurosaki T. Memory B cells. *Nat Rev Immunol*. 2023. Online ahead of print.
173. Irby RB, McCarthy SM, Yeatman TJ. Osteopontin regulates multiple functions contributing to human colon cancer development and progression. *Clin Exp Metastasis*. 2004. 21(6):515-23.
174. Jha BK, Polyakova I, Kessler P et al. Inhibition of RNase L and RNA-dependent protein kinase (PKR) by sunitinib impairs antiviral innate immunity. *J Biol Chem*. 2011. 286(30):26319-26.
175. Ju C, Tacke F. Hepatic macrophages in homeostasis and liver diseases: from pathogenesis to novel therapeutic strategies. *Cell Mol Immunol*.2016, 13(3):316-27.
176. Kaku Y, Imaoka H, Morimatsu Y et al. Overexpression of CD163, CD204 and CD206 on alveolar macrophages in the lungs of patients with severe chronic obstructive pulmonary disease. PLoS One. 2014. 30;9(1):e87400.
177. Kambayashi T, Laufer TM. Atypical MHC class II-expressing antigen-presenting cells: can anything replace a dendritic cell? *Nat Rev Immunol*. 2014. 14(11):719-30.
178. Kang Q, Li L, Pang Y. An update on Ym1 and its immunoregulatory role in diseases. *Front Immunol*. 2022. 13:8912220.
179. Kany S, Vollrath JT, Relja B. Cytokines in Inflammatory Disease. *Int J Mol Sci*. 2019. 20(23):6008.

180. Kapsenberg ML. Dendritic-cell control of pathogen-driven T-cell polarization. *Nat Rev Immunol*. 2003. 3(12):984-93.
181. Kariya Y, Kariya Y. Osteopontin in Cancer: Mechanisms and Therapeutic Targets. *Int. J. Transl. Med.* 2022. 2:419-447.
182. Kawai T, Akira S. TLR signaling. *Cell Death Differ*. 2006. 13(5):816-25.
183. Kawai T, Akira S. The role of pattern-recognition receptors in innate immunity: update on Toll-like receptors. *Nat Immunol*. 2010. 11(5):373-84.
184. Kawakami T, Lichtnekert J, Thompson LJ et al. Resident renal mononuclear phagocytes comprise five discrete populations with distinct phenotypes and functions. *J Immunol*. 2013. 191(6):3358-3372.
185. Kim H. Cerulein Pancreatitis: Oxidative Stress, Inflammation, and Apoptosis. *Gut Liver*. 2008. 2:74-80.
186. Kim R, Emi M, Tanabe K. Cancer immunoediting from immune surveillance to immune escape. *Immunology*. 2007. 121(1):1-14.
187. Kim SK, Cho SW. The Evasion Mechanisms of Cancer Immunity and Drug Intervention in the Tumor Microenvironment. *Front Pharmacol*. 2022 May 24;13:868695.
188. King C. New insights into the differentiation and function of T follicular helper cells. *Nat Rev Immunol*. 2009 Nov;9(11):757-66.
189. Köhler C. Allograft inflammatory factor-1/Ionized calcium-binding adapter molecule 1 is specifically expressed by most subpopulations of macrophages and spermatids in testis. *Cell tissue res*. 2007. 330(2), 291–302.
190. Kotsias F, Cebrian I, Alloatti A. Antigen processing and presentation. *Int Rev Cell Mol Biol*. 2019. 348:69-121.
191. Kovats S. Estrogen receptors regulate innate immune cells and signaling pathways. *Cell Immunol*. 2015. 294(2): 63–69.
192. Kraal G, van der Laan LJ, Elomaa O, Tryggvason K. The macrophage receptor MARCO. *Microbes Infect*. 2000 Mar;2(3):313-6.
193. Kroger CJ, Spidale NA, Wang B et al. Thymic dendritic cell subsets display distinct efficiencies and mechanisms of intercellular MHC transfer. *J Immunol*. 2017. 198(1):249-256.
194. Kubat E, Mahajan S, Liao M, Ackerman L, Ohara P, Grady E et al. Corticotropin-releasing factor receptor 2 mediates sex-specific cellular stress responses. *Mol Med*. 2013. 19:212-222.
195. Kulle A, Thanabalasuriar A, Cohen TS et al. Resident macrophages of the lung and liver: The guardians of our tissues. *Front Immunol*. 2022. 13:1029085.
196. Kumar V, Abbas AK, Aster JC. Inflammation and repair. In: Robbins & Cotran Pathologic basis of disease. 10th ed. Elsevier; 2018 (a)
197. Kumar V, Abbas AK, Aster JC. Diseases of the Immune System. In: Robbins & Cotran Pathologic basis of disease. 10th ed. Elsevier; 2018.(b)
198. Kunz P, Fellenberg J, Moskovszky L, Sápi Z, Krenacs T, Poeschl J et al. Osteosarcoma microenvironment: whole-slide imaging and optimized antigen detection overcome major limitations in immunohistochemical quantification. *PLoS One*. 2014. 9(3):e90727.
199. Kurotaki D, Uede T, Tamura T. Functions and development of red pulp macrophages. *Microbiol Immunol*. 2015 Feb;59(2):55-62.
200. Lau AH and Thomson AW. Dendritic cells and immune regulation in the liver. *Gut*. 2003. 52(2):307-314.
201. Lawrence T. The nuclear factor NF-kappaB pathway in inflammation. *Cold Spring Harb Perspect Biol*. 2009 Dec;1(6):a001651.
202. Lazaratos AM, Annis MG, Siegel PM. GPNMB: a potent inducer of immunosuppression in cancer. *Oncogene*. 2022. 41(41):4573-4590.
203. Lelouard, H, Henri S, De Bovis B et al. Pathogenic bacteria and dead cells are internalized by a unique subset of Peyer's patch dendritic cells that express lysozyme. *Gastroenterology*. 2010. 138:173-184.

204. Lewis-Wambi JS, Craig VJ. Estrogen regulation of apoptosis: how can one hormone stimulate and inhibit? *Breast Cancer Res.* 2009. 11(3):206.
205. Li Y, Yang B, Miao H et al. Nicotinamide N-methyltransferase promotes M2 macrophage polarization by IL6 and MDSC conversion by GM-CSF in gallbladder carcinoma. *Hepatology*. *Online first*, 2023.
206. Liguori M, Digifico E, Vacchini A et al. The soluble glycoprotein NMB (GPNMB) produced by macrophages induces cancer stemness and metastasis via CD44 and IL-33. *Cell Mol Immunol*. 2021. 18(3):711-722.
207. Linehan SA, Martínez-Pomares L, Stahl PD, Gordon S. Mannose receptor and its putative ligands in normal murine lymphoid and nonlymphoid organs: In situ expression of mannose receptor by selected macrophages, endothelial cells, perivascular microglia, and mesangial cells, but not dendritic cells. *J Exp Med*. 1999. 189(12):1961-72.
208. Liu C, Chu D, Kalantar-Zadeh K, George J, Young HA, Liu G. Cytokines: From Clinical Significance to Quantification. *Adv Sci (Weinh).* 202. 8(15):e2004433.
209. Liu S, Galat V, Galat Y, Lee YKA, Wainwright D, Wu J. NK cell-based cancer immunotherapy: from basic biology to clinical development. *J Hematol Oncol*. 2021. 14(1):7.
210. Liu T, Soong L, Liu G, König R, Chopra AK. CD44 expression positively correlates with Foxp3 expression and suppressive function of CD4+ Treg cells. *Biol Direct*. 2009. 4:40.
211. Le K, Sun J, Khawaja H, Shibata M, Maggirwar SB, Smith MR et al. Mantle cell lymphoma polarizes tumor-associated macrophages into M2-like macrophages, which in turn promote tumorigenesis. *Blood Adv. 2021*. 5(14), 2863-2878.
212. Lehrer RI, Szklarek D, Barton A, Ganz T, Hamann KJ, Gleich GJ. Antibacterial properties of eosinophil major basic protein and eosinophil cationic protein. *J Immunol*. 1989. 142(12):4428-34.
213. Lenschow DJ, Walunas TL, Bluestone JA. CD28/B7 system of T cell costimulation. *Annu Rev Immunol*. 1996;14:233-58.
214. Lerch MM, Gorelick FS. Models of acute and chronic pancreatitis. *Gastroenterology*. 2013. 144:1180-1193.
215. Ley K. M1 means kill; M2 means heal. *J Immunol*. 2017, 199(7):2191-2193.
216. Li C, Jiang P, Wei S, Xu X, Wang J. Regulatory T cells in tumor microenvironment: new mechanisms, potential therapeutic strategies and future prospects. *Mol Cancer*. 2020. 19(1):116.
217. Li D, Wu M. Pattern recognition receptors in health and diseases. *Signal Transduct Target Ther*. 2021. 6(1):291.
218. Li Y, Wang W, Yang F, Xu Y, Feng C, Zhao Y. The regulatory roles of neutrophils in adaptive immunity. *Cell Commun Signal*. 2019. 14;17(1):147.
219. Li Y, Jiang Q, Wang L. Appetite Regulation of TLR4-Induced Inflammatory Signaling. *Front Endocrinol (Lausanne)*. 2021. 12:777997.
220. Li W, Wang Y, Zhao H, Zhang H, Xu Y, Wang S et al. Identification and transcriptome analysis of erythroblastic island macrophages. *Blood*. 2019. 134(5):480-491.
221. Lieberman J. The ABCs of granule-mediated cytotoxicity: new weapons in the arsenal. *Nat Rev Immunol*. 2003. 3(5):361-70.
222. Liu C, Yang M, Zhang D, Chen M, Zhu D. Clinical cancer immunotherapy: Current progress and prospects. *Front Immunol*. 2022. 13:961805.
223. Liu S, Liu Z, Shang A et al. CD44 is a potential immunotherapeutic target and affects macrophage infiltration leading to poor prognosis. *Sci Rep*. 2023. 13(1):9657.
224. Lokka E, Lintukorpi L, Cisneros-Montalvo S et al. Generation, localization and functions of macrophages during the development of testis. *Nat Commun*. 2020. 11(1):4375.
225. Long H, Liao W, Wang L, Lu Q. A Player and Coordinator: The Versatile Roles of Eosinophils in the Immune System. *Transfus Med Hemother*. 2016. 43(2):96-108.
226. Lopes-Ramos C, Quackenbush J, DeMeo DL. Genome-wide sex and gender differences in cancer. *Front Oncol*. 2020. 10:597788.

227. Lu Y, Lu G, Gao L. The Pro-resolving Lipid Mediator Maresin1 Alleviates Experimental Pancreatitis via Switching Macrophage Polarization. *Mediators Inflamm.* 2021. 6680456.
228. Luchian A, Ressel L. Combined colour deconvolution and artificial intelligence approach for region-selective immunohistochemical labelling quantification: The example of alpha smooth muscle actin in mouse kidney. *J Biophotonics*. 2023. e202300244.
229. Lugea A, Nan L, French SW, Bezerra JA, Gukovskaya A, Pandol SJ. Pancreas Recovery Following Caerulein-induced Pancreatitis is Impaired in Plasminogen Deficient Mice . *Gastroenterol*ogy. 2006. 131(3):885-899.
230. Lumeng CN, Bodzin JL, Saltiel AR. Obesity induces a phenotypic switch in adipose tissue macrophage polarization. *J Clin Invest*. 2007. 117(1):175-184.
231. Ma CS, Tangye SG, Deenick EK. Human Th9 cells: inflammatory cytokines modulate IL-9 production through the induction of IL-21. *Immunol Cell Biol*. 2010. 88(6):621-3.
232. Mackey JBG, Coffelt SB, Carlin LM. Neutrophil Maturity in Cancer. *Front Immunol*. 2019. 10:1912.
233. Majde JA, Krueger JM. Links between the innate immune system and sleep. *J Allergy Clin Immunol*. 2005.116(6):1188-98.
234. Madiji S, Golembioski A, Wilson S, Thompson E. Acute Pancreatitis: Etiology, Pathology, Diagnosis and Treatment. *South Med J*. 2017. 110, 11: 727-732.
235. Majoros A, Platanitis E, Kernbauer-Hölzl E, Rosebrock F, Müller M, Decker T. Canonical and Non-Canonical Aspects of JAK-STAT Signaling: Lessons from Interferons for Cytokine Responses. *Front Immunol*. 2017;8:29.
236. Malek TR, Bayer AL. Tolerance, not immunity, crucially depends on IL-2. *Nat Rev Immunol*. 2004. 4(9):665-74.
237. Mareninova OA, Sung KF, Hong P, Lugea A, Pandolf SJ, Gukovsky I et al. Cell death in pancreatitis: caspases protect from necrotizing pancreatitis. *J Biol Chem*. 2006. 281(6):3370-3381.
238. Mariuzza RA, Agnihotri P, Orban J. The structural basis of T-cell receptor (TCR) activation: An enduring enigma. *J Biol Chem*. 2020. 295(4):914-925.
239. Martinon F, Tschopp J. Inflammatory caspases and inflammasomes: master switches of inflammation. *Cell Death Differ*. 2007. 14(1):10-22.
240. Masopust D, Sivula CP, Jameson SC. Of Mice, Dirty Mice, and Men: Using Mice To Understand Human Immunology. *J Immunol*. 2017. 199(2):383-388.
241. Mauri C, Bosma A. Immune regulatory function of B cells. *Annu Rev Immunol*. 2012;30:221-41.
242. Mawhorter SD, Kazura JW, Boom WH. Human eosinophils as antigen-presenting cells: relative efficiency for superantigen- and antigen-induced CD4+ T-cell proliferation. *Immunology*. 1994. 81(4):584-91.
243. McGaha TL, Chen Y, Ravishankar B, van Rooijen N, Karlsson MC. Marginal zone macrophages suppress innate and adaptive immunity to apoptotic cells in the spleen. *Blood*. 2011. 117(20):5403-12.
244. McGrath KE, Frame JM, Palis J. Early hematopoiesis and macrophage development. *Semin Immunol*. 2015. 27(6):379-87.
245. McIlroy D, Troadec C, Grassi F et al. Investigation of human spleen dendritic cell phenotype and distribution reveals evidence of in vivo activation in a subset of organ donors. *Blood*. 2011. 97(11):3470-3477.
246. Maguire AS, Woodie LN, Judd RL, Martin DR, Greene MW, Graff EC. Whole-slide image analysis outperforms micrograph acquisition for adipocyte size quantification. *Adipocyte*. 2020. 9(1):567-575.
247. Marselli L, Bosi E, De Luca C et al. Arginase 2 and polyamines in human pancreatic beta cells: possible role in the pathogenesis of type 2 diabetes. Int J Mol Sci. 2021. 22(22):12099.
248. McIntire PJ, Irshaid L, Liu Y, Chen Z, Menken F, Nowak E, Shin SJ, Ginter PS. Hot Spot and Whole-Tumor Enumeration of $CD8^+$ Tumor-Infiltrating Lymphocytes Utilizing

Digital Image Analysis Is Prognostic in Triple-Negative Breast Cancer. *Clin Breast Cancer*. 2018. 18(6):451-458.e1.

249. Menzies-Gow A, Ying S, Phipps S, Kay AB. Interactions between eotaxin, histamine and mast cells in early microvascular events associated with eosinophil recruitment to the site of allergic skin reactions in humans. *Clin Exp Allergy*. 2004. 34(8):1276-82.

250. Merle NS, Church SE, Fremeaux-Bacchi V, Roumenina LT. Complement System Part I - Molecular Mechanisms of Activation and Regulation. *Front Immunol*. 2015. 6:262.

251. Mesa MA, Vasquez G. NETosis. *Autoimmune Dis*. 2013; 2013:651497.

252. Mestas J, Hughes CC. Of mice and not men: differences between mouse and human immunology. *J Immunol*. 2004. 172(5):2731-8.

253. Miceli MC, Parnes JR. The roles of CD4 and CD8 in T cell activation. Semin Immunol. 1991. 3(3):133-41.

254. Michaud D, Steward CR, Mirlekar B, Pylayeva-Gupta Y. Regulatory B cells in cancer. *Immunol Rev*. 2021. 299(1):74-92.

255. Mills CD, Kincaid K, Alt JM, Heilman MJ, Hill AM. M-1/M-2 macrophages and the Th1/Th2 paradigm. *J Immunol*. 2000 Jun 15;164(12):6166-73.

256. Milne SA, McGregor AL, McCulloch J, Sharkey J. Increased expression of macrophage receptor with collagenous structure (MARCO) in mouse cortex following middle cerebral artery occlusion. *Neurosci Lett*. 2005. 383(1-2):58-62.

257. Mirlekar B. Tumor promoting roles of IL-10, TGF-β, IL-4, and IL-35: Its implications in cancer immunotherapy. *SAGE Open Med*. 2022. 10:20503121211069012.

258. Mittal D, Gubin MM, Schreiber RD, Smyth MJ. New insights into cancer immunoediting and its three component phases--elimination, equilibrium, and escape. *Curr Opin Immunol*. 2014. 27:16-25.

259. Misharin AV, Morales-Nebreda L, Mutlu GM et al. Flow cytometric analysis of macrophages and dendritic cell subsets in the mouse lung. *Am J Respir Cell Mol Biol*. 2013. 49(4):503-10.

260. Mishra MN, Chandavarkar V, Sharma R, Bhargava D. Structure, function and role of CD44 in neoplasia. *J Oral Maxillofac Pathol*. 2019 May-Aug;23(2):267-272.

261. Miyake Y, Toyonaga K, Mori D et al. C-type lectin MCL is an FcRγ-coupled receptor that mediates the adjuvanticity of mycobacterial cord factor. *Immunity*. 2013. 38(5):1050-62.

262. Moens E and Veldhoen M. Epithelial barrier biology: good fences make good neighbors. *Immunology*. 135(1):1-8, 2012.

263. Molawi K, Wolf Y, Kandalla PK et al. Progressive replacement of embryo-derived cardiac macrophages with age. *J Exp Med*. 2014. 211(11):2151-8.

264. Mondanelli G, Bianchi R, Pallotta MT et al. A Relay Pathway between Arginine and Tryptophan Metabolism Confers Immunosuppressive Properties on Dendritic Cells. *Immunity*. 2017. 21;46(2):233-244.

265. Morel L. Mouse models of human autoimmune diseases: essential tools that require the proper controls. *PLoS Biol*. 2004 Aug;2(8):E241.

266. Mori D, Watanabe N, Kaminuma O et al. IL-17A induces hypo-contraction of intestinal smooth muscle via induction of iNOS in muscularis macrophages. *J Pharmacol Sci*. 2014. 125(4):394-405.

267. Molnar C, Gair J. *Adaptive immune response*. In: *Concepts of Biology-1st Canadian edition.*. 1st ed. BCCampus, Open edition; 2021.

268. Mott FE. Mesothelioma: a review. *Ochsner J*. 12(1):70-9, 2012.

269. Mossadegh-Keller N, Gentek R, Gimenez G et al. Developmental origin and maintenance of distinct testicular macrophage populations. *J Exp Med*. 2017. 214(10):2829-2841.

270. Muller PA, Koscsó B, Rajani GM et al. Crosstalk between muscularis macrophages and enteric neurons regulates gastrointestinal motility. *Cell*. 2014. 158(2):300-313.

271. Munder M, Mollinedo F, Calafat J, Canchado J, Gil-Lamaignere C, Fuentes JM et al. Arginase I is constitutively expressed in human granulocytes and participates in fungicidal activity. *Blood*. 2005. 105(6):2549-56.
272. Muñoz-Wolf N, Lavelle EC. Innate Immune Receptors. *Methods Mol Biol*. 2016;1417:1-43.
273. Munsell MA, Buscaglia JM. Acute Pancreatitis. *J Hosp Med*. 2010. 5(4):241-250.
274. Murtaugh LC, Keefe M. Regeneration and repair of the exocrine pancreas. *Annu Rev Physio*l. 2015. 77: 229–249, 2015.
275. Mysona BA, Segar S, Hernandez C, Kim C, Zhao J, Mysona D et al. QuPath Automated Analysis of Optic Nerve Degeneration in Brown Norway Rats. *Transl Vis Sci Technol*. 2020. 9(3):22.
276. Nadkarni S, Smith J, Sferruzzi-Perri AN et al. Neutrophils induce proangiogenic T cells with a regulatory phenotype in pregnancy. *Proc Natl Acad Sci U S A*. 2016. 113(52):E8415-E8424.
277. Nagy L, Lee TH, Goetzl EJ, Pickett WC, Kay AB. Complement receptor enhancement and chemotaxis of human neutrophils and eosinophils by leukotrienes and other lipoxygenase products. *Clin Exp Immunol*. 1982. 47(3):541-7.
278. Naito M, Hasegawa G, Takahashi K. Development, differentiation, and maturation of Kupffer cells. *Microsc Res Tech*. 1997. 39(4):350-364.
279. Nakagawa T, Ohnishi K, Kosaki Y, Saito Y, Horlad H, Fujiwara Y et al. Optimum immunohistochemical procedures for analysis of macrophages in human and mouse formalin fixed paraffin embedded tissue samples. *J Clin Exp Hematop*. 2017. 57(1):31-36.
280. Nandakumar V, Hebrink D, Jenson P et al. Differential Macrophage Polarization from Pneumocystis in Immunocompetent and Immunosuppressed Hosts: Potential Adjunctive Therapy during Pneumonia. *Infect Immun*. 2017. 85(3):e00939-16.
281. Nauseef WM. How human neutrophils kill and degrade microbes: an integrated view. *Immunol Rev*. 2007. 219:88-102.
282. Negishi H, Taniguchi T, Yanai H. The Interferon (IFN) Class of Cytokines and the IFN Regulatory Factor (IRF) Transcription Factor Family. *Cold Spring Harb Perspect Biol*. 2018. 10(11):a028423.
283. Nelson MP, Christmann BS, Werner JL et al. IL-33 and M2a alveolar macrophages promote lung defense against the atypical fungal pathogen Pneumocystis murina. *J Immunol*. 2011. 186(4):2372-2381.
284. Niederau C, Ferrell LD, Grendell JH. Caerulein-induced acure necrotizing pancreatitis in mice: protective effects if proglumide, benzotript and secretin. *Gastroenterology*. 2018. 88:1192-1204.
285. Nielsen MC, Hvidbjerg Gantzel R, Clària J et al. Macrophage Activation Markers, CD163 and CD206, in Acute-on-Chronic Liver Failure. *Cells*. 2020 May 9;9(5):1175.
286. Nikolakopoulou C, Willment JA, Brown GD. C-Type Lectin Receptors in Antifungal Immunity. *Adv Exp Med Biol*. 2020. 1204:1-30.
287. Nio J, Jujimoto W, Kon Y. Cellular expression of murine Ym1 and Ym2, chitinase family proteins, as revealed by in situ hybridization and immunohistochemistry. *Histochem Cell Biol*. 2004. 121(6):473-482.
288. Nofallah S, Wu W, Liu K, Ghezloo F, Elmore JG, Shapiro LG. Automated analysis of whole slide digital skin biopsy images. *Front Artif Intell*. 2022. 5:1005086.
289. Nordlohne J, Hulsmann I, Schwaferzt S, Zgrajek J, Grundmann M, Von Vietinghof et al. A flow cytometry approach reveals heterogeneity in conventional subsets of murine renal mononuclear phagocytes. *Sci Rep*. 2021. 11(1):13251.
290. Norkina O, Graf R, Appenzeller P and De Lisle RC. Caerulein-induced acute pancreatitis in mice that constitutively overexpress *Reg/PAP* genes. *BMC Gastroenterol*. 2006. 6:16.
291. Obafemi TF, Yu P, Li J, Davis JM, Liu K, Cheng B et al. Comparable responses in male and female mice to caerulein induced chronic pancreatic injury and recovery. *JOP*. 2018. 19:236-243.

292. Obilor EI, Chikweru E. Test for Significance of Pearson's Correlation Coefficient (r). *Int Jour Innov Math Stat*. 2018. 6(1):11-23.
293. Odegaard JI, Ricardo-Gonzalez RR, Red Eagle A, Vats D, Morel CR, Goforth MH et al. Alternative M2 activation of Kupffer cells by PPARdelta ameliorates obesity-induced insulin resistance. *Cell Metab*. 2008. *7*(6): 496-507.
294. O'Neill LA, Bowie AG. The family of five: TIR-domain-containing adaptors in Toll-like receptor signaling. *Nat Rev Immunol*. 2007. 7(5):353-64.
295. Onai N, Obata-Onai A, Schmid MA, Ohteki T, Jarrossay D, Manz MG. Identification of clonogenic common Flt3+M-CSFR+ plasmacytoid and conventional dendritic cell progenitors in mouse bone marrow. *Nat Immunol*. 2007. 8(11):1207-16.
296. Oshawa K, Imai Y, Sasaki Y, Kohsaka S. Microglia/macrophage-specific protein Iba1 binds to fimbrin and enhances its actin-bundling activity. *J Neurochem*. 2004 Feb;88(4):844-56.
297. Ozbek A, Ozbek E. Histologic demonstration of adrenal macrophages as a member of mononuclear phagocytic system in guinea pig models. *Mikrobiyol Bul.* 2006. 40(4):325-32.
298. Pae HO, Oh GS, Choi BM, Chae SC, Chung HT. Differential expressions of heme oxygenase-1 gene in CD25- and CD25+ subsets of human CD4+ T cells. *Biochem Biophys Res Commun*. 2003. 306(3):701-5.
299. Pan Y, Yu Y, Wang X, Zhang T. Tumor-associated macrophages in tumor immunity. *Front Immunol*. 2020. 11:583084.
300. Paolicelli RC, Bolasco G, Pagani F, Maggi L, Scianni M, Panzanelli, P et al. Synaptic pruning by microglia is necessary for normal brain development. *Science.* 2011. 333(6048):1456-1458.
301. Paris J, Henderson NC. Liver zonation, revisited. *Hepatology.* 2022. 76(4):1219-1230.
302. Peng C, Li Z, Yu X. The role of pancreatitis infiltrating innate and immune cells in acute pancreatitis. *Int. J. Med. Sci.* 2021. 18(2): 534-545.
303. Perry VH, Humes DA, Gordon S. Immunohistochemical localization of macrophages and microglia in the adult and developing mouse brain. *Neuroscience.* 1985. 15(2):313-326, 1985.
304. Pöllänen P, Maddocks S. Macrophages, lymphocytes and MHC II antigen in the ram and the rat testis. 1988. *J Reprod Fertil*. 82(2):437-445.
305. Ponomarev AV, Shubina IZ. Insights Into Mechanisms of Tumor and Immune System Interaction: Association with Wound Healing. *Front Oncol*. 2019 Oct 25;9:1115.
306. Pieper K, Grimbacher B, Eibel H. B-cell biology and development. *J Allergy Clin Immunol*. 2013. 131(4):959-71.
307. Pillai S, Cariappa A. The follicular versus marginal zone B lymphocyte cell fate decision. *Nat Rev Immunol*. 2009. 9(11):767-77.
308. Pinto C, Giordano DM, Maroni L et al. Role of inflammation and proinflammatory cytokines in cholangiocyte pathophysiology. *Biochim Biophys Acta Mol Basis Dis.* 2018. 1864(4 Pt B):1270-1278.
309. Prinz M, Priller J, Sisodia SS, Ransohoff RM. Heterogeneity of CNS myeloid cells and their roles in neurodegeneration. *Nat Neurosci*. 2011. 14(10):1227-35.
310. Prinz M, Priller J. The role of peripheral immune cells in the CNS in steady state and disease. *Nat Neurosci*. 2017. 20(2):136-144.
311. Puhr S, Lee J, Zvezdova E, Zhou YJ, Liu, K. Dendritic cell development: History, advances, and open questions. *Semin Immunol*. 2015. *27*(6), 388–396.
312. Raes G, Noël W, Beschin A, Brys L, de Baetselier P, Hassanzadeh GH. FIZZ1 and Ym as tools to discriminate between differentially activated macrophages. *Dev Immunol*. 2002 Sep;9(3):151-9.
313. Rahman AH and Aloman C. Dendritic cells and liver fibrosis. *Biochim Biophys Acta*. 2013.1832(7):998-1004.

314. Ramirez GA, Yacoub MR, Ripa M, Mannina D, Cariddi A, Saporiti N et al. Eosinophils from Physiology to Disease: A Comprehensive Review. *Biomed Res Int*. 2018. 2018:9095275.
315. Rangaswami H, Bulbule A, Kundu GC. Osteopontin: role in cell signaling and cancer progression. *Trends Cell Biol*. 2006 Feb;16(2):79-87.
316. Rankin LC, Artis D. Beyond Host Defense: Emerging Functions of the Immune System in Regulating Complex Tissue Physiology. *Cell*. 2018. 173(3):554-567.
317. Rao KN, Eagon PK, Okamura K, Van Thiel DH, Gavaler JS, Kelly RH et al. Acute hemorrhagic pancreatic necrosis in mice Induction in male mice treated with estradiol. *Am J Pathol*. 1982. 109:1-8.
318. Remon J, Lianes P, Martínez S, Velasco M, Querol R, Zanui M. Malignant mesothelioma: new insights into a rare disease. *Cancer Treat Rev*. 39(6):584-91, 2013.
319. Rehwinkel J, Gack MU. RIG-I-like receptors: their regulation and roles in RNA sensing. *Nat Rev Immunol*. 2020. 20(9):537-551.
320. Revelo XS, Parthiban P, Chen C et al. Cardiac Resident Macrophages Prevent Fibrosis and Stimulate Angiogenesis. *Circ Res*. 2021. 129(12):1086-1101.
321. Reynolds G, Vegh P, Fletcher J, Poyner EFM, Stephenson E, Goh Iet al. Developmental cell programs are co-opted in inflammatory skin disease. *Science*. 2021. 371(6527):eaba6500.
322. Risso A. Leukocyte antimicrobial peptides: multifunctional effector molecules of innate immunity. *J Leukoc Biol*. 2000. 68(6):785-92.
323. Roberts SE, Morrison-Rees S, John A, Williams JG, Brown TH, Samuel DG. The incidence and aetiology of acute pancreatitis across Europe. *Pancreatology*. 2017. 17:155-165.
324. Rodriguez PC, Ochoa AC, Al-Khami AA. Arginine Metabolism in Myeloid Cells Shapes Innate and Adaptive Immunity. *Front Immunol*. 2017. 8:93.
325. Rossi M, Korpak K, Doefler A. Deciphering the Role of Heme Oxygenase-1 (HO-1) Expressing Macrophages in Renal Ischemia-Reperfusion Injury. *Biomedicines*. 2021. 9(3):306, 2021.
326. Rőszer T. Understanding the Mysterious M2 Macrophage through Activation Markers and Effector Mechanisms. *Mediators Inflamm*. 2015:816460.
327. Sakamoto C, Otsuki M, Ohki A, Okabayashi Y, Yuu H Maeda M et al. Interaction of Caerulein, Glucose, and Amino Acids on Insulin Secretion from the Perfused Rat Pancreas. *Endocrinol Jpn*. 1985. 32(1):1-7.
328. Samokhvalov IM, Samokhvalova NI, Nishikawa S. Cell tracing shows the contribution of the yolk sac to adult haematopoiesis. *Nature*. 2007. 446(7139):1056-61.
329. Sánchez-Jaramillo EA, Gasca-Lozano LE, Vera-Cruz JM, Hernández-Ortega LD, Salazar-Montes AM. Automated Computer-Assisted Image Analysis for the Fast Quantification of Kidney Fibrosis. *Biology (Basel)*. 2022. 11(8):1227
330. Sanmarco LM, Eberhardt N, Ponce NE et al. New insights into the immunobiology of mononuclear phagocytic cells and their relevance to the pathogenesis of cardiovascular diseases. *Front Immunol*. 2018. 8:1921.
331. Sansonetti M, Waleczek FJG, Jung M et al. Resident cardiac macrophages: crucial modulators of cardiac (patho)physiology. *Basic Res Cardiol*. 2020. 115(6):77.
332. Sartor RB. Microbial influences in inflammatory bowel diseases. *Gastroenterology*. 2008. 134(2):577-94.
333. Sathe P, Shortman K. The steady-state development of splenic dendritic cells. *Mucosal Immunol.* 2008. 1(6):425-431.
334. Scatena M, Liaw L, Giachelli CM. Osteopontin: a multifunctional molecule regulating chronic inflammation and vascular disease. *Arterioscler Thromb Vasc Biol*. 2007. 27(11):2302-2309.
335. Sellers RS. Translating Mouse Models. *Toxicol Pathol*. 2017. 45(1):134-145.
336. Sendler M et al. Cathepsin B-Mediated Activation of Trypsinogen in Endocytosing Macrophages Increases Severity of Pancreatitis in Mice. *Gastroenterol*. 2018. 154:704-718.

337. Sharma JN, Al-Omran A, Parvathy SS. Role of nitric oxide in inflammatory diseases. *Inflammopharmacology*.15(6):252-9, 2007.
338. Shibuya T, Kamiyama A, Sawada H et al. Immunoregulatory Monocyte Subset Promotes Metastasis Associated with Therapeutic Intervention for Primary Tumor. *Front Immunol*. 2021;12:663115.
339. Schillebeeckx E, van Meerbeeck JP, Lamote K. Clinical utility of diagnostic biomarkers in malignant pleural mesothelioma: a systematic review and meta-analysis. *Eur Respir Rev*. 30(162):210057, 2021.
340. Schlitzer A, Sivakamasundari V, Chen J, Sumatoh HR, Schreuder J, Lum J et al. Identification of cDC1- and cDC2-committed DC progenitors reveals early lineage priming at the common DC progenitor stage in the bone marrow. *Nat Immunol*. *16*(7): 718-728, 2015.
341. Schneider CA, Rasband WS, Eliceiri KW. NIH Image to ImageJ: 25 years of image analysis. *Nat Methods*. 2012. 9(7):671-5
342. Scott NA and Mann ER. Regulation of mononuclear phagocyte function by the microbiota at mucosal sites. *Immunology*. 159(1):26-38, 2020.
343. Shao Y, Saredy J, Yang WY, Sun Y, Lu Y, Saaoud F et al. Vascular Endothelial Cells and Innate Immunity. *Arterioscler Thromb Vasc Biol*. 2020. 40(6):e138-e152.
344. Shi-Ping D, Ji-cheng L, Chang J. A mouse model of severe acute pancreatitis induced with caerulein and lipopolysaccharide. *World J Gastroenterol*. 2003. 9(3):584-589.
345. Shi N, Li N, Duan X, Niu H. Interaction between the gut microbiome and mucosal immune system. *Mil Med Res*. 2017. 4:14.
346. Shi X, Zhao H, Kang Y et al. The role of mononuclear phagocytes in the testes and epididymis. 2022. *Int J Mol Sci*. 24(1):53.
347. Shrivastava P, Bhatia M. Essential role of monocytes and macrophages in the progression of acute pancreatitis. *World J Gastroenterol*. 2010. 16(32): 3995-4002.
348. Schrumpf E, Tan C, Karlsen TH, Sponheim J, Björkström NK, Sundnes O, Alfsnes K, Kaser A, Jefferson DM, Ueno Y, Eide TJ, Haraldsen G, Zeissig S, Exley MA, Blumberg RS, Melum E. The biliary epithelium presents antigens to and activates natural killer T cells. Hepatology. 2015. 62(4):1249-59.
349. Silva-Vaz P, Abrantes AM, Castelo-Branco M, Botelho MF, Tralhao JG. Murine models of acute pancreatitis: a critical appraisal of clinical relevance. *Int J Mol Sci*. 2019. 20, 2794-2813.
350. Soos TJ, Sims TN, Barisoni L et al. CX3CR1+ interstitial dendritic cells form a contiguous network throughout the entire kidney. *Kidney int*. 2006. 70(3):591-596.
351. Smythies LE, Sellers M, Clements RH et al. Human intestinal macrophages display profound inflammatory anergy despite avid phagocytic and bactericidal activity. *J Clin Invest*. 2005. 115(1):66-75.
352. Snapper CM, Finkelman FD. Immunoglobulin class switching. In: Fundamental Immunology. WE Paul, ed. Lippincott-Raven, 1999.
353. Snyder PW. Diseases of Immunity. Adaptive immunity (specific immunity). In: Zachary Pathologic basis of veterinary diseases. 7th ed. Elsevier; 2022.
354. Sprent J. Antigen-presenting cells. Professionals and amateurs. *Curr Biol*. 1995. 1;5(10):1095-7.
355. Sproston NR, Ashworth JJ. Role of C-Reactive Protein at Sites of Inflammation and Infection. *Front Immunol*. 2018. 13;9:754.
356. Storz P. Acinar cell plasticity and development of pancreatic ductal adenocarcinoma. *Nat Rev Gastroenterol Hepatol*. 2017. 14(5):296–304.
357. Takaoka A, Hayakawa S, Yanai H et al. Integration of interferon-alpha/beta signaling to p53 responses in tumour suppression and antiviral defence. *Nature*. 2003. 424(6948):516-23.
358. Tamoutounour S, Guilliams M, Montanana S et al. Origins and functional specialization of macrophages and of conventional and monocyte-derived dendritic cells in mouse skin. *Immunity*. 2013. 39(5):925-38.
359. Taylor PR, Martinez-Pomares L, Stacey M et al. Macrophage receptors and immune recognition. *Annu Rev Immunol.* 2005. 23:901-944.

360. Thaiss CA, Zmora N, Levy M, Elinav E. The microbiome and innate immunity. *Nature*. 2016. 535(7610):65-74..
361. Thalmann GN, Sikes RA, Devoll RE et al. Osteopontin: possible role in prostate cancer progression. *Clin Cancer Res*. 1999. 5(8):2271-7.
362. Tizard I. Cellular innate Immunity: Macrophages and Recovery from Inflammation. In: Veterinary Immunology. 10th ed. Elsevier; 2018.
363. Tizard I. Dendritic cells and antigen processing. In: Veterinary Immunology. 10th ed. Elsevier; 2018.
364. Tsai TL, Zhou TA, Hsieh YT et al. Multiomics reveal the central role of pentose phosphate pathway in resident thymic macrophages to cope with efferocytosis-associated stress. *Cell Rep*. 2022. 40(2):111065.
365. Tumino N, Fiore PF, Pelosi A, Moretta L, Vacca P. Myeloid derived suppressor cells in tumor microenvironment: Interaction with innate lymphoid cells. *Semin Immunol*. 2022. 61-64:101668.
366. Turner MW. The role of mannose-binding lectin in health and disease. *Mol Immunol*. 2003. 40(7):423-9.
367. Uzé G, Monneron D. IL-28 and IL-29: newcomers to the interferon family. *Biochimie*. 2007. 89(6-7):729-34.
368. Van Coillie S, Wiernicki B, Xu J. Molecular and Cellular Functions of CTLA-4. *Adv Exp Med Biol*. 2020. 1248:7-32.
369. Van der Borght K, Lambrecht BN. Heart macrophages and dendritic cells in sickness and in health: A tale of a complicated marriage. *Cell Immunol*. 2018 Aug;330:105-113.
370. Van Furth R, Cohn ZA, Hirsch JG, Humphrey JH, Spector WG, Langevoort HL. Mononuclear phagocytic system: new classification of macrophages, monocytes and of their cell line. *Bull Word Health Organ*. 47:651-658, 1972.
371. Van Gassen N, Overmeire EV, Leuck G. Macrophage dynamics are regulated by local macrophage proliferation and monocyte recruitment in injured pancreas. *Eur J Immunol*. 2015. 45(5): 1482-1493.
372. Van Kooten C, Banchereau J. CD40-CD40 ligand. *J Leukoc Biol*. 2000. 67(1):2-17.
373. Vermaelen K, Pauwels R. Accurate and simple discrimination of mouse pulmonary dendritic cell and macrophage populations by flow cytometry: methodology and new insights. *Cytometry A*. 2004. 61(2):170-77.
374. Vijayan V, Wagener FADTG, Immenschuh S. The macrophage heme-heme oxygenase-1 system and its role in inflammation. *Biochem Pharmacol*. 2018. 153:159-167.
375. Vijayan V, Pradhan P, Braud L et al. Human and murine macrophages exhibit differential metabolic responses to lipopolysaccharide - A divergent role for glycolysis. *Redox Biol*. 2019. 22:101147.
376. Viola MF and Boeckxstaens G. Intestinal resident macrophages: Multitaskers of the gut. *Neurogastroenterol Motil*. 2020. 32(8):e13843.
377. Vos Q, Lees A, Wu ZQ, Snapper CM, Mond JJ. B-cell activation by T-cell-independent type 2 antigens as an integral part of the humoral immune response to pathogenic microorganisms. *Immunol Rev*. 2000. 176:154-70.
378. Wakahara K, Baba N, Van VQ et al. Human basophils interact with memory T cells to augment Th17 responses. *Blood*. 2012. 120(24):4761-71.
379. Walker LS, Sansom DM. The emerging role of CTLA4 as a cell-extrinsic regulator of T cell responses. *Nat Rev Immunol*. 2011. 11(12):852-63.
380. Wallace JL. Nitric oxide in the gastrointestinal tract: opportunities for drug development. *Br J Pharmacol*. 2019. 176(2):147-154.
381. Walsh MJ, Stump CT, Kureshi R et al. IFNγ is a central node of cancer immune equilibrium. *Cell Rep*. 2023. 42(3):112219.
382. Wang H, Zúñiga-Pflücker. Thymic microenvironment: Interactions between innate immune cells and developing thymocytes. *Front Immunol*. 2022. 13;885280.
383. Wang J, Ohmuraya M, Suyama K et al. Relationship of strain-dependent susceptibility to experimentally induced acute pancreatitis with regulation of Prss1 and Spink3 expression. *Lab Invest.* 2010.

384. Wang M, Gorelick F, Bhargava A. Differences in the Exocrine Pancreas and Associated Diseases. *Cell Mol Gastroenterol Hepatol*. 2021. 12(2): 427–441.
385. Watanabe T, Kudo M, Strober W. Immunopathogenesis of pancreatitis. *Mucosal Immunol*. 2017. 10(2): 283-298.
386. Waterston RH, Lindblad-Toh K, Birney E et al. Initial sequencing and comparative analysis of the mouse genome. *Nature*. 2002. 420(6915):520-62.
387. Webb LM, Tait Wojno ED. The role of rare innate immune cells in Type 2 immune activation against parasitic helminths. *Parasitology*. 2017. 144(10):1288-1301.
388. Weisel F, Shlomchik M. Memory B Cells of Mice and Humans. *Annu Rev Immunol*. 2017. 35:255-284.
389. Weitz JR, Makhmuota M, Almaca J et al. Mouse pancreatic islet macrophages use locally released ATP to monitor beta cell activity. *Diabetologia*. 2019. 61(1):182-192.
390. Willemer S, Elsasser HP, Adler G. Hormone-induced pancreatitis. *Eur Surg Res*. 1992. 1: 29-39.
391. Wood GW. Macrophages in the thymus. *Surv Immunol Res*. 4(3): 179-191, 1985.
392. Wosen JE, Mukhopadhyay D, Macaubas C, Mellins ED. Epithelial MHC Class II Expression and Its Role in Antigen Presentation in the Gastrointestinal and Respiratory Tracts. *Front Immunol*. 2018. 25;9:2144.
393. Wynn TA, Chawla A, Pollard JW. Macrophage biology in development, homeostasis and disease. *Nature*. 2013. 496(7446):445-55.
394. Wucherpfennig KW, Gagnon E, Call MJ, Huseby ES, Call ME. Structural biology of the T-cell receptor: insights into receptor assembly, ligand recognition, and initiation of signaling. *Cold Spring Harb Perspect Biol*. 2010. 2(4):a005140.
395. Wu J, Zhang L, Shi J et al. Macrophage phenotypic switch orchestrates the inflammation and repair/regeneration following acute pancreatitis injury. *EBioMedicine*. 2020. 58:102920.
396. Wu Y, Hirschi KK. Tissue-Resident Macrophage Development and Function. *Front Cell Dev Biol*. 2021. 8:617879.
397. Xu A, Zhou H, Yu DZ, Hei TK. Mechanisms of the genotoxicity of crocidolite asbestos in mammalian cells: implication from mutation patterns induced by reactive oxygen species. *Environ Health Perspect*. 110(10):1003-8, 2002.
398. Xue Q, Yan Y, Zhang R, Xiong H. Regulation of iNOS on Immune Cells and Its Role in Diseases. *Int J Mol Sci*. 2018. 19(12):3805.
399. Yang CW, Strong BS, Miller MJ, Unanue ER. Neutrophils influence the level of antigen presentation during the immune response to protein antigens in adjuvants. *J Immunol*. 2010. 185(5):2927-34.
400. Yang X, Yao L, Fu X, Mukherjee R, Xia Q, Jakubowska A et al. Experimental Acute Pancreatitis Models: History, Current Status and Role in Translational Research. *Front Physiol*. 2020, 11:614591.
401. Yang Z, Ming XF. Functions of arginase isoforms in macrophage inflammatory responses: impact on cardiovascular diseases and metabolic disorders. *Front Immunol*. 2014. 27;5:533.
402. Yip JLK, Balasuriya GK, Spencer SJ et al. The Role of Intestinal Macrophages in Gastrointestinal Homeostasis: Heterogeneity and Implications in Disease. *Cell Mol Gastroenterol Hepatol*. 2021. 12(5):1701-1718.
403. Yona S, Gordon S. From the Reticuloendothelial to Mononuclear Phagocyte System - The Unaccounted Years. *Front Immunol*. 2015. 1;6:328.
404. Yoshida H, Kawane K, Koike M, Mori Y, Uchiyama Y, Nagata S. Phosphatidylserine-dependent engulfment by macrophages of nuclei from erythroid precursor cells. *Nature*. 2005. *437*(7059):754–758.
405. Yuan SF, Hung AC, Hsu CW et al. CD44 Mediates Oral Squamous Cell Carcinoma-Promoting Activity of MRE11 via AKT Signaling. *J Pers Med*. 2022. 12(5):841.
406. Yunna C, Mengru H, Lei W, Weidong C. Macrophage M1/M2 polarization. *Eur J Pharmacol*. 2020. 877:173090.

407. Zhang L, Zhang J, Shea K, Xu L, Tobin G, Knapton A et al. Autophagy in Pancreatic Acinar Cells in Caerulein-treated Mice: Immunolocalization of Related Proteins and Their Potential as Markers of Pancreatitis. *Toxicol Pathol*. 2014. 42: 435-457.
408. Zhang SS, Park CG, Zhang P et al. Plasminogen activator Pla of Yersinia pestis utilizes murine DEC-205 (CD205) as a receptor to promote dissemination. *J Biol Chem.* 2008. 283(46):31511-21.
409. Zhang W, Cao D, Wang M et al. XBP1s repression regulates Kupffer cell polarization leading to immune suppressive effects protecting liver allograft in rats. *Int Immunopharmacol*. 2021. 91;107294.
410. Zhang X, Shi Q, Wang C, Wang G. Differential susceptibility of mouse strains on pancreatic injury and regeneration in cerulein-induced pancreatitis. *Int J Clin Exp Pathol.* 2017. 10(9):9934-9944.
411. Zhao Y, Zou W, Du J, Zhao Y. The origins and homeostasis of monocytes and tissue-resident macrophages in physiological situation. *J Cell Physiol*. 2018. 233(10):6425-6439.
412. Zheng W, Yang L, Jiang S et al. Role of Kupffer cells in tolerance induction after liver transplantation. *Front Cell Dev Biol*. 2023. 11:1179077.
413. Zheng Z, Xuan-Ding Y, Qu Y, Cao F, Li F. A narrative review of acute pancreatitis and its diagnosis, pathogenetic mechanism, and management. *Ann Transl Med*. 2021. 9(1):69.
414. Zhou TA, Hsu HP, Tu YH et al. Thymic macrophages consist of two populations with distinct localization and origin. *Elife*. 2022. 11:e75148.
415. Zhou Y, Dai DL, Martinka M et AL. Osteopontin expression correlates with melanoma invasion. *J Invest Dermatol*. 2005. 124(5):1044-52.
416. Zhu Y, Zhang L, Lu Q et al. Identification of different macrophage subpopulations with distinct activities in a mouse model of oxygen-induced retinopathy. *Int J Mol Med*. 2017. 40(2):281-292.
417. Zinselmeyer BH, Vomund AN, Saunders BT, Johnson MW, Carrero JA, Unanue ER. The resident macrophages in murine pancreatic islets are constantly probing their local environment, capturing beta cell granules and blood particles. *Diabetologia*. 2018. 61(6):1374-1383.
418. Zschaler J, Schlorke D, Arnhold J. Differences in innate immune response between man and mouse. *Crit Rev Immunol*. 2014. 34(5):433-54.

Appendix I - LIST OF PAPERS RELATED TO THE PhD PROJECT

Digifico E, Erreni M, Mannarino L, Marchini S, Ummarino A, Anfray C, **Bertola L**, Recordati C, Pistillo D, Roncalli M, Bossi P, Zucali PA, D'Incalci M, Belgiovine C, Allavena P. Important functional role of the protein osteopontin in the progression of malignant pleural mesothelioma. *Front Immunol*. 2023 Jun 16;14:1116430.

Bertola L, Pepe G., Dolce A, Cappelleri A, Canesi S, Sala L, Moretti P, Giordano A, Ressel L, Scanziani E, Vegeto E, Recordati C. Sex-Dependent Modulation of Caerulein-Induced Acute Pancreatitis in C57BL/6J Mice: Histopathological and Immunohistochemical Characterization. *Veterinary pathology,* under review.

Manuscripts in preparation

Bertola L, Pepe G, Dolce A Canesi S, Sala G, Scanziani E, Vegeto E, Recordati C. A comparison between hot spot fields and whole slide image analysis for immune cell infiltrates investigation in a murine model of caerulein-induced acute pancreatitis.

Bertola L, Valenti AG, Cappelleri A, Canesi S, Scanziani E, Recordati C, Minoli L. Immunohistochemical characterization of cells of the mononuclear phagocyte system in the mouse*. Veterinary pathology.*

Appendix II - LIST OF PAPERS NOT RELATED TO THE PhD PROJECT

1. Cappelleri A, **Bertola L**, Caniatti M, Recordati C. Diagnostic challenge in veterinary pathology: Disseminated tumor in a young dog. *Vet Pathol*. 2022 May;59(3):394-396.

2. Bertola L, Cappelleri A, Tomba RM, Dotti E, Caniatti M, Dall'Ara P, Recordati C. Vaccine-Associated Anaphylactic Shock in a Springer Spaniel Dog with Arrhythmogenic Right Ventricular Cardiomyopathy. *J Comp Pathol*. 2022. 194:34-38.

3. Epis S, Varotto-Boccazzi I, Manenti A, Rubolini D, Gabrieli P, Cattaneo GM, Gourlay L, Dapporto F, Monti M, Razzano I, Leonardi M, Iannacone M, Recordati C, **Bertola L**, Fiorina P, Marvasi L, Montomoli E, Zuccotti G, Bandi C. Efficacy of mucosal vaccination using a protozoan parasite as a vehicle for antigen delivery: IgG and neutralizing response after rectal administration of LeCoVax-2, a candidate vaccine against COVID-19. *Pharmacol Res*. 2022. 186:106546.

4. Dander E, Vinci P, Vetrano S, Recordati C, Piazza R, Fazio G, Bardelli D, Bugatti M, Sozio F, Piontini A, Bonanomi S, **Bertola L**, Tassistro E, Valsecchi MG, Calza S, Vermi W, Biondi A, Del Prete A, Sozzani S, D'Amico G. The chemerin/CMKLR1 axis regulates intestinal graft-versus-host disease. *JCI Insight*. 2023. 8(5):e154440.

5. Cino M, Gariboldi EM, Stefanello D, Spindler KP, Ferraris EI, Morello EM, **Bertola L**, Maniscalco L, Martano M. Ki67 Index in Patnaik Grade 2/Kiupel Low-Grade Canine Cutaneous Mast Cell Tumors with Early Lymph Node Metastasis: A Descriptive Study. *Vet Sci*. 2023 Jul 5;10(7):436.

6. Bertola L, Pellizzoni B, Giudice C, Grieco V, Ferrari R, Chiti LE, Stefanello D, Manfredi M, De Zani D, Recordati C. Tumor Associated Macrophages and Tumor Infiltrating Lymphocytes in Canine Cutaneous and Subcutaneous Mast Cell Tumors. *Veterinary Pathology*. Apr 22:3009858241244851. Epub ahead of print.

7. Cappelleri A, Canesi S, **Bertola L**, Capo V, Zecchillo A, Albano L, Villa A, Scanziani E, Recordati C. Histological and Immunohistochemical Characterization of Pulmonary Lesions in CD40L-/- Mice Experimentally Infected with Pneumocystis. *Veterinary Pathology*. 2024 May 17:3009858241252409. Epub ahead of print.

8. Guarnieri C †, **Bertola L** †, Ferrari L, Quintavalla C, Corradi A, Di Lecce R. Myocarditis in an FIP-Diseased Cat with FCoV M1058L Mutation: Clinical and Pathological Changes. *Animals (Basel)*. 2024 Jun 3;14(11):1673. *† These authors contributed equally to the work and share first authorship.*

Appendix III – Supplementary Material

Supplemental Table 1. Primary antibodies used in the thesis.

Antigen	Supplier	Clonality	Clone/ Code no	Antigen Retrieval	Working Dilution	Incubation Time	Positive Controls
Iba1	Dako	Rb poly[a]	A0452	HIER	1:2000	1h RT	Spleen
F4/80	Biorad	Rat mono[b]	MCA497G	PIER	1:100	1h RT	Spleen
MARCO	Abcam	Rb mono[c]	ab239369	HIER	1:1000	1h RT	Spleen
CD206	Abcam	Rb poly[a]	ab64693	HIER	1:4000	1h RT	Spleen
Arginase 1	Santa Cruz	Goat poly[d]	sc-18354	HIER	1:2000	1h RT	Spleen
Ym1	StemCell Technologies	Rb poly[a]	#01404	HIER	1:1000	1h RT	Spleen
iNOS	Abcam	Rb poly[a]	ab15323	HIER	1:100	1h RT	Hepatitis
HO-1	Biorad	Rb poly[a]	4915-1050	HIER	1:500	1h RT	Spleen
MHC-II	Biolegend	Rat mono[b]	M5/114.15.2	HIER	1:300	1h RT	Spleen
CD3ε	Santa Cruz	Goat poly[d]	s-1127	HIER	1:1000	1h RT	Spleen
B220	BD Biosciences	Rat mono[b]	AB394614	HIER	1:500	1h RT	Spleen
Ly6G	BD Biosciences	Rat mono[b]	AB551459	HIER	1:2000	1h RT	Spleen
Cytokeratin 19	Abcam	Rb poly[a]	ab133496	HIER	1:2000	1h RT	Pancreas
Cleaved caspase 3	Cell Signaling	Rb poly[a]	Asp175	HIER	1:2000	1h RT	Thymus
CD4	Invitrogen	Rat mono[b]	#14-0041-82	HIER	1:600	1h RT	Spleen
CD8	Invitrogen	Rat mono[b]	#14-0808-82	HIER	1:800	1h RT	Spleen
FoxP3	eBioscience	Rat mono[b]	FJK-16S	HIER	1:200	1h RT	Spleen
CD31	Abcam	Rb poly[a]	ab182981	HIER	1:2000	1h RT	Lung
OPN	R&D System	Rb poly[a]	MAB808	HIER	1:400	1h RT	Mesothelioma
GPNMB	R&D System	Goat poly[d]	AF2330	HIER	1:200	1h RT	Mesothelioma

aRabbit polyclonal; bRat monoclonal; cRabbit monoclonal; dGoat polyclonal; HIER: Heat-induced epitope retrieval in dewaxing buffer H pH=9; PIER: Protease-induced epitope retrieval with trypsin; 1h RT: 1 hour at room temperature

Supplemental Table 2. Liver immunohistochemical evaluation.

Organ/structure		Marker	Location	Cellular count	Shape (%)	Staining Intensity	Staining Pattern	ID
Liver	Parenchyma	Iba-1	Capsule	+	Spindle	+++	Cytoplasm	CMφs
			Sinusoids	+++	Stellate	+++	Cytoplasm	Kupffer cells
			Centrilobular veins	+	Round	+++	Cytoplasm	Circulating Monocytes
			Portal Spaces	++	Stellate	+++	Cytoplasm	MoMφs/ MoDCs / cDCs
			Portal Vessels	+/-	Round	+++	Cytoplasm	Circulating Monocytes
		F4/80	Capsule	+	Spindle	+/+++	Cytoplasm	CMφs
			Sinusoids	+++	Stellate	+/+++	Cytoplasm	Kupffer cells
			Centrilobular veins	+	Round	+/+++	Cytoplasm	Circulating Monocytes
			Portal Spaces	+/++	Stellate	+/++	Cytoplasm	MoMφs
			Portal Vessels	+	Round	+/+++	Cytoplasm	Circulating Monocytes
		MARCO	Capsule	\	\	\	\	\
			Sinusoids	++	Stellate	+++	Cytoplasm	Kupffer cells
			Centrilobular veins	+	Round/Spindle	+++	Cytoplasm	Circulating Monocytes
			Portal Spaces	+/-	Stellate	+++	Cytoplasm	MoMφs/ MoDCs / cDCs
			Portal Vessels	+	Round/Spindle	+++	Cytoplasm	Circulating Monocytes
		CD206	Capsule	\	\	\	\	\
			Sinusoids	\	\	\	\	\
			Centrilobular veins	\	\	\	\	\
			Portal Spaces	+	Stellate	++	Cytoplasm	MoMφs/ MoDCs / cDCs
			Portal Vessels	\	\	\	\	\
		Arg-1	Capsule	\	\	\	\	\
			Sinusoids	\	\	\	\	\
			Centrilobular veins	\	\	\	\	\
			Portal Spaces	\	\	\	\	\
			Portal Vessels	\	\	\	\	\
		Ym1	Capsule	\	\	\	\	\
			Sinusoids	+	Round	++	Cytoplasm	Circulating Monocytes
			Centrilobular veins	+/-	Round	++	Cytoplasm	Circulating Monocytes
			Portal Spaces	\	\	\	\	\
			Portal Vessels	+/-	Round	++	Cytoplasm	Circulating Monocytes
		iNOS	Capsule	\	\	\	\	\
			Sinusoids	\	\	\	\	\
			Centrilobular veins	\	\	\	\	\
			Portal Spaces	\	\	\	\	\
			Portal Vessels	\	\	\	\	\
		HO1	Capsule	\	\	\	\	\
			Sinusoids	+	Stellate	++	Cytoplasm	Kupffer cells
			Centrilobular veins	+/-	Round	++	Cytoplasm	Circulating Monocytes
			Portal Spaces	\	\	\	\	\
			Portal Vessels	+/-	Round	++	Cytoplasm	Circulating Monocytes
		MHC-II	Capsule	\	\	\	\	\
			Sinusoids	+	Stellate	++	Cytoplasm	Kupffer cells/ MoDCs / cDCs
			Centrilobular veins	\	\	\	\	\
			Portal Spaces	++	Stellate	++	Cytoplasm	MoMφs/ MoDCs / cDCs
			Portal Vessels	\	\	\	\	\

Supplemental Table 3. Gallbladder immunohistochemical evaluation.

Organ/structure		Marker	Location	Cellular count	Shape (%)	Staining Intensity	Staining Pattern	**ID**
Gallbladder	Mucosa	Iba-1	Lamina propria	++	Stellate/Spindle (80%)	+++	Cytoplasm	MoMφs/ MoDCs/ cDCs
					Round (20%)	+++	Cytoplasm	MoMφs
		F4/80	Lamina propria	++	Stellate/Spindle (70%)	++	Cytoplasm	MoMφs
					Round (30%)	+++	Cytoplasm	MoMφs
		MARCO	Lamina propria	\	\	\	\	\
		CD206		+/++	Spindle	++	Cytoplasm	MoMφs/ MoDCs/ cDCs
		Arg-1	Lamina propria	\	\	\	\	\
		Ym1		\	\	\	\	\
		iNOS	Lamina propria	\	\	\	\	\
		HO1		\	\	\	\	\
		MHC-II	Lamina propria	+/-	Stellate	+	Cytoplasm	MoMφs/ MoDCs/ cDCs
	Muscular Layer	Iba-1	Muscular layer	+/++	Spindle	++	Cytoplasm	MoMφs/ MoDCs/ cDCs
		F4/80	Muscular layer	+	Spindle	+	Cytoplasm	MoMφs
		MARCO	Muscular layer	\	\	\	\	\
		CD206	Muscular layer	+/++	Spindle	+/++	Cytoplasm	MoMφs/ MoDCs/ cDCs
		Arg-1	Muscular layer	\	\	\	\	\
		Ym1	Muscular layer	\	\	\	\	\
		iNOS	Muscular layer	\	\	\	\	\
		HO1	Muscular layer	\	\	\	\	\
		MHC-II	Muscular layer	\	\	\	\	\

Supplemental Table 4. Spleen immunohistochemical evaluation.

Organ/structure		Marker	Location	Cellular count	Shape (%)	Staining Intensity	Staining Pattern	ID
Spleen	Red pulp	Iba-1	Chords/Sinuses	++++	Polymorphic	++/+++	Cytoplasmic/Membranous	RPMφs, MoDCs/ cDCs / pDCs
		F4/80	Chords/Sinuses	++++	Polymorphic	++/+++	Cytoplasmic/Membranous	RPMφs
		MARCO	Chords/Sinuses	+	Polymorphic	+	Cytoplasmic	RPMφs
		CD206	Chords/Sinuses	+	Polymorphic	+/++	Cytoplasmic	RPMφs
		Arg-1	Chords/Sinuses	+	Round	+++	Cytoplasmic	RPMφs
		Ym1	Chords/Sinuses	+/-	Polymorphic	+++	Cytoplasmic	RPMφs
		iNOS	Chords/Sinuses	\	\	\	\	\
		HO1	Chords/Sinuses	+++	Polymorphic	++/+++	Cytoplasmic	RPMφs/ MoDCs/ cDCs/ pDCs
		MHC II	Chords/Sinuses	++	Polymorphic	+/++	Cytoplasmic	RPMφs, MoDCs/ cDCs / pDCs
	White pulp	Iba-1	PALS	+++/++++	Stellate	++	Cytoplasmic/Membranous	MoMφs/ MoDCs/ cDCs / pDCs
			Follicle - Mantle zone	++/+++	Stellate	++/+++	Cytoplasmic/Membranous	MoMφs/ MoDCs/ cDCs / pDCs
			Follicle - GCs	+++	Stellate (70%)	++/+++	Cytoplasmic	FDCs
					Round (30%)	++	Cytoplasmic	TBMφs
			Marginal zone Inner/Outer layer	+++	Stellate	+++	Cytoplasmic	MZMφs/ MMMφs/ MoDCs/ cDCs
		F4/80	PALS	+	Stellate	+/++	Cytoplasmic	MoMφs
			Follicle - Mantle zone	+/-	Stellate	+/++	Cytoplasmic	MoMφs
			Follicle - GCs	\	\	\	\	\
			Marginal zone Inner/Outer layer	\	\	\	\	\
		MARCO	PALS	\	\	\	\	\
			Follicle - Mantle zone	\	\	\	\	\
			Follicle - GCs	\	\	\	\	\
			Marginal zone outer layer	++++	Stellate	+++	Cytoplasmic	MZMφs
		CD206	PALS	\	\	\	\	\
			Follicle - Mantle zone	\	\	\	\	\
			Follicle - GCs	\	\	\	\	\
			Marginal zone Inner/Outer layer	\	\	\	\	\
		Arg-1	PALS	\	\	\	\	\
			Follicle - Mantle zone	\	\	\	\	\
			Follicle - GCs	\	\	\	\	\
			Marginal zone Inner/Outer layer	\	\	\	\	\
		Ym1	PALS	\	\	\	\	\
			Follicle - Mantle zone	\	\	\	\	\
			Follicle - GCs	\	\	\	\	\
			Marginal zone Inner/Outer layer	\	\	\	\	\
		iNOS	PALS	\	\	\	\	\
			Follicle - Mantle zone	\	\	\	\	\
			Follicle - GCs	\	\	\	\	\
			Marginal zone Inner/Outer layer	\	\	\	\	\
		HO1	PALS	++	Polymorphic	+/++	Cytoplasmic	MoMφs
			Follicle - Mantle zone	+	Polymorphic	+	Cytoplasmic	MoMφs
			Follicle - GCs	+/++	Stellate (60%)	+/++	Cytoplasmic	FDCs
					Round (40%)	+/++	Cytoplasmic	TBMφs
			Marginal zone Inner/Outer layer	+/-	Polymorphic	+	Cytoplasmic	MoMφs / MZMφs(?) / MMMφs (?)
		MHC II	PALS	++	Stellate	+	Cytoplasmic	MoMφs/ MoDCs/ cDCs
			Follicle - Mantle zone	++	Stellate	+	Cytoplasmic	MoMφs/ MoDCs/ cDCs
			Follicle - GCs	++	Stellate (70%)	+	Cytoplasmic	FDCs
					Round (30%)	++	Cytoplasmic	TBMφs
			Marginal zone Inner/Outer layer	+/++	Polymorphic	+	Cytoplasmic	MoDCs/ cDCs/ pDCs

Supplemental Table 5. Thymus immunohistochemical evaluation.

Organ/structure		Marker	Location	Cellular count	Shape (%)	Staining Intensity	Staining Pattern	**ID**
Thymus	Cortex	Iba-1	Cortex	++	Stellate	+++	Membrane/Cytoplasmic	ThyMΦs /MoMφs
		F4/80	Cortex	+/-	Stellate	+	Cytoplasm	ThyMΦs/ MoMΦs
		MARCO	Cortex	\	\	\	\	\
		CD206	Cortex	\	\	\	\	\
		Arg-1	Cortex	\	\	\	\	\
		Ym1	Cortex	+	Stellate	+++	Cytoplasm	ThyMΦs/ MoMΦs
		iNOS	Cortex	\	\	\	\	\
		HO1	Cortex	++	Stellate	+	Membrane/Cytoplasmic	ThyMΦs/ MoMΦs
		MHC II	Cortex	\	\	\	\	\
	Medulla	Iba-1	Medulla	+++	Stellate	+++	Membrane/Cytoplasmic	ThyMΦs/ MoMφs/ MoDCs/ cDCs
		F4/80	Medulla	+	Stellate	+	Cytoplasm	ThyMΦs /MoMφs
		MARCO	Medulla	+	Stellate	+++	Cytoplasm	ThyMΦs / MoMφs
		CD206	\	\	\	\	\	\
		Arg-1	Medulla	++	Round/Stellate	+++	Cytoplasm/nuclear	ThyMΦs / MoMφs
		Ym1	Medulla	++	Round/Stellate	+++	Cytoplasm	ThyMΦs / MoMφs
		iNOS	Medulla	++	Round/Stellate	+++	Cytoplasm	ThyMΦs / MoMφs / MoDCs/ cDCs / pDCs
		HO1	Medulla	+	Stellate	+	Membrane/Cytoplasmic	ThyMΦs / MoMφs
		MHC II	Medulla	+++	Stellate	+/++	Cytoplasm	ThyMΦs / MoMφs/ MoDCs/ cDCs

Supplemental Table 6. Lymph node immunohistochemical evaluation.

Organ/structure		Marker	Location	Cellular count	Shape (%)	Staining Intensity	Staining Pattern	**ID**
Lymphnode	Capsule	Iba-1	Subcapsular sinus	++++	Round	+++	Cytoplasmic/Membranous	SCSMφs
		F4/80	Subcapsular sinus	+	Round	+	Cytoplasmic	SCSMφs
		MARCO	Subcapsular sinus	++++	Round	+++	Cytoplasmic	SCSMφs
		CD206	Subcapsular sinus	+++	Round	++	Cytoplasmic	SCSMφs
		Arg-1	Subcapsular sinus	+	Round	+++	Cytoplasmic/Nuclear	SCSMφs
		Ym1	Subcapsular sinus	\	\	\	\	\
		iNOS	Subcapsular sinus	\	\	\	\	\
		HO1	Subcapsular sinus	+++/++++	Round	++	Membrane/ Cytoplasmic	SCSMφs
		MHC II	Subcapsular sinus	+/++	Round	+	Cytoplasmic	SCSMφs
	Cortex	Iba-1	Germinal Center	++	Round	+++	Cytoplasmic	TBMφs
				++	Stellate	+++	Cytoplasmic	FDCs
			Mantle zone	++	Stellate	+++	Cytoplasmic	MoMφs / MoDCs/ cDCs / pDCs
			Marginal zone	+	Stellate	+++	Cytoplasmic	MoMφs / MoDCs/ cDCs / pDCs
		F4/80	Germinal Center	\	\	\	\	\
			Mantle zone	\	\	\	\	\
			Marginal zone	\	\	\	\	\
		MARCO	Germinal Center	\	\	\	\	\
			Mantle zone	\	\	\	\	\
			Marginal zone	\	\	\	\	\
		CD206	Germinal Center	\	\	\	\	\
			Mantle zone	\	\	\	\	\
			Marginal zone	\	\	\	\	\
		Arg-1	Germinal Center	\	\	\	\	\
			Mantle zone	+	Round	+++	Cytoplasmic/Nuclear	MoMφs
			Marginal zone	+	Round	+++	Cytoplasmic/Nuclear	MoMφs
		Ym1	Germinal Center	\	\	\	\	\
			Mantle zone	\	\	\	\	\
			Marginal zone	\	\	\	\	\
		iNOS	Germinal Center	\	\	\	\	\
			Mantle zone	\	\	\	\	\
			Marginal zone	\	\	\	\	\
		HO1	Germinal Center	\	\	\	\	\
			Mantle zone	\	\	\	\	\
			Marginal zone	\	\	\	\	\
		MHC II	Germinal Center	++	Round (80%)	++	Cytoplasmic	TBMφs
					Stellate (20%)	+	Cytoplasmic	FDCs
			Mantle zone	+/-	Round/Stellate	+/++	Cytoplasmic	MoDCs/ cDCs / pDCs
			Marginal zone	+/-	Round/Stellate	+/++	Cytoplasmic	MoDCs/ cDCs / pDCs
	Paracortex	Iba-1	Paracortex	+++	Stellate	+++	Cytoplasmic	MoMφs / TZMφs/ MoDCs/ cDCs / pDCs
		F4/80	Paracortex	\	\	+	\	\
		MARCO	Paracortex	\	\	+	\	\
		CD206	Paracortex	+/-	Stellate	+	Cytoplasmic	MoMφs
		Arg-1	Paracortex	++	Round	+++	Cytoplasmic/Nuclear	MoMφs
		Ym1	Paracortex Cortico-medullary region	++	Round	+	Cytoplasmic	MoMφs (?)

		iNOS	Paracortex	\	\	+	\	\
		HO1	Paracortex	+	Round	+	Membrane/ Cytoplasmic	MoMφs
		MHC II	Paracortex	+++	Stellate	+/++	Cytoplasmic	TZMφs / MoDCs/ cDCs / pDCs
	Medulla	Iba-1	Chords	+++	Round/Spindle	+++	Cytoplasmic	MCMφs/DCs
			Sinuses	++++	Round	+++	Cytoplasmic	MSMφs
		F4/80	Chords	\	\	\	\	\
			Sinuses	+++	Round	++/+++	Cytoplasmic	MSMφs
		MARCO	Chords	\	\	\	\	\
			Sinuses	++++	Round	+++	Cytoplasmic	MSMφs
		CD206	Chords	\	\	\	\	\
			Sinuses	++/+++	Round	+	Cytoplasmic	MSMφs
		Arg-1	Chords	\	\	\	\	\
			Sinuses	+/-	Round	+	Cytoplasmic/Nuclear	
		Ym1	Chords	++	Polymorphic	+	Cytoplasmic	MCMφs (?)
			Sinuses	\	\	\	\	\
		iNOS	Chords	\	\	\	\	\
			Sinuses	\	\	\	\	\
		HO1	Chords	\	\	\	\	\
			Sinuses	+++/++++	Round	+	Membrane/ Cytoplasmic	MSMφs
		MHC II	Chords	+/++	Round	+/++	Cytoplasmic	MCMφs / DCs
			Sinuses	+/++	Round	+/++	Cytoplasmic	MSMφs

Supplemental Table 7. Kidney immunohistochemical evaluation.

Organ/structure		Marker	Location	Cellular count	Shape (%)	Staining Intensity	Staining Pattern	ID
Kidney	Capsule	Iba-1	Intracapsular	+/++	Spindle	++	Cytoplasmic	MoMφs / ReMφs
			Pericapsular fat	+	Round/Spindle	++	Cytoplasmic	WAT Mφs
		F4/80	Intracapsular	+/++	Spindle	+/++	Cytoplasmic	MoMφs / ReMφs
			Pericapsular fat	+	Round/Spindle	+	Cytoplasmic	WAT Mφs
		MARCO	Intracapsular	\	\	\	\	\
			Pericapsular fat	\	\	\	\	\
		CD206	Intracapsular	+	Spindle	++/+++	Cytoplasmic	MoMφs / ReMφs
			Pericapsular fat	+	Round	++/+++	Cytoplasmic	WAT Mφs
		Arg-1	Intracapsular	+/-	Spindle	+++	Nuclear, cytoplasmic	MoMφs / ReMφs / Circulating monocytes
			Pericapsular fat	+	Round	+++	Nuclear, cytoplasmic	WAT Mφs
		Ym1	Intracapsular	+/-	Spindle	+	Cytoplasmic	MoMφs / ReMφs / Circulating monocytes
			Pericapsular fat	\	\	\	\	\
		iNOS	Intracapsular	\	\	\	\	\
			Pericapsular fat	\	\	\	\	\
		HO-1	Intracapsular	\	\	\	\	\
			Pericapsular fat	\	\	\	\	\
		MHC II	Intracapsular	\	\	\	\	\
			Pericapsular fat	\	\	\	\	\
	Cortex	Iba-1	Interstitium	++	Stellate	++/+++	Cytoplasmic	MoMφs/ ReMφs/ cDCs / MoDCs
		F4/80	Interstitium	++	Stellate	++	Cytoplasmic	MoMφs/ ReMφs
		MARCO	\	\	\	\	\	\
		CD206	Interstitium	++	Round/Stellate	++	Cytoplasmic	MoMφs/ ReMφs
		Arg-1	Interstitial blood vessels	+/-	Round	+++	Nuclear, cytoplasmic	Circulating monocytes
		Ym1	Interstitial blood vessels	+/-	Round (60%)	++	cytoplasmic (stippled)	Circulating monocytes
			Interstitium		Spindle/Stellate (40%)	++	cytoplasmic (stippled)	MoMφs/ ReMφs
		iNOS	\	\	\	\	\	\
		HO-1	\	\	\	\	\	\
		MHC II	Interstitium	+	Stellate	++	Cytoplasmic	MoMφs/ ReMφs/ cDCs / MoDCs
	Medulla	Iba-1	Interstitium	++	Stellate	++	Cytoplasmic	MoMφs/ ReMφs/ cDCs / MoDCs
		F4/80	Interstitium	++/+++	Stellate	++	Cytoplasmic	MoMφs/ ReMφs
		MARCO	\	\	\	\	\	\
		CD206	Interstitium	++	Round/Stellate	++	Cytoplasmic	MoMφs/ ReMφs
		Arg-1	Interstitial blood vessels	+/-	Round (80%)	+++	Nuclear, cytoplasmic	Circulating monocytes
			Interstitium		Spindle/Stellate (20%)	+++	Nuclear, cytoplasmic	MoMφs/ ReMφs/ cDCs
		Ym1	Interstitial blood vessels	+/-	Round (80%)	+++	cytoplasmic (stippled)	Circulating monocytes
			Interstitium		Spindle/Stellate (20%)	+++	cytoplasmic (stippled)	MoMφs/ ReMφs
		iNOS	\	\	\	\	\	\
		HO-1	\	\	\	\	\	\
		MHC II	Interstitium	+	Stellate	++	Cytoplasmic	MoMφs/ ReMφs/ cDCs / MoDCs
	Renal papilla	Iba-1	Interstitium	+/++	Round/Stellate	++	Cytoplasmic	MoMφs/ ReMφs
		F4/80	\	\	\	\	\	\
		MARCO	\	\	\	\	\	\
		CD206	Interstitium	+/++	Round/Stellate	+++	Cytoplasmic	MoMφs/ ReMφs
		Arg-1	\	\	\	\	\	\
		Ym1	\	\	\	\	\	\

		iNOS	\	\	\	\	\	\
		HO-1	\	\	\	\	\	\
		MHC II	\	\	\	\	\	\
	Pelvis	Iba-1	Lamina propria	+/++	Polymorphic	++	Cytoplasmic	MoMφs/ ReMφs/ cDCs / MoDCs
		F4/80	Lamina propria	+/++	Stellate/Spindle	++	Cytoplasmic	MoMφs/ ReMφs
		MARCO	\	\	\	\	\	\
		CD206	Lamina propria	+	Round (40%) Spindle (60)	+++	Cytoplasmic	MoMφs/ ReMφs
		Arg-1	Lamina propria	+	Round (80%) Spindle (20%)	+++	Nuclear, cytoplasmic	MoMφs/ ReMφs
		Ym1	\	\	\	\	\	\
		iNOS	\	\	\	\	\	\
		HO-1	\	\	\	\	\	\
		MHC II	Lamina propria	+	Stellate/Spindle	+	Cytoplasmic	MoMφs/ ReMφs/ cDCs / MoDCs

Supplemental Table 8. Adrenal glands immunohistochemical evaluation.

Organ/structure		Marker	Location	Cellular count	Shape (%)	Staining Intensity	Staining Pattern	ID
Adrenals	Cortex	Iba-1	Zona glomerulosa	+++	Stellate	++/+++	Cytoplasmic	AdMφs/ MoMφs/ cDCs / MoDCs
			Zona fasciculata	++	Stellate	++	Cytoplasmic	AdMφs/ MoMφs/ cDCs / MoDCs
		F4/80	Zona glomerulosa	n/a	n/a	n/a	n/a	n/a
			Zona fasciculata	n/a	n/a	n/a	n/a	n/a
		MARCO	Zona glomerulosa	\	\	\	\	\
			Zona fasciculata	\	\	\	\	\
		CD206	Zona glomerulosa	\	\	\	\	\
			Zona fasciculata	\	\	\	\	\
		Arg-1	Zona glomerulosa / Blood vessels	+/-	Round	+++	Nuclear, Cytoplasmic	Monocytes
			Zona fasciculata	\	\	\	\	\
		Ym1	Zona glomerulosa	\	\	\	\	\
			Zona fasciculata	\	\	\	\	\
		iNOS	Zona glomerulosa	\	\	\	\	\
			Zona fasciculata	\	\	\	\	\
		HO-1	Zona glomerulosa	\	\	\	\	\
			Zona fasciculata	\	\	\	\	\
		MHC II	Zona glomerulosa	+/-	Stellate	++	Cytoplasmic	AdMφs/ MoMφs/ cDCs / MoDCs
			Zona fasciculata	+/-	Stellate	++	Cytoplasmic	AdMφs/ MoMφs/ cDCs / MoDCs
	Medulla	Iba-1	Medulla	+	Stellate	++/+++	Cytoplasmic	AdMφs/ MoMφs/ cDCs / MoDCs
		F4/80	Medulla	n/a	n/a	n/a	n/a	n/a
		MARCO	\	\	\	\	\	\
		CD206	\	\	\	\	\	\
		Arg-1	\	\	\	\	\	\
		Ym1	\	\	\	\	\	\
		iNOS	\	\	\	\	\	\
		HO-1	\	\	\	\	\	\
		MHC II	Medulla	+	Stellate	++/+++	Cytoplasmic	AMφs/ MoMφs/ cDCs / MoDCs

Supplemental Table 9. Forestomach immunohistochemical evaluation.

Organ/structure			Marker	Location	Cellular count	Shape (%)	Staining Intensity	Staining Pattern	ID
Stomach	Forestomach	Tunica mucosa	Iba-1	Lamina Propria	+++	Round/Spindle	+++	Cytoplasm	MoMφs / MoDCs/ cDCs
			F4/80	Lamina Propria	++	Round/Spindle	+/++	Membrane/Cytoplasm	MoMφs
			MARCO	Lamina Propria	\	\	\	\	\
			CD206	Lamina Propria	+	Round/Spindle	+++	Cytoplasm	MoMφs
			Arg-1	Lamina Propria	+/-	Round	+++	Cytoplasmic nuclear	MoMφs
			Ym1	Lamina Propria	\	\	\	\	\
			iNOS	Lamina Propria	\	\	\	\	\
			HO1	Lamina Propria	\	\	\	\	\
			MHC-II	Lamina Propria	\	\	\	\	\
		Tunica sub-mucosa	Iba-1	Submucosa	+	Round/Spindle	+++	Cytoplasm	MoMφs / MoDCs/ cDCs
			F4/80	Submucosa	+	Round/Spindle	+/++	Cytoplasm	MoMφs
			MARCO	Submucosa	\	\	\	\	\
			CD206	Submucosa	+	Round/Spindle	+++	Cytoplasm	MoMφs
			Arg-1	Submucosa	+/-	Round	+++	Cytoplasmic nuclear	MoMφs
			Ym1	Submucosa	\	\	\	\	\
			iNOS	Submucosa	\	\	\	\	\
			HO1	Submucosa	+	Round	++	Cytoplasm	MoMφs
			MHC-II	Submucosa	\	\	\	\	\
		Tunica muscularis	Iba-1	Tunica muscolaris	+	Round/Spindle	+++	Cytoplasm	MoMφs
			F4/80	Tunica muscolaris	+/-	Round/Spindle	+/++	Cytoplasm	MoMφs
			MARCO	Tunica muscolaris	\	\	\	\	\
			CD206	Tunica muscolaris	+	Round/Spindle	+++	Cytoplasm	MoMφs
			Arg-1	Tunica muscolaris	\	\	\	\	\
			Ym1	Tunica muscolaris	\	\	\	\	\
			iNOS	Tunica muscolaris	\	\	\	\	\
			HO1	Tunica muscolaris	\	\	\	\	\
			MHC-II	Tunica muscolaris	\	\	\	\	\
		Serosa	Iba-1	Serosal lining	\	\	\	\	\
			F4/80	Serosal lining	\	\	\	\	\
			MARCO	Serosal lining	\	\	\	\	\
			CD206	Serosal lining	\	\	\	\	\
			Arg-1	Serosal lining	\	\	\	\	\
			Ym1	Serosal lining	\	\	\	\	\
			iNOS	Serosal lining	\	\	\	\	\
			HO1	Serosal lining	\	\	\	\	\
			MHC-II	Serosal lining	\	\	\	\	\

Supplemental Table 10. Glandular stomach immunohistochemical evaluation.

Organ/structure			Marker	Location	Cellular count	Shape (%)	Staining Intensity	Staining Pattern	ID
Stomach	Glandular Stomach	Tunica mucosa	Iba-1	Lamina Propria	+++	Stellate/Spindle (80%)	+++	Cytoplasm	MoMφs / MoDCs/ cDCs
						Round (20%)			MoMφs
			F4/80	Lamina Propria	++	Stellate/Spindle (80%)	+/++	Cytoplasm	MoMφs
						Round (20%)			MoMφs
			MARCO	Lamina Propria	\	\	\	\	\
			CD206	Lamina Propria	+	Round/Spindle	+++	Cytoplasm	MoMφs
			Arg-1	Lamina Propria	+	Round	++	Cytoplasm	MoMφs
			Ym1	Lamina Propria	\	\	\	\	\
			iNOS	Lamina Propria	\	\	\	\	\
			HO1	Lamina Propria	+/-	Round	++	Cytoplasm	MoMφs
			MHC-II	Lamina Propria	++	Stellate/Spindle	+++	Cytoplasm	MoMφs / MoDCs/ cDCs
		Tunica sub-mucosa	Iba-1	Submucosa	++/+++	Stellate/Spindle	+++	Cytoplasm	MoMφs / MoDCs/ cDCs
			F4/80	Submucosa	++/+++	Stellate/Spindle	+	Cytoplasm	MoMφs
			MARCO	Submucosa	\	\	\	\	\
			CD206	Submucosa	++	Round/Spindle	+++	Cytoplasm	MoMφs
			Arg-1	Submucosa	+/-	Round	++	Cytoplasm	MoMφs
			Ym1	Submucosa	\	\	\	\	\
			iNOS	Submucosa	\	\	\	\	\
			HO1	Submucosa	+	Round	++	Cytoplasm	MoMφs
			MHC-II	Submucosa	\	\	\	\	\
		Tunica muscularis	Iba-1	Tunica muscolaris	++	Round/Spindle	+++	Cytoplasm	MoMφs / MoDCs/ cDCs
			F4/80	Tunica muscolaris	+/-	Round/Spindle	+++	Cytoplasm	MoMφs
			MARCO	Tunica muscolaris	\	\	\	\	\
			CD206	Tunica muscolaris	+	Round/Spindle	+++	Cytoplasm	MoMφs
			Arg-1	Tunica muscolaris	\	\	\	\	\
			Ym1	Tunica muscolaris	\	\	\	\	\
			iNOS	Tunica muscolaris	\	\	\	\	\
			HO1	Tunica muscolaris	\	\	\	\	\
			MHC-II	Tunica muscolaris	\	\	\	\	\
		Serosa	Iba-1	Serosal lining	+	Round/Spindle	+++	Cytoplasm	MoMφs
			F4/80	Serosal lining	\	\	\	\	\
			MARCO	Serosal lining	\	\	\	\	\
			CD206	Serosal lining	+	Round/Spindle	+++	Cytoplasm	MoMφs
			Arg-1	Serosal lining	\	\	\	\	\
			Ym1	Serosal lining	\	\	\	\	\
			iNOS	Serosal lining	\	\	\	\	\
			HO1	Serosal lining	\	\	\	\	\
			MHC-II	Serosal lining	\	\	\	\	\

Supplemental Table 11. Small intestine immunohistochemical evaluation.

Organ/structure		Marker	Location	Cellular count	Shape (%)	Staining Intensity	Staining Pattern	ID
Small intestine	Tunica mucosa	Iba-1	Lamina propria	++++	Stellate/Spindle (80%)	+++	Membrane/Cytoplasm	MoMφs / MoDCs/ cDCs
					Round (20%)	+++	Membrane/Cytoplasm	MoMφs / MoDCs/ cDCs / pDCs
			Lymphoid follicles- Mantle zone	++	Polymorphic	+++	Membrane/Cytoplasm	MoMφs / MoDCs/ cDCs / pDCs
			Lymphoid follicles- Germinal center	++	Round	+++	Cytoplasmic	TBMφs
					Stellate	+++	Cytoplasmic	FDCs
		F4/80	Lamina propria	+++	Stellate/Spindle (70%)	++	Membrane/Cytoplasm	MoMφs
					Round (30%)	++	Membrane/Cytoplasm	MoMφs
			Lymphoid follicles- Mantle zone	n/a	n/a	n/a	n/a	n/a
			Lymphoid follicles- Germinal center	n/a	n/a	n/a	n/a	n/a
		MARCO	Lamina propria	\	\	\	\	\
			Lymphoid follicles- Mantle zone	\	\	\	\	\
			Lymphoid follicles- Germinal center	\	\	\	\	\
		CD206	Lamina propria	+	Round (80%)	++	Cytoplasmic	MoMφs
					Spindle (20%)	++	Cytoplasmic	MoMφs
			Lymphoid follicles- Mantle zone	\	\	\	\	\
			Lymphoid follicles- Germinal center	\	\	\	\	\
		Arg-1	Lamina propria	++	Round	+++	Nuclear, cytoplasmic	MoMφs
			Lymphoid follicles- Mantle zone	++	Round	+++	Nuclear, cytoplasmic	MoMφs
			Lymphoid follicles- Germinal center	\	\	\	\	\
		Ym1	Lamina propria	+	Round	++	Cytoplasmic (granular)	MoMφs
			Lymphoid follicles- Mantle zone	+/-	Round	++	Cytoplasmic (granular)	MoMφs
			Lymphoid follicles- Germinal center	\	\	\	\	\
		iNOS	Lamina propria	+/-	Round/Spindle	++	Cytoplasmic	MoMφs
			Lymphoid follicles- Mantle zone	+++	Stellate	++	Cytoplasmic	MoMφs
			Lymphoid follicles- Germinal center	++	Stellate	++	Cytoplasmic	FDCs
		HO-1	Lamina propria	+	Round	+	Cytoplasmic	MoMφs
			Lymphoid follicles- Mantle zone	+/-	Stellate	+	Cytoplasmic	MoMφs
			Lymphoid follicles- Germinal center	\	\	\	\	\
		MHC II	Lamina propria	++/+++	Stellate	++	Cytoplasmic	MoMφs / MoDCs/ cDCs
			Lymphoid follicles- Mantle zone	++	Stellate	++	Cytoplasmic	MoMφs / MoDCs/ cDCs / pDCs
			Lymphoid follicles- Germinal center	+	Round	++	Cytoplasmic	MoMφs / MoDCs/ cDCs / pDCs
	Tunica sub-mucosa	Iba-1	Submucosa	++	Polymorphic	++	Cytoplasmic	MoMφs / MoDCs/ cDCs
		F4/80	Submucosa	+/-	Polymorphic	+/++	Cytoplasmic	MoMφs
		MARCO	Submucosa	\	\	\	\	\
		CD206	Submucosa	+	Round/spindle	+++	Cytoplasmic	MoMφs
		Arg-1	Submucosa	+	Round	+++	Nuclear, cytoplasmic	MoMφs
		Ym1	Submucosa	\	\	\	\	\
		iNOS	Submucosa	\	\	\	\	\
		HO-1	Submucosa	\	\	\	\	\
		MHC II	Submucosa	\	\	\	\	\
	Tunica muscularis	Iba-1	Inner and outer layer	+	Round/Spindle	+++	Cytoplasmic	MoMφs
		F4/80	Inner and outer layer	n/a	n/a	n/a	n/a	n/a
		MARCO	Inner and outer layer	\	\	\	\	\
		CD206	Inner and outer layer	+	Round/Spindle	+++	Cytoplasmic	MoMφs

		Arg-1	Inner and outer layer	\	\	\	\	\
		Ym1	Inner and outer layer	\	\	\	\	\
		iNOS	Inner and outer layer	\	\	\	\	\
		HO-1	Inner and outer layer	\	\	\	\	\
		MHC II	Inner and outer layer	\	\	\	\	\
	Serosa	Iba-1	Serosal lining	+	Round/Spindle	+++	Cytoplasmic	MoMφs
		F4/80	Serosal lining	n/a	n/a	n/a	n/a	n/a
		MARCO	Serosal lining	\	\	\	\	\
		CD206	Serosal lining	+	Round/Spindle	+/++	Cytoplasmic	MoMφs
		Arg-1	Serosal lining	+	Round	++	Nuclear, cytoplasmic	MoMφs
		Ym1	Serosal lining	\	\	\	\	\
		iNOS	Serosal lining	\	\	\	\	\
		HO-1	Serosal lining	\	\	\	\	\
		MHC II	Serosal lining	\	\	\	\	\

Supplemental Table 12. Testis immunohistochemical evaluation.

Organ/structure		Marker	Location	Cellular count	Shape (%)	Staining Intensity	Staining Pattern	ID
Testes	Interstitium	Iba1	Intertubular	+++	Stellate	+++	Cytoplasmic	IntMφs/ MoMφs
		F4/80	Intertubular	+	Stellate	+	Cytoplasmic	IntMφs/ MoMφs
		MARCO	\	\	\	\	\	\
		CD206	Intertubular	++	Round/Spindle	+++	Cytoplasmic	IntMφs/ MoMφs
		Arg-1	\	\	\	\	\	\
		Ym1	\	\	\	\	\	\
		iNOS	\	\	\	\	\	\
		HO-1	\	\	\	\	\	\
		MHCII	\	\	\	\	\	\
	Peritubular	Iba1	Peritubular	+	Spindle	+++	Cytoplasmic	PTMφs
		F4/80	\	\	\	\	\	\
		MARCO	\	\	\	\	\	\
		CD206	\	\	\	\	\	\
		Arg-1	\	\	\	\	\	\
		Ym1	\	\	\	\	\	\
		iNOS	\	\	\	\	\	\
		HO-1	\	\	\	\	\	\
		MHCII	\	\	\	\	\	\
	Tubular lumen	Iba1	\	\	\	\	\	\
		F4/80	\	\	\	\	\	\
		MARCO	\	\	\	\	\	\
		CD206	\	\	\	\	\	\
		Arg-1	\	\	\	\	\	\
		Ym1	\	\	\	\	\	\
		iNOS	\	\	\	\	\	\
		HO-1	\	\	\	\	\	\
		MHCII	\	\	\	\	\	\

Supplemental Table 13. Heart immunohistochemical evaluation.

Organ/structure		Marker	Location	Cellular count	Shape (%)	Staining Intensity	Staining Pattern	ID
Heart	Epicardium	Iba1	Epicardium	+	Round/Spindle	+++	Cytoplasmic	CaMφs / MoMφs
		F4/80	Epicardium	+/-	Round/Spindle	++	Cytoplasmic	CaMφs / MoMφs
		MARCO	Epicardium	\	\	\	\	\
		CD206	Epicardium	+	Round/Spindle	++	Cytoplasmic	CaMφs / MoMφs
		Arg-1	Epicardium	\	\	\	\	\
		Ym1	Epicardium	\	\	\	\	\
		iNOS	Epicardium	\	\	\	\	\
		HO-1	Epicardium	\	\	\	\	\
		MHCII	Epicardium	\	\	\	\	\
	Myocardium	Iba1	Myocardium	++	Polymorphic	+++	Cytoplasmic	CaMφs / MoMφs
		F4/80	Myocardium	\	\	\	\	\
		MARCO	Myocardium	\	\	\	\	\
		CD206	Myocardium	+	Round/Spindle	++	Cytoplasmic	CaMφs / MoMφs
		Arg-1	Myocardium	\	\	\	\	\
		Ym1	Myocardium	\	\	\	\	\
		iNOS	Myocardium	\	\	\	\	\
		HO-1	Myocardium	\	\	\	\	\
		MHCII	Myocardium	\	\	\	\	\
	Endocardium	Iba1	Endocardium	+	Round/Spindle	+++	Cytoplasmic	CaMφs / MoMφs
		F4/80	Endocardium	\	\	\	\	\
		MARCO	Endocardium	\	\	\	\	\
		CD206	Endocardium	\	\	\	\	\
		Arg-1	Endocardium	\	\	\	\	\
		Ym1	Endocardium	\	\	\	\	\
		iNOS	Endocardium	\	\	\	\	\
		HO-1	Endocardium	\	\	\	\	\
		MHCII	Endocardium	\	\	\	\	\
	Valves	Iba1	Valvular stroma	+	Round/Spindle	+++	Cytoplasmic	CaMφs / MoMφs
		F4/80	Valvular stroma	\	\	\	\	\
		MARCO	Valvular stroma	\	\	\	\	\
		CD206	Valvular stroma	\	\	\	\	\
		Arg-1	Valvular stroma	\	\	\	\	\
		Ym1	Valvular stroma	\	\	\	\	\
		iNOS	Valvular stroma	\	\	\	\	\
		HO-1	Valvular stroma	\	\	\	\	\
		MHCII	Valvular stroma	\	\	\	\	\

Supplemental Table 14. Lung immunohistochemical evaluation.

Organ/structure		Marker	Location	Cellular count	Shape (%)	Staining Intensity	Staining Pattern	ID
Lungs	Alveolar System	Iba-1	Alveoli, Bronchioles	\	\	\	\	\
		F4/80	Alveoli, Bronchioles	++	Round	+	Cytoplasmic, Membranous	AMφs
		MARCO	Alveoli, Bronchioles	++/+++	Round	+++	Cytoplasmic, Membranous	AMφs
		CD206	Alveoli, Bronchioles	+/++	Round	++/+++	Cytoplasmic	AMφs
		Arg-1	Alveoli, Bronchioles	+/-	Round	+	Cytoplasmic	AMφs
		Ym1	Alveoli, Bronchioles	++++	Round	+++	Cytoplasmic	AMφs
		iNOS	Alveoli, Bronchioles	\	\	\	\	\
		HO1	Alveoli, Bronchioles	+	Round	+++	Cytoplasmic	AMφs
		MHC II	Alveoli, Bronchioles	+/-	Round	+	Cytoplasmic	AMφs
	Interstitium	Iba-1	Perivascular/Peribronchial	+++	Polymorphic	+++	Cytoplasmic	IMφs (MoMΦs) / MoDCs/ cDCs
			Alveolar Septa	+/++	Round (40%)	++		IMφs (MoMΦs) / MoDCs/ cDCs
					Spindle (60%)			
		F4/80	Perivascular/Peribronchial	+	Spindle/Stellate	+	Cytoplasmic, Membranous	IMφs (MoMΦs)
			Alveolar Septa	+/++	Round (40%)			Circulating monocytes
					Spindle (60%)			IMφs (MoMΦs)
		MARCO	Perivascular/Peribronchial	\	\	\	\	\
			Alveolar Septa	\	\	\	\	\
		CD206	Perivascular/Peribronchial	++/+++	Polymorphic	+++	Cytoplasmic	IMφs (MoMΦs)
			Alveolar Septa	+	Spindle	++/+++	Cytoplasmic	IMφs (MoMΦs)
		Arg-1	Perivascular/Peribronchial	+/++	Round/Spindle	+++	Cytoplasmic, Nuclear	IMφs (MoMΦs)
			Alveolar Septa	++	Round	++	Cytoplasmic	Circulating monocytes
					Spindle	+		IMφs (MoMΦs)
		Ym1	Perivascular/Peribronchial	+	Spindle/Stellate	+++	Cytoplasmic	IMφs (MoMΦs)
			Alveolar Septa	+	Round	+++	Cytoplasmic	Circulating monocytes
		iNOS	Perivascular/Peribronchial	\	\	\	\	\
			Alveolar Septa	\	\	\	\	\
		HO1	Perivascular/Peribronchial	\	\	\	\	\
			Alveolar Septa	\	\	\	\	\
		MHC II	Perivascular/Peribronchial	++	Spindle/Stellate	++	Cytoplasmic	IMφs (MoMΦs) / MoDCs/ cDCs
			Alveolar Septa	+	Spindle	++	Cytoplasmic	IMφs (MoMΦs) / MoDCs/ cDCs

Supplemental Table 15. Pancreas immunohistochemical evaluation.

Organ/structure		Marker	Location	Cellular count	Shape (%)	Staining Intensity	Staining Pattern	ID
Pancreas	Exocrine Pancreas	Iba-1	Interacinar interstitium	+	Stellate/Spindle	+++	Cytoplasmic	MoMφs / cDCs / MoDCs
			Peri-tubular interstitum	++	Stellate/Spindle	+++	Cytoplasmic	PaMφs (MoMφs)
		F4/80	Interacinar interstitium	+	Stellate/Spindle	+	Cytoplasmic	MoMφs
			Peri-tubular interstitum	+/-	Stellate/Spindle	+	Cytoplasmic	\
		MARCO	Interacinar interstitium	\	\	\	\	\
			Peri-tubular interstitum	\	\	\	\	\
		CD206	Interacinar interstitium	\	\	\	\	MoMφs
			Peri-tubular interstitum	+	Stellate/Spindle	+/++	Cytoplasmic	\
		Arg-1	Interacinar interstitium	\	\	\	\	MoMφs / circulating monocytes
			Peri-tubular interstitum	+	Round	+++	Cytoplasmic	\
		Ym-1	Interacinar interstitium	\	\	\	\	\
			Peri-tubular interstitum	\	\	\	\	\
		iNOS	Interacinar interstitium	\	\	\	\	\
			Peri-tubular interstitum	\	\	\	\	\
		HO-1	Interacinar interstitium	\	\	\	\	MoMφs
			Peri-tubular interstitum	+/-	Round	+	Cytoplasmic	PaMφs (MoMφs) / cDCs / MoDCs
		MHC II	Interacinar interstitium	+	Stellate/Spindle	++	Cytoplasmic	MoMφs / MoDCs/ cDCs / MoDCs
			Peri-tubular interstitum	+	Stellate	++	Cytoplasmic	IslMφs
	Endocrine Pancreas	Iba-1	Langerhans Island	+	Stellate	+++	Cytoplasmic	IslMφs
		F4/80	Langerhans Island	+	Stellate	++	Cytoplasmic	\
		MARCO	Langerhans Island	\	\	\	\	\
		CD206	Langerhans Island	\	\	\	\	\
		Arg-1	Langerhans Island	\	\	\	\	\
		Ym-1	Langerhans Island	\	\	\	\	\
		iNOS	Langerhans Island	\	\	\	\	\
		HO-1	Langerhans Island	\	\	\	\	IslMφs
		MHC II	Langerhans Island	+/-	Stellate	++	Cytoplasmic	IslMφs

Supplemental Table 16. Necrosuppurative hepatitis immunohistochemical evaluation.

Organ/structure		Marker	Location	Cellular count	Shape (%)	Staining Intensity	Staining Pattern	ID
Liver	Necro suppurative foci	Iba-1	Perinecrotic area	++++	Stellate	++	Membrane / cytoplasmic	MoMφs / MoDCs/ cDCs
			Peripheric area	++++	Stellate	++/+++	Membrane / cytoplasmic	MoMφs / MoDCs/ cDCs
		F4/80	Perinecrotic area	\	\	\	\	\
			Peripheric area	+/-	Stellate	+	Cytoplasmic	MoMφs
		MARCO	Perinecrotic area	++	Round/Stellate	++	Membrane/ cytoplasmic	MoMφs
			Peripheric area	+	Round/Stellate	++	Membrane/ cytoplasmic	MoMφs
		CD206	Perinecrotic area	\	\	\	\	\
			Peripheric area	\	\	\	\	\
		Arg-1	Perinecrotic area	+++	Stellate	+++	Cytoplasm	MoMφs
			Peripheric area	\	\	\	\	\
		Ym-1	Perinecrotic area	+	Round	+++	Cytoplasm	MoMφs
			Peripheric area	+/++	Round	+++	Cytoplasm	MoMφs
		iNOS	Perinecrotic area	+++	Stellate	++	Cytoplasm	MoMφs
			Peripheric area	\	\	\	\	\
		HO1	Perinecrotic area	+	Stellate	+	Cytoplasm	MoMφs
			Peripheric area	\	\	\	\	\
		MHCII	Perinecrotic area	++/+++	Stellate	+++	Cytoplasmic	MoMφs / MoDCs/ cDCs
			Peripheric area	++/+++	Stellate	+++	Cytoplasmic	MoMφs / MoDCs/ cDCs

Supplemental Table 17. *Pneumocystis murina* infected lung immunohistochemical evaluation.

Organ	Anatomical region	Marker	Location	Cellular count	Shape (%)	Staining Intensity	Staining Pattern	ID
Lung	Alveolar System	Iba-1	Alveoli, Bronchioles	++++	Round	+++	Membrane	MoMφs / AMφs
		F4/80	Alveoli, Bronchioles	n/a	n/a	n/a	n/a	n/a
		MARCO	Alveoli, Bronchioles	+/-	Round	++	Membrane/cytoplasmic	MoMφs / AMφs
		CD206	Alveoli, Bronchioles	+	Round	+	Membrane/cytoplasmic	MoMφs / AMφs
		Arg-1	Alveoli, Bronchioles	++++	Round	+++	Membrane/cytoplasmic	MoMφs / AMφs
		Ym-1	Alveoli, Bronchioles	+++	Round	+++	Cytoplasmic (granular)	MoMφs / AMφs
		iNOS	Alveoli, Bronchioles	+++	Round	+++	Cytoplasmic	MoMφs / AMφs
		HO1	Alveoli, Bronchioles	+++	Round	+/++	Cytoplasmic	MoMφs / AMφs
		MHCII	Alveoli, Bronchioles	+/-	Round	+	Cytoplasmic	MoMφs / AMφs
	Interstitium	Iba-1	Perivasal/Peribronchial	+++/++++	Polymorphic	+++	Membrane/Cytoplasm	IMφs (MoMφs) / MoDCs / cDCs
			Alveolar Septa	+++	Polymorphic	+++	Membrane/Cytoplasm	IMφs (MoMφs) / MoDCs / cDCs
		F4/80	Perivasal/Peribronchial	n/a	n/a	n/a	n/a	n/a
			Alveolar Septa	n/a	n/a	n/a	n/a	n/a
		MARCO	Perivasal/Peribronchial	\	\	\	\	\
			Alveolar Septa	\	\	\	\	\
		CD206	Perivasal/Peribronchial	+	Spindle	+++	Cytoplasmic dots	IMφs (MoMφs)
			Alveolar Septa	\	\	\	\	\
		Arg-1	Perivasal/Peribronchial	+/++	Stellate	+++	Cytoplasmic	IMφs (MoMφs)
			Alveolar Septa	\	\	\	\	\
		Ym-1	Perivasal/Peribronchial	+/-	Stellate	+++	Cytoplasmic (granular)	IMφs (MoMφs)
			Alveolar Septa	+/-	Stellate	+++	Cytoplasmic (granular)	IMφs (MoMφs)
		iNOS	Perivasal/Peribronchial	\	\	\	\	\
			Alveolar Septa	\	\	\	\	\
		HO1	Perivasal/Peribronchial	+	Stellate	++	Cytoplasmic	IMφs (MoMφs)
			Alveolar Septa	+/-	Spindle/ stellate	+	Cytoplasmic	IMφs (MoMφs)
		MHCII	Perivasal/Peribronchial	+++	Stellate	++	Cytoplasmic	IMφs (MoMφs) / MoDCs /cDCs
			Alveolar Septa	++	Round	+	Cytoplasmic	IMφs (MoMφs) / MoDCs /cDCs

Supplemental Table 18. Human synovial sarcoma xenograft immunohistochemical evaluation.

Organ	Case	Marker	Location	Cellular count	Shape	Staining Intensity	Staining Pattern	ID
Skeletal muscle	Human synovial sarcoma xenograft	Iba-1	Periphery	++++	Spindle	+++	Membrane/cytoplasmic	TAMφs / TADCs
			Bulk of the tumor	+++	Polymorphic	+++	Membrane/cytoplasmic	TAMφs / TADCs
			Perinecrotic area	++	Polymorphic	+++	Membrane/cytoplasmic	TAMφs / TADCs
		F4/80	Periphery	++++	Spindle	+++	Membrane/cytoplasmic	TAMφs
			Bulk of the tumor	+++	Polymorphic	+++	Membrane/cytoplasmic	TAMφs
			Perinecrotic area	++	Round/stellate	++	Membrane/cytoplasmic	TAMφs
		MARCO	Periphery	+	Spindle	+++	Membrane/cytoplasmic	TAMφs
			Bulk of the tumor	\	\	\	\	\
			Perinecrotic area	\	\	\	\	\
		CD206	Periphery	+++	Spindle	+++	cytoplasmic	TAMφs (M2-oriented)
			Bulk of the tumor	+	Round/spindle	+	cytoplasmic	TAMφs (M2-oriented)
			Perinecrotic area	\	\	\	\	\
		Arg-1	Periphery	+++	Spindle	+++	cytoplasmic, nuclear	TAMφs / MDSCs
			Bulk of the tumor	+++	Stellate	+++	cytoplasmic, nuclear	TAMφs / MDSCs
			Perinecrotic area	+++	Polymorphic	++/+++	cytoplasmic, nuclear	TAMφs / MDSCs
		Ym-1	Periphery	+/-	Stellate	+/++	cytoplasmic (stippled)	TAMφs (M2-oriented)
			Bulk of the tumor	+/-	Stellate	+/++	cytoplasmic (stippled)	TAMφs (M2-oriented)
			Perinecrotic area	\	\	\	\	\
		iNOS	Periphery	\	\	\	\	\
			Bulk of the tumor	\	\	\	\	\
			Perinecrotic area	\	\	\	\	\
		HO1	Periphery	+/++	Polymorphic	++	Cytoplasmic	TAMφs (M2-oriented)
			Bulk of the tumor	+/++	Polymorphic	++	Cytoplasmic	TAMφs (M2-oriented)
			Perinecrotic area	+	Round/stellate	++	Cytoplasmic	TAMφs (M2-oriented)
		MHC-II	Periphery	\	\	\	\	\
			Bulk of the tumor	\	\	\	\	\
			Perinecrotic area	\	\	\	\	\

Supplemental Table 19. Murine fibrosarcoma syngraft immunohistochemical evaluation.

Organ	Case	Marker	Location	Cellular count	Shape	Staining Intensity	Staining Pattern	ID
Skeletal muscle	Syngeneic murine fibrosarcoma	Iba-1	Periphery	++++	Polymorphic	+++	Membrane/cytoplasmic	TAMφs / TADCs
			Bulk of the tumor	++++	Polymorphic	+++	Membrane/cytoplasmic	TAMφs / TADCs
			Perinecrotic area	+++	Polymorphic	++/+++	Membrane/cytoplasmic	TAMφs / TADCs
		F4/80	Periphery	n/a	n/a	n/a	n/a	n/a
			Bulk of the tumor	n/a	n/a	n/a	n/a	n/a
			Perinecrotic area	n/a	n/a	n/a	n/a	n/a
		MARCO	Periphery	+	Spindle	++	cytoplasmic	
			Bulk of the tumor	\	\	\	\	
			Perinecrotic area	\	\	\	\	
		CD206	Periphery	++/+++	polymorphic	+++	Cytoplasmic	TAMφs (M2-oriented)
			Bulk of the tumor	+	polymorphic	+/++	Membrane/cytoplasmic	TAMφs (M2-oriented)
			Perinecrotic area	+/-	polymorphic	+/++	Membrane/cytoplasmic	TAMφs (M2-oriented)
		Arg-1	Periphery	+++/++++	polymorphic	++	cytoplasmic, nuclear	TAMφs / MDSCs
			Bulk of the tumor	+++	polymorphic	+++	cytoplasmic, nuclear	TAMφs / MDSCs
			Perinecrotic area	++/+++	polymorphic	++/+++	cytoplasmic, nuclear	TAMφs / MDSCs
		Ym-1	Periphery	+/-	Stellate	+/++	cytoplasmic (stippled)	TAMφs (M2-oriented)
			Bulk of the tumor	+/-	Stellate	+/++	cytoplasmic (stippled)	TAMφs (M2-oriented)
			Perinecrotic area	\	\	\	\	\
		iNOS	Periphery	\	\	\	\	\
			Bulk of the tumor	\	\	\	\	\
			Perinecrotic area	+/++	Stellate	++	Cytoplasmic	TAMφs (M1-oriented)
		HO1	Periphery	+/++	Round/spindle	++	Cytoplasmic	TAMφs (M2-oriented)
			Bulk of the tumor	+/++	Polymorphic	++	Cytoplasmic	TAMφs (M2-oriented)
			Perinecrotic area	+	Round	++	Cytoplasmic	TAMφs (M2-oriented)
		MHC-II	Periphery	\	\	\	\	\
			Bulk of the tumor	\	\	\	\	\
			Perinecrotic area	\	\	\	\	\

Supplemental Table 20. Histologic grading system for caerulein-induced pancreatitis severity assessment.

	EDEMA Entire section	**INTERSTITIAL INFLAMMATORY CELLS INFILTRATES** 4 hot spot fields 400x	**APOPTOSIS** 4 Hot spot fields 400x	**ADM** 4 Hot spot fields 400x	**PANCREATITIS EXTENSION** Entire section
SCORE					
0	Absent	No inflammatory cells	0 total apoptotic cells	Absent	0%
1	Optically empty space slightly separates lobules	< 10 inflammatory cells per field	1-5 total apoptotic cells	1-10 ducts	0-25 %
2	Optically empty space separates lobules	10-40 inflammatory cells per field	6-10 total apoptotic cells	11-20 ducts	26- 50 %
3	Optically empty space separates single acini	40-80 inflammatory cells per field	11-14 total apoptotic cells	> 20 ducts	51-75 %
4	n/a	> 80 inflammatory cells per field	>15 total apoptotic cells	n/a	76-100 %

Supplemental Table 21. Histologic grading system for caerulein-induced pancreatitis severity assessment in male mice. Colored lines contain median values

SEX	TIME POINT	GROUP	MOUSE ID	EDEMA	INTERSTITIAL INFILTRATES	INFLAMMATORY CELLS TYPES	APOPTOSIS	ADM	EXTENT	TOTAL HISTOLOGY SCORE
♂	0 day	Not manipulated	**13.0**	0	0	\	0	0	0	0
				0	0	\	0		0	0
	12h	Control (PBS)	**13.1**	0	0	\	0	0	0	0
	12h	Control (PBS)	**13.2**	0	0	\	0	0	0	0
	12h	Control (PBS)	**13.3**	0	0	\	0	0	0	0
				0	0	\	0	0	0	0
	12h	Caerulein	**13.4**	3	3	N, M, rare L and P	1	0	2	14
	12h	Caerulein	**13.5**	3	3	N, M, rare L and P	1	0	2	14
	12h	Caerulein	**13.6**	3	4	N, M, rare L and P	1	0	3	24
				3	3	n/a	1	0	2	14
	48h	Control (PBS)	**13.7**	0	0	\	0	0	0	0
	48h	Control (PBS)	**13.8**	0	0	\	0	0	0	0
				0	0	\	0	0	0	0
	48h	Caerulein	**13.9**	2	3	N, M, rare L and P	4	2	3	27
	48h	Caerulein	**13.10**	2	3	M, N, rare L and P	4	2	2	18
	48h	Caerulein	**13.11**	2	2	N, M, rare L and P	4	2	1	8
				2	3	n/a	4	2	2	18
	7 days	Control (PBS)	**13.12**	0	0	\	0	0	0	0
	7 days	Control (PBS)	**13.13**	0	0	\	0	0	0	0
				0	0	\	0	0	0	0
	7 days	Caerulein	**13.14**	0	1	M, L, P and rare N	2	3	1	3
	7 days	Caerulein	**13.15**	0	1	M, L, P and rare N	3	3	1	4
	7 days	Caerulein	**13.16**	0	1	M, L, P and rare N	3	3	1	4
				0	1	n/a	3	3	1	4

Supplemental Table 22. Histologic grading system for caerulein-induced pancreatitis severity assessment in female mice. Colored lines contain median values

SEX	TIME POINT	GROUP	MOUSE ID	EDEMA	INTERSTITIAL INFILTRATES	INFLAMMATORY CELLS TYPES	APOPTOSIS	ADM	EXTENT	TOTAL HISTOLOGY SCORE
♀	0 day	Not manipulated	**13.17**	0	0	\	0	0	0	0
				0	0	\	0	0	0	0
	12h	Control (PBS)	**13.18**	0	0	\	0	0	0	0
	12h	Control (PBS)	**13.19**	0	0	\	0	0	0	0
	12h	Control (PBS)	**13.20**	0	0	\	0	0	0	0
				0	0	\	0	0	0	0
	12h	Caerulein	**13.21**	2	2	N, M, rare L and P	0	0	1	4
	12h	Caerulein	**13.22**	3	4	N, M, rare L and P	0	0	4	28
	12h	Caerulein	**13.23**	3	4	N, M, rare L and P	0	0	4	28
	12h	Caerulein	**13.24**	2	3	N, M, rare L and P	0	2	3	15
				2.5	3.5	n/a	0	0	3.5	21.5
	48h	Control (PBS)	**13.25**	0	0	\	0	0	0	0
	48h	Control (PBS)	**13.26**	0	0	\	0	0	0	0
				0	0	\	0	0	0	0
	48h	Caerulein	**13.27**	2	2	N, M, rare L and P	2	2	2	12
	48h	Caerulein	**13.28**	1	2	N, M, rare L and P	2	2	1	5
	48h	Caerulein	**13.29**	1	1	N, M, rare L and P	3	1	1	5
				1	2	n/a	2	2	1	5
	7 days	Control (PBS)	**13.30**	0	0	\	0	0	0	0
	7 days	Control (PBS)	**13.31**	0	0	\	0	0	0	0
				0	0	\	0	0	0	0
	7 days	Caerulein	**13.32**	0	1	M, L, P and rare N	1	2	1	2
	7 days	Caerulein	**13.33**	0	2	M, L, P and rare N	2	2	1	4
	7 days	Caerulein	**13.34**	0	1	M, L, P and rare N	0	0	1	1
	7 days	Caerulein	**13.35**	0	1	M, L, P and rare N	0	2	1	1
				0	1	n/a	0.5	2	1	1.5

Supplemental Table 23. QuPath and ImageJ (hot spot) % of positive areas.

CASE	IBA1 QuPath	Iba1 Hot Spot	F480 QuPath	F4/80 Hot Spot	HO1 QuPath	HO1 Hot Spot	CD206 QuPath	CD206 Hot Spot
13.4	0.05530	0.04836	0.00697	0.01306	0.02494	0.02494	0.01397	0.02295
13.5	0.04763	0.03485	0.00476	0.01559	0.01682	0.01682	0.00490	0.01373
13.6	0.04658	0.05112	0.02274	0.02425	0.01645	0.01645	0.01485	0.02106
13.9	0.03649	0.01574	0.02290	0.01068	0.00960	0.00869	0.00478	0.01057
13.10	0.02799	0.06389	0.03257	0.03060	0.01416	0.01953	0.01933	0.01646
13.11	0.03228	0.03965	0.03787	0.03897	0.00993	0.02942	0.02726	0.01668
13.14	0.02692	0.03306	0.00737	0.01404	0.00878	0.02428	0.02161	0.01602
13.15	0.09138	0.09688	0.01919	0.02803	0.00738	0.00960	0.00461	0.01803
13.16	0.07526	0.06016	0.03248	0.02033	0.00711	0.01416	0.00728	0.03644
13.21	0.08327	0.07010	0.01557	0.01867	0.00869	0.00993	0.00593	0.02587
13.22	0.04617	0.04009	0.02032	0.01383	0.01953	0.01337	0.00690	0.02002
13.23	0.04793	0.03768	0.04104	0.01763	0.02942	0.01006	0.00432	0.01925
13.24	0.02031	0.01266	0.00720	0.01992	0.02428	0.00405	0.00088	0.00696
13.27	0.17395	0.10578	0.01319	0.01978	0.01337	0.00878	0.00391	0.02930
13.28	0.10301	0.07149	0.02628	0.01513	0.01006	0.00738	0.00090	0.02791
13.29	0.11780	0.09095	0.00780	0.02953	0.00405	0.00711	0.00201	0.00930
13.32	0.09469	0.09821	0.01774	0.01942	0.01083	0.01083	0.00479	0.01448
13.33	0.10076	0.09839	0.01269	0.01311	0.02749	0.02749	0.01163	0.01471
13.34	0.10773	0.10794	0.00798	0.00720	0.03112	0.03112	0.00673	0.00708
13.35	0.07023	0.06674	0.03319	0.02580	0.00770	0.00770	0.00188	0.00354

Supplemental Table 24. QuPath and ImageJ (hot spot) % of positive areas.

CASE	MHC-II QuPath	MHC-II Hot Spot	B220 QuPath	B220 Hot Spot	CD3e QuPath	CD3e Hot Spot	Caspase QuPath	Caspase Hot Spot
13.4	0.00098	0.00222	0.00040	0.00059	0.00037	0.00113	0.00580	0.01333
13.5	0.00050	0.00084	0.00017	0.00062	0.00029	0.00120	0.00670	0.03433
13.6	\	\	0.00029	0.00102	0.00054	0.00186	0.01030	0.05933
13.9	0.00322	0.00183	0.00027	0.00028	0.00053	0.00113	0.02880	0.02300
13.10	0.00087	0.00164	0.00038	0.00093	0.00145	0.00318	0.02660	0.05067
13.11	0.00005	0.00269	0.00041	0.00137	0.00248	0.00448	0.02060	0.08233
13.14	0.00066	0.00227	0.00066	0.00123	0.00067	0.00223	0.03540	0.03833
13.15	0.00030	0.00071	0.00050	0.00208	0.00026	0.00085	0.37580	0.54467
13.16	0.00095	0.00191	0.00050	0.00093	0.00029	0.00113	0.41750	0.90200
13.21	0.00154	0.00070	0.00040	0.00089	0.00075	0.00210	0.30870	0.54467
13.22	0.00004	0.00062	0.00058	0.00121	0.00091	0.00194	0.17300	0.38300
13.23	0.01365	0.01107	0.00077	0.00131	0.00174	0.00204	0.21030	0.47000
13.24	0.00905	0.00656	0.00039	0.00066	0.00040	0.00101	0.06110	0.11033
13.27	0.00840	0.00747	0.00053	0.00072	0.00647	0.00585	0.02220	0.03300
13.28	0.00239	0.00122	0.00246	0.00490	0.00341	0.00569	0.14910	0.29933
13.29	\	\	0.00166	0.00309	0.00134	0.00332	0.10230	0.17000
13.32	0.00010	0.00052	0.00142	0.00230	0.00207	0.00231	0.05630	0.04667
13.33	0.00244	0.00056	0.00270	0.00432	0.00715	0.00640	0.01760	0.03733
13.34	0.01365	0.01107	0.00292	0.00061	0.01356	0.00478	0.00000	0.01633
13.35	0.00000	0.00000	0.00193	0.00219	0.00402	0.00354	\	\